UNIVERSITÀ DEGLI STUDI DI UDINE
hic sunt futura

www.uniud.it

Doctor of Philosophy in:

"ENVIRONMENTAL AND ENERGY ENGINEERING SCIENCE"

XXXVI cycle

Thesis title:

"DEVELOPMENT OF NOVEL RUTHENIUM(II) BIS(NHC) COMPLEXES AS A CHEMICAL PLATFORM FOR HOMOGENEOUS CATALYSIS"

Ph.D. Student:

Filippo Campagnolo

Supervisor

Prof. Daniele Zuccaccia

Co-supervisor

Dr. Eleonora Aneggi

Year 2024

PREFACE

This thesis is dedicated to the synthesis of novel ruthenium(II) bis(N-heterocyclic carbene) organonitrile complexes. The work covers the design and development of a synthetic pathway, the mechanistic analysis of complex formation, and the preliminary evaluation of these compounds in reactions of interest. However, it is essential to acknowledge the parallel progression of other significant research projects undertaken during this period as, despite the overarching themes of organometallic chemistry and catalysis, the different nature of these research projects made it challenging to include them in the present work.

Gold(I) catalysis is a prosperous research field, and over the years, our research group has specialized in the study of the counterion effect, a critical aspect of many gold-catalyzed transformations. Following the existing research line, a multinuclear DOSY NMR study was conducted to correlate the anion effect to the ion-pairing ratio between the free catalyst and the counterion under reaction conditions. The study tied the ion-pairing ratio to reactivity, corroborating previous experimental observations and confirming p-toluenesulfonate as the optimal counterion due to its balanced coordination and basic properties. In addition, in collaboration with Professor Andrea Biffis's group from the University of Padua, the anion effect was also studied for dinuclear bis(NHC) gold(I) catalysts. The study proved how the dinuclear systems feature a reduced ionization barrier, increasing the reactivity at the expense of stability, thus requiring careful tuning of reaction conditions.

During my Ph.D. I also had the opportunity to spend six months abroad at the Technical University of Munich (TUM) under the supervision of Prof. Fritz E. Kühn, whose research group is deeply involved in transfer hydrogenation catalysis. A collaborative project was initiated to investigate mechanistically the reaction rate dependence on the catalysts' steric hindrance. The catalysts, bearing mixed phosphine-aNHC ligands, were observed to be affected by the base-driven activation process, leading to a reduced reaction rate in proportion to steric bulkiness.

As additional noteworthy contributions, I actively participated in a project focused on the metabolomic analysis of blood serum and in the development of heterogeneous ruthenium(II)-based catalysts. A concise abstract for all contributions is provided at the conclusion of this thesis.

ABSTRACT

N-heterocyclic carbenes (NHCs) rapidly emerged as versatile ligands in coordination chemistry due to their adaptable stereoelectronic properties, enhanced stability, and strong σ-donating power, presenting an appealing alternative to conventional ligands like phosphines. Moreover, integrating NHCs into polydentate ligands has resulted in more robust coordination compounds, which, for instance, has led to decreased catalyst-to-substrate ratios in catalysis. Remarkably, limited examples exist of ruthenium(II) complexes bearing bis(NHC) ligands, despite the blooming field of ruthenium(II) coordination chemistry, prompting further investigation.

Our research led to the development of a novel synthetic pathway giving access to a branch of ruthenium(II) bis(NHC) dicationic organonitrile complexes, successfully functionalized with diverse bidentate ligands of the amino, bipyridine, and phosphine types. The reaction mechanism was thoroughly studied, identifying a key reactive intermediate species, the dicationic tetrakis(acetonitrile)[bis(NHC)]ruthenium(II), which was isolated. Additionally, our investigation unveiled the pivotal role of triethylamine, revealing its function as an internal base in the formation of a ruthenium(II)-triethylamino complex, which then reacts with the bis(NHC) precursor.

The synthesized catalysts have been tested in the transfer hydrogenation reaction, displaying moderate reactivity, with the exception of the dicationic *cis*-bis(acetonitrile)(2,2'-bipyridine) [bis(NHC)]ruthenium(II) complex, which reached a TOF of 50,000 h^{-1}. A significant result for catalysts in an early stage of development.

In conclusion, the developed synthetic protocol is remarkably efficient, demanding mild reaction conditions and minimal workup. It relies on commercially available reagents and consistently returns high yields. The nearly unlimited range of ligands that can be accommodated in the coordination sphere of these complexes - whether novel bis(NHC) ligands, mixed bidentate ligands, or even pincer ligands - enables the tailored synthesis of catalysts for specific applications. This versatility makes of the dicationic tetrakis(acetonitrile)[bis(NHC)]ruthenium(II) a critical platform for catalyst development.

TABLE OF CONTENTS

LIST OF ABBREVIATIONS

ACN	Acetonitrile
AcPh	Acetophenone
AMPY	2-picolylamine
aNHC	Abnormal N-heterocyclic carbene
Ar	Aryl group
B(MI)M	1,1-Bis(3-methylimidazol-2-ylidene)methylene
BIPY	2,2'-bipyridine
B(MI)MI2	1,1-Bis(3'-methylimidazolium)methylene diiodide
bisNHC	Bidentate N-heterocyclic carbene
bTM	1,1-Bis(3'-mesytil-1',2',3'-triazol-5'-ylidene)methylene
COD	1,5-Cyclooctadiene
DCM	Dichloromethane
NMP	N-methyl-2-pyrrolidone
DPPB	1,4-Bis(diphenylphosphino)butane
DPPE	1,2-Bis(diphenylphosphino)ethane
DPPP	1,3-Bis(diphenylphosphino)propane
DSSC	Dye-sensitized solar cell
EN	Ethylenediamine
HOMO	Highest Occupied Molecular Orbital
IS	Internal Standard
iPr_2-bimy	1,3-(diisopropyl)benzimidazole
LUMO	Lowest Unoccupied Molecular Orbital
NHC	N-heterocyclic carbene
p-cymene	1-Methyl-4-(propan-2-yl)benzene
rNHC	Remote N-heterocyclic carbene
RT	Room Temperature
TEA	Triethylamine
TEP	Tolman Electronic Parameter
TH	Transfer hydrogenation
THF	Tetrahydrofuran

1 INTRODUCTION

1.1 N-heterocyclic carbenes (NHCs)

Carbenes are neutral compounds containing carbon atoms engaged in two covalent bonds while retaining a lone electron pair, accounting for a total of six valence electrons.[1] The electronic structure of carbenes points to extreme reactivity, and carbenes were treated as particularly unstable compounds.[2] This perspective radically changed after the introduction of persistent carbenes by the end of the 20th century, thanks to the discovery of N-heterocyclic carbenes (NHCs), a class of singlet carbenes. Defined as heterocycles containing at least one nitrogen atom and a carbene carbon within the ring structure,[1] NHCs now include a comprehensive library of structurally diversified compounds. Nevertheless, it would be arduous to present NHCs properties without speaking of 1,3-disubstituted imidazole-derived carbenes since Arduengo's *1,3-di(adamantyl)imidazol-2-ylidene* is the first example of isolated stable carbene (Figure 1a).[3]

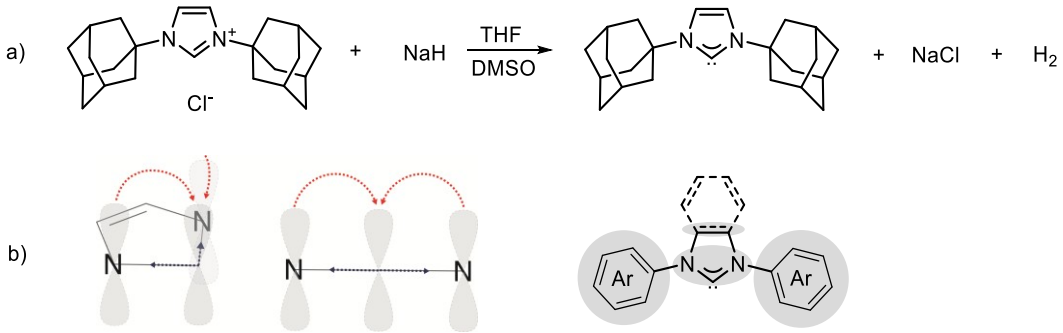

Figure 1 - a) The reaction used by Arduengo to produce *1,3-di(adamantyl)imidazol-2-ylidene*, also known as IAd b) An illustration of the stabilizing stereoelectronic effects on an imidazole-based carbene, and the critical structural feature affecting *imidazol-2-ylidenes* stability.

1.1.1 Stereoelectronic properties of NHCs

The stability of *imidazole*-derived carbenes arises from the steric and electronic properties of the heterocycle structure. The carbene carbon is strategically placed between two nitrogen atoms, which concertedly exert a σ electron-withdrawing and a π electron-donating effects, stabilizing the singlet carbene state (Figure 1b).[4] Indeed, the σ electron-withdrawing effect lowers the energy of the *1,3-disubstituted-imidazol-2-ylidenes* highest occupied molecular orbital (HOMO), increasing the energy gap with the lower unoccupied molecular orbital (LUMO) above 40 kcal/mol, determining the inaccessibility of the triplet carbene state.[5] Germilene and silylene homologs do not necessarily follow this trend.[6,7] Meanwhile, the π electron-donating effect stabilizes the empty p orbital on the carbene atom via π-backdonation (or mesomeric effect).[8] Moreover, the eventual presence of an unsaturated bond in the backbone of the *1,3-disubstituted-imidazol-2-ylidenes* originates partial aromaticity that further stabilizes the carbene,[9] and the electron-rich aryl groups placed at nitrogen atoms, commonly

referred to as the wingtips, amplify this effect. Nevertheless, it should be noted that the unsaturated backbone is not required to produce stable NHC and that stable compounds with alkylic backbones have also been reported.[10] The wingtips fragment of *1,3-disubstituted-imidazol-2-ylidenes* is also essential in producing kinetically stable carbenes, as the steric bulkiness reduces the carbene reactivity and inhibits the dimerization process by which an olefine generates from the condensation of two carbenes. Interestingly, the dimerization reaction is not irreversible, and the dimer is in equilibrium with the free carbene form; hence, the dimer acts as a carbene reservoir. This process is known as Wanzlick's equilibrium and is shifted toward the dimeric form (Figure 2a).[11] While unhindered *1,3-disubstituted-imidazol-2-ylidenes* tend to dimerize, results from experiments designed to study the dimerization process showed that the free *1,3-disubstituted-imidazol-2-ylidenes* are stable and that dimerization is not trivial (Figure 2b).[12]

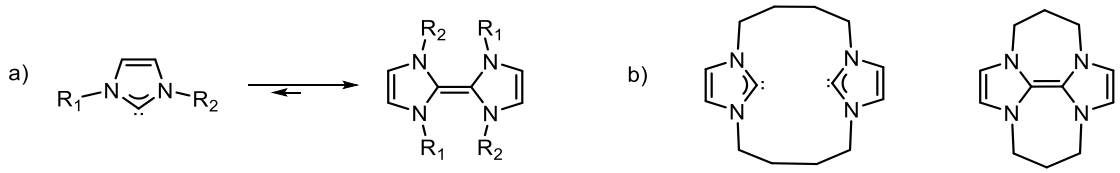

Figure 2 - a) The general scheme of Wanzlick's equilibrium reaction, b) Experimental results showed that carbene dimerization is not trivial, with dimerization occurring only from cyclic bis-carbene under steric strain.

The steric and electronic properties of the wingtip substituents are essential in tuning the *1,3-disubstituted-1,3-imidazol-2-ylidenes* stability and reactivity. The steric properties have been thoroughly studied over the years, with the *buried volume* that emerged as a fundamental parameter to understand the *1,3-disubstituted-imidazol-2-ylidenes* reactivity,[13] and which can be considered as the analog of the Tolman cone angle used to model the steric properties of phosphines.[14] The electronic properties have also been studied in depth and are commonly described using the Tolman Electronic Parameter (TEP), which was also initially developed for phosphines. The TEP specifically evaluates the electron-donating ability of ligands by measuring the difference between the infrared-stretching frequencies of carbonyl ligands in model transition metal carbonyl complexes.[14] Another crucial tool for assessing the σ-donor strength of NHCs is Huynh's Electronic Parameter (HEP).[15] This method operates on the principle of evaluating the change in the ^{13}C chemical shift of the carbene probe in *trans-(dibromo)[1,3-bis(isopropyl)benzimidazole-2-ylidene](L)palladium(II)* complex, where the 1,3-bis(isopropyl)benzimidazole-2-ylidene fragment represents the carbene probe, and L is the ligand under investigation (Figure 3).[16] While other factors may contribute to this scale, a more deshielded carbon atom, evidenced by an upfield shift in the spectrum of the carbene probe signal, signifies a less effective σ-donor NHC. Importantly, this parameter enables the comparison of Werner-type and organometallic ligands on a unified scale.

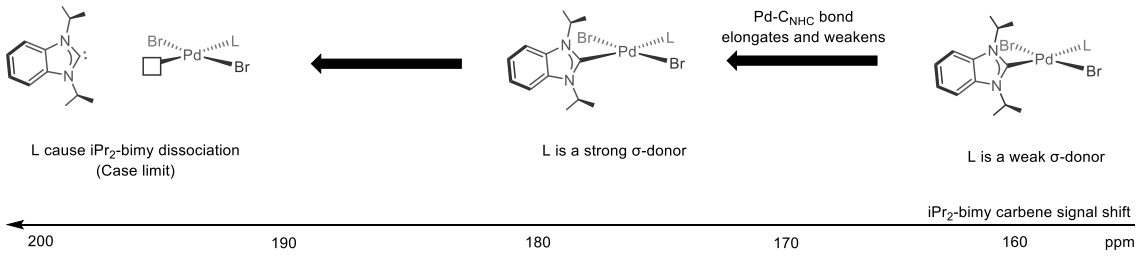

Figure 3 - Relationship of carbene chemical shifts and ligand donor strength in HEP.

Overall, the unique stereoelectronic properties of *1,3-imidazol-2-ylidenes* generate neutral chemical species with a lone pair that can act as a substantial sigma donor in bonding, making these compounds useful as nucleophiles and in coordination chemistry.

1.1.2 Different classes of NHCs

The chemistry of NHC is not limited to *imidazole-2-ylidene* carbenes but is instead characterized by a rich and structurally diversified library of compounds.[1] It is indeed this formidable tunability that makes NHCs such potent tools in coordination chemistry. Regardless of the structural differences between NHCs, they all share a similar base structural motif, and thus their reactivity can be rationalized via the same stereoelectronic parameters discussed above for *imidazole-2-ylidenes*. Nevertheless, given the impressive amount of reported NHCs, a categorization into three main classes has been developed based on the free carbene structure: 1) *normal NHCs* (nNHC), where the free NHC must have a neutral resonance form among the possible structures, 2) *mesoionic or abnormal NHCs* (aNHC), where the free carbene must be mesoionic, and 3) *remote NHCs* (rNHC) where the carbene carbon must not be bound to any heteroatom (Figure 3).[17]

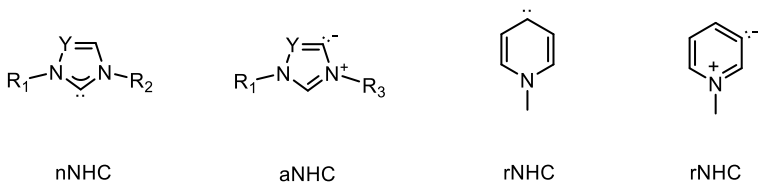

Figure 4 – Four schematic examples depicting possible NHC structural motifs. The generic element Y represents either carbon or nitrogen.

Abnormal NHCs are gaining attention in the literature as they exhibit improved σ-donors capabilities compared to normal NHCs due to the mesoionic nature of these compounds,[18] and of which a quick explanation would be the inclusion of carbanionic species among the possible limit resonance structures. It should be noticed, though, that the carbon atom hosting the free doublet features eight valence electrons, making aNHCs not strictly carbenes by definition.[19] The formation of free aNHCs is challenging compared to free nNHCs, given the increased pKa of the protons involved. For example, when Bertrand et al. isolated the first free aNHC from a triazolium salt, the reaction required the use of *potassium bis(trimethylsilyl)amide* (KHMDS) as even *n-butyl lithium* (BuLi) did not afford the

desired product, but instead resulted in carbon lithiation.[20] Moreover, aNHCs do not dimerize, and processes such as the Wanzlick equilibrium have not been reported,[21] but different decomposition pathways affect these compounds. For instance, 1,2,3-triazolium-related salts decompose via intermolecular nucleophilic attack, leading to the intermediacy of an ion pair before neutral inactive triazoles are produced.[22] The discussion up to this point might misleadingly suggest a clear separation between nNHCs and aNHCs. Instead, whereas the two types of NHCs display different reactivities, they behave similarly in the bound state, making them suitable for the same applications.[17] Overall, aNHCs extend the range of electronic effects in the strong donor direction from phosphines.[23,24]

1.1.3 Coordination chemistry of NHCs

The excellent σ-donor properties make NHCs powerful tools for coordination chemistry, to such an extent that examples exist of NHCs coordinated to every transition metal,[21] with NHCs finding use in different fields as part of metal-organic materials, metallopharmaceuticals, nanomaterials, and homogeneous catalysts.[1] The synthesis of complexes does not generally require the formation of the free carbene, as one may infer from the discussion above, but instead, an in situ deprotonation of an azolium salt is commonly conducted in the presence of a suitable transition metal precursor. However, strategies involving α-elimination or oxidative addition at the carbene carbon, carbene transfer from pre-formed NHC-silver(I) or copper(I) complexes, and metal-templated controlled formation of NHC may also be used.[1] Coordination compounds bearing NHC ligands mediate many catalyzed chemical transformations, and notable examples include iridium and ruthenium-catalyzed hydrogenation and hydrogen auto-transfer reactions,[26] gold-catalyzed activation of unsaturated bonds,[27] and rhodium, and platinum-catalyzed hydrosilylation. However, the most relevant are cross-coupling (catalyzed by palladium,[28–31] nickel,[32] copper,[33] and other metals) and ruthenium-catalyzed olefin metathesis reactions (Figure 5).[34,35]

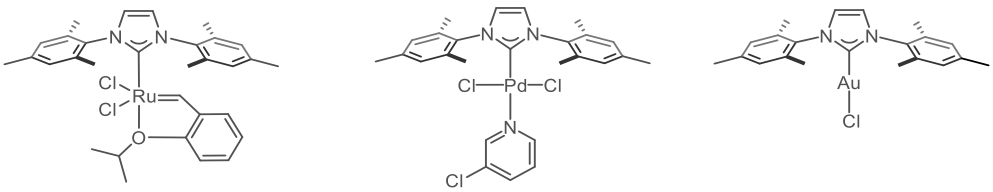

Figure 5 - Three examples of NHC-metal complexes employed in homogeneous catalysis. From left to right: Grubb's 2nd generation catalysts for olefin metathesis, Organ's Pd-PEPPSI-NHC pre-catalyst employed in cross-coupling reactions, and an Au(I)-NHC complex used in catalyzed nucleophilic addition to alkynes.

The interest behind developing NHC complexes in catalysis can be understood upon comparison with the closest class of ligands by stereoelectronic properties: phosphines (Figure 6). NHCs and phosphines are strong σ-donors ligands while also being low-demanding π-acceptors via back donation.[23] The main difference between the two classes of ligands originates from the tunability of

stereoelectronic parameters, as with NHCs these properties can be varied almost independently, whereas this is not possible with phosphines.[1]

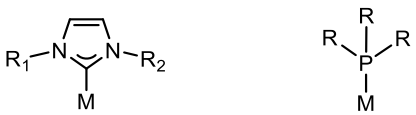

Figure 6 - NHC- and phosphine-metal bonds in coordination compounds, the two ligands possess similar properties, being both strong σ-donors.

Moreover, the increased electron donor properties of NHCs lead to thermodynamically stronger metal-ligand bonds, which are reflected in typically greater bond dissociation energies. The stronger metal-ligands interaction renders NHCs less labile, and the complexes are generally more thermally and oxidatively stable.[25] A drawback in using NHCs ligands comes instead from steric bulkiness and strain, as variations in the wingtips have significant effects on the steric environment at the metal center. As an example, Nolan et al. plotted relative bond dissociation energy values for a range of *imidazol-2-ylidene-ruthenium(II)* against the related buried volumes, showing a marked linear decrease in NHC-Ru bond strength of about 12 kcal as the ligand steric bulkiness increased.[13] Even so, for all carbene ligands except the most sterically demanding, the bond dissociation energies remained greater than that of the phosphine-based analog complexes.

1.2 Coordination chemistry of bidentate NHCs

Polydentate ligands have been critical in synthesizing novel coordination compounds, benefiting from the chelate effect's improvement in entropical stability.[36] While monodentate NHC ligands have received considerable attention in research, the literature also extensively reports the use of multi-dentate ligands, covering bidentate, pincer, scorpionate, and macrocyclic motifs, as well as their respective transition metal complexes. Since bidentate NHC (bis(NHC)) ligands are the main focus of this work, we will not dwell further on other types of polydentate NHC ligands that are already comprehensively discussed in the literature. Similar to monodentate ligands, bis(NHC) ligands predominantly feature the *imidazol-2-ylidene* structural motif. Nevertheless, it is worth noting that alternative forms, including triazole-based heterocycles and abnormal carbenes, are not uncommon. Moreover, bis(NHC) ligands exhibit high moisture, air, and temperature sensitivity in their free form. They are generally less stable than their monodentate counterparts and are typically stored as bis-imidazolium salts.[37] Well-established synthetic routes are available to obtain bis-imidazolium salts, with the simplest compounds being obtained from the direct alkylation of *1,1'-methylenbis(1H-imidazol)*. Furthermore, since numerous procedures are available for synthesizing N-substituted imidazoles through one-pot diimine cyclization,[38] N,N'-symmetrical bis-imidazolium salts can be easily obtained via a two-step process involving the disubstitution of haloalkanes with suitable N-substituted imidazoles (Scheme 1).[39–42]

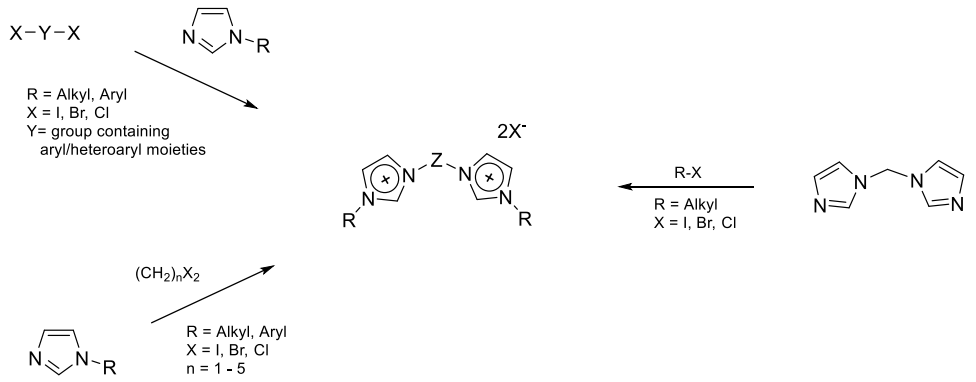

Scheme 1 – Common strategies for the synthesis of N,N'-symmetrical bis(imidazolium) salts.

Despite the structural diversity of bis(NHC) ligands, three synthetic strategies are commonly used to obtain bis(NHC) coordination compounds, all closely related to the approaches employed for synthesizing monodentate NHC metal complexes. These strategies include 1) *in situ* deprotonation and metallation using metal precursors with basic ligands, such as *diacetate palladium(II)*, 2) transmetallation through silver(I) bis(NHC) complexes, and 3) direct metallation of preformed free bis(NHC)s or their *in situ* generation with an external base (Scheme 2).

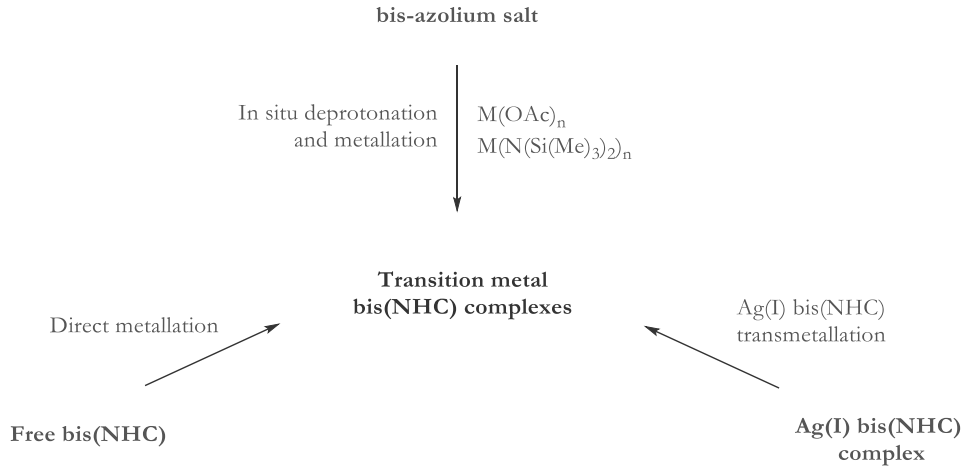

Scheme 2 – Scheme depicting the most common strategies employed in the synthesis of bis(NHC) metal complexes.

Due to milder conditions and efficient atom economy, the in situ deprotonation and metallation route is usually preferred in generating bis(NHC) metal complexes. However, the reaction is commonly required to be conducted under anhydrous conditions. Moreover, while in principle any metal acetate salt could react following this strategy, in reality, few examples exist apart from *palladium(II), nickel(II),* and *manganese (II) diacetate* complexes.[43–45] Therefore, when the metal-acetate approach is not feasible, *bis(trimethylsilylamide) metal* salts can also provide similar reactivity, as demonstrated in the generation of iron(II) bis(NHC) complexes. A versatile alternative to access a broader range of metal complexes, including palladium(II), nickel(II), and cobalt(II), is transmetallation from silver(I) bis(NHC) complexes.[46] This strategy is tolerant to both air and moisture, and the generation of silver(I) bis(NHC) complexes can be achieved through various methods,[47] with the primary approach being the in situ deprotonation and metallation of bis-azolium salts with silver(I) oxide. A final well-documented approach consists of generating the free bis(NHC) with an external base, a step directly followed by metallation to yield the desired complex. A wide range of bases can be utilized for proton abstraction to generate the carbene species, including alkali metal carbonates,[48] acetates, alkoxides,[49] silylamides, tertiary amines[50], and alkyl lithium reagents.[51] This final strategy extends access to bis(NHC) complexes to nearly all transition metals on the periodic table (Figure 7).

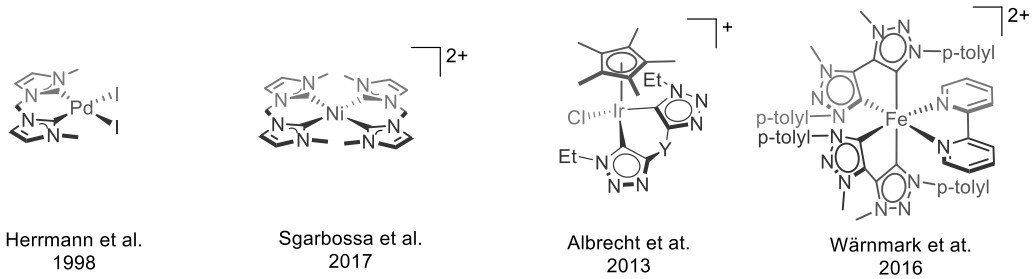

Figure 7 – Examples of relevant transition metal-based coordination compounds, with application as catalysts in coupling reactions,[52,53] transfer-hydrogenation reactions,[54] and photochemistry.[55]

The bidentate nature of bis(NHC) ligands gives rise to various possible coordination modes, even for simple methylene-bridged bidentate ligands (Figure 8).

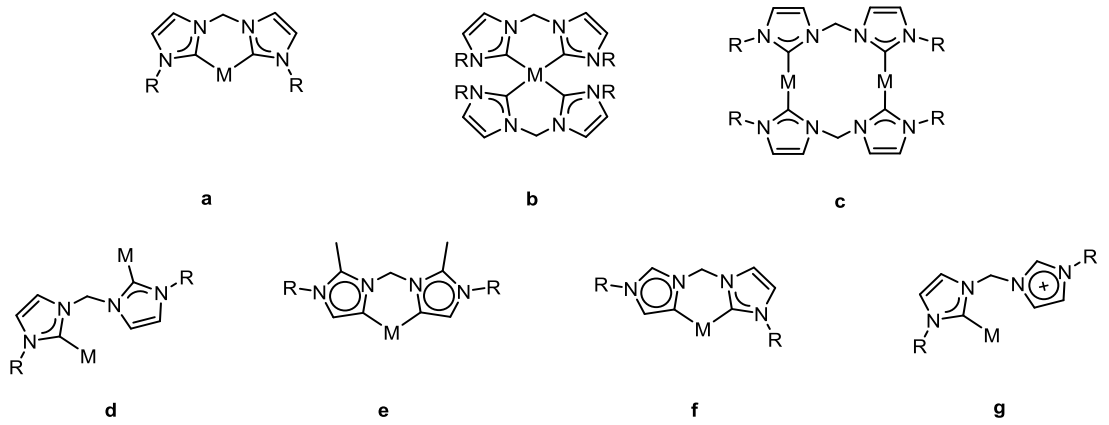

Figure 8 – Various coordination modes of bis(NHC) ligands to generic metals (M): a) 1:1 chelated, b) 2:1 chelated,[56] c) 1:1 bridged,[57–61] d) 1:2 bimetallic,[62] e) 1:1 abnormal chelated, f)1:1 mixed normal/abnormal chelated and g) 1:1 pendant.[63]

The most common motif involves the methylene bridge in a chelated arrangement. However, bridging conformations are frequently reported in the case of late-transition metals like silver and gold.[64,65] Aside from chelation entropic stability, the methylene linker's length is optimal for forming six-membered rings with the least relative steric hindrance when coordinated to a metal center. Moreover, the boat conformation adopted by the six-membered ring also minimizes steric interference between substituents and their interactions with other bound ancillary ligands. As the steric bulk at the wingtips of bis(NHC) ligands increases, the boat conformation of the metal-NHC ring becomes flatter to prevent steric interactions between the N-substituents, effectively spacing them farther apart. Furthermore, as the metal-NHC ring flattens, the methylene-to-metal coordination plane distance decreases, bringing bis(NHC) N-substituents closer to the ancillary ligands in the metal coordination plane.[36,66,67]

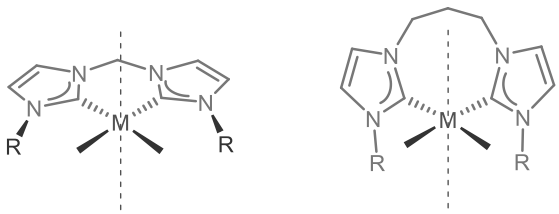

Figure 9 – The bridging alkyl chain length effect on ligand orientation.

As for monodentate NHCs, understanding the electron-donating properties of the ligand is crucial as these affect the metal complex's electronic structure and reactivity. Bidentate ligands are, however, far less studied, and literature examples investigating the electronic properties of bidentate ligand systems are mostly limited to studies involving TEP conversion equations.[68,69] Parameters that cannot always be obtained experimentally due to the synthetic inaccessibility of some nickel carbonyl

complexes. Alternatively, HEP can be used to evaluate bis(NHC) σ-donor strength, as a new scale to account for bidentate ligands has been introduced. Named HEP2, the new scale is based on the same fundamental principles (Section 1.1.1), where a downshift of the carbene probe signal still serves as an indicator of enhanced electron-donating power of the ligand under examination, with typical values on this scale ranging from 177.0 to 180.3 ppm (Figure 10).[70]

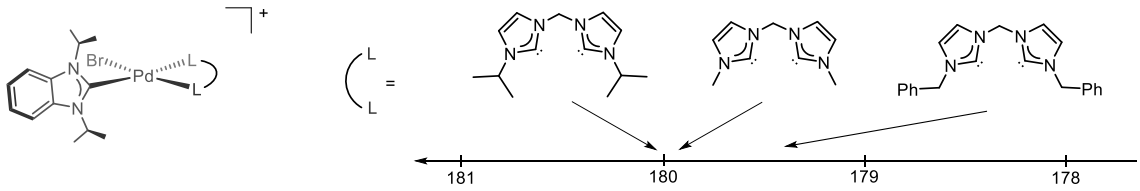

Figure 10 – The effect of N-substituents steric hindrance on the chemical shift of different palladium complexes with the general formula: PdBr(iPr-bimy)(LL). An increase in steric hindrance reduces the σ-donor capabilities of the complex.

Bis(NHC) metal complexes have seen applications in many metal-mediated reactions. The nature of the metal primarily directs the reactivity, though the properties of the bis(NHC) ligand also modulate the complexes' activity. The first examples of bis(NHC) complexes in catalysis originated from the Hermann group and were initially applied in palladium-catalyzed Heck-type coupling reactions.[53] Shortly after, other palladium complexes were examined in Suzuki coupling reactions using iodobenzene and 4-bromotoluene as substrates.[71] These reactions featured low catalyst loadings (0.002–0.0002 mol%), high temperatures (140 °C) for extended times, high turnover numbers (TONs), and reasonable conversions. These results highlight the robust stability of bis(NHC) complexes even under the harsh reaction conditions required for unactivated substrates. Numerous other research groups have employed chelated palladium, nickel, and platinum bis(NHC) complexes in various cross-coupling processes, including Kumada–Corriu,[72] Fujiwara alkyne hydroarylation,[73–75] and Buchwald–Hartwig amination reactions (Figure 11).[52]

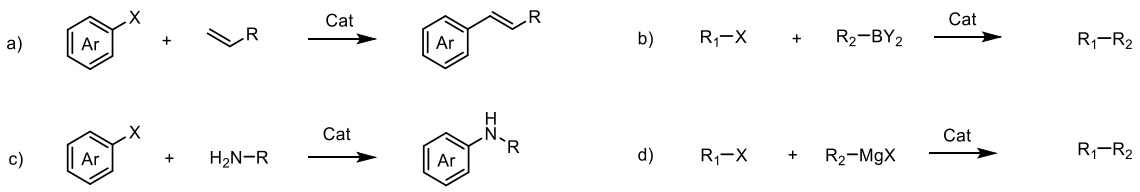

Figure 11 – Examples of coupling reactions catalyzed by metal-bisNHC complexes: a) Heck, b) Suzuki- Miyaura, c) Buchwald-Hartwig, and d) Kumada-Corriu reactions.

Examples of bis(NHC) complexes as catalysts in polymerization reactions also exist, with chromium(III) bis(NHC) complexes exhibiting limited activity and resulting in broad polymer molecular weight distributions in ethylene oligomerization when exposed to methylaluminoxane.[76] The authors suggest that the catalytic activity may be influenced by the ease with which chromium(III) complexes are reduced to chromium(II), which is known not to polymerize ethylene.

In addition, ruthenium, rhodium, and iridium bis(NHC) complexes have found numerous applications in transfer hydrogenation chemistry (Scheme 3).[77–80]

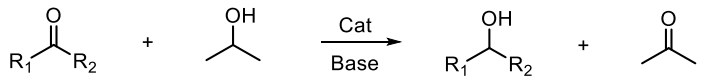

Scheme 3 – General reaction scheme of the catalyzed transfer hydrogenation reaction.

Furthermore, a report by Albrecht and colleagues demonstrated the utility of chelated bis(NHC) palladium(II) complexes in the catalytic hydrogenation of cyclooctene at room temperature with 1.0 atm of hydrogen.[81,82] Moreover, bis(NHC) ligands have emerged as promising ligands for generating photosensitive organometallic complexes,[55,83] due to their exceptional σ-donating capabilities, which are hypothesized to extend the excited state lifetime of photoactive metal complexes.

1.3 Coordination chemistry of ruthenium

Ruthenium is an essential metal with many applications in different industrial fields, including alloy metals, material science, medicinal chemistry, and catalysis. In the interest of time, we will not linger on the rich history or the general inorganic chemistry concerning the metal. Instead, in this brief section, we will cite a few general applications in coordination chemistry and catalysis. The main fields of application of ruthenium(II) coordination compounds are 1) the olefin metathesis reaction, 2) the hydrogenation and transfer-hydrogenation reactions, 3) the sensitizers contained in solar cells, and 4) the water oxidation reaction.

1.3.1 The olefin metathesis reaction

The olefin metathesis reaction is a critical set of chemical transformations involving the distribution of alkene fragments by scission and regeneration of C-C double bonds. Among these useful synthetic transformations are 1) ring-closure metathesis involving terminal vinyl groups, 2) intermolecular cross-metathesis, and 3) ring-opening metathesis of strained alkenes (Figure 12).[84] In the homogeneous phase, the olefine metathesis reaction is catalyzed by ruthenium(II) catalysts, which have demonstrated astonishing reactivity since their discovery in the early 2000s. In particular, ruthenium(II) NHC reported by Herrmann,[85] Nolan,[86] and Grubbs[87] displayed significantly improved metathesis activity and enhanced thermal stability.

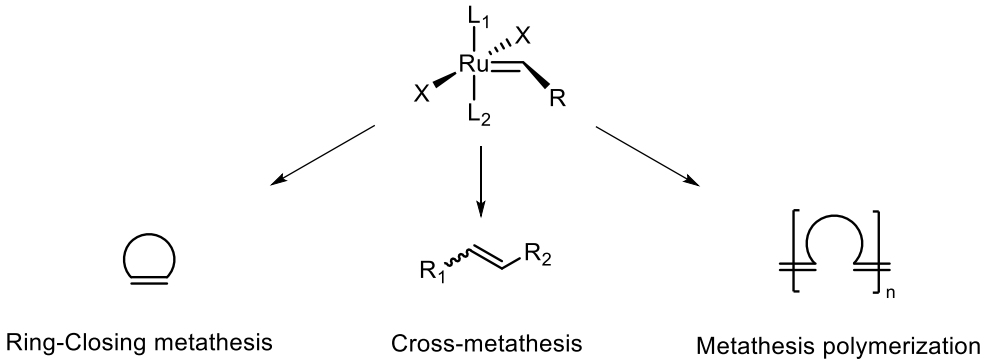

Figure 12 – General ruthenium(II) catalyst structure and metathesis applications.

1.3.2 Hydrogenation and hydrogen auto-transfer reactions

Hydrogenation is an essential chemical transformation with countless applications, from synthesizing fine chemicals to producing margarine.[88] More than a hundred ruthenium homogeneous hydrogenation catalysts have been developed in the last decades, which proved to be some of the most effective catalysts for these reactions since they displayed high reactivity and selectivity, especially in the catalytic reduction of polar bonds, often surpassing rhodium and iridium complexes.[82,89–93] Noticeably, ruthenium(II) complexes with amine ligands are incredibly reactive in the hydrogenation of ketones. In all these reactions, ruthenium hydride and dihydrogen complexes have been recognized as the active species in the catalytic cycle.[94–96] A critical subset of hydrogenation reactions is transfer hydrogenations, where hydrogen is transferred from one sacrificial molecule to

another rather than utilizing hydrogen gas.[97] Furthermore, when a pair of transfer hydrogenations is coupled with an intermediate reaction on the in situ-generated reactive intermediate, a hydrogen borrowing reaction (also known as hydrogen auto-transfer reaction) occurs (Scheme 4).[98–101]

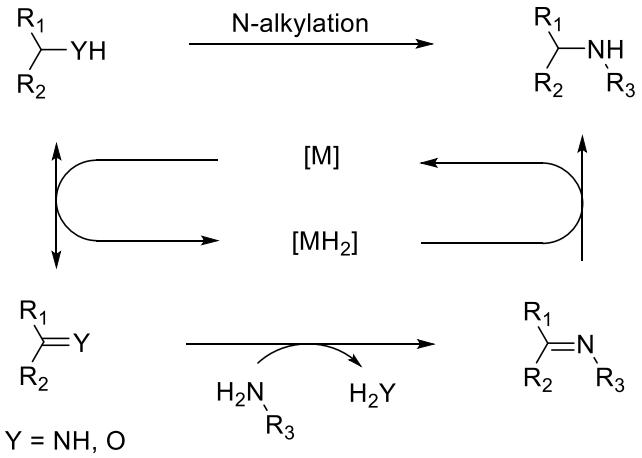

Scheme 4 – Schematic generalization of transition metal-catalyzed hydrogen-borrowing reactions.

The borrowing hydrogen approach is widely employed to facilitate the functionalization of alcohols. Most of these transformations involve the direct use of commodity alcohols as alkylating agents in a wide range of C−N and C−C bond-forming processes. An essential application of ruthenium(II) catalyzed hydrogen auto-transfer reactions involves improving biomass-derived compounds' synthetic utility. In particular, the levulinic acid produced from lignocellulosic biomass is gaining attention as a critical platform chemical in future biorefineries, given the now available high-yield production processes and the inexpensive nature .[102] From the catalytic hydrogenation of levulinic acid, key intermediate compounds such as γ-valerolactone, and valeric acid, 1,4-pentanediol, and 2-methyltetrahydrofuran can be obtained.

1.3.3 Ruthenium(II) coordination compounds as sensitizers

The increasing demand for new, sustainable energy sources to replace fossil fuels has reached a critical point due to the urgent need to reduce the impact of climate change. In this context, photovoltaic technology is one of the most promising solutions.[103,104] By taking advantage of sunlight as a clean, affordable, and consistent energy source, photovoltaic systems are growing as a convenient choice in pursuing sustainable energy.[105,106] Typical solid-state photovoltaic cells are based on inorganic semiconductors and are very efficient. However, they display some drawbacks, such as high production costs and limits in their mass utilization.[107,108] Dye-sensitized cells (DSSCs) are growing as an appealing alternative to conventional solid-state cells, given their relatively low cost, operating temperatures, transparency, and flexibility.[109–111] DSSCs are based on nanocrystalline metal oxide semiconductors sensitized by molecular dyes.[112] In these cells, the dye absorbs visible light, generating photoelectrons, which are injected into the semiconductor.

Recently developed state-of-the-art DSSCs are based on heteroleptic ruthenium(II) sensitizers and achieve remarkable power conversion efficiencies of up to 15% (Figure 13).[113–116]

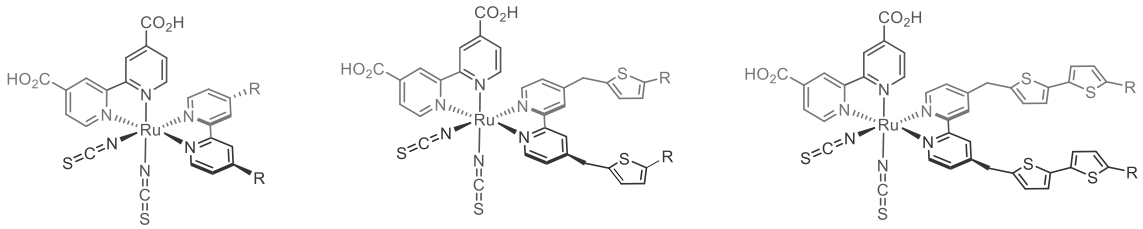

Figure 13 - Molecular structures of common heteroleptic ruthenium(II) dyes.

The reason behind these sensitizers' success is found in the ligand's extended conjugated system and the long alkylic chains. In fact, the extended conjugation enhances the optical absorptivity of titanium dioxide, while the hydrophobic chains increase tolerance to water.[117]

1.3.4 The water oxidation reaction

The molecular water oxidation reaction is a critical transformation that has experienced impressive development over the last decade, given the promise of generating a more sustainable and carbon-neutral society. The water oxidation reaction is based on water-splitting, and most recent advances have been possible thanks to a detailed understanding of reactions and intermediates involved in the catalytic cycles. Still, the primary challenge in this field remains the development of more robust and faster catalysts to employ in the light-driven water-splitting reaction under neutral to acidic conditions. Water oxidation catalysts based on ruthenium(II) coordination compounds are among the most efficient and reach turnover frequencies that are orders of magnitude higher than that of the natural oxygen-evolving center in photosystem II (Figure 14).[118]

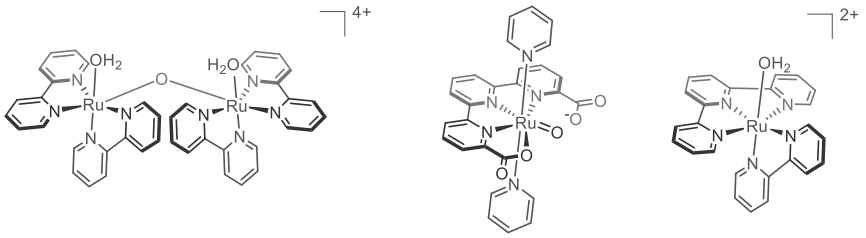

Figure 14 – Examples of current state-of-the-art ruthenium catalysts used in the water oxidation reaction.

1.4 Scope of the project

Ruthenium(II) homogeneous catalysis is a well-developed and constantly growing field in organometallic chemistry. Interestingly, few examples of ruthenium(II) complexes bearing bis(NHC) ligands exist to our knowledge, despite the widely recognized properties of this class of ligands (Figure 15).[119]

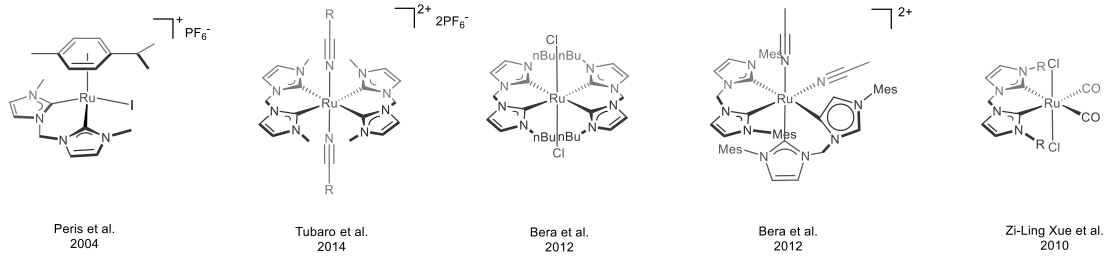

Figure 15 – Literature examples of ruthenium(II) coordination compounds bearing bis(NHC) ligands.[69,81,120–122]

The lack of development in this field is particularly surprising, given the widespread use of strong σ-donating bis(phosphine) ligands in the hydrogenation and transfer-hydrogenation reactions. Moreover, NHC-based complexes' acknowledged improved tolerance toward oxidative and harsher reaction conditions could prove essential in developing ruthenium(II) catalyzed oxidative processes. Accordingly, the aim of the present work concerns the design of new ruthenium(II) complexes bearing bis(NHC) ligands, to be developed as ductile and robust catalysts for different organic transformations, and which should answer the following criteria: 1) ease of synthesis, aligning with the principles of green chemistry, 2) use of commercially available reactants, to enhance cost-effectiveness and practicality, 3) tunability and functionalization, enabling optimization for various catalytic requirements, and 4) stability, ensuring long-term storage. A strategy to achieve these goals would be the introduction of the bis(NHC) ligands at an early stage of synthesis to enable further downstream reactivity by not saturating the complex coordination sphere. On top of this, introducing a second bidentate ancillary ligand still leaves two potential coordination sites for catalysis, in contrast to ancillary pincer ligands. In summary, we seek to produce ruthenium(II) complexes bearing a bis(NHC) ligand, a second ancillary ligand, and two displaceable monodentate ligands (Figure 16).

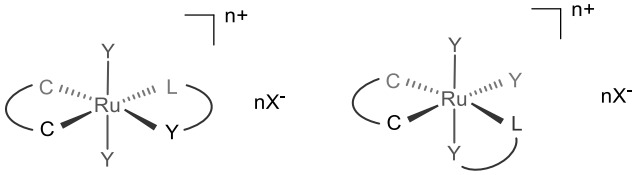

Figure 16 – General structure of our target *trans* and *cis*-compounds, which should feature a bis(NHC) ancillary ligand (C-C), a general bidentate ligand (L-Y), and two monodentate ligands (Y). The Y symbol represents either an L or X ligand.

2 RESULTS AND DISCUSSION

2.1 Screening of suitable ruthenium precursors

The synthesis of novel ruthenium(II) bis(NHC) complexes poses a challenge given the few available examples. With little data available, identifying the general conditions under which reactivity can be directed toward the desired compounds is critical. Therefore, a set of screening reactions was conducted to determine the best conditions to activate the ligand in the presence of a receptive ruthenium(II) precursor. The metal complex was chosen following the rationale that it should either feature an internal base as a ligand, an available coordination site, or an emilable leaving group, and, for these reasons, 1) *bis(triphenylphosphine)(diacetate)ruthenium(II)*, 2) *tris(carbonyl)(dichloride)ruthenium(II) dimer* and 3) *tris(triphenylphosphine)(dichloro)ruthenium(II)* were selected (Figure 17).

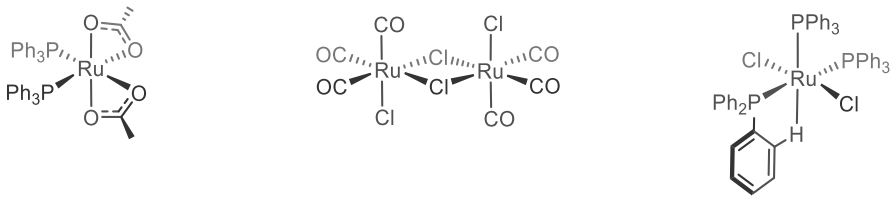

Figure 17 – The chemical structure of the three precursors employed in the initial screening (from left to right*): bis(triphenylphosphine)(diacetate)ruthenium(II)*, *tris(carbonyl)(dichloride)ruthenium(II) dimer* and *tris(triphenylphosphine)(dichloro)ruthenium(II)*.

Once a suitable metal complex candidate is chosen, different strategies for the coordination of NHC exist, all of which rely on different approaches to activate the ligand and produce the complex, such as 1) generating the reactive free carbene, 2) generating the free carbene in situ using a weak base, and 3) via ligand-exchange with a silver-NHC cluster complex. For this initial screening, both the strong and weak base approaches were tested following the general reaction scheme reported in Scheme 5.

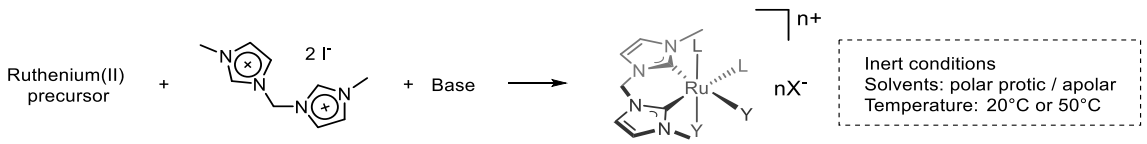

Scheme 5 – Concept reaction scheme showing the rationale behind the screening experiments.

As for the ligand, *1,1-bis(3'-methylimidazolium)methylene diiodide* was considered ideal for two reasons. First, the methyl groups at the NHCs moieties wingtips are not sterically demanding, compared to, for example, isopropyl or aromatic groups. Second, the short methylene bridge forms a six-membered ring once coordination with the metal occurs, which is usually more stable than other cyclic structures due to steric strain.

Table 1 – Screening experiments, conducted at 25 and 60°C, sampled at 24 and 48 h. *1,1-bis(3'-methylimidazolium)methylene diiodide* was used as bis-imidazolium salt in the reaction, if not otherwise stated, and was always added stoichiometrically with respect to the ruthenium(II) precursor. All reactions were conducted under Schlenk conditions. The reactions in THF were also conducted at 0°C.

Ruthenium(II) precursor	n	Solvent	V	Base	n
[formula]	[mmol]	[formula]	[mL]	[formula]	[mmol]
$Ru(OAc)_2(PPh_3)_2$	0.05	MeOH	5	K_2CO_3	0.25
	0.05	MeOH	5	NaOAc	0.25
	0.05	EtOH	5	NaOAc	0.25
	0.05	tBuOH	5	tBuOK	0.10
	0.05	THF	5	tBuOK	0.10
$Ru(CO)_3Cl_2$	0.05	MeOH	5	K_2CO_3	0.25
	0.05	MeOH	5	NaOAc	0.25
	0.05	EtOH	5	NaOAc	0.25
	0.05	tBuOH	5	tBuOK	0.10
	0.05	THF	5	tBuOK	0.10
$Ru(PPh_3)_3Cl_2$	0.05	MeOH	5	K_2CO_3	0.25
	0.05	MeOH	5	NaOAc	0.25
	0.05	EtOH	5	NaOAc	0.25
	0.05	tBuOH	5	tBuOK	0.10
	0.05	THF	5	tBuOK	0.10

The initial screening results have been reported in Table 1, and the reactions did not produce the desired target compounds. Even after analyzing the samples via NMR spectroscopy, no traces of ruthenium(II)-NHC complexes were found. When weak bases were used in the reactions, the original ruthenium complex remained the primary component in the mixture, indicating that the desired transformation did not occur. On the other hand, when strong bases were used, the reaction mixture showed signs of overreaction, resulting in a mixture of products. We also conducted another screening test using two different approaches: 1) preactivated imidazole salt, in the form of a cluster complex with silver(I), and 2) a bis-imidazolium salt with an internal base in the form of hydrogen carbonate. These tests were conducted at both 25°C and 60°C, using methanol and THF as solvents. However, in both cases, the reactions did not proceed as expected, which required us to reconsider our approach.

2.2 Assessing the synthetic accessibility of the target ruthenium(II) bis(NHC) complexes

The screening reactions did not yield the desired ruthenium(II) bis(NHC) complexes despite testing different ruthenium(II) precursors and employing the most typical synthetic strategies to produce metal-NHC complexes. These results suggested that two problems subsided: 1) the activation of the ruthenium(II) precursor toward nucleophilic attacks from active carbene species and 2) stabilizing the intermediates that would lead to a stable ruthenium(II) bis(NHC) complex. Since few examples of ruthenium(II) bis(NHC) complexes exist, the accessibility of the desired species was to be probed using one of these complexes as the precursor. Crabtree et al. described a synthetic pathway from *(p-cymene)(dichloro)ruthenium(II) dimer* (**1**), a piano-stool complex, leading to the formation of *[bis-1,1'-(3-methylimidazol-2-ylidene)methylene](p-cymene)(iodide)ruthenium(II) hexafluorophosphate* (**2**) (Scheme 1, Section 4.4).[123]

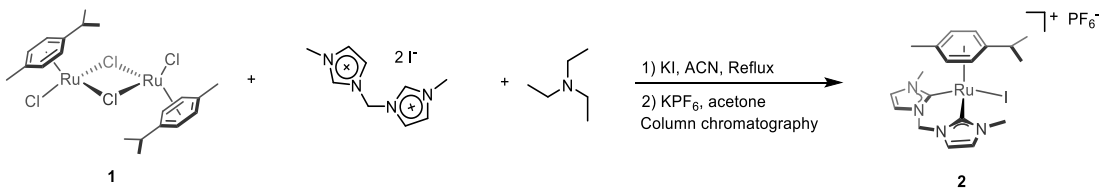

Scheme 6 - The general reaction scheme to produce *[bis-1,1'-(3-methylimidazol-2-ylidene)methylene](p-cymene)(iodide)ruthenium(II) hexafluorophosphate* (**2**) from *(p-cymene)(dichloro)ruthenium(II) dimer* (**1**) as reported by Crabtree et al.

This complex holds particular interest because the displacement of the arene ligand is a well-documented reaction for other ruthenium(II) systems, which involves the complex activation with a silver salt in *acetonitrile* (*ACN)* at mild temperatures, forming an organonitrile complex.[124] As expected, refluxing *[bis-1,1'-(3-methylimidazol-2-ylidene)methylene](p-cymene)(iodide)ruthenium(II) hexafluorophosphate* (**2**) in *ACN* did not result in the formation of an organonitrile complex. Hence, a metathesis reaction with silver salts was performed in ACN at 25 °C over 24 h to abstract the halide; *[bis-1,1'-(3-methylimidazol-2-ylidene)methylene](p-cymene)(iodide)ruthenium(II) hexafluorophosphate* (**2**) (150 mg, 0.20 mmol) reacted with *silver tetrafluoroborate* (220 mg, 1.20 mmol) under inert conditions in *ACN*, resulting in iodide abstraction, and precipitating *silver iodide* along unreacted *silver tetrafluoroborate.*[125,126] The residue silver salts were then removed via filtration over Celite, a necessary step to avoid undesired side reactions in downstream transformations. After removing the solvent *(acetonitrile)[bis-1,1'-(3-methylimidazol-2-ylidene)methylene](p-cymene)ruthenium(II) ditetrafluoroborate* (**3**) was isolated (85% yield), the brown solid proved to be highly hygroscopic, and the solvating *ACN* could not be removed entirely applying vacuum (Scheme 7).

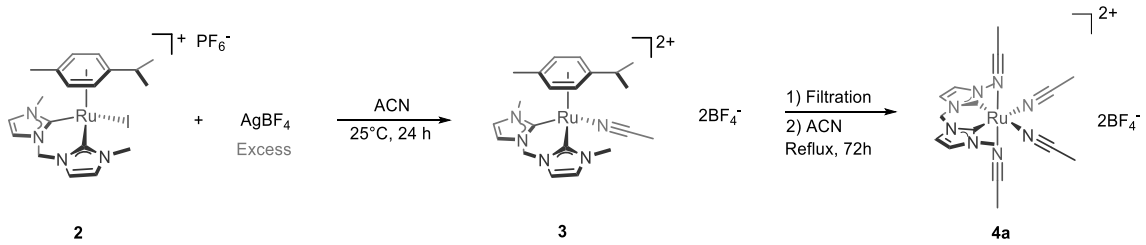

Scheme 7 - Reaction scheme depicting the chemical transformations required to obtain *tetrakis(acetonitrile)[bis-1,1'-(3-methylimidazol-2-ylidene)methylene]ruthenium(II) ditetrafluoroborate* (**4a**) from *[bis-1,1'-(3-methylimidazol-2-ylidene)methylene](p-cymene)(iodide)ruthenium(II) hexafluorophosphate* (**2**), going through the intermediate *(acetonitrile)[bis-1,1'-(3-methylimidazol-2-ylidene)methylene](p-cymene)ruthenium(II) ditetrafluoroborate* (**3**).

The identity of the newly synthesized complex was verified by conducting a comprehensive analysis via NMR spectroscopy (Section 4.5). The successful abstraction of the anionic iodide, followed by the coordination of an *ACN* molecule, was assessed at the ^{1}H NMR spectrum as a new sharp singlet peak rose at 2.30 ppm. Furthermore, when comparing the spectra of the product with those of the reagent, a notable upfield shift in the NHC and cymene moieties' signals was detected. This observation aligned with the dicationic nature of the newly formed complex (Figure 18).

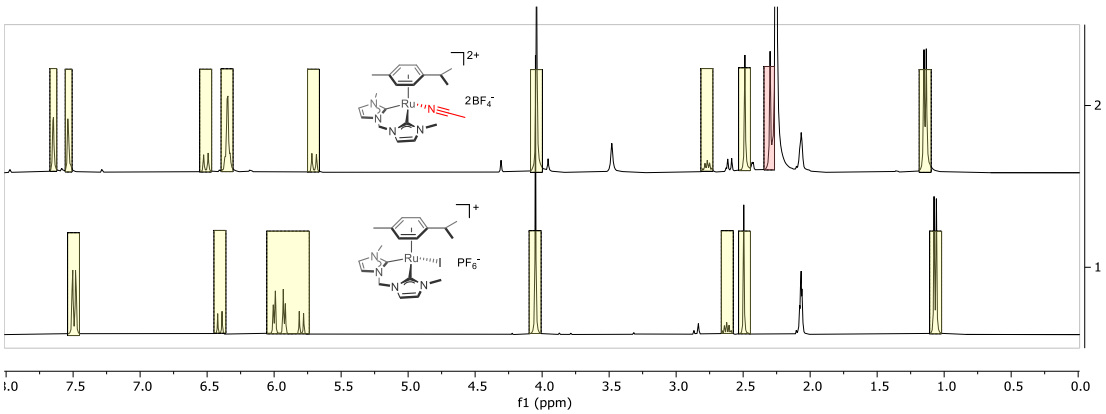

Figure 18 - The ^{1}H NMR spectra of *[bis-1,1'-(3-methylimidazol-2-ylidene)methylene](p-cymene)(iodide) ruthenium(II) hexafluorophosphate* (**2**) (below) and of *(acetonitrile)[bis-1,1'-(3-methylimidazol-2-ylidene)methylene](p-cymene)ruthenium(II) ditetrafluoroborate* (**3**) (above). The yellow highlight marks the signals originating from the ligands in common between the two complexes, while the red mark highlights the newly introduced *ACN*.

From the ^{1}H NMR spectra, it was not possible to unequivocally ascertain the exact nature of the singlet. Therefore, the assignment was confirmed as coordinated acetonitrile through ^{13}C and ^{1}H-^{13}C correlation spectroscopies. These spectroscopic techniques revealed the presence of two distinct acetonitrile species: 1) coordinated ACN, characterized by two ^{13}C signals at 128 ppm and 2.92 ppm, which correlated with the signal at 2.30 ppm in the proton spectrum, and 2) free ACN, with carbon signals at 118.30 and 0.30 ppm, correlating at 2.07 ppm in the proton spectrum.

At this point, the *(acetonitrile)bis-1,1'-(3-methylimidazol-2-ylidene)methyleneruthenium(II) ditetrafluoroborate* (**3**) complex underwent a further reaction aimed at displacing the arene ligand. To achieve this, the complex (100 mg, 0.18 mmol) was refluxed in *ACN* (10 mL) for 72 hours under inert conditions. Leveraging on the solvent mass effect and coordination properties, the reaction yielded a reactive and air-sensitive intermediate. After drying the solution, *tetrakis(acetonitrile) [bis-1,1'-(3-methylimidazol-2-ylidene)methylene] ruthenium(II) ditetrafluoroborate* (**4a**) was successfully isolated. The air-sensitive nature did not allow for a comprehensive characterization at the time, with the powder turning slowly from bright orange to green in the presence of air, indicating an incipient decomposition process. The complete characterization was later achieved from a sample obtained following an improved synthetic route (Section 4.6). A characterization attempt via ^{1}H NMR spectroscopy has been reported in Figure 19; from the NMR spectra, it is clear that arene cleavage occurred as no *p-cymene* signals are observed in the characteristic regions. Moreover, two distinct *ACN* signals are present in addition to the bis(NHC) framework, consistent with the apical and equatorial positions assumed in the octahedral geometry. Interestingly, the -CH_2- bridging the NHCs moieties appears as a broad rather than sharp singlet, suggesting that *ACN* ligands are involved in exchange processes with the deuterated *acetone* or *water* traces (Figure 19). Consistent with the complex reactivity.

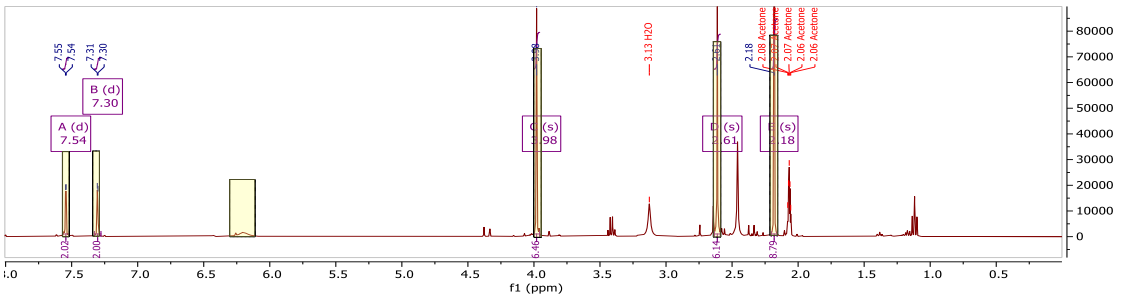

Figure 19 - The ^{1}H NMR spectra of *tetrakis(acetonitrile)[bis-1,1'-(3-methylimidazol-2-ylidene)methylene] ruthenium(II) ditetrafluoroborate* (**4a**). The compound's significant signals have been highlighted in yellow. The other peaks have been assigned to trace *diethyl ether* and *water* impurities (spectrum acquired in deuterated *acetone*).

The *tetrakis(acetonitrile)[bis-1,1'-(3-methylimidazol-2-ylidene)methylene] ruthenium(II) ditetrafluoroborate* (**4a**) complex holds four *ACN* ligands, which offer up to four different coordination sites for further functionalization given the solvent-complexes' inherent reactivity. In order to verify this thesis and the accessibility of our target compounds, the complex reactivity toward LL-type ligands was probed by adding a stoichiometric amount of *2,2'-bipyridine* (28 mg, 0.18 mmol) in *acetone* (4 mL) at RT (Scheme 8).

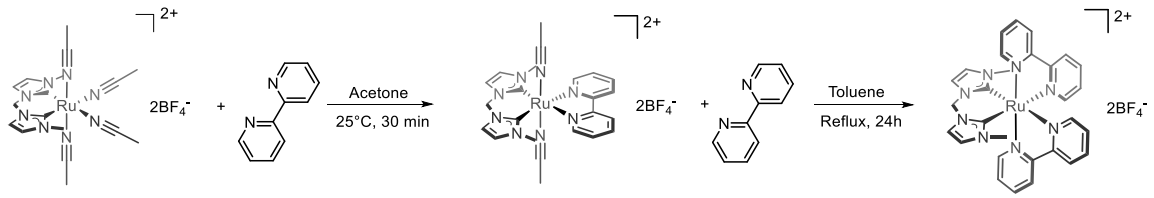

Scheme 8 - General scheme depicting the reactions required for the subsequent addition of two *2,2'-bipyridine* ligands to *tetrakis(acetonitrile)[bis-1,1'-(3-methylimidazol-2-ylidene)methylene] ruthenium(II) ditetrafluoroborate* (**4a**).

The first reaction, involving coordination of the first *2,2'-bipyridine,* reached completion at room temperature within 30 minutes, as confirmed by ^{1}H NMR spectroscopy (Figure 20). The ligand coordination was assessed by the high-field shift of *2,2'-bipyridine* signals, with the most distinctive peak shifting from 8.60 ppm for the free ligand to 9.20 ppm. No residual signals ascribed to the ruthenium(II) precursor were detected, but by integration, unreacted *2,2'-bipyridine* accounted for an unisolated yield of 50% considering *(acetonitrile)[bis-1,1'-(3-methylimidazol-2-ylidene)methylene](p-cymene)ruthenium(II) ditetrafluoroborate* (**3**) as starting material. The lack of 2D experiments did not allow us to determine unequivocally the structure of the isolated compounds, which was later identified as *trans-(diacetonitrile)(2,2'-bipyridine)[1,1-Bis(3'-methyl-imidazol-1'-ylidene)methylene]ruthenium(II) ditetrafluoroborate* (**5**) (Section 4.7).

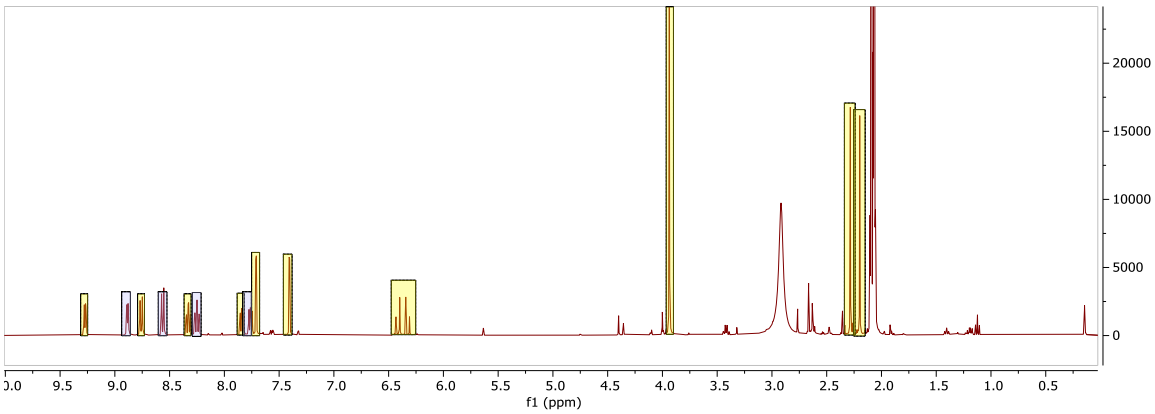

Figure 20 - The ^{1}H NMR spectra of the reacting mixture sample with the relevant species highlighted by color: *trans-(diacetonitrile)(2,2'-bipyridine)[1,1-Bis(3'-methyl-imidazol-1'-ylidene)methylene]ruthenium(II) ditetrafluoroborate* (**5**) (yellow), and free *2,2'-bipyridine* (light blue). The spectrum was acquired in deuterated *acetone*.

To further assess the reactivity of the newly synthesized complex, an attempt was carried out to replace the remaining coordinated *ACN* by adding an excess of *2,2'-bipyridine*. However, no observable reaction occurred after the addition of 2,2'-bipyridine (28 mg, 0.18 mmol), even after placing the solution at reflux. The absence of the desired bis-bipyridine complex was attributed to the *trans*-geometry of the complex, as the *trans*-to-*cis* isomerization reaction may be associated with a high activation energy or a slow kinetic, which might have prevented the coordination of the chelating

ligand. This hypothesis was confirmed when the reaction finally reached completion after drying the solution, adding toluene (5 mL), and refluxing the mixture for 24 hours. The solvent was then removed, and the product was isolated by precipitating it from *acetone* (1 mL) using *diethyl ether* (6 mL), resulting in the formation of *bis(2,2'-bipyridine)[1,1-Bis(3'-methyl-imidazol-1'-ylidene)methylene]ruthenium(II) ditetrafluoroborate* (**6**) with a yield of 70 %. Given the scarce synthetic utility, the compound was not wholly purified nor characterized via NMR spectroscopy. Nonetheless, the coordination of the second *2,2'-bipyridine* was confirmed by analyzing the corresponding signals in the aromatic region (Figure 21). Furthermore, two distinct spectral features strongly suggest the occurrence of coordination. First, the bis(NHC) moiety -CH_2- bridge manifests as a sharp singlet, indicating the absence of exchange phenomena similar to those observed in the presence of coordinated *ACN*. Second, the signal multiplicity of both bis(NHC) and bipyridine fragments aligns with a symmetry plane bisecting the complex.

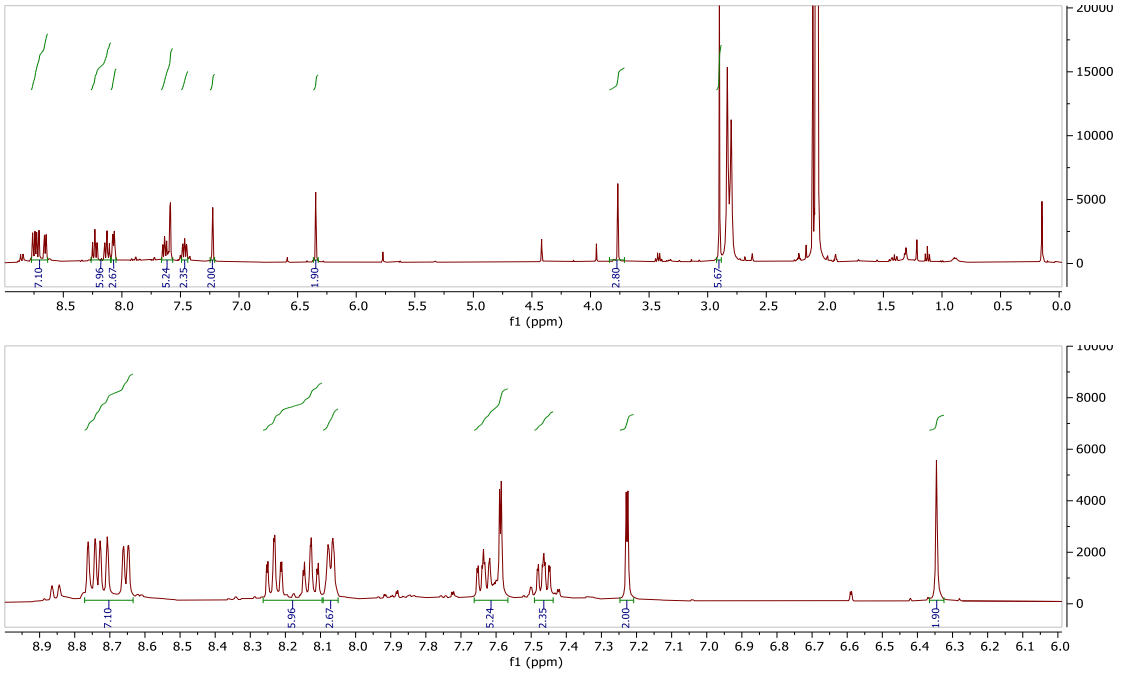

Figure 21 - The ^{1}H NMR spectra of the isolated *bis(2,2'-bipyridine)[1,1-Bis(3'-methyl-imidazol-1'-ylidene)methylene]ruthenium(II) ditetrafluoroborate* (**6**) complex (above), and a spectrum fragment highlighting the high-field region where the 2,2'-bipyridine signals lie (below).

The synthetic route proved that the target compounds are both thermodynamically and kinetically accessible. However, with a cumulative yield of approximately 9%, many synthetic steps, and purifications, the process must be redesigned and optimized to meet improved sustainability standards.

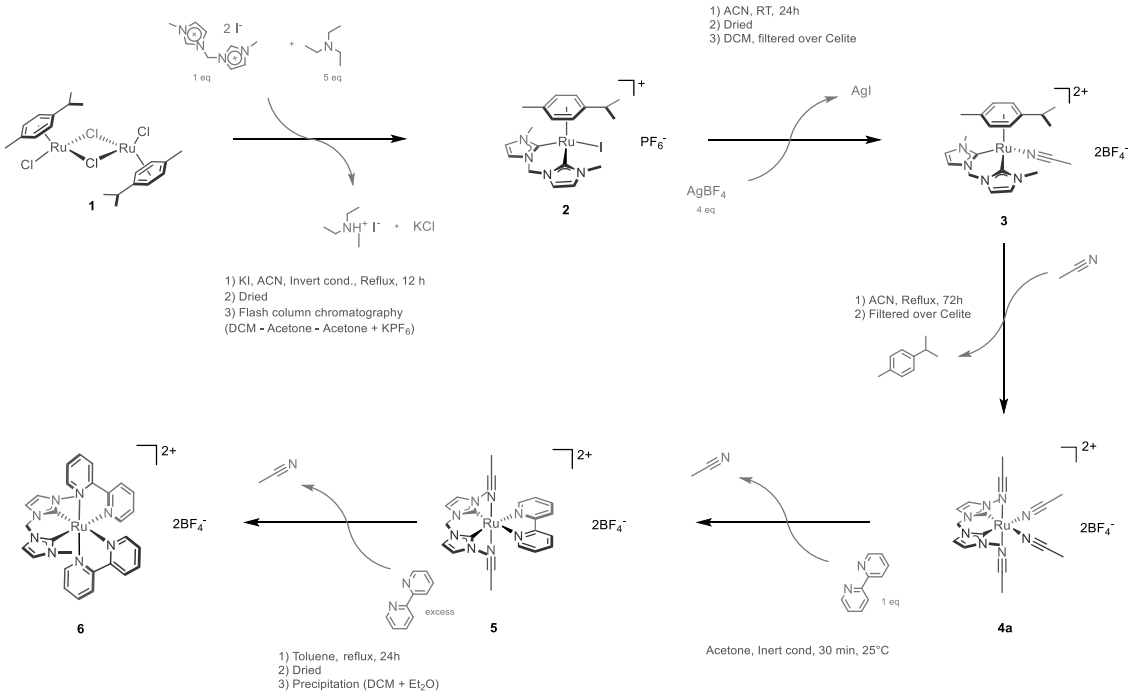

Scheme 9 - The reaction scheme summarizing the synthetic route developed to access ruthenium(II) complexes bearing bis(NHC) ligands, an LL ligand, and two available coordination sites.

2.3 Synthesis of $Ru(ACN)_4(b(MI)M)(PF_6)_2$

The *(p-cymene)(dichloro) ruthenium(II) dimer* (**1**) is a reactive compound belonging to the class of ruthenium(II) arene/polyene complexes, which are prone to arene/polyene substitution owing to the free ligand stability, in contrast to polyenyl complexes where the ligand must dissociate as a radical or an anion. Correspondingly, arenes/polyenes react as active ligands, whereas polyenyls act as spectator ligands, a ductile property granting ruthenium(II) arene/polyene complexes wide application as precursors in coordination chemistry. Among them, *(1,5-cyclooctadiene)(dichloro) ruthenium(II) polymer* (**7**) is another common precursor with a liable alicyclic ligand instead of an arene ligand.[127] Nevertheless, the polymeric nature of *(1,5-cyclooctadiene)(dichloro) ruthenium(II)* (**7**) requires the monomer release to take advantage of the increased reactivity. The depolymerization of *(1,5-cyclooctadiene)(dichloro)ruthenium(II) polymer* (**7**) is known to occur in acetonitrile at reflux, producing *(1,5-cyclooctadiene)(diacetonitrile)(dichloro)ruthenium(II)* (**8**) (Figure 22), but the reaction is not quantitative.[128] Moreover, the addition of *potassium hexafluorophosphate* promotes the first chloride ionization yielding the cationic *(1,5-cyclooctadiene)(triacetonitrile)(chloro)ruthenium(II) hexafluorophosphate,* which can react further with silver salts to afford the dicationic *tetrakis(acetonitrile)*(1,5-*cyclooctadiene)ruthenium(II) dihexafluorophosphate.*[123,129,130]

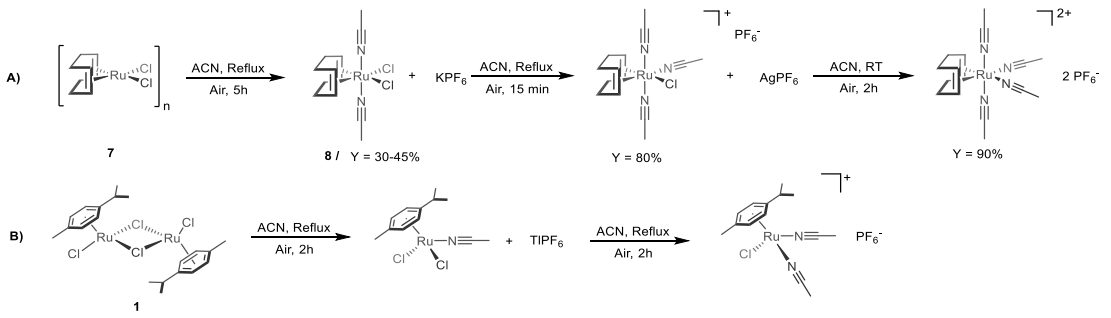

Figure 22 - A flow diagram describing the reactions involving *(1,5-cyclooctadiene) ruthenium(II) dichloride polymer* (**7**) to afford the organonitrile complexes (A). The analog diagram depicts the same process but involving *(p-cymene)(dichloro) ruthenium(II) dimer* (**1**) (B).

The depolymerization of *(1,5-cyclooctadiene)(dichloro)ruthenium(II) polymer* (**7**) in *ACN* generates organonitrile complexes, part of a more comprehensive class of transition metal organosolvent complexes that incorporate easily dissociable solvent ligands.[131] While *(arene)(dichloro) ruthenium(II) dimers* also generate organonitrile complexes, these complexes are less reactive due to steric hindrance and denticity of the arene ligand, making the *in situ* generated *(1,5-cyclooctadiene)(diacetonitrile)(dichloro)ruthenium(II)* (**8**) an attractive intermediate for the synthesis of ruthenium(II) bis(NHC) complexes. Consequently, *(1,5-cyclooctadiene)(dichloro)ruthenium(II) polymer* (**7**) (84 mg, 0.3 mmol) was refluxed in acetonitrile under Schlenk conditions for 2 h prior to the addition of *1,1-bis(3'-methylimidazolium)methylene diiodide* (130 mg, 0.3 mmol) and *triethylamine* (200 uL, 1.5 mmol).

The mixture reacted for 24 h producing the *tetrakis(acetonitrile)[1,1-bis(3'-methylimidazol-2'-ylidene)methylene]ruthenium(II) dihalide* (**4x**)(Scheme 10).

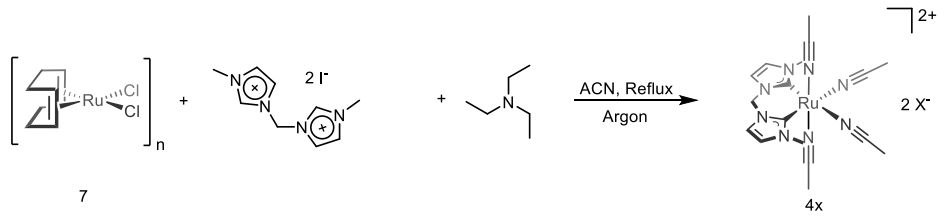

Scheme 10 - General reaction scheme depicting the synthesis of *tetrakis(acetonitrile)[1,1-bis(3'-methylimidazol-2'-ylidene)methylene]ruthenium(II) dihalide* (**4x**).

The isolation of the organonitrile complex posed a considerable challenge due to its sensitivity to air and inherent instability, which required working under tight Schlenk conditions at each purification step. Therefore, the reacting mixture was initially charged with *potassium hexafluorophosphate* (220 mg, 1.2 mmol) and allowed to react for 2 h. Subsequently, the solution was concentrated by reducing its volume and then transferred via a cannula into a 50 mL Schlenk flask equipped with sintered glass septa and filled with neutral deactivated alumina. Then, flash chromatography was carried out using degassed *ACN* under an inert atmosphere. Following these controlled conditions and after removing the solvent, the air-sensitive product was successfully isolated, resulting in a yield of 60% (Section 4.6). The complete characterization via NMR spectroscopy has been reported in Section 4.6, and the ^{1}H NMR spectrum of the complex has already been discussed (Section 2.2). It should be noted that *TEA* traces were detected in the isolated compound, free and coordinated (Figure 23). Samples previously collected from the reaction mixture did not suggest *TEA* coordination.

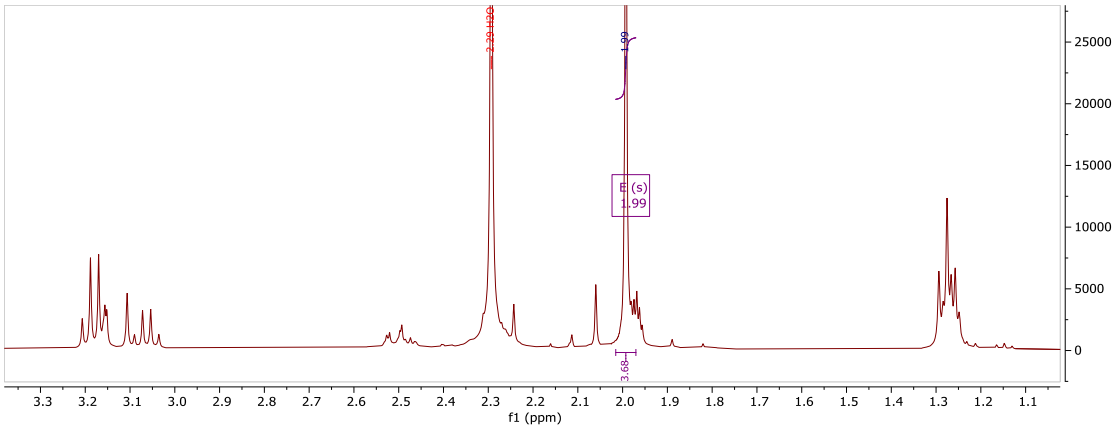

Figure 23 – A section of *tetrakis(acetonitrile)[1,1-bis(3'-methylimidazol-2'-ylidene)methylene]ruthenium(II) dihalide* (**4x**) ^{1}H NMR spectrum collected in deuterated *ACN* displaying the peaks assigned to coordinated and free *TEA* (cross-referenced via ^{13}C and 2D NMR experiments).

The *tetrakis(acetonitrile)[1,1-bis(3'-methylimidazol-2'-ylidene)methylene]ruthenium(II) dihalide* (**4x**) complex exhibits extreme reactivity, which makes it more suitable as an interesting intermediate rather than a stable precursor. Due to this reactivity, instead of isolating the complex separately each time from

the mixture, we conducted reactions directly within the mixture using various ligands. This approach allowed us to produce a series of further functionalized ruthenium(II) complexes, as discussed in Section 4.5. However, it is essential to note that although one might initially perceive the synthesis of *tetrakis(acetonitrile)[1,1-bis(3'-methylimidazol-2'-ylidene)methylene]ruthenium(II) dihalide* (**4x**) as a straightforward process, the data presented till now do not provide a complete understanding of the underlying complexities involved in this synthesis. The *ACN* role in the activation of *(1,5-cyclooctadiene)(dichloro)ruthenium(II) polymer* (**7**) might appear as critical, with the mass effect of the weakly σ-donor solvent being a key factor in the substitution reaction. A possible mechanism could hence involve the formation of *(1,5-cyclooctadiene)(diacetonitrile)(dichloro)ruthenium(II)* (**8**) by treating *(1,5-cyclooctadiene)(dichloro)ruthenium(II) polymer* (**7**) in *ACN* at reflux, which later react with bis-imidazolium salt activated by *TEA*. Interestingly, refluxing *(1,5-cyclooctadiene)(dichloro)ruthenium(II) polymer* (**7**) for a week does not provide quantitatively *(1,5-cyclooctadiene) (diacetonitrile)* (*dichloro)ruthenium(II)* (**8**), when conversely the formation *tetrakis(acetonitrile)[1,1-bis(3'-methylimidazol-2'-ylidene)methylene]ruthenium(II) dihalide* (**4x**) only requires 36 h. As Crabtree et al. suggested, a trivial explanation could be the influence of the activated bis-imidazolium salt, implying that the free carbene drives the precursor activation by subtracting the intermediate *(1,5-cyclooctadiene)(diacetonitrile)(dichloro)ruthenium(II)* (**8**).[132] However, upon further inquiry, a mixture of unidentified products was observed upon replacing *TEA* with stronger bases such as *sodium acetate*, *cesium carbonate*, *potassium hydroxide*, or *potassium tert butoxide*. Moreover, while replacing *ACN* with *acetone* and *THF* produced similar results, the presence of ruthenium(II) triethylamino complexes was unexpectedly detected, suggesting that *TEA* does not simply react as a base (Figure 24). These results prompted us to study the role of *TEA*, a topic to which the next section will be dedicated (Section 2.4).

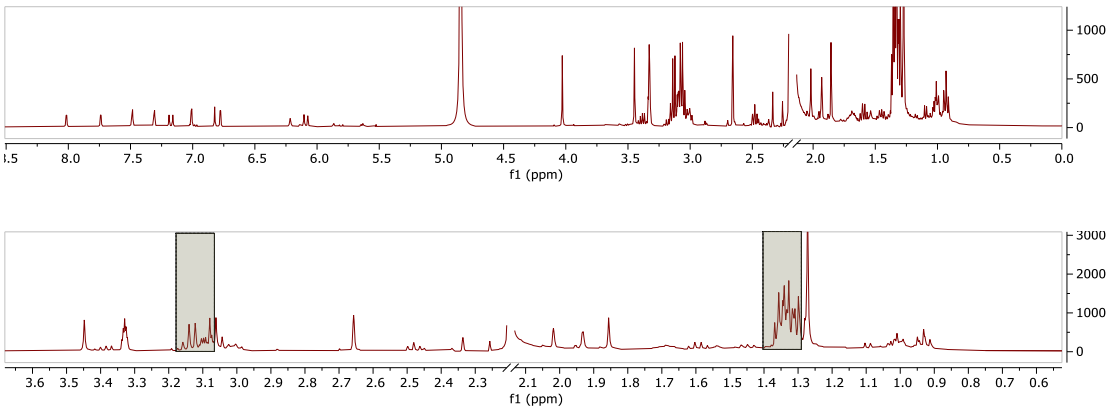

Figure 24 – Most significative ^{1}H NMR spectrum of the crude reaction mixture obtained by following the protocol for the synthesis of *tetrakis(acetonitrile)[1,1-bis(3'-methylimidazol-2'-ylidene)methylene]ruthenium(II) dihalide* (**4x**, Section 4.6), but replacing *ACN* with *acetone* (above). A highlight of the same spectrum, displaying the peaks assigned to coordinate *TEA* (below).

2.4 Mechanistic analysis of $[Ru(COD)Cl_2]_n$ activation

The reaction mechanism leading to the formation of *tetrakis(acetonitrile)[1,1-bis(3'-methylimidazol-2'-ylidene)methylene]ruthenium(II) dihalide* (**4x**) was inquired with a kinetic experiment followed via ^{1}H NMR spectroscopy, aimed to identify the relevant intermediates. A 5 mm J-young NMR tube was charged with 10.1 mg *(1,5-cyclooctadiene)(dichloro)ruthenium(II) polymer* (**7**), 500 uL of deuterated *ACN*, 25 uL of *TEA* and 15.6 mg of *1,1-bis(3'-methylimidazolium)methylene diiodide*, according to the developed synthetic protocol. A ^{1}H NMR spectrum of the heterogeneous mixture was acquired before starting the reaction by placing the tube at reflux (Figure 25). The bis-imidazolium salt was slightly soluble, and the related signals are highlighted in yellow. Instead, the ruthenium precursor and the related organonitrile complexes were not observed at this time. The only other compounds observed in solution were *TEA* and *water*.

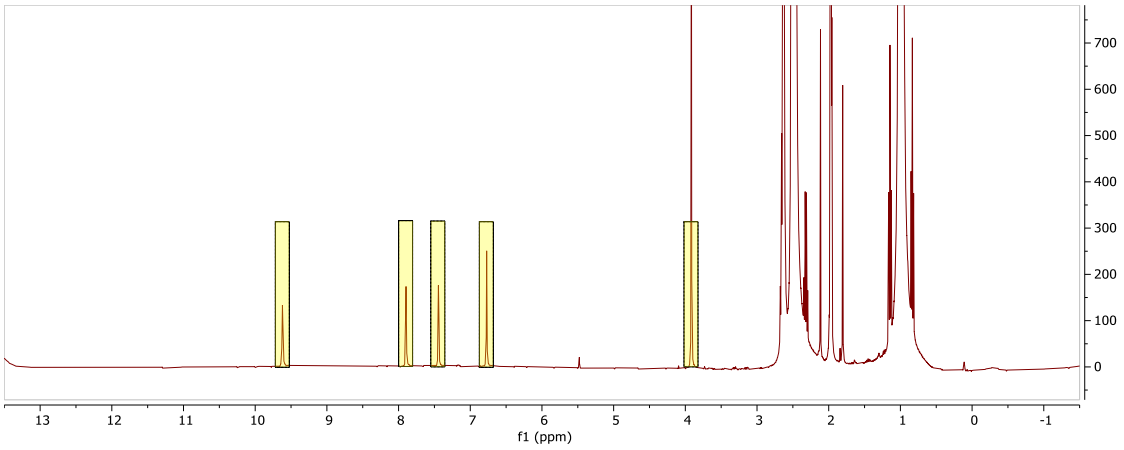

Figure 25 - The ^{1}H NMR spectra of the unreacted mixture at time t=0h, containing: 10.1mg of *(1,5-cyclooctadiene)(dichloro)ruthenium(II) polymer* (**7**), 15.6mg of *1,1-bis(3'-methylimidazolium)methylene diiodide*, 25 uL of *TEA*, and 500 uL of CD_3CN.

The tube was placed in a stirred oil bath at 80°C for 30 h and ^{1}H-NMR spectra were acquired at different times to monitor the reaction progress at 2, 4, 6, 8, 12, 16, 20, 24, and 28 h. All the acquired spectra are reported stacked in Figure 26, and the assignments of the relevant chemical species have been highlighted with different colors. The kinetic experiment shows the formation of *tetrakis(acetonitrile)[1,1-bis-(3'-methylimidazol-2'-ylidene)methylene]ruthenium(II) dihalide* (**4x**), a triethylamino complex and cyclooctadiene, as well as the progressive consumption of the *1,1-bis(3'-methylimidazolium)methylene diiodide*.

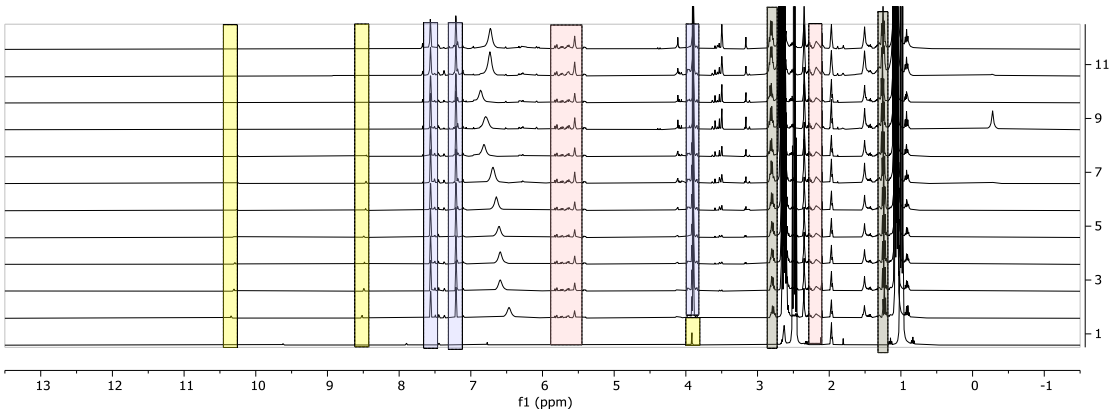

Figure 26 - The ^{1}H-NMR kinetic experiment of the reacting mixture at times t=0, 2, 4, 6, 8, 10, 12, 16, 20, 24, 28, 32h, T = 80°C. Reagents: 10.1mg of *(1,5-cyclooctadiene)ruthenium(II) dichloride polymer* (**7**), 15.6mg of *1,1-bis(3'-methylimidazolium)methylene diiodide*, 25 uL of *TEA*, and 500 uL of *CD_3CN*.

The spectrum collected after 10 hours was chosen as the most representative since most of the species involved in the reaction were detected jointly. Hence, the relative spectra was extracted from the overall kinetic experiment, reported in Figure 27, and divided into two fragments to improve visual observation of the relevant species. In the high field fragment (Figure 27, above), from left to right, the first compound identified was *1,1-bis(3'-methylimidazolium)methylene diiodide*, which is highlighted in yellow. The two identified peaks have been assigned to the -CH from the imidazole moiety backbone, falling respectively at 10.40 and 8.52 ppm. The acidic proton (-CH) and the proton from the methylene bridge (-CH_2-) of the bis-imidazolium salt are either in exchange or covered by the broad peak of *water* and the triethylammonium cation falling in the 6.5 ppm region. The main product, the assumed *tetrakis(acetonitrile)[1,1-bis(3'-methylimidazol-2'-ylidene)methylene]ruthenium(II) dihalide* (**4x**) has two identifiable peaks highlighted in blue, two doublets falling respectively at 7.55 and 7.23 ppm, also from the imidazole moiety of the product. Different cyclooctadiene species were observed in the 5.50 ppm region, but the assignment attempts of these peaks to single species failed. In the low field fragment (Figure 27, below), the two singlets in the 3.90 ppm region were ascribed to the free ligand (*1,1-bis(3'-methylimidazolium)methylene diiodide*) and (*tetraacetonitrile)[bis-1,1'-(3-methylimidazol-2-ylidene)methylene]ruthenium(II) dihalide* (**4x**), specifically to the (-CH_3) moiety of the ligands. *TEA* was observed more downfield, with two peaks assigned to the (-CH_2-) and (-CH_3) moieties falling respectively at 2.50 and 1.08 ppm. A species consistent with coordinated TEA was also observed slightly upfield, at 2.80 and 1.25 ppm. The formation of the triethylammonium cation was also inferred by the presence of a rising peak at 6.50 ppm, consistent with the protonated amine being in exchange with water.

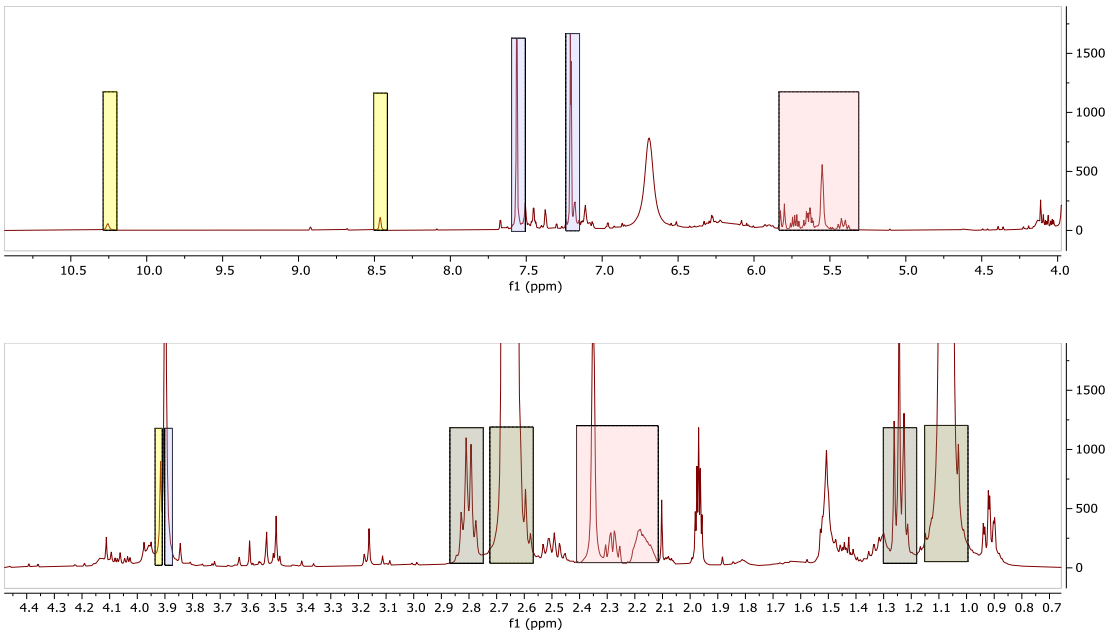

Figure 27 - The ^{1}H NMR spectra extracted from the kinetic experiment of the reacting mixture after 10 h at 80 °C. The spectra has been divided into two fragments to ease consultation: the fragment above reports the high-field portion, and the fragment below the low-field portion. Reagents: 10.1 mg of *(1,5-cyclooctadiene)(dichloro)ruthenium(II) polymer* (**7**), 15.6 mg of *1,1-bis(3'-methylimidazolium)methylene diiodide*, 25 uL of *TEA*, and 500 uL of CD_3CN.

The TEA peaks were integrated and used as an internal standard to determine the soluble species' concentration. At a temperature of 25°C, the maximum concentration of *1,1-bis(3'-methylimidazolium)methylene diiodide* was observed to be 5 mM. The salt concentration steadily fell as the reaction progressed beyond 12 h till no residual signal was detected after 24 h, marking reaction completion. Notably, the concentration of *tetrakis(acetonitrile)[1,1bis-(3'-methylimidazol-2'-ylidene)methylene]ruthenium(II) dihalide* (**4x**) is also constant for the whole experiment after the first acquired point, the solubility limit being at 30 mM which translated to 60% conversion. It should be noted that TEA is not a reliable standard but rather a reagent. The same kinetic experiment was carried out without *1,1-bis(3'-methylimidazolium)methylene diiodide* to asses if the salt is directly involved in complex activation. After 20 minutes at reflux, the sample of *(1,5-cyclooctadiene)(dichloride)ruthenium(II) polymer* (**7**) was completely dissolved, but the reaction did not reach equilibrium, as shown in Figure 28 as an unidentified specie related to *1,5-cyclooctadiene* kept rising in concentration till the experiment was halted after 32h. Even if the intermediate was not identified, this experiment proves that TEA is involved in the precursor activation as the coordinated TEA peak at 2.5 ppm increased proportionally to the *1,5-cyclooctadiene* peaks. Moreover, simply placing *(1,5-cyclooctadiene)(dichloride)ruthenium(II) polymer* (**7**) in a 9:1 mixture of degassed *ACN* and deuterated *ACN* will not afford the same product, but *(1,5-cyclooctadiene)(diacetonitrile) ruthenium(II) dichloride* (**7**) (Figure 28),[129] and the reaction will take 7 days to complete.

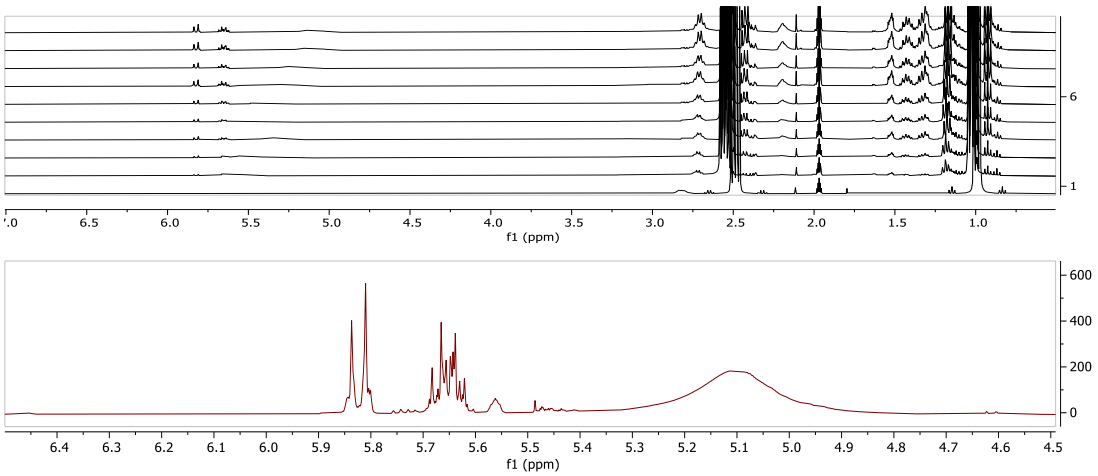

Figure 28 - The ^{1}H NMR kinetic experiment of the reacting mixture at times t=0, 2, 4, 6, 8, 10, 12, 16, 20, 24, 28, 32h, T = 80°C. Reagents: 10.1 mg of *(1,5-cyclooctadiene)ruthenium(II) dichloride polymer* (**7**), 25 uL of *TEA*, and 500 uL of *CD_3CN* (above). A highlight of the spectrum region where the signals from the protons bound to unsaturated carbons in *1,5-cyclooctadiene* fall, acquired at t=32 h (middle). The ^{1}H NMR of a solution containing *(1,5-cyclooctadiene)(diacetonitrile)(dichloro) ruthenium(II)* (**8**) originated from 10.1 mg of *(1,5-cyclooctadiene)ruthenium(II) dichloride polymer* (**7**) placed at reflux in *ACN* for 7 days.

The *(1,5-cyclooctadiene)ruthenium(II) dichloride polymer* activation is a critical step in the formation of the alleged *tetrakis(acetonitrile)[1,1-bis(3'-methylimidazole-2'-ylidene)methylene]ruthenium(II) dihalide* (**4x**), and *TEA* proved essential in the depolymerization step as the base produces reactive intermediates that will further react with the bis-imidazolium salt.

2.5 Synthesis of *trans*-$Ru(ACN)_2(b(MI)M)(Bipy)(PF_6)_2$

The *tetrakis(acetonitrile)[1,1-bis(3'-methylimidazole-2'-ylidene)methylene] ruthenium(II) dihalide* (**4x**) complex proved susceptible to nucleophilic attacks from LL ligands under mild conditions (Section 2.2) and thus is an ideal candidate to generate a comprehensive library of coordination compounds (Scheme 11), like the desired target species.

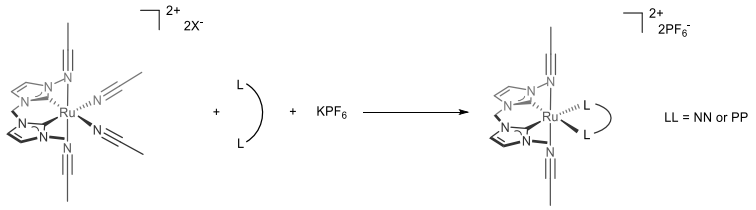

Scheme 11 - The general reaction scheme depicting the coordination of an LL-ligand to *tetrakis(acetonitrile) [1,1-bis(3'-methylimidazole-2'-ylidene)methylene] ruthenium(II) dihalide* (**4x**) complex resulting in the formation of the trans product, also regarded as the kinetic product, and the release of two *ACN* molecules.

To streamline the synthetic process, an attractive alternative to isolating the reactive complex as an intermediate would be to carry out further reactions directly on the reacting mixture. Thus, prior to the LL ligand additions, the mixture containing the reactive intermediate was cannula filtered using a Whatman filter to remove ruthenium black traces. The filtrate was dried, isolating an air-sensitive orange powder that must be stored under argon. The first attempt to coordinate a new ligand was carried out with *2,2'-bipyridine*, which was added stoichiometrically (46 mg, 0.30 mmol) to the initial amount of ruthenium precursor (84 mg, 0.30 mmol); then, all the compounds were dissolved in *chloroform* (4 mL) and put at reflux resulting in an immediate change of color from orange to deep red. After 2 h, the solution was dried, and the product was isolated via gradient flash chromatography. The stationary phase consisted of neutral deactivated alumina, and the complex was charged as a liquid. The first fraction collected was eluted with *acetone* and was characterized by a deep red color. Upon investigation via NMR spectroscopy, this mixture was ruled to contain the unreacted *2,2'-bipyridine* ligand. The target complex, instead, does not effectively elute under these conditions, and it can be isolated only after anion exchange; this was accomplished using a saturated solution of *potassium hexafluorophosphate* in *acetone*. The anion exchange affected the complex's solubility, releasing it from the stationary phase and producing a single compound from the initial mixture of complexes with different counterions. The solvent was removed at the rotary evaporator, and the product was extracted using *dichloromethane (DCM,* 40 ml) and filtered. Again, the solvent was removed, and after drying overnight, *trans-(diacetonitrile)(2,2'-bipyridine)[1,1-Bis(3'-methyl-imidazol-2'-ylidene)methylene] ruthenium(II) dihexafluorophosphate* (**9a**) was obtained with a cumulative yield of 40% (Scheme 12).

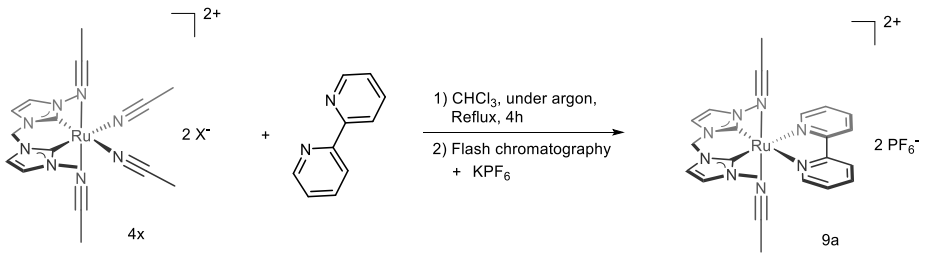

Scheme 12 – The first attempt at the coordination of *2,2'-bipyridine* to *tetrakis(acetonitrile)[1,1-bis(3'-methylimidazole-2'-ylidene)methylene] ruthenium(II) dihalide* (**4x**).

Even if a 40% yield determined an overall improvement from the initially obtained 7%, the process was still not satisfactory as consisting of many synthetic steps and time-consuming purification procedures. A first improvement to the process was introduced by changing the reaction temperature to reduce the formation of unidentified side products after ligand addition, which likely consist of polypyridine-related ruthenium(II) species. Hence, the ligand addition occurred at 25 °C in *DCM* (4 mL) in the next synthesis, resulting in a cleaner reaction as a reduced amount of side products was observed from the ^{1}H NMR spectra of the reaction's crude. Since less undesired product was detected, the isolation was performed via precipitation instead of flash column chromatography. After drying the solution, the solid residue was dissolved in the minimum amount of boiling *methanol*, and subsequently, *potassium hexafluorophosphate* (220 mg, 1.20 mmol) was added. The solution was placed at -18 °C resulting in the crystallization of the product, which was isolated by filtration over gooch and washed with *diethyl ether* (3 x 5 mL). The process of crystallizing the product from a *methanol* solution, taking advantage of the hexafluorophosphate complex solubility, concluded with a comparable yield of 45%. Adding *sodium tetraphenylborate* to the filtrate resulted in immediate precipitation of the *trans-(diacetonitrile)(2,2'-bipyridine)[1,1-Bis(3'-methyl-imidazol-2'-ylidene)methylene]ruthenium(II) ditetraphenylborate* (**9b**), highlighting that the solubility of the complex in *methanol* is higher than expected and thus limiting the overall yield. The synthesis was thus repeated, but this time precipitating only with *sodium tetraphenylborate (410 mg, 1.2 mmol)* from the *methanol* solution, resulting in a 75% yield. The *trans-(diacetonitrile)(2,2'-bipyridine)[1,1-Bis(3'-methyl-imidazol-2'-ylidene)methylene] ruthenium(II) ditetraphenylborate* (**9b**), unfortunately, proved to be insoluble in most solvents except for *dimethyl sulfoxide*, which prompted us to optimize further the synthetic process for future catalytic application where the catalyst solubility could affect reactivity. To solve the solubility problem and further simplify the synthetic procedure, a "one-pot" synthesis was designed, taking advantage of the insolubility of cationic complexes bearing hexafluorophosphate counterions in *water*. Starting from the reactive mixture containing *tetrakis(acetonitrile)[1,1-bis(3'-methylimidazole-2'-ylidene)methylene] ruthenium(II) dihalide* (**4x**) complex (0.30mmol) in *ACN*, *2,2'-bipyridine* (46 mg, 0.30 mmol) was added at room temperature under argon counterflow, and the solution was left reacting for 2 h. As expected, the mass effect of *ACN* slowed the reaction, and the temperature was raised to 50 °C for 2 h to reach reaction completion. At this point, to isolate the product, *potassium hexafluorophosphate* (440 mg, 2.40 mmol) was added, resulting in partial product precipitation. The

mixture was reduced in volume, then *water* (10 mL) was added to precipitate the product and the organic residue as an oily glue while removing the inorganic salts. The mixture was left crushing under stirring, producing a fine orange powder after 4 h. The mixture was filtrated over gooch, and the powder was washed with *water* (2 x 5 mL) and *diethyl ether* (3 x 5 mL) to remove the unreacted *2,2'-bipyridine*. The recovered orange powder was later dried overnight, affording the product (80% yield). The coordination process of *2,2'-bipyridine* to *tetrakis(acetonitrile)[1,1-bis(3'-methylimidazole-2'-ylidene)methylene] ruthenium(II) dihalide* (**4x**) complex was studied in a j-young tube, the same tube containing the mixture previously employed to study the activation of *(1,5-cyclooctadiene)ruthenium(II) dichloride polymer* (**7**) (Section 2.4). The experiment started by adding *2,2'-bipyridine* (6 mg) under argon counterflow to the reactive mixture, then, immediately after, the reaction profile was monitored via ^{1}H NMR spectroscopy using the kin2d pulse sequence, acquiring a spectrum every 5 minutes. The final reaction profile is reported in Figure 29. The concentrations of the detected reactants, intermediates, and products have been reported relative to the sum of *2,2'-bipyridine* signals used as an internal standard. The signals used in the summation originated from the product and the free ligand (the original ^{1}H NMR spectra have been reported in Section 4.20).

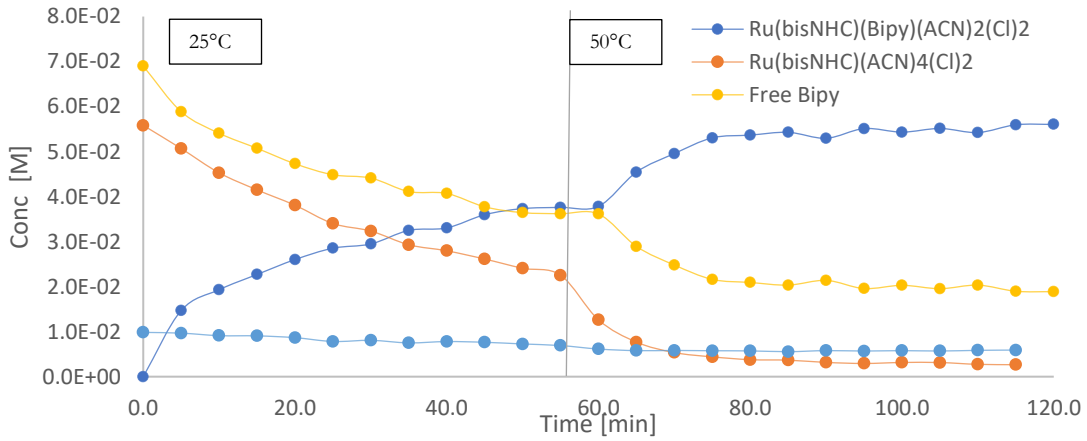

Figure 29 - The reaction profile was obtained from a collection of ^{1}H NMR spectra, each acquired every 5 minutes for 1 h at 25°C, and for 1 h at 50°C. The tube contained 10.1 mg of *(dichloro)(1,5-cyclooctadiene)ruthenium(II) polymer* (**7**), 15.6 mg of *1,1-bis(3'-methylimidazolium)methylene diiodide*, 25 uL of *TEA*, and 500 uL of deuterated *ACN*, which reacted for 32 h at reflux before the addition of 6.0 mg of *2,2'-bipyridine*.

From the kinetic profiles, it can be inferred that *2,2'-bipyridine* reacts at room temperature but that the reaction is not quantitative as after 1 h the reaction reaches a plateau, and the product concentration does not increase further, limiting at 53% conversion. Hence, the reaction reaches an equilibrium at room temperature where the reaction stops before consuming the reagent completely; then, either an excess of the ligand or a temperature increase is required to shift the equilibrium. The shift was achieved by raising the temperature to 50°C for 1 h, resulting in the complete consumption of *tetrakis(acetonitrile)[1,1-bis(3'-methylimidazole-2'-ylidene)methylene] ruthenium(II) dihalide* (**4x**), which was converted up to 80% into the *trans-(diacetonitrile)(2,2'-bipyridine)[1,1-Bis(3'-methyl-imidazol-1'-*

ylidene)methylene]ruthenium(II) dihalide (**9x**), as shown in Figure 29. An impurity was also detected, accounting for a 7% conversion of the initial precursor. The species was not isolated, but the signals in the ^{1}H NMR spectrum were consistent with the formation of *cis-di(acetonitrile)bis[1,1-bis(3'-methylimidazole-2'-ylidene)methylene] ruthenium(II) dihalide* (**10x**) (Figure 30).

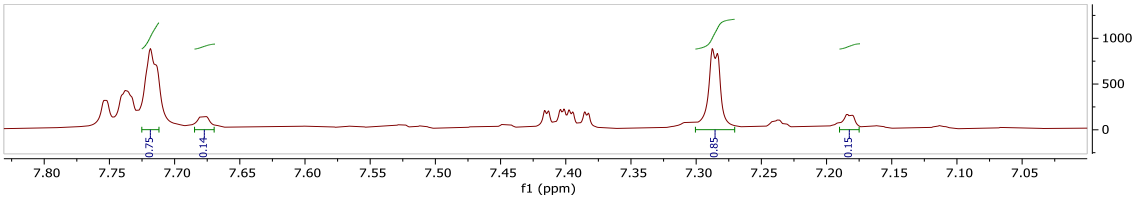

Figure 30 - A fragment of the ^{1}H NMR spectrum collected 2 h after the addition of *2,2'-bipyridine* to the mixture containing the alleged *tetrakis(acetonitrile) [1,1-bis(3'-methylimidazole-2'-ylidene)methylene] ruthenium(II) dihalide* (**4x**) intermediate. The fragment highlights the region where the signals of the imidazole moiety fall. Two species are detected, the main identified as *trans-(diacetonitrile)(2,2'-bipyridine)[1,1-bis(3'-methyl-imidazol-2'-ylidene)methylene]ruthenium(II) dihalide* (**9x**) and a second consistent with *cis-di(acetonitrile)bis[1,1-bis(3'-methylimidazole-2'-ylidene)methylene] ruthenium(II) dihalide* (**10x**).

Following the compound isolation, 20 mg of *trans-(diacetonitrile)(2,2'-bipyridine)[1,1-Bis(3'-methyl-imidazol-2'-ylidene)methylene]ruthenium(II) dihexafluorophosphate* (**9a**) (Figure 31) were dissolved in deuterated *ACN* to determine the compound structure using the ^{1}H, ^{13}C, ^{19}F, ^{31}P, ^{1}H-^{13}C HSQC, ^{1}H-^{13}C HMBC, ^{1}H-^{15}N HMBC and ^{1}H-^{1}H NOESY NMR methods (Section 4.7).

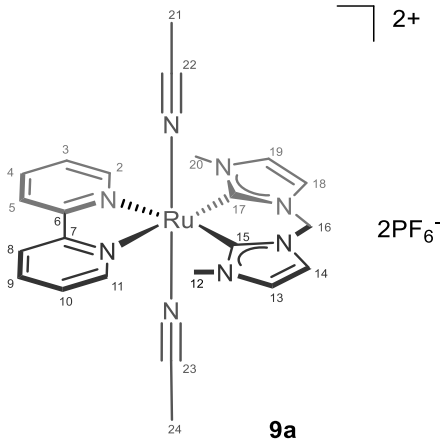

Figure 31 - The structure of *trans-(diacetonitrile)(2,2'-bipyridine)[1,1-bis(3'-methyl-imidazol-2'-ylidene)methylene]ruthenium(II) dihexafluorophosphate* (**9a**) as determined via NMR analysis, the carbon atoms have been numbered to ease the discussion of the structure elucidation.

First, the coordination of *2,2'-bipyridine* to the metal center was assessed by the high-field shift of all signals compared to the free ligand, the most distinctive signal related to hydrogens H2 and H11 shifting from 8.56 ppm to 9.20 ppm. Similarly, although the coordination of *1,1-bis(3'-methyl-imidazolium)methylene diiodide* was already known from the study on the precursor reactivity, the presence of a ruthenium-carbene bond was observed at the ^{13}C NMR with a peak falling at 183 ppm,

the characteristic region of coordinated NHCs[133]. The ^{1}H-^{13}C HMBC spectra confirmed that the signal belonged to carbons C15 and C17, as the trough-bond correlation from the signal relates to all the relevant imidazole moiety protons (Figure 32).

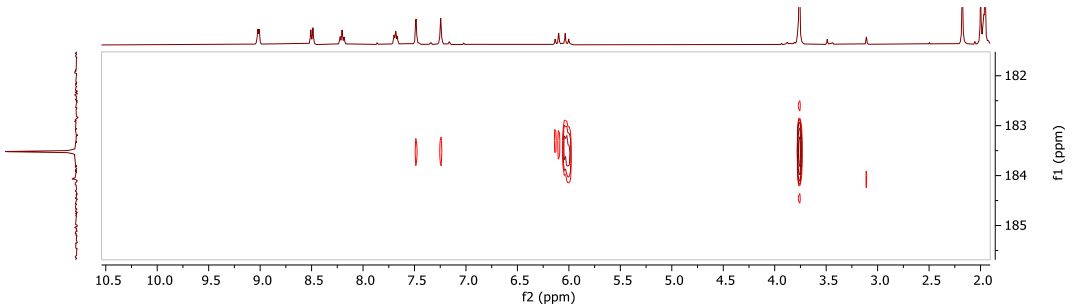

Figure 32 - A section of the acquired ^{1}H-^{13}C HMBC of the *trans-(diacetonitrile)(2,2'-bipyridine)[1,1-bis(3'-methyl-imidazol-2'-ylidene)methylene]ruthenium(II) dihexafluorophosphate* (**9a**) complex, highlighting the correlations between C15, C17 and the related protons.

The signals identified from the two chelating ligands also let us determine the complex's geometry since, in the ^{1}H NMR spectra, the number of signals observed changes based on the complex symmetry. As both the *2,2'-bipyridine* and *[1,1-bis(3'-methylimidazole-2'-ylidene)methylene]* moieties signals retain their symmetry in the final product, like in the free ligand, the *trans* complex has formed. Taking as an example *2,2'-bipyridine,* if the final complex had been the *cis*-product, then eight different signals would have arisen in the ^{1}H NMR spectra from *2,2'-bipyridine's* two heteroaromatic rings, as they would have experienced a different coordination sphere and *trans* effect with respect to each other. In contrast, only four signals are observed as in the free ligand, meaning the ligands in the relative *trans* position are equal. The same applies when reasoning on the *1,1-bis(3'-methylimidazole-2'-ylidene)methylene* moiety.

Interestingly, when integrating the signal originating from the -CH_3 moiety of *ACN* against the other signals from the target compound, the integration accounts for only one coordinated *ACN* molecule. This evidence could suggest that the complex is mono-cationic instead of di-cationic, with a halide ligand coordinated to the metal center. However, exchange with the deuterated solvent could also have occurred since the spectra were acquired in deuterated *ACN* due to solubility.[134] The latter proved the case, as acquiring the same spectra in deuterated *acetone* or *DCM* gave rise to two singlets ascribed to *ACN* -CH_3 groups. Moreover, in a more coordinating solvent the chemical shift of the second *ACN* molecule drifts closer to the free *ACN* chemical shift suggesting an exchange regime is occurring with the *water* traces or the solvent itself (**Figure 33**).

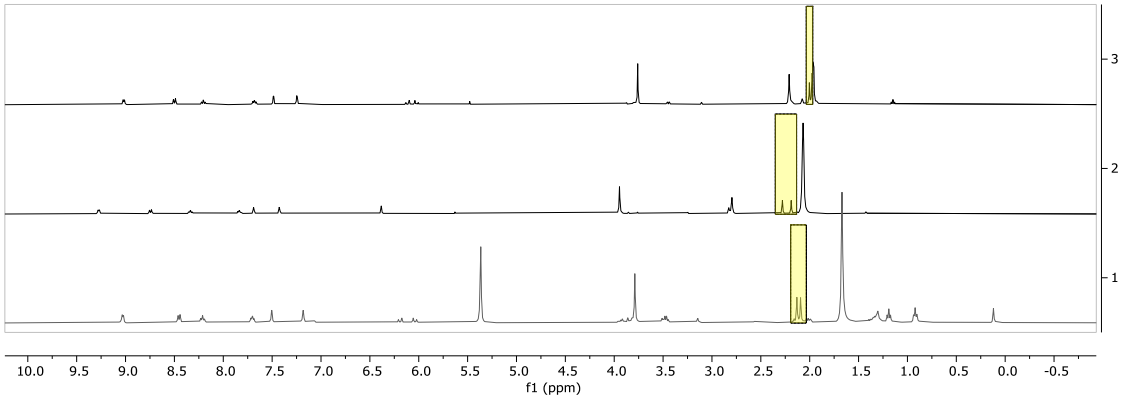

Figure 33 - Three ^{1}H NMR spectra of *trans-(diacetonitrile)(2,2'-bipyridine)[1,1-Bis(3'-methyl-imidazol-2'-ylidene)methylene]ruthenium(II) dihexafluorophosphate* (**9a**) acquired in different deuterated solvents: *ACN* (above), *acetone* (center), and *DCM* (below).

The effect of the counterion on the ligands' chemical shift was tested in situ by adding 4 eq of different silver salts to a deuterated *acetone* solution containing 10 mg of *trans-(diacetonitrile)(2,2'-bipyridine)[1,1-Bis(3'-methyl-imidazol-1'-ylidene)methylene]ruthenium(II) ditetraphenylborate* (**9b**). Immediate flocculation of *silver tetraphenylborate* was always observed. The experiment produced four ^{1}H NMR spectra of the complex with four different counterions: trifluoroacetate, hexafluorophosphate, trifluoromethanesulfonate, and tetraphenylborate (Figure 34).

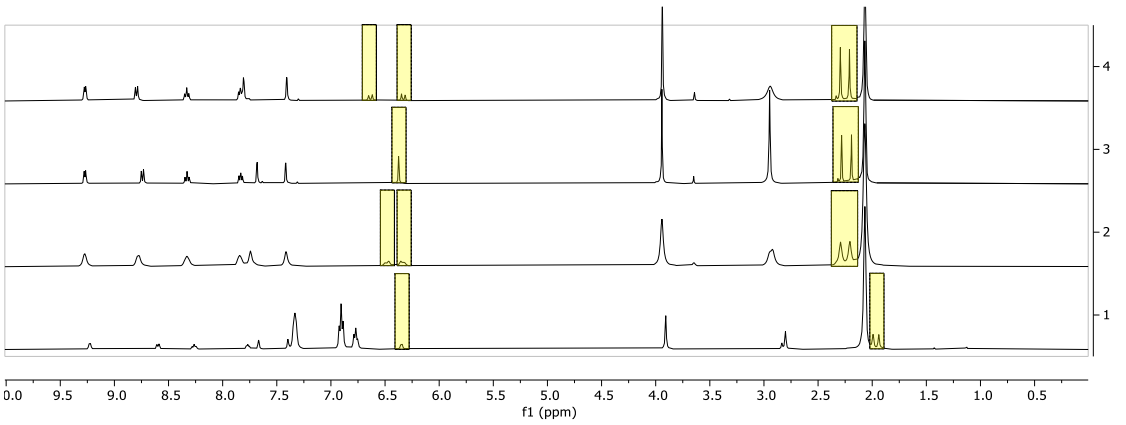

Figure 34 - The acquired spectra of *trans-(diacetonitrile)(2,2'-bipyridine)[1,1-Bis(3'-methyl-imidazol-1'-ylidene)methylene]ruthenium(II) ditetraphenylborate* (**9b**) (10 mg) after the addition of 4 eq of a silver salt, from top to bottom: AgTFA, $AgPF_6$, AgOTf, and no silver salt. Solvent: deuterated *acetone* (500 uL).

The *ACN* peaks structure did not change significantly to suggest that the anion is involved in an exchange equilibrium, as highlighted by the yellow bars in the low field region (Figure 34). The -CH_2- bridging the two bis-carbene moieties, highlighted in yellow in the upfield region (Figure 34), is instead affected in multiplicity. More coordinating anions differentiate the two protons generating two doublets, implying a possible exchange with coordinated *ACN*. From the available NMR experimental data, we conclude that the complex's apically coordinated *ACN* molecules are in

dynamic equilibrium with *water* traces in the deuterated solvent and with slightly coordinating counterions.

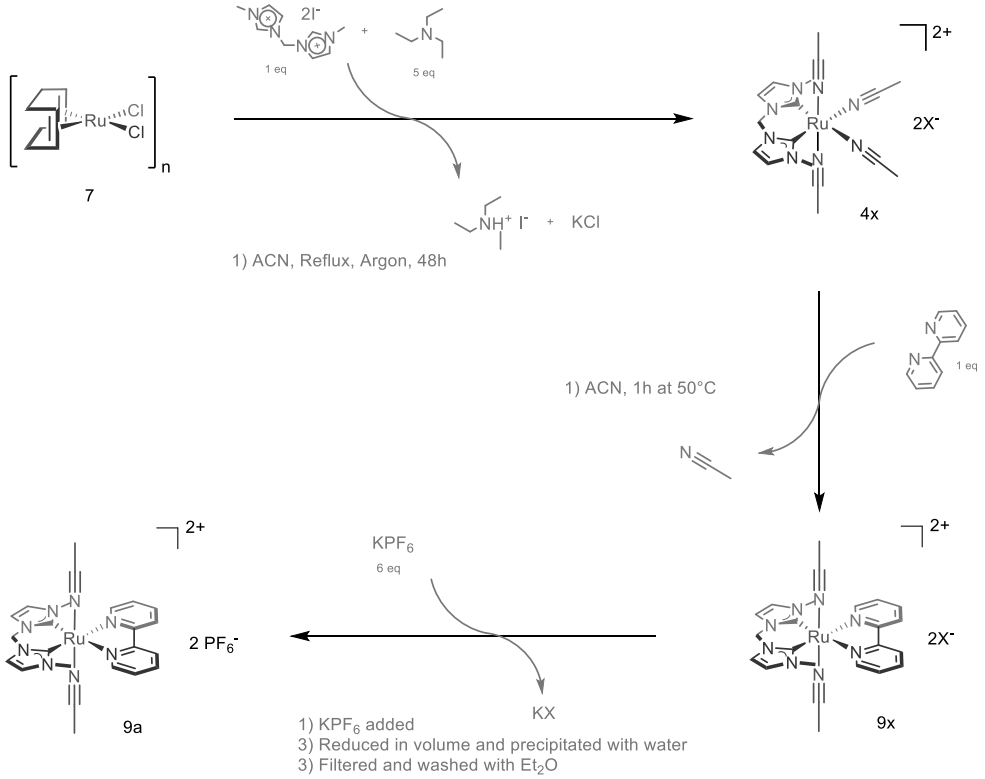

Scheme 13 - The optimized *one-pot* process for the synthesis of *trans-(diacetonitrile)(2,2'-bipyridine)[1,1-Bis(3'-methyl-imidazol-2'-ylidene)methylene] ruthenium(II) dihexafluorophosphate* (**9a**).

2.6 Synthesis of *cis*-Ru(ACN)$_2$(b(MI)M)(Bipy)(PF$_6$)$_2$

Since *trans-(diacetonitrile)(2,2'-bipyridine)[1,1-Bis(3'-methyl-imidazol-2'-ylidene)methylene]ruthenium(II) dihexafluorophosphate* was obtained, attempts were made to obtain also *cis-(diacetonitrile)(2,2'-bipyridine)[1,1-Bis(3'-methyl-imidazol-2'-ylidene)methylene]ruthenium(II) dihexafluorophosphate*, as depicted in Scheme 14.

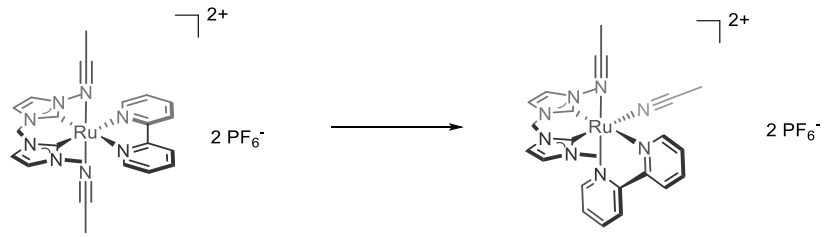

Scheme 14 - Isomerization reaction of *trans-(diacetonitrile)(2,2'-bipyridine)[1,1-Bis(3'-methyl-imidazol-2'-ylidene)methylene]ruthenium(II) dihexafluorophosphate* (**9a**) to *cis-(diacetonitrile)(2,2'-bipyridine)[1,1-Bis(3'-methyl-imidazol-2'-ylidene)methylene]ruthenium(II) dihexafluorophosphate* (**10a**).

The *trans*-product, i.e., the one featuring two *trans* acetonitriles, is the kinetic product as the carbene projects a strong *trans* effect increasing the dissociation constant of the *trans* ligands, which are more liable and easily undergo substitution with *2,2'-bipyridine.* Given this assumption, the thermodynamic *cis*-product could technically be obtained via the isomerization reaction of the *trans*-product. This process is known to proceed thermally, but that does not apply to all complexes as side reactions leading to complex decomposition or unintended products may occur before the isomerization. Different mechanisms have been proposed for *trans* to *cis* thermal isomerization of complexes over the decades. However, since the synthesized complexes feature the solvent in the coordination sphere, i.e., they are solvent-derived complexes, we assumed that the mechanism follows *ACN* temporary displacement, ending in the *2,2'-bipyridine* rearrangement. Following this strategy, thermic isomerization was initially carried out in *ACN* at reflux, leaving the *trans*-complex (120 mg, 0.20 mmol) reacting for 3 days, resulting in 30% isomerization as determined via ^{1}H NMR spectroscopy. After drying the solution and switching to *isopropanol* as a solvent, the reaction reached completion 3 days later. Since the two solvents have similar boiling points, we assumed that the reaction was not accelerated by temperature but rather slowed by the *ACN* mass effect, which is probably driven by bounded *ACN* dissociation. As unidentified side-products were observed, flash column chromatography was carried out to isolate the pure product, which consisted of neutral deactivated alumina for the stationary phase and *acetone* as eluent. After the first product isolation, the process was optimized to avoid the lengthy purification step. Since *ACN* should be preferred over alcohols to prevent decomposition, the reaction should be carried out inside a pressure tube to increase the isomerization rate by raising the reaction temperature. Hence, 120mg (0.20 mmol) of the *trans* complex were placed in a pressure tube, dissolved in *ACN*, and placed at 120°C for 2 days resulting

in total conversion to the *cis*-product, which was later isolated via subsequent recrystallizations in *methanol-diethylether* 2:1 (80% yield).

Similarly to the *trans*-complex, the isolated *cis-(diacetonitrile)(2,2'-bipyridine)[1,1-Bis(3'-methyl-imidazol-2'-ylidene)methylene]ruthenium(II) dihexafluorophosphate* (**10a**) (Figure 35) structure was determined using the ^{1}H, ^{13}C, ^{19}F, ^{31}P, ^{1}H-^{13}C HSQC, ^{1}H-^{13}C HMBC, ^{1}H-^{15}N HMBC and ^{1}H-^{1}H NOESY NMR methods (Section 4.8).

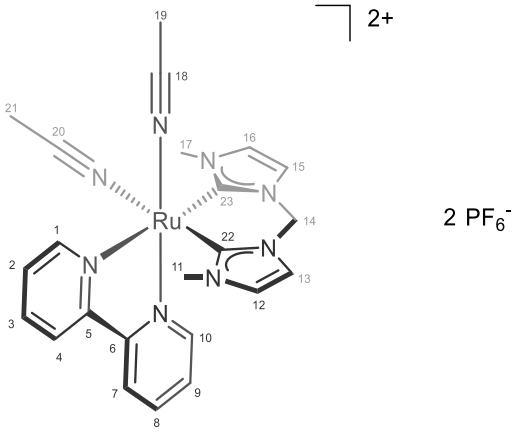

Figure 35 - The structure of *cis-(diacetonitrile)(2,2'-bipyridine)[1,1-Bis(3'-methyl-imidazol-2'-ylidene)methylene]ruthenium(II) dihexafluorophosphate* (**10a**) as determined via NMR analysis, the carbon atoms have been numbered to ease the discussion of the structure elucidation.

The general structure of the complex was initially determined via ^{1}H NMR spectroscopy. Indeed, as discussed before, the loss of symmetry from the *cis*-complex to the *trans*-complex doubles the signals from the ligands as each pyridine and imidazole moiety experiences a different chemical environment (Figure 36).

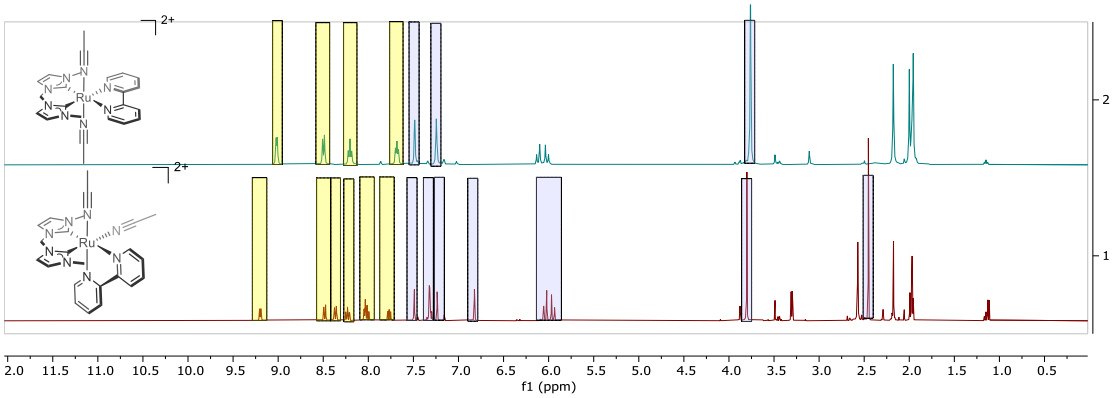

Figure 36 - A comparison of the ^{1}H NMR spectra of the *trans* (above) and *cis* (below) (*diacetonitrile)(2,2'-bipyridine)[1,1-Bis(3'-methyl-imidazol-2'-ylidene)methylene]ruthenium(II)dihexafluorophosphate* (**9a**,**10a**) complexes, highlighting the symmetry loss of the cis complex as the *2,2'-bipyridine* signals (yellow) and the *[1,1-Bis(3'-methyl-imidazol-2'-ylidene)methylene]* signals (blue) doubles.

The same conclusion was inferred from the ^{1}H-^{13}C HSQC and ^{1}H-^{13}C HMBC spectra. A fragment of the ^{1}H-^{13}C HMBC has been reported in (Figure 37), highlighting the correlation between the carbenes at C22 and C23 and the related protons in each imidazole moiety.

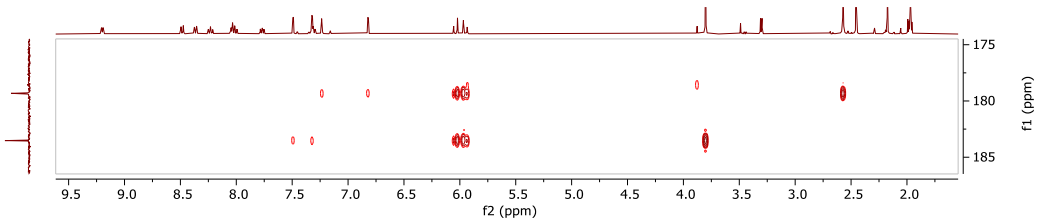

Figure 37 - A section of the acquired ^{1}H-^{13}C HMBC of the *cis-(diacetonitrile)(2,2'-bipyridine)[1,1-Bis(3'-methyl-imidazol-2'-ylidene)methylene]ruthenium(II) dihexafluorophosphate* (**10a**) complex, highlighting the correlations between C22, C23 and the related protons.

As for the *trans*-complex, the coordinated *ACN* does not integrate correctly with the other molecule signals due to exchange with the deuterated solvent. Moreover, the *ACN* signal accounts for 1.8 nuclides compared to 3.0 nuclides in the *trans*-complex spectrum, suggesting that *ACN* is more liable in the *cis*-complex.

2.7 Expansion of the ligand scope

A broad ligand scope is essential for fine-tuning complex reactivity, such as improving catalytic performances. Following the synthetic protocol developed for the *2,2'-bipyridine* complexes, *2-picolylamine* and *1,2-ethylenediamine* were introduced as new ligands (Scheme 15). The synthesis did not require any adaptation, and the *trans*-complexes (**11-12**) were obtained with consistent yields (Sections 4.7 and 4.8). The related *cis*-complexes have not been obtained for all compounds yet.

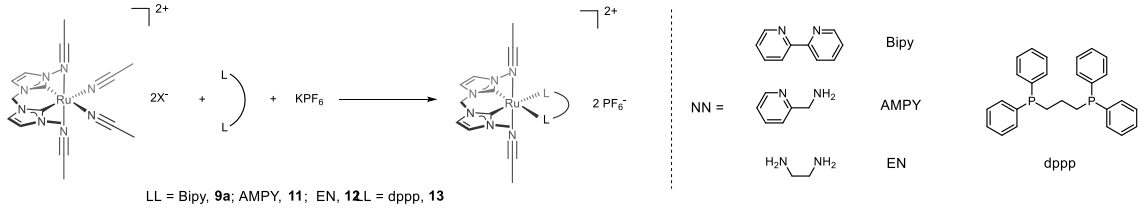

Scheme 15 – Addition of LL-type ligands to *tetrakis(acetonitrile)[1,1-bis(3'-methylimidazole-2'-ylidene)methylene] ruthenium(II) dihalide*, producing the corresponding trans-complexes.

The coordination of bis(phosphine) ligands to the *tetrakis(acetonitrile)[1,1-bis(3'-methylimidazole-2'-ylidene)methylene]ruthenium(II) dihalide* (**4x**) complex proved instead more challenging. The addition of *1,3-bis(diphenylphosphino)propane* (124 mg, 0.3 mmol) to the reactive *ACN* mixture containing the ruthenium(II) bis(NHC) intermediate (220 mg, 0.30 mmol) resulted in a mixture of products. The NMR spectrum of the reactions' crude indicated the bis(phosphine) successful coordination, but the broad peaks in the aromatic region suggested the presence of polynuclear ruthenium(II) species, bridged by the newly introduced ligand. The target compound, *trans-[1,1-bis(3'-methylimidazol-1'-ylidene)methylene] [1,3-bis(diphenylphosphino)propane] (diacetonitrile) ruthenium(II) dihexafluorophosphate* (**13**) was isolated upon purification via flash column chromatography, eluted with *DCM* over neutral deactivated alumina. After removing the solvent, the product was obtained as a pale-yellow powder (30 % yield) and fully characterized via NMR spectroscopy (Section 4.11). The alleged polynuclear species were collected after changing the mobile phase of the column to *ACN,* and their nature was inquired via NMR spectroscopy (40% approx. yield). Further attempts to coordinate bis(phosphine) ligands were conducted employing *1,2-bis(diphenylphosphino)ethane* and *1,4-bis(diphenylphosphino)butane*, which did not yield the desired mononuclear product. These results suggested that, while the mononuclear product is obtainable, only the coordination compound originating from *1,3-bis(diphenylphosphino)propane* can be obtained under these conditions, as forming a six-membered ring structure drives the coordination process. To kinetically limit the formation of multinuclear species, the bis(diphenylphosphino)propane addition was carried out at -10°C, leaving the mixture reacting till RT was reached. Under such conditions, the mononuclear complexes formed selectively, and no column chromatography was required to isolate the product which was precipitated with *water* (8 mL) and washed with *diethyl ether* (3 x 5 mL) after reducing the mixture in volume (70 % yield). The *trans-[1,1-bis(3'-methylimidazol-1'-ylidene)methylene][1,3-bis(diphenylphosphino)propane](diacetonitrile)ruthenium(II) dihexafluorophosphate* (**13**) (150 mg, 0.1 mmol) was isomerized to the corresponding *cis*-complex in

ACN (10 mL) at reflux. The reaction was monitored via ^{31}P NMR spectroscopy, which slowly reached completion after 15 days (Scheme 16).

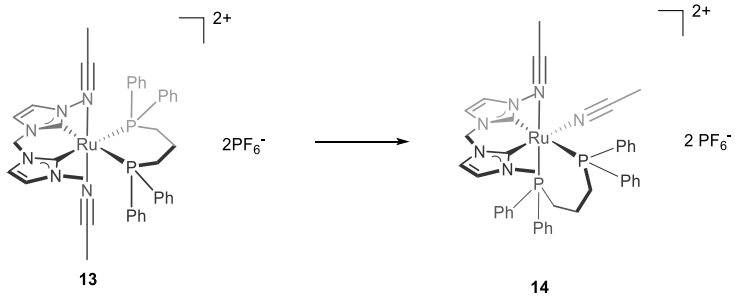

Scheme 16 - The thermal isomerization of *trans-[1,1-bis(3'-methylimidazol-1'-ylidene)methylene][1,3-bis(diphenylphosphino)propane](diacetonitrile)ruthenium(II) dihexafluorophosphate* (**13**) to *cis-[1,1-bis(3'-methylimidazol-1'-ylidene)methylene] [1,3-bis(diphenylphosphino)propane] (diacetonitrile) ruthenium(II) dihexafluorophosphate* (**14**) (Left).

2.8 Catalytic application in transfer hydrogenation reactions

The transfer hydrogenation (TH) reaction is a critical chemical transformation for improving the synthetic utility of alcohols, belonging to the broader field of hydrogenation processes (Section 1.3). In contrast to direct hydrogenations, TH involves reducing a substrate by hydrogen addition from sources other than molecular hydrogen. In the most common example, a ketone is reduced at the expense of a cheaper alcohol, and, typically, *2-propanol* is used as the reducing agent as it is available, non-toxic, and environmentally friendly. Moreover, given the low boiling point, the acetone formed as a byproduct can be easily removed from the reaction mixture. Formiate salts are also employed as reducing agents since they oxidize, producing carbon dioxide.

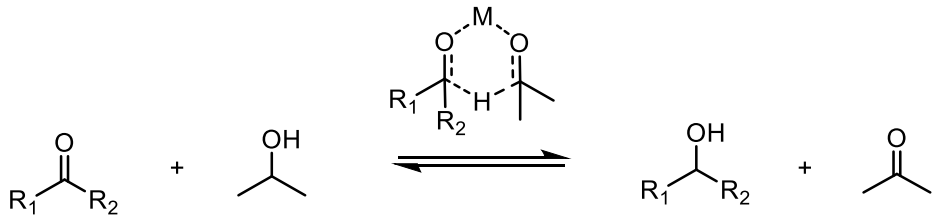

Scheme 17 – Example of transfer hydrogenation reactions involving the reduction of a ketone with *2-propanol*. On top of the equilibrium arrows, the proposed transition state according to the Meerwein, Ponndorf, and Verley (MVP) mechanism.

The first TH reaction was reported in 1925 by Meerwein, [135] Ponndorf,[136] and Verley (MVP) and is driven by the addition of a stoichiometric amount of aluminum alkoxides. Despite the disadvantage of the stoichiometric process, the MVP reduction found industrial applications in the synthesis of fine chemicals and in the fragrance industry.[97] Since the discovery of TH, other promoters have been discovered, and a considerable effort has been applied to develop a catalytic process. In the 1960s, the first late-transition metal complex was used as a catalyst for MPV reduction, and by the 1970s, the *triphenylphosphine dichloro ruthenium(II)* complex was employed in the reduction of α,β-unsaturated ketones.[137] The turning point was reached in the 1990s with the discovery that catalytic amounts of base enhanced the reaction rate by a factor of 10^3 - 10^4,[138] and shortly after, by the development of the asymmetric TH.[91,92,139] Current state-of-the-art catalysts display turnover frequencies (TOF) in the order of 10^5 h^{-1}.[140,141] Notable examples include the catalyst Yu developed, reaching a TOF of 114 000 h^{-1} in the reduction of acetophenone.[142] Similarly, Kühn reported a slightly higher TOF of 140,000 h^{-1} under the same conditions,[143] a value further improved to 500,000 h^{-1} with a recently developed catalyst.[144]

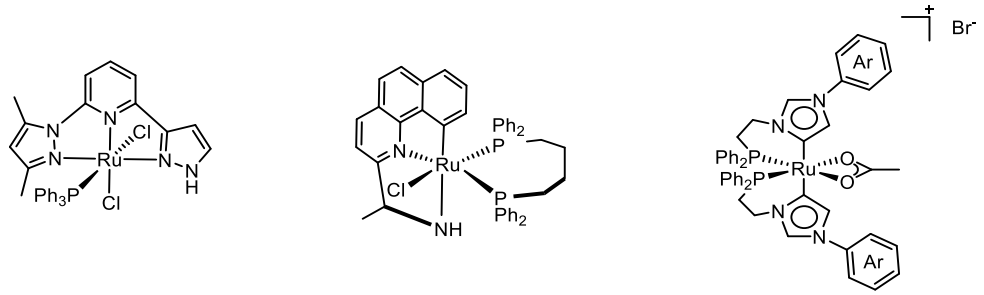

Figure 38 – The structure of prominent current state-of-the-art TH catalysts.

The continuous improvement in catalyst design proved crucial to achieving low catalyst loading and high reactivity, and since different reaction mechanisms are possible for TH, structurally diversified catalysts were conceived to leverage different strategies in driving the reaction. Aside from the MVP mechanism, which still finds some examples in modern catalyzed TH reactions, all the other proposed mechanisms involve the formation of ruthenium(II) hydrides. These ruthenium(II) hydride species are generally generated via β-hydride elimination after a hydride source coordinates with the metal complex. Once the reactive ruthenium(II) hydride is formed, the reaction commonly proceeds via three possible mechanisms: 1) the inner-sphere monohydride mechanism, 2) the outer-sphere ligand-assisted mechanism, and 3) the inner-sphere dihydride mechanism (Figure 39).[88] Conventionally, catalysts exploiting the outer sphere ligand-assisted mechanism outperform others following the inner-sphere mechanism. However, the recent examples reported by Kühn considerably narrowed the reactivity gap.

Figure 39 – The TH reaction has different possible reaction mechanisms, and here, four examples of the key reaction steps involving the hydride transfer have been reported. From left to right, 1) inner sphere, 2) inner sphere ligand assisted, 2) outer sphere, 3) outer sphere ligand assisted.

The reduction of *acetophenone* is a standard benchmark reaction for the catalytic TH, and correspondingly, it was chosen to evaluate the catalytic performances of the synthesized complexes. The reaction conditions were selected based on previously published work and have been reported in Sections 4.21 and 4.21, alongside an accurate description of how reagents were processed prior to use (Scheme 18).

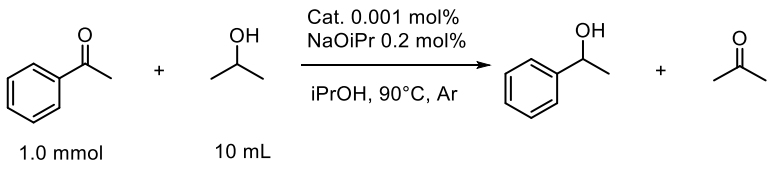

Scheme 18 – Reaction scheme summarizing the reaction conditions employed in the catalytic TH of *acetophenone*.

Before effectively testing the catalysts, a control reaction in their absence was performed to define baseline reactivity. *Acetophenone* (117 uL, 0.1 mmol) was placed at reflux in *2-propanol* (10 mL), and *sodium isopropoxide* (200 uL, 0.1 M) was added to the solution. After five days, the reaction was incomplete, with the solution turning pale brown from colorless. Nevertheless, no side products were detected via ^{1}H NMR spectroscopy, and the conversion of *acetophenone* to *1-phenylethanol* accounted for 80%. Performing the same reaction under non-inert conditions did not yield different results. In order to evaluate the catalyst performance, the TOF value was calculated for each reaction, defined as the conversion per mole of catalyst per hour at 50% conversion. The results have been reported in Table 2.

Table 2 – Summary of the catalytic results obtained by testing the synthesized catalysts in the TH reaction (the reaction protocol is disclosed in Section 4.22).

Complex	Temperature	Catalyst loading	TOF	Conversion	Time
[Codename]	[°C]	[%]	[h-1]	[%]	[h]
trans-Ru(bisNHC)(Bipy)$(ACN)_2(PF6)_2$ (**9a**)	90	0.1	4286	95	2
trans-Ru(bisNHC)(AMPY)$(ACN)_2(PF6)_2$ (**11**)	90	0.1	2000	99	3
trans-Ru(bisNHC)(EN)$(ACN)_2(PF6)_2$ (**12**)	90	0.1	1000	90	24
trans-Ru(bisNHC)(dppp)$(ACN)_2(PF6)_2$ (**13**)	90	0.1	100	95	8
cis-Ru(bisNHC)(Bipy)$(ACN)_2(PF6)_2$ (**10**)	90	0.1	50000	90	24
cis-Ru(bisNHC)(dppp)$(ACN)_2(PF6)_2$ (**14**)	90	0.1	2000	95	8
cis-Ru(bisNHC)(Bipy)$(ACN)_2(PF6)_2$ (**10**)	90	0.01	1000	50	2
White	90	0.1	10	80	128

The first set of catalytic tests was conducted with the *trans*-complexes. All reactions reached total conversion within 24 h, with the *2,2'-bipyridine* complex displaying the highest TOF at 4286h^{-1}. This is an unexpected result, as the complexes bearing amino groups are commonly acknowledged to

significantly improve the reactivity in TH by taking advantage of the outer sphere ligand-assisted mechanism. The catalytic tests were repeated using the two available *cis*-complexes. The TOF considerably improved for both the bis(phosphine) and *2,2'-bipyridine* complexes. The TOF's one-fold increase for both catalysts suggests that the *cis*-complex is more reactive, as one would expect if the reaction follows the inner-sphere mechanism. Moreover, the experimental results highlight that the isomerization reaction between the *cis*-kinetic and *trans*-thermodynamic isomers does not appreciably take place under catalytic conditions. The *cis-(diacetonitrile)(2,2'-bipyridine) [1,1-Bis(3'-methyl-imidazol-2'-ylidene)methylene] ruthenium(II) dihexafluorophosphate* (**10a**) is very active in the TH reaction when compared to the few available examples of complexes bearing similar bis(NHC) ligands (Section 1.4). A direct comparison is not trivial as the authors did not calculate a TOF values, but limited to report the time when the reaction reached completion. In general, piano-stool ruthenium(II) complexes featuring bis(NHC) ligands have exhibited either inactivity or required several hours to achieve reaction completion.[69,132] Another category of ruthenium(II) catalysts, employing distinct bis(NHC) ligands as developed by Xue et al., has demonstrated higher reactivity.[122] However, even the fastest catalyst operating under similar reaction conditions requires more than 40 minutes to reach completion, against our *2,2'-bipyridine* catalysts which requires less than 20 minutes. Notably, the conversion is limited to 91% of the initial acetophenone, while our catalysts achieve conversions of up to 99% In conclusion, the *cis-(diacetonitrile)(2,2'-bipyridine) [1,1-Bis(3'-methyl-imidazol-2'-ylidene)methylene] ruthenium(II) dihexafluorophosphate* (**10a**) is the most active complex in the TH reactions among the tested catalysts, and, to the best of our knowledge, the fastest ruthenium(II) complex bearing bis(NHC) a ligand in TH.

2.9 Catalytic application in direct C-H arylation

Chemical transformations involving the formation of novel carbon-carbon bonds, also known as C-C coupling reactions, are critical for synthesizing complex molecules. Conducting reactions within this specific class utilizing ruthenium(II) complexes as catalysts poses considerable challenges due to the unique electronic configuration of the metal, as these complexes are usually characterized by an octahedral geometry and a low spin d^6 configuration.[145] The complexes thus feature a low-lying set of fully occupied $t2_g$ orbitals and a higher-lying set of empty e_g orbitals, increasing stability and accounting for the unreactive nature. In recent years, innovative reaction protocols have emerged for direct arylation reactions, leading to the synthesis of bi-aryls through the application of ruthenium(II) complexes.[145,146,147] These protocols are strategically designed to incorporate a directing group within the substrate, facilitating its coordination with the metal. The utilization of a directing group in the direct arylation not only enhances selectivity but also enables the late-stage functionalization of complex molecules, thereby improving the overall atom economy.[148] A common approach in synthesizing bi-aryl compounds involves employing substrates with amino branches capable of coordinating with the metal. This coordination induces C-H activation through cyclometallation, activating the metal complex for subsequent oxidative addition with an aryl halide. The resulting transient species undergo reductive elimination, forming the desired bi-aryl compound (Scheme 19).[148]

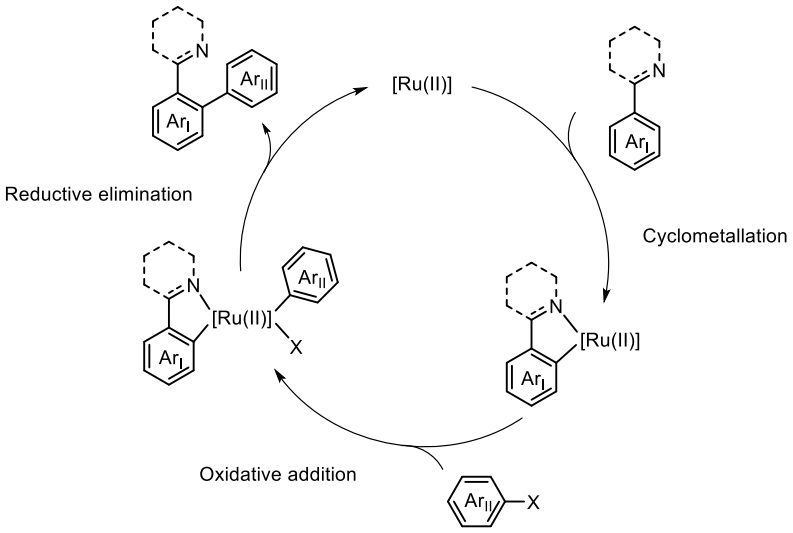

Scheme 19 – General reaction mechanism of the ruthenium(II) catalyzed C-H arylation. A more detailed version is proposed for the present work in Section 4.23.

Different research groups have documented various examples of catalysts promoting these reactions. Broadly, two classes of ruthenium(II) complexes have been recognized as effective catalysts for this process: 1) ruthenium(II) piano stool complexes and 2) ruthenium(II) organonitrile complexes (Figure 40). [147–154]

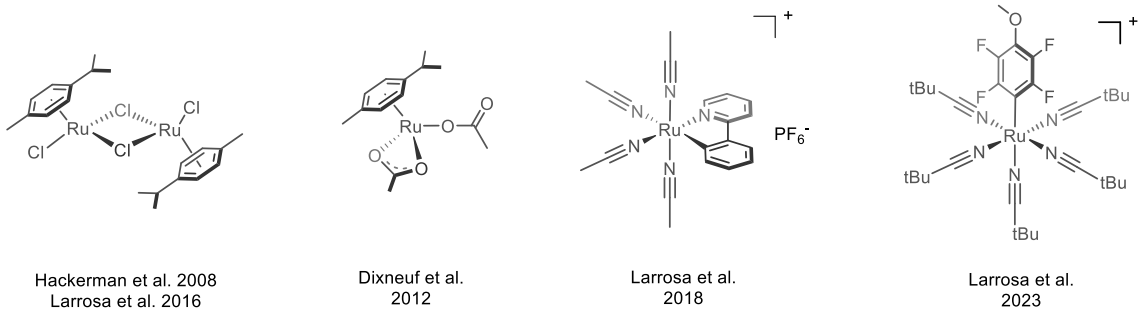

Figure 40 - Examples of current state-of-the-art catalysts for the arylation of C-H bonds.

In this regard, the dicationic *tetrakis(acetonitrile)[1,1-Bis(3'-methylimidazol-1'-ylidene)methylene] ruthenium(II) dihexafluorophosphate* (**4x**) complex early presented (Section 2.3) is an ideal candidate as a catalyst to employ in the direct C-H arylation reaction. The dicationic nature of the complex should promote cyclometallation, which, alongside the inherent strong σ-donor character of the bis(NHC) ligand, should produce an electron-rich complex capable of undergoing oxidative addition. This hypothesis was tested by probing the reactivity of *tetrakis(acetonitrile)[1,1-Bis(3'-methylimidazol-1'-ylidene)methylene] ruthenium(II) dihexafluorophosphate* (**4x**) in the direct C-H arylation of *2-phenylpyridine* using *iodobenzene* (Scheme 20).

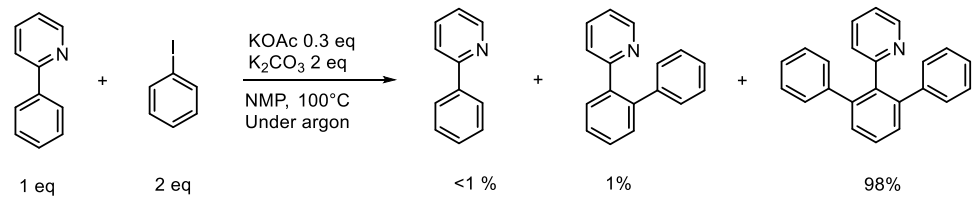

Scheme 20 – The general reaction scheme of the direct C-H arylation of *2-phenylpyridine* with *iodobenzene*. The general reaction conditions employed to achieve reaction completion have been summarized in the scheme. Notice that the monoarylated compound was not detected, if not as a trace.

The compound *2-phenylpyridine* was selected as a substrate due to the pyridine fragment's effective directing properties in facilitating the reaction's cyclometallation step, while *iodobenzene* was chosen as a substrate because it lacks activation towards oxidative addition. The reactivity test was conducted following common reaction conditions reported in the literature, summarized in Table 3.

Table 3 - Summary of the conducted catalytic tests. The ratio between *2-phenylpyridine* and *iodobenzene* was varied according to the table (Column 3). The acetate was added relative to *2-phenylpyridine* moles, and 3 eq of *potassium carbonate* were always added. Further information is available in Section 4.23.

Entry	Catalyst loading	Ar/ArX	Temperature	KOAc	Yield	Time
[num]	[%]	[ratio]	[°C]	[eq]	[%]	[h]
1	10.0	1:1	35	0.30	8	24
2	10.0	1:1	120	0.30	50	36
3	10.0	1:2	120	0.30	99	24
4	10.0	1:2	70	0.30	40	36
5	2.5	1:2	100	0.30	97	12
6	2.5	1:2	100	0.03	7	24
7	2.5	1:2	100	1.00	22	24
8	2.0	1:2	100	0.30	98	12
9	1.0	1:2	100	0.30	35	12

The initial reactivity trials were conducted at 35°C with a stoichiometric amount of reagents, aiming to assess selectivity. At this temperature and with a 10% catalyst loading, the reaction exhibited limited conversion, and no observable progress occurred. Subsequently, the experiment was repeated at 120°C with the same loading, leading to the complete consumption of *iodobenzene*. Notably, the reaction displayed selectivity towards the diarylated compound, as no monoarylated product was detected via NMR spectroscopy. This suggests that either the intermediate monoarylated product does not undergo cleavage after the initial arylation or, if it does, the local molar concentration prevents competition with unsubstituted *2-phenylpyridine*. Recognizing the inaccessibility of the monoarylated product under these conditions, the substrate ratio was increased, resulting in the total conversion of *2-phenylpyridine* to *2-[(2',6'-diphenyl)phenyl]pyridine* and yielding a satisfactory 98% yield under the same reaction conditions. The product was isolated for NMR characterization through flash column chromatography. The reaction crude was diluted with a 9:1 mixture of *pentane* and *ethyl acetate* and charged as a liquid in the column. *NMP* eluted in the head fraction, while the product, *2-[(2',6'-diphenyl)phenyl]pyridine* (R_f = 0.60), was isolated after collecting *2-phenylpyridine* traces (R_f = 0.65). Moreover, a tentative trial was carried out to isolate a cyclometallated intermediate. Unfortunately, placing the ruthenium(II) complex alongside *2-phenylpyridine* in deuterated *acetone* at reflux and in presence of *potassium acetate* did not yield the desired complex. Concluding the catalytic tests, a successful reduction in catalyst loading from 10% to 2% at a temperature of 100°C was achieved, leading to complete conversion within less than 12 hours. However, further reduction in the loading resulted in an incomplete reaction. Upon comparison with literature results, *tetrakis(acetonitrile)[1,1-Bis(3'-methylimidazol-1'-ylidene)methylene] ruthenium(II) dihexafluorophosphate* (**4x**) is placed among the fastest.[147–154] Notably, despite the elevated operating temperature, the catalyst demonstrates remarkable efficiency with a relatively low loading, in contrast to numerous examples found in the

literature that typically range from 2.5% to 10%. The catalytic process achieves completion in less than 12 h, a noteworthy improvement when compared to the average of 24 h reported in the literature. It is worth highlighting that the fastest-known catalyst, developed by Larrosa et al., to the best of the author's knowledge, accomplishes the same reaction in under 6 h at 35°C with comparable loadings.[146,157]

2.10 Design, synthesis, and coordination of a novel bis(triazole) ligand

In the present work, the leading synthetic effort was focused on introducing different bidentate ligands to the *tetrakis(acetonitrile)[1,1-bis(3'-methylimidazol-2'-ylidene)methylene]ruthenium(II) dihalide* (**4x**) complex while keeping the same bis(imidazolium) as bis(NHC) precursor in all the syntheses. As stated in the introduction (Section 1.2), expanding the bis(NHC) ligand scope is challenging due to the concerted effects of the wingtip's steric hindrance and bridge length on the complex geometry. The *(1,5-cyclooctadiene)(dichloro)ruthenium(II) polymer* (**7**) and the related organonitrile complexes may accommodate more sterically demanding bis(NHC) ligands when compared to less reactive and sterically hindered ruthenium(II) systems. However, it might come at the cost of complicating further functionalization processes. Within this context, we sought the development of a new bis(NHC) ligand that should feature 1) increased steric bulkiness without affecting the other complex coordination sites and 2) increased σ-donors capabilities. Mesoionic carbenes, in particular 1,2,3-triazoles, are well-suited for this purpose, as they possess the optimal geometry to accommodate bulky wingtip substituents without directly interfering with other ligands in the trans position, and they are stronger σ-donors than nNHCs. Numerous synthetic routes for 1-substituted-1,2,3-triazoles and their coordination with various transition metal compounds are well-documented in the literature. However, to the best of our knowledge, there are no reported examples of N-bridged bis(1,2,3-triazolium) salts. A widely used strategy for accessing 1-substituted-1,2,3-triazoles consists of synthesizing aryl azides from the corresponding substituted anilines and, subsequently, performing a copper-catalyzed azide-alkyne cycloaddition (CuAAC, Scheme 21) with an alkyne. In this synthetic pathway, it is noteworthy that the steric hindrance of the aryl azide has a significant impact on the CuAAC reaction. As a result, we have opted for *mesitylamine* as the starting material, a compromise between the bulky *2,6-diisopropylaniline*, and the more explosive *phenylazide*, as per the rule of six.[158]

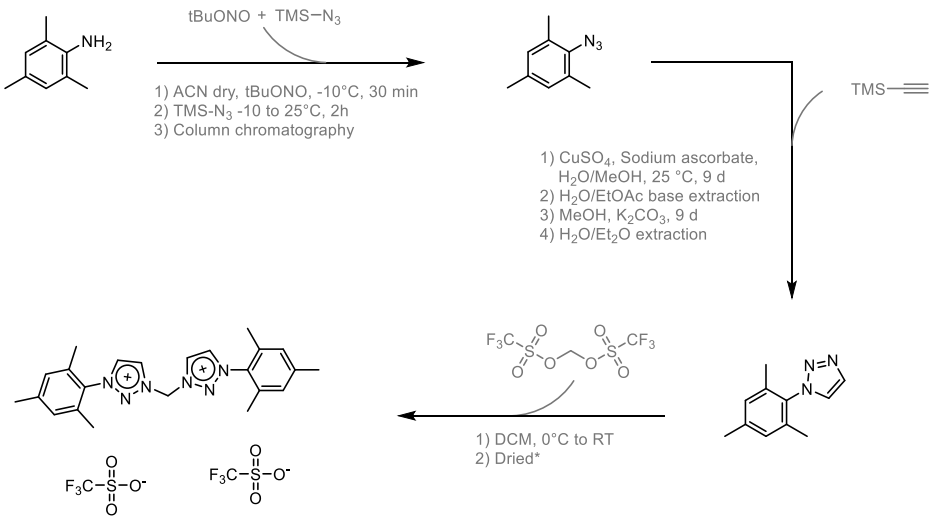

Scheme 21 – Synthetic route to access *1,1-bis(1'-mesityl-1',2',3'-triazolium) methylene ditrifluromethanesulfonate* from mesitylamine as starting material.

Hence, following the established literature procedure, the synthesis of *1-mesityl-1,2,3-triazole* was successfully accomplished. However, a new protocol was required to produce the corresponding bis(triazolium) salt. The primary challenge in linking two triazoles lies in the fact that triazoles exhibit lower nucleophilicity when compared to imidazoles. As a result, achieving a successful nucleophilic substitution with alkyl dihalides would require harsh conditions to activate the substrate. Preliminary experiments were conducted by reacting *1-mesityl-1,2,3-triazole* (320 mg, 1.8 mmol) with *diiodomethane* or 1*,3-dibromopropane* in *THF* (15 mL) within a pressure tube at 120°C. Unfortunately, this initial attempt did not yield the desired product, suggesting the need for a more suitable leaving group. Following precedents in the literature, the same reaction was repeated using *methylenebistriflate* (267 mg, 0.9 mmol) in *DCM* (15 mL). This modification led to the formation of the desired product, *1,1-bis(1'-mesityl-1',2',3'-triazolium) methylene ditrifluromethanesulfonate*, which was subsequently isolated by solvent removal. The new compound was characterized via NMR spectroscopy (Section 4.16). The heterocycles -CH bonds are considerably acidic compared to bis(imidazolium) salts, as confirmed by the considerable downfield shift (Figure 41).

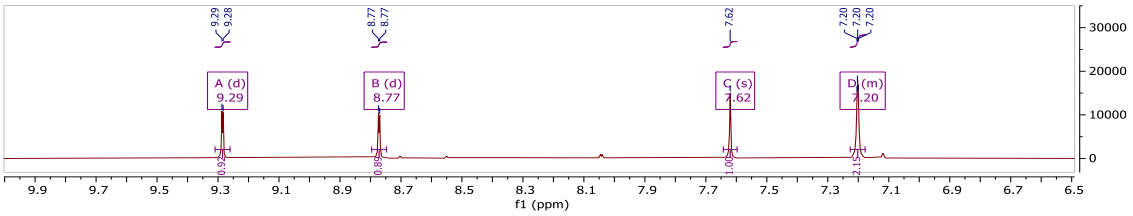

Figure 41 - A fragment of the ^{1}H NMR spectrum of *1,1-bis(1'-mesityl-1',2',3'-triazolium) methylene ditrifluromethanesulfonate* showing the signal in the aromatic region (*CD_2Cl_2*). The peaks on the left side have been assigned to the 1,2,3-triazole -CH moieties, while the remaining two have been assigned respectively to the methylene bridge and the mesitylene aromatic signals.

The methylene -CH_2- bridge signal's chemical shift falls at 7.62 ppm, while the same signal in standard bis(imidazolium) salts falls at around 6.20 ppm. Moreover, the signal is broader, signaling that some form of chemical exchange may be taking place, and the increased acidity of this proton raises concerns about the stability of the ligand under basic conditions.

The ligand's practical capability of coordinating to a metal center was inquired in the synthesis of ruthenium(II) complexes, following the developed reaction protocol (Scheme 22).

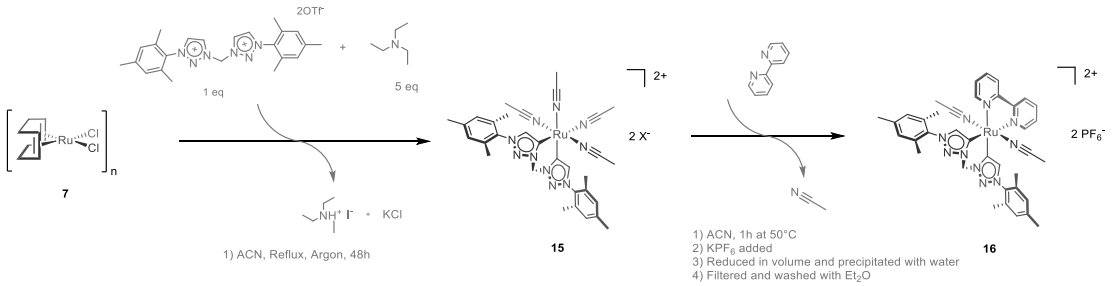

Scheme 22 – The synthesis of *trans-(diacetonitrile) (2,2'-bipyridine) [1,1-Bis(3'-mesytil-1',2',3'-triazol-5'-ylidene)methylene] ruthenium(II) dihexafluorophosphate* (**16**).

A mixture containing *(1,5-cycloctadiene) dichloro ruthenium(II) polymer* (**7**) (84 mg, 0.30 mmol), *1,1-bis(1'-mesityl-1',2',3'-triazolium) methylene ditrifluromethanesulfonate* (220 mg, 0.30 mmol), TEA (200 uL, 1.50 mmol) and *ACN* (4 mL) was left reacting for 48h. The formation of *tetrakis(acetonitrile)[1,1-Bis(3'-mesytil-1',2',3'-triazol-5'-ylidene)methylene]ruthenium(II) ditrifluoromethanesulfonate* (**15**) was witnessed via ^{1}H NMR spectroscopy, by the disappearance of the bis(triazolium) salt most acidic proton. Subsequently, the addition of *2,2'-bipyridine* (46 mg, 0.3 mmol) and *potassium hexafluorophosphate* (110 mg, 1.20 mmol) to resulted in the formation of *trans-(diacetonitrile) (2,2'-bipyridine) [1,1-Bis(3'-mesytil-1',2',3'-triazol-5'-ylidene)methylene] ruthenium(II) dihexafluorophosphate* (**16**) (70% yield). The isolated complex was extensively characterized using NMR spectroscopy (Section 4.17). The presence of a ruthenium-carbene bond was confirmed through the observation of a distinctive peak at 177 ppm in the ^{13}C NMR spectrum. Notably, the chemical shift of this signal appears more upfield compared to previously reported metal-coordinated triazoles, suggesting that the new ligand has a weaker σ-donor character. Furthermore, when compared to the closely related *trans-(diacetonitrile) (2,2'-bipyridine) [1,1-Bis(3'-methyl-imidazol-2'-ylidene)methylene] ruthenium(II) dihexafluorophosphate* (**9a**), where the carbene signal is observed at 184 ppm, it becomes apparent that the metal center in the newly formed complex is relatively electron-deficient. This observation is supported by the shift in the chemical shift of the coordinated *2,2'-bipyridine* ligand, which shifted from 9.05 ppm in the bis(imidazole) complex to 9.42 ppm in the bis(triazole) complex.

3 CONCLUSIONS AND OUTLOOK

A novel synthetic pathway was developed to synthesize dicationic organonitrile ruthenium(II) complexes featuring bis(NHC) ligands, of which few examples exist in the literature. To assess the accessibility of these compounds, a preliminary investigation was conducted involving screening reactions, which highlighted the non-trivial nature of coordinating bis(NHC) ligands to common ruthenium(II) precursors. Starting from the complex *(p-cymene)(dichloro)ruthenium(II) dimer* (**7**), a synthetic route was established to yield the *tetrakis(acetonitrile) [1,1-Bis(3'-methyl-imidazol-1'-ylidene)methylene] ruthenium(II) ditetrafluoroborate* (**4a**) complex. This organonitrile complex exhibited high reactivity towards nucleophilic substitution of the weakly bound ACN ligands, even under mild conditions, enabling further functionalization with LL-type ligands. However, substituting the remaining ACN ligands posed a more significant challenge, necessitating the use of harsher conditions, likely due to a sluggish isomerization process. Decided that the organonitrile complex could be an ideal platform for catalyst development, a novel synthetic method was designed to obtain the closely related *tetrakis(acetonitrile) [1,1-Bis(3'-methyl-imidazol-1'-ylidene)methylene] ruthenium(II) dihexafluorophosphate* (**4b**) complex. The new protocol involves starting from the alicyclic *(1,5-cyclooctadiene)(dichloro)ruthenium(II) polymer* (**7**) and leveraging on cyclooctadiene's lability. Furthermore, the role of the base was investigated, revealing that *TEA* plays an active role by coordinating with the metal center and acting as an internal base, effectively driving the reaction. The *ACN* also plays a crucial role both as solvent and ligand, stabilizing the reactive intermediates, while keeping the coordination sites of the metal accessible by being involved in a dynamic equilibrium with the other reagents. To investigate the reactivity of *tetrakis(acetonitrile) [1,1-Bis(3'-methyl-imidazol-1'-ylidene)methylene] ruthenium(II) dihexafluorophosphate* (**4b**), we synthesized four organonitrile complexes using *2,2'-bipyridine, 2-picolylamine*, *1,2-ethylenediamine*, and *1,3-bis(diphenylphosphino)propane* as ligands. Subsequently, we achieved the transformation from kinetic trans products to thermodynamic cis products in the complexes involving *2,2'-bipyridine* and *1,3-bis(diphenylphosphino)propane* ligands through a thermal isomerization reaction. Overall the processes demonstrated high favorability, yielding an average final yield of 75% for the trans products, and 60% for the cis products.

All of the synthesized complexes were subjected to testing in the TH reaction, and, with the exception of *cis-(diacetonitrile)(2,2'-bipyridine) [1,1-Bis(3'-methyl-imidazol-1'-ylidene)methylene] ruthenium(II) dihexafluorophosphate* (**10a**), the compounds exhibited comparatively lower performance against state-of-the-art catalysts. Despite being in the early stages of development, the maximum TOF of 50,000 h^{-1} achieved with the cis 2,2'-bipyridine complex stands as a remarkable outcome. Notably, within the pool of reported ruthenium(II) complexes featuring bis(NHC) ligands, this complex demonstrates exceptional speed, marking it as one of the fastest known.

In conclusion, this study concerned the synthesis of novel ruthenium(II) bis(NHC) organonitrile complexes and highlights their accessibility with the development of an efficient reaction protocol that relies on commercially available compounds. Additionally, the highly reactive nature of the *tetrakis(acetonitrile) [1,1-Bis(3'-methyl-imidazol-1'-ylidene)methylene] ruthenium(II) dihexafluorophosphate* (**4b**) complex is of particular interest, as, due to its exceptional reactivity, the complex may serve as a promising chemical platform for developing new branches of ruthenium(II) coordination compounds. In this regard, the early stage of development of these complexes opens several promising directions for future research. From the synthetic point of view, the ligand scope is currently limited to bidentate L-type ligands, and its expansion could prove essential in widening the catalytic applications of these species. For instance, introducing cyclometallated ligands would reduce the complex's formal charge. Furthermore, considering the ligand environment, replacing the weakly bound ACN with anionic ligands, such as halides or bidentate acetate, may enhance the stability of the synthesized complexes. Moreover, while there are a few documented examples of ruthenium(II) bis(bis(NHC)) complexes in the literature, our initial attempts following the developed synthetic protocol did not yield the desired compounds in significant quantities, and further investigation will be required. Additionally, beyond synthesis, the catalytic potential of these complexes has been narrowly explored. Starting with TH, a broader substrate scope should be explored by testing the catalysts in reducing molecules of interest, such as biomass-derived compounds, or in the late-stage transformation of pharmaceutical ingredients. A protocol for the closely related Oppenauer oxidation reaction should also be developed. Furthermore, *tetrakis(acetonitrile) [1,1-Bis(3'-methyl-imidazol-1'-ylidene)methylene] ruthenium(II) dihexafluorophosphate* (**4b**) proved active in the -CH arylation of biaryls, catalyzing the orto-diarylation of *2-phenylpyridine* in under 24 h, with low catalyst loading. This is a reaction of interest, given that this transformation is a cost-effective strategy for building these structural motifs instead of traditional cross-coupling reactions. Finally, the strong σ-donating ligand environment, alongside the improved stability exhibited by these complexes under oxidative conditions, in contrast to their phosphine analogs, could stabilize the high oxidation state of ruthenium despite the complex charge. This would potentially open at homogeneously catalyzed oxidation reactions, a rapidly growing field given the sensitivity of related environmental aspects, with critical applications concerning the functionalization of the unreactive polyolefins in commodity plastics, [159] and the procurement of sustainable energy via the water oxidation reaction.

4 EXPERIMENTAL PART

4.1 Material and apparatus

- All reactants have been purchased from Merk® (formerly Sigma-Aldrich®) and used as delivered if not otherwise stated.
- The employed Schlenk techniques are discussed in the literature.[160]
- The ^{1}H NMR spectra were acquired using a Bruker Avance III HD 400 MHz spectra equipped with a broadband 5 mm probe (^{1}H/BBF iProbe) with a z-axis gradient (50 G/cm).

4.2 Materials and apparatus for the synthesis of ruthenium(II) complexes

- 10, 25, 50, and 100 mL Schlenk tubes equipped with Rotaflo stopcocks, glass stoppers, and Glindemann O-rings.
- Schlenk tube equipped with Gooch G3 filter.
- Schlenk line connected to a vacuum pump capable of reaching a 10^{-3} mbar pressure.
- Airtight Hamilton syringes (100 uL, 500 uL, 1 mL, and 5 mL).
- Neutral deactivated alumina was obtained by adding 9 mL of water to 300 g of neutral alumina.
- The solids were accurately dried under vacuum before use.
- All the liquids were freeze-pump-towed (FPT) to remove oxygen before addition, except for the solvents employed in flash column chromatography (if not otherwise stated).
- Acetonitrile purification: 1) Treated with *calcium hydride* overnight, 2) fractionally distilled under argon, 3) FPT.
- Isopropyl alcohol purification: 1) Treated with *calcium hydride* overnight, 2) fractionally distilled under argon, 3) FPT.

4.3 Synthesis of 1,1-bis(3'-methylimidazolium)methylene diiodide

Procedure

The synthesis of *1,1-bis(3'-methylimidazolium)methylene diiodide* is known, and a literature available procedure was followed.[161] A 15 mL pressure tube was charged with 3.88 mL (48.0 mmol, 2 eq) of *1-methylimidazole*, 2.0 mL (24 mmol, 1 eq) of *diiodomethane* and 8 mL of *tetrahydrofuran (THF)*. The tube was sealed and placed in an oil bath at 120 °C under stirring. After 24 h, the product was removed from the bath, and the white powder precipitated was filtered over Gooch. The solid was washed with *THF* (2 x 5 mL), *pentane* (3 x 5 mL) and dried under vacuum (80% yield).

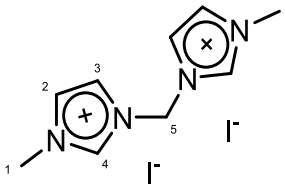

Figure 42 - The structure of *1,1-bis(3'-methylimidazolium)methylene diiodide*.

Characterization

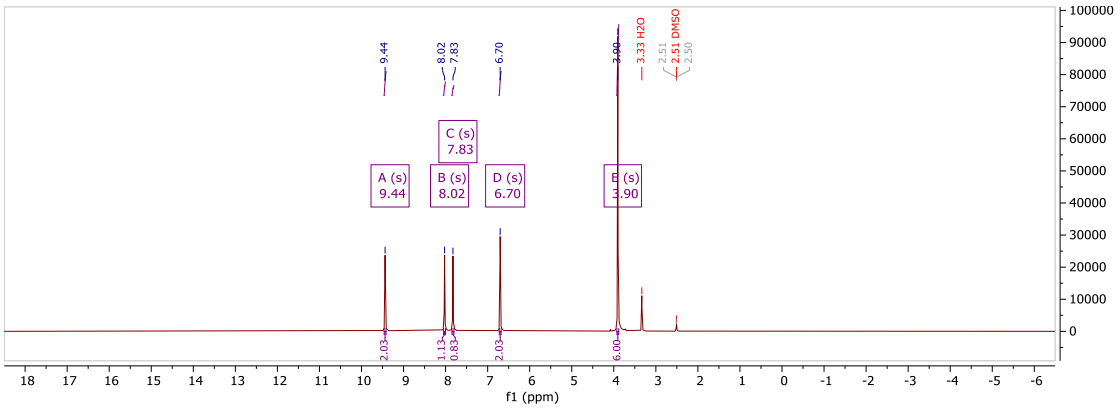

Spectrum 1 - ^{1}H NMR spectrum of *1,1-bis(3'-methylimidazolium)methylene diiodide*.

$C_9H_{16}N_4I_2$: ^{1}H NMR(C_2D_6OS, 400MHz): δ 9.44 (s, 2H, **4**), 8.02 (s, 1H, **3**), 7.83 (s, 1H, **2**), 6.70 (s, 2H, **5**), 3.90 (s, 5H, **1**).

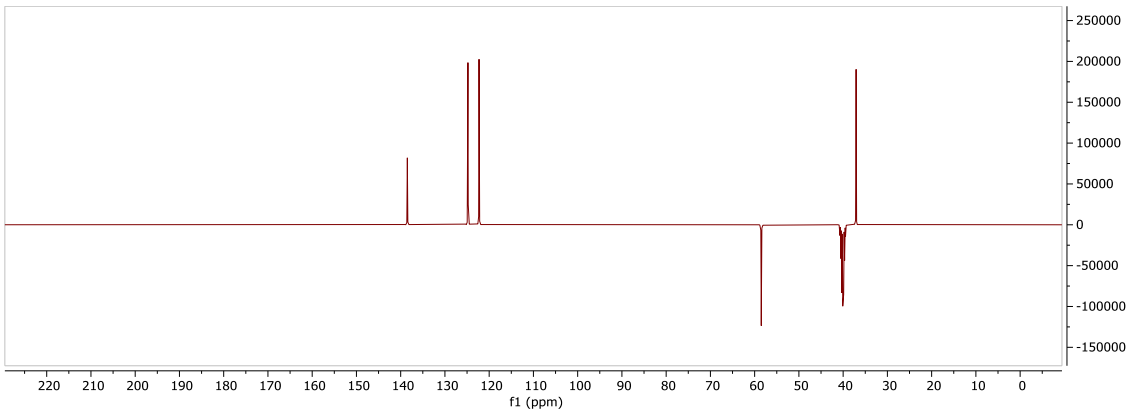

Spectrum 2 - ^{13}C NMR spectrum of *1,1-bis(3'-methylimidazolium)methylene diiodide.*

$C_9H_{16}N_4I_2$: ^{13}C-NMR(C_2D_6OS, 400MHz): δ 138.58 (**4**), 124.88 (**3**), 122.25 (**2**), 58.55 (**5**), 37.02 (**1**).

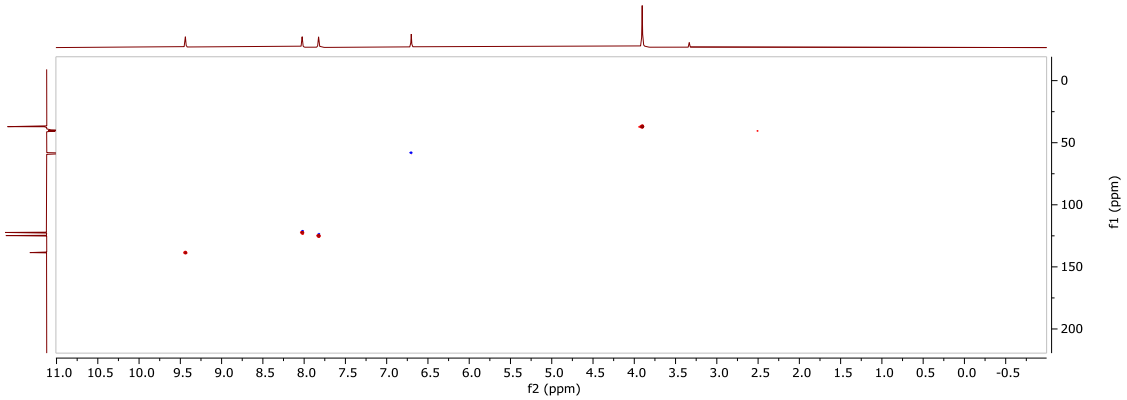

Spectrum 3 - ^{1}H-^{13}C HSQC NMR spectrum of *1,1-bis(3'-methylimidazolium)methylene diiodide.*

4.4 Synthesis of Ru(p-cymene)(b(MI)M)(I)PF_6 (**2**)

Procedure

The synthesis of *1,1-bis(3'-methylimidazolium)methylene diiodide* is known, and a slightly modified procedure was followed.[132] A Schlenk type 250 mL round bottom flask was charged with 1.0 g (1.6 mmol, 1 eq) of *(p-cymene)(dichloro) ruthenium(II) dimer*, 2.0 g (12.0 mmol, 8 eq) of *potassium iodide*, 1.4 g (3.2 mmol, 2 eq) of *1,1-bis(3'-methylimidazolium)methylene diiodide*. The air was removed from the container, cycling vacuum, and argon. Then, 80 mL of dry and degassed ACN were added to dissolve the solids alongside 2.3 mL (16 mmol, 10 eq) of *TEA*. The mixture was left reacting for 16 h, and then the solvent was removed at the rotary evaporator. The product was isolated using gradient flash liquid column chromatography; neutral deactivated alumina was used as the stationary phase while a mixture of *DCM/acetone* was used as eluent, with a ratio spanning from 10:1 to 1:1. To elute the product, *potassium hexafluorophosphate* was added to the eluent after the elution of the first neutral subproducts. The solvent was removed, and the final product was obtained after recrystallization from *methanol* (35% yield).

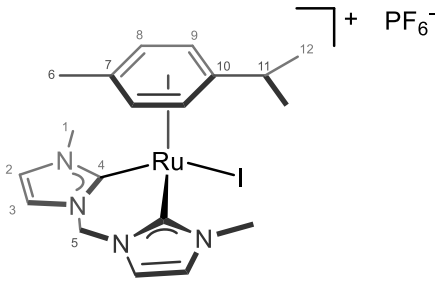

Figure 43 - The structure of *[1,1-Bis(3'-methylimidazol-1'-ylidene)methylene](p-cymene) (iodide) ruthenium(II) hexafluorophosphate.*

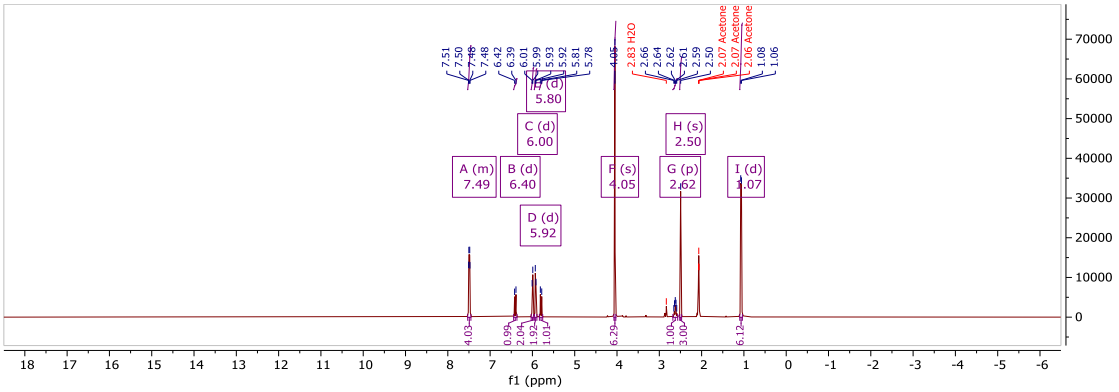

Spectrum 4 - ^{1}H NMR spectrum of *[1,1-Bis(3'-methylimidazol-1'-ylidene)methylene](p-cymene) (iodide) ruthenium(II) hexafluorophosphate.*

$Ru(C_9H_{14}N_4)(C_{10}H_{14})(I)(PF_6)$: ^{1}H-NMR($CD_6O$, 400MHz): δ 7.50 (d, 2H, $^{3}J_{H3-H2}$, 2.15 Hz, **3**), 7.48 (d, 2H, $^{3}J_{H2-H3}$, 2.15 Hz, **2**), 6.40 (d, 1H, $^{2}J_{H5-H5}$, 11.40 Hz, **5**), 5.99 (d, 2H, $^{3}J_{H8-H9}$, 6.90 Hz, **8**), 5.92 (d, 2H, $^{3}J_{H9-H8}$, 6.90 Hz, **9**), 5.79 (d, 1H, $^{2}J_{H5-H5}$, 11.40 Hz, **5**), 4.04 (s, 6H, **1**), 2.62 (hept, 1H, $^{3}J_{H11-H12}$, 6.95 Hz, **11**), 2.50 (s, 3H, **6**), 1.06 (d, 6H, $^{3}J_{H12-H11}$, 6.90 Hz, **12**).

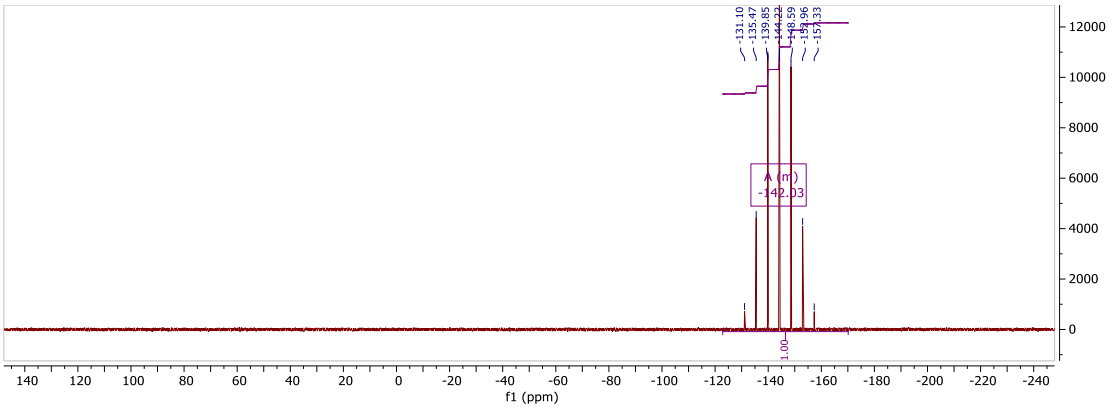

Spectrum 5 - ^{31}P NMR spectrum of *[1,1-Bis(3'-methylimidazol-1'-ylidene)methylene](p-cymene) (iodide) ruthenium(II) hexafluorophosphate.*

$Ru(C_9H_{14}N_4)(C_{10}H_{14})(I)(PF_6)$: ^{31}P-NMR($C_3D_6O$, 400 MHz): δ -144.46 (hept, 2P, ^{1}J= 626.6 Hz).

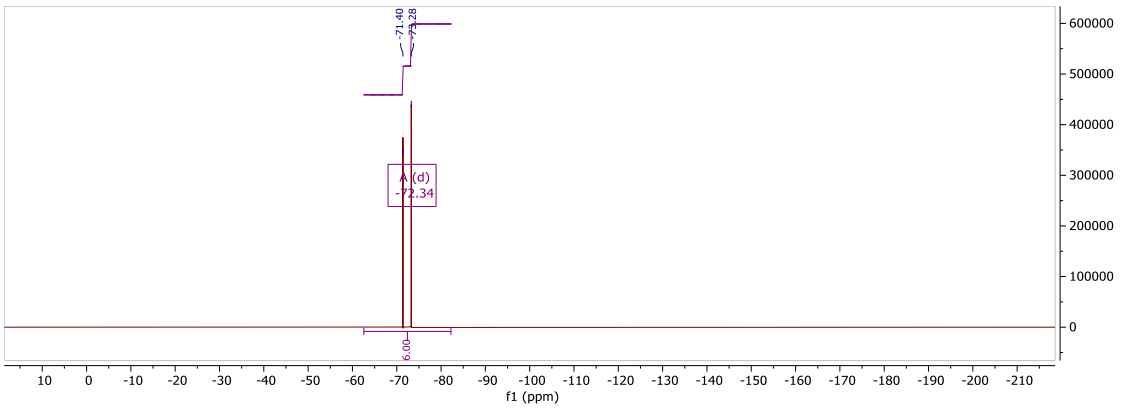

Spectrum 6 - ^{19}F NMR spectrum of *[1,1-Bis(3'-methylimidazol-1'-ylidene)methylene](p-cymene) (iodide) ruthenium(II) hexafluorophosphate.*

$Ru(C_9H_{14}N_4)(C_{10}H_{14})(I)(PF_6)$: ^{19}F-NMR(C_3D_6O, 400 MHz): δ -72.29 (hept, 6F, ^1J= 618.98 Hz).

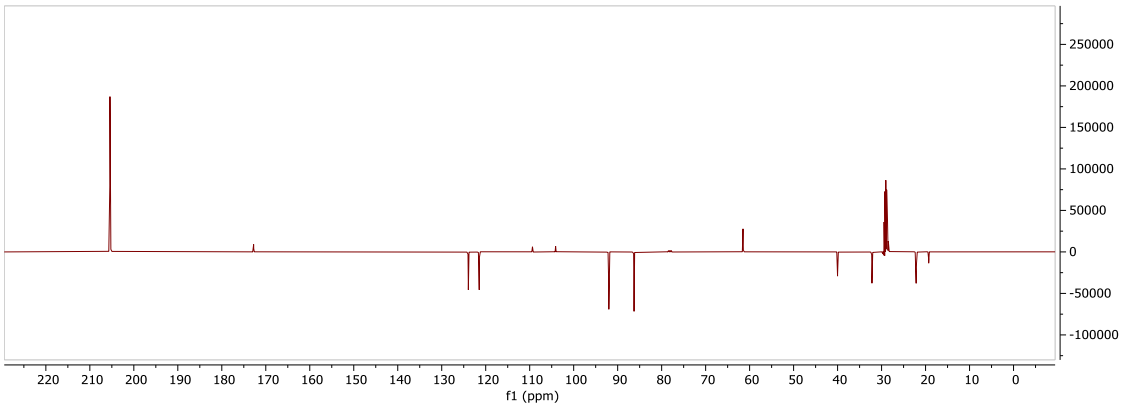

Spectrum 7 - ^{13}C NMR spectrum of *[1,1-Bis(3'-methylimidazol-1'-ylidene)methylene](p-cymene) (iodide) ruthenium(II) hexafluorophosphate.*

$Ru(C_9H_{14}N_4)(C_{10}H_{14})(I)(PF_6)$: ^{13}C-NMR(C_3D_6O, 400 MHz): δ 172.76 (**4**), 123.98 (**2**), 121.34 (**3**), 109.37 (**7** or **10**), 103.80 (**7** or **10**), 92.14 (**8**), 86.34 (**9**), 61.49 (**5**), 39.88 (**1**), 31.98 (**11**), 22.19 (**12**), 19.36 (**6**).

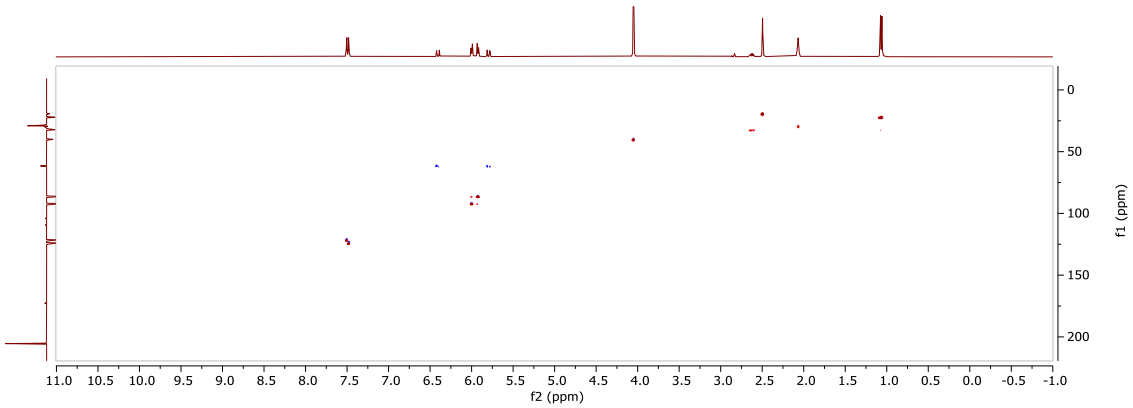

Spectrum 8 - ^{1}H-^{13}C HSQC NMR spectrum of *[1,1-Bis(3'-methylimidazol-1'-ylidene)methylene](p-cymene) (iodide) ruthenium(II) hexafluorophosphate.*

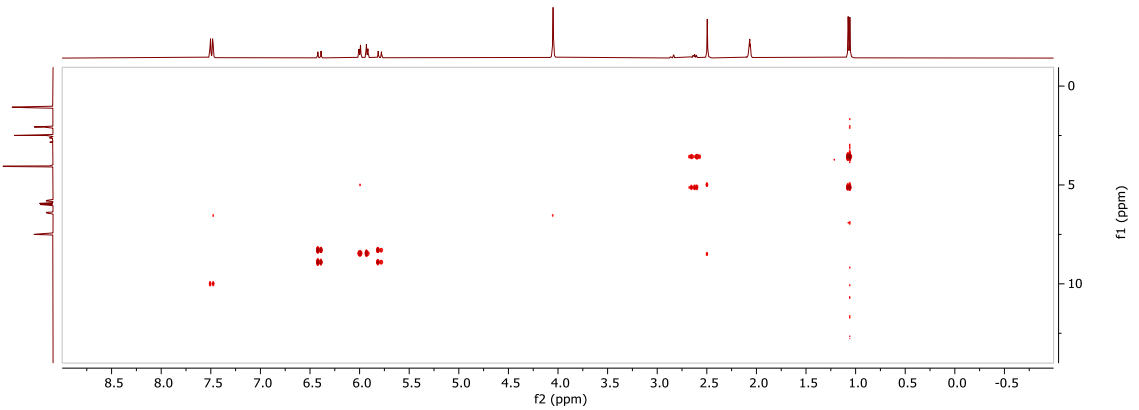

Spectrum 9 - ^{1}H-^{1}H COSY NMR spectrum of *[1,1-Bis(3'-methylimidazol-1'-ylidene)methylene](p-cymene) (iodide) ruthenium(II) hexafluorophosphate.*

4.5 Synthesis of Ru(p-cymene)(b(MI)M)(ACN)(BF_4)$_2$(**3**)

Procedure

A 25 mL Schlenk tube was charged with 150 mg (0.22 mmol, 1 eq) of *[1,1-Bis(3'-methylimidazol-1'-ylidene)methylene](p-cymene) (iodide) ruthenium(II) hexafluorophosphate*. The tube was sealed and placed under an inert atmosphere by cycling vacuum and argon, then 220 mg (1.13 mmol, 5 eq) of silver tetrafluoroborate were added under argon counterflow. Next, 10 mL of dry and degassed *ACN* were added to dissolve the solids, and the tube was placed in an oil bath at the temperature of 45°C. After 12 h, the solution was dried under a vacuum, the product was dissolved in *DCM* (3 x 5 mL), and the residue salts were separated via gooch filtration. The pure product was isolated after removing the solvent and drying the brown solid for 24 h (yield = 80%).

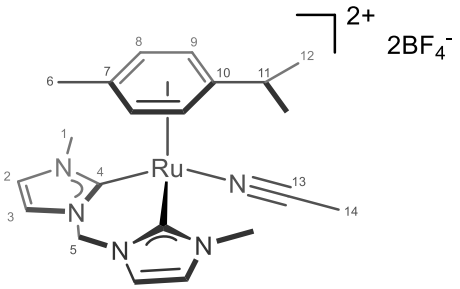

Figure 44 - The structure of *[1,1-Bis(3'-methylimidazol-1'-ylidene)methylene](p-cymene) (acetonitrile) ruthenium(II) ditetrafluoroborate.*

Characterization

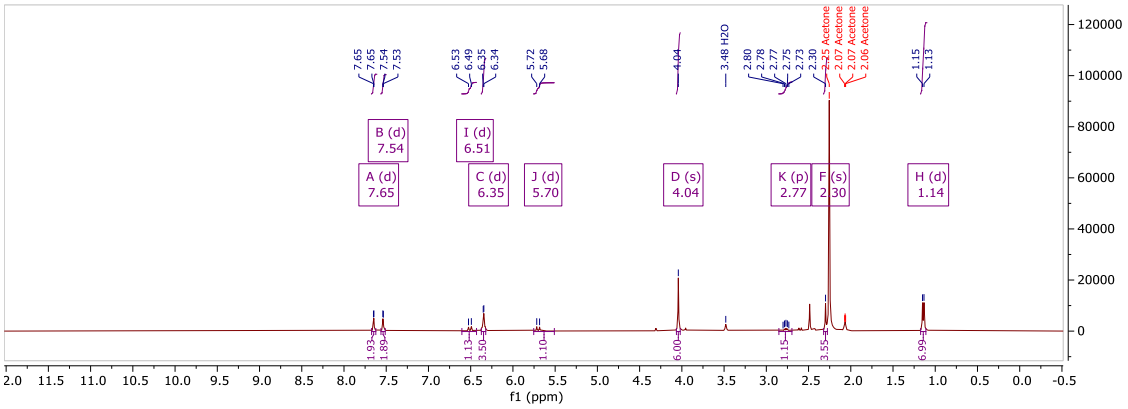

Spectrum 10 - ^{1}H NMR spectrum of *[1,1-Bis(3'-methylimidazol-1'-ylidene)methylene](p-cymene) (acetonitrile) ruthenium(II) ditetrafluoroborate.*

$Ru(C_9H_{14}N_4)(C_{10}H_{14})(CH_3CN)(BF_4)_2$: ^{1}H-NMR($C_3D_6O$, 400MHz): δ 7.64 (d, 2H, $^3J_{H3\text{-}H2}$, 2.20 Hz, **3**), 7.53 (d, 2H, $^3J_{H2\text{-}H3}$, 2.20 Hz, **2**), 6.50 (d, 1H, $^2J_{H5\text{-}H5}$, 13.70 Hz, **5**), 6.34 (m, 2H, **8 + 9**), 5.70 (d, 1H, $^2J_{H5\text{-}H5}$, 13.70 Hz, **5**), 4.04 (s, 6H, **1**), 2.77 (hept, 1H, $^3J_{H11\text{-}H12}$, 6.82 Hz, **11**), 2.48 (s, 3H, **14**), 2.29 (s, 3H, **6**), 1.13 (d, 6H, $^3J_{H12\text{-}H11}$, 6.97 Hz, **12**).

Note: from the 2D NMR experiments, the singlet at 2.25 ppm was assigned to free acetonitrile.

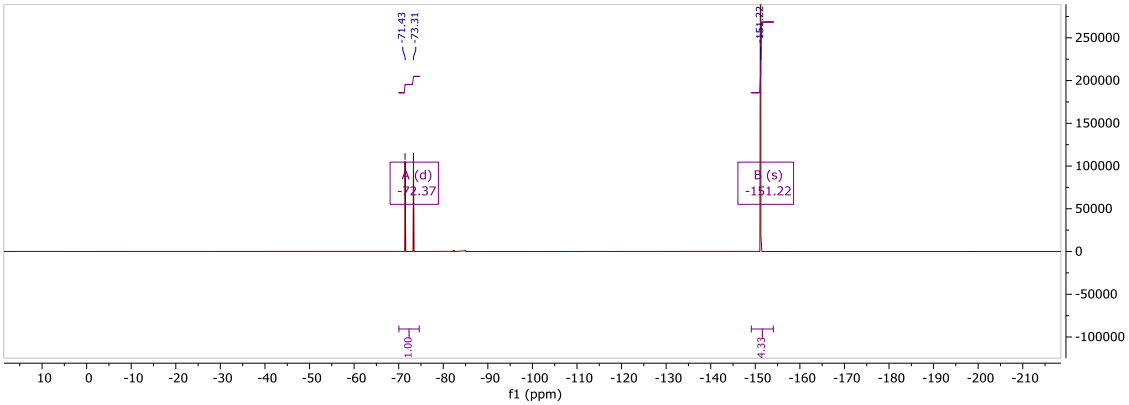

Spectrum 11 - ^{19}F NMR spectrum of *[1,1-Bis(3'-methylimidazol-1'-ylidene)methylene](p-cymene) (acetonitrile) ruthenium(II) ditetrafluoroborate.*

$Ru(C_9H_{14}N_4)(C_{10}H_{14})(CH_3CN)(BF_4)_2$:^{19}F-NMR($C_3D_6O$, 400MHz): δ -72.29 (d, ^1J = 759.66 Hz), -151.28 (s)

Note: The ratio between the hexafluorophosphate and tetrafluoroborate anions originating from the original compound and the silver salt employed in the halide abstraction reaction was 1:5, which is then preserved in the counterion ratio in the final product.

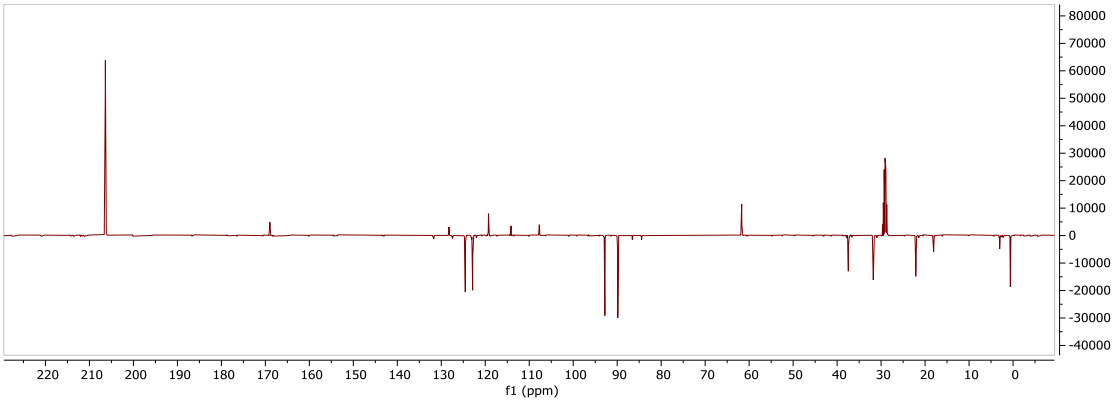

Spectrum 12 - ^{13}C NMR DEPTQ spectrum of *[1,1-Bis(3'-methylimidazol-1'-ylidene)methylene](p-cymene) (acetonitrile) ruthenium(II) ditetrafluoroborate.*

$Ru(C_9H_{14}N_4)(C_{10}H_{14})(CH_3CN)(BF_4)_2$:^{13}C-NMR($C_3D_6O$, 400MHz): δ 168.92 (**4**), 128.27 (**13**), 124.58 (**2**), 122.92 (**3**), 114.12 (**10**), 107.49 (**7**), 92.88 (**9**), 89.87(**8**), 61.49 (**5**) 37.48 (**1**), 31.84 (**11**), 22.19 (**12**), 18.05 (**6**), 2.92 (**14**)

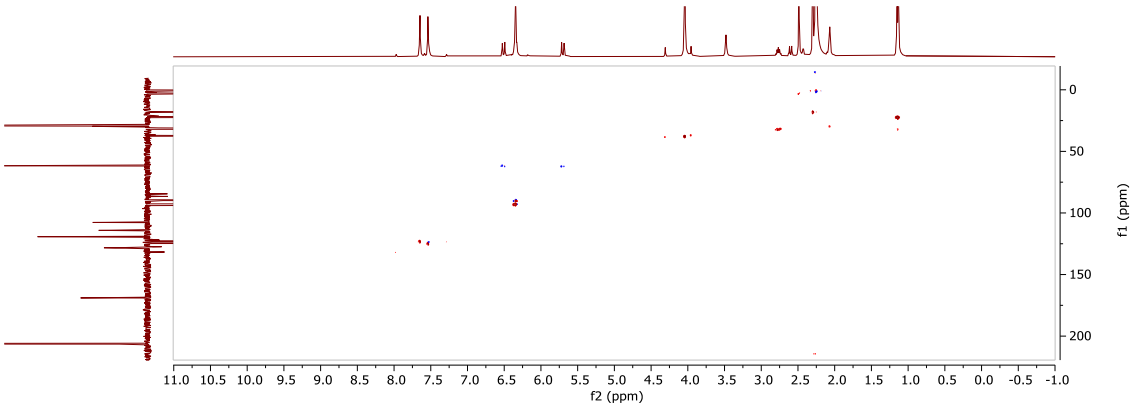

Spectrum 13 - ^{1}H-^{13}C HSQC NMR spectrum of *[1,1-Bis(3'-methylimidazol-1'-ylidene)methylene](p-cymene) (acetonitrile) ruthenium(II) ditetrafluoroborate.*

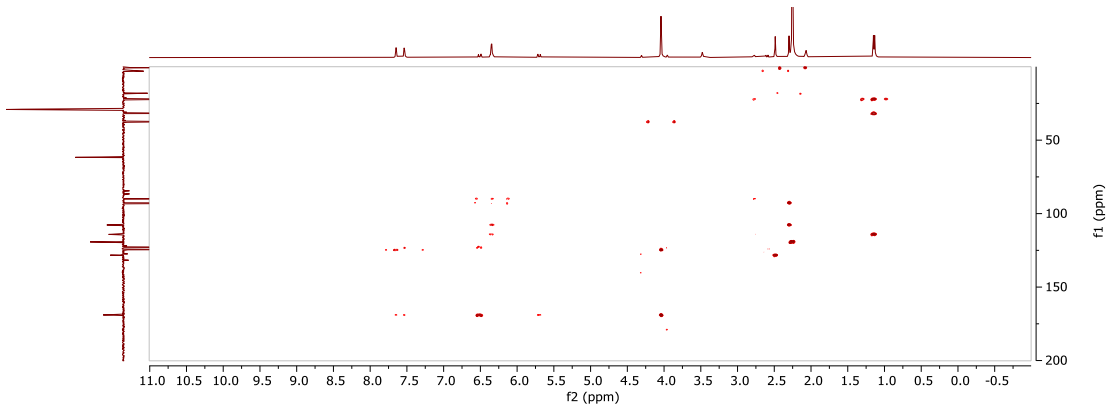

Spectrum 14 - ^{1}H-^{13}C HMBC NMR spectrum of *[1,1-Bis(3'-methylimidazol-1'-ylidene)methylene](p-cymene) (acetonitrile) ruthenium(II) ditetrafluoroborate.*

4.6 Synthesis of $Ru(ACN)_4(b(MI)M)(PF6)_2$ (**4b**)

Procedure

A 25 mL Schlenk was charged with 84 mg (0.30 mmol, 1 eq) of *(1,5-cyclooctadiene)(dichloro) ruthenium(II) polymer* and with 130 mg (0.30 mmol, 1 eq) of *1,1-bis(3'-methylimidazolium)methylene diiodide*. The tube was set under argon by cycling vacuum and argon three times, and then 4 mL (75 eq) of anhydrous and degassed *ACN* were added. The solution was left stirring at reflux for 2 h, then 200 uL (1.50 mmol, 5 eq) of degassed *TEA* were added. The mixture was left reacting for 48 h at reflux, or till the red solution was homogeneous, and 110 mg of *potassium hexafluorophosphate* were added under argon counterflow (110 mg, 4 eq). A second 25 mL Schlenk equipped with a gooch filter was charged with neutral deactivated alumina and placed under inert gas; subsequently, *ACN* was adsorbed in the stationary phase. The hot solution containing the product was transferred under argon using a cannula and deposited over the wet alumina, then filtration was carried out to isolate the product, which was obtained after drying for 36 h under vacuum.

Note: The air-sensitive product should be handled under glove box conditions. It is unstable in solution with a shelf life below 5 minutes; even the solid form darkens until decomposition. For these reasons, the yield was not calculated.

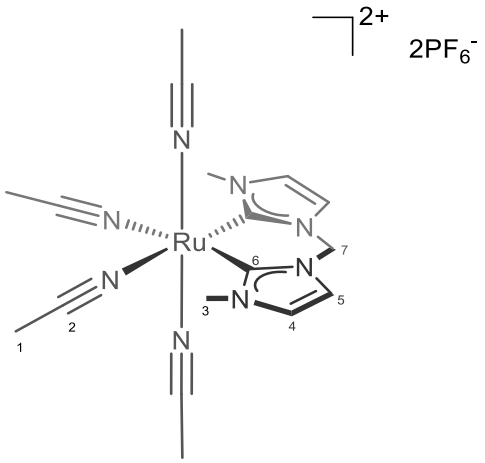

Figure 45 - The structure of *tetrakis(acetonitrile)[1,1-Bis(3'-methylimidazol-1'-ylidene)methylene] ruthenium(II) dihexafluorophosphate.*

Characterization

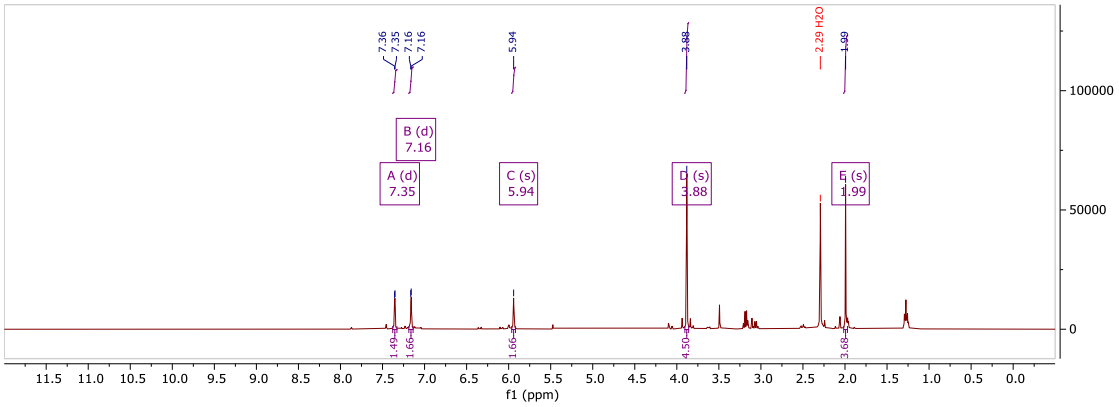

Spectrum 15 - ^{1}H NMR spectrum of *tetrakis(acetonitrile) [1,1-Bis(3'-methylimidazol-1'-ylidene)methylene] ruthenium(II) dihexafluorophosphate.*

$Ru(C_9H_{14}N_4)(CH_3CN)_4(PF_6)_2$: ^{1}H-NMR($C_2D_3N$, 400MHz): δ 7.35 (d, 2H, $^{3}J_{H5\text{-}H4}$, 2.23 Hz, **5**), 7.16 (d, 2H, $^{3}J_{H4\text{-}H5}$, 2.23 Hz, **4**), 5.94 (s, 2H, **7**), 3.88 (s, 6H, **3**), 2.29 (s, 6H, **1**), 1.99 (s, 6H, **1**).

Note: The purification of this compound is not trivial; hence, the analysis was carried out despite the subproduct traces. From the ^{1}H-NMR spectra, clear peaks belonging to TEA, coordinated and free, are observed, accounting for most of the detected impurities.

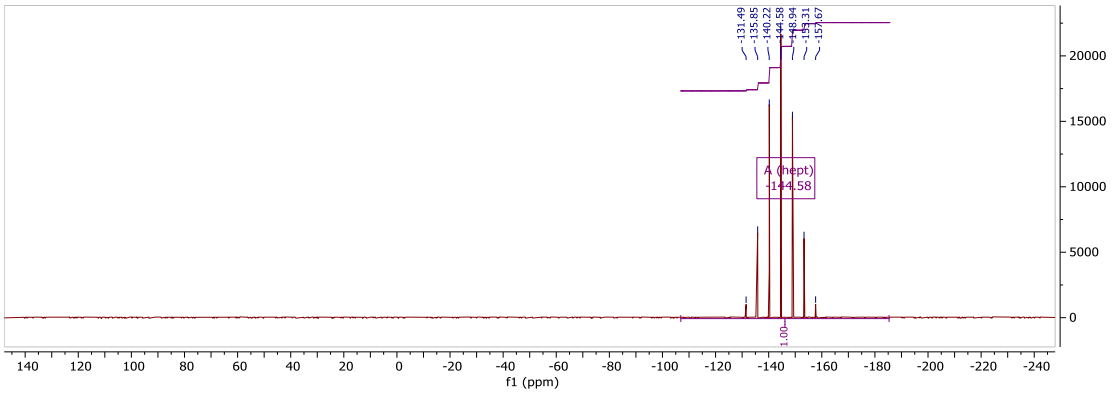

Spectrum 16 - ^{31}P NMR spectrum of *tetrakis(acetonitrile) [1,1-Bis(3'-methylimidazol-1'-ylidene)methylene] ruthenium(II) dihexafluorophosphate.*

$Ru(C_9H_{14}N_4)(CH_3CN)_4(PF_6)_2$: ^{31}P-NMR($C_2D_3N$, 400MHz): δ -144.61 (hept, 2P, ^{1}J= 716.03 Hz).

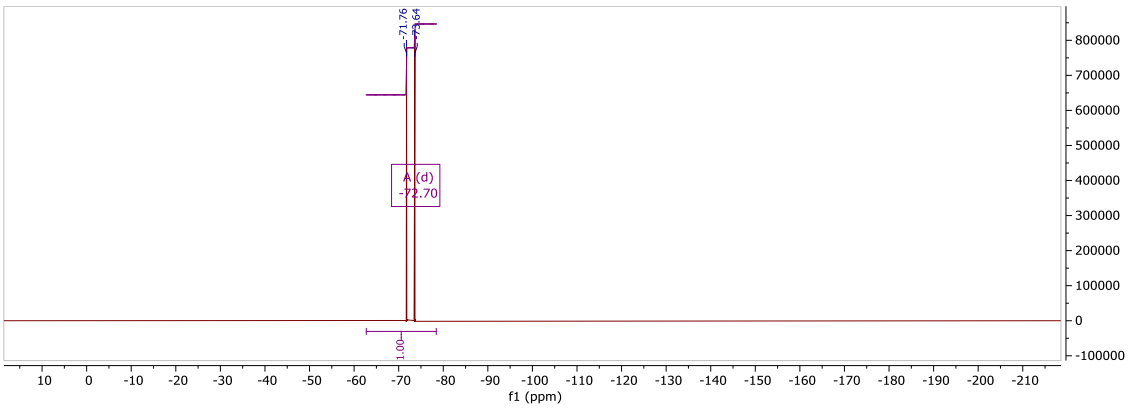

Spectrum 17 - ^{19}F NMR spectrum of *tetrakis(acetonitrile) [1,1-Bis(3'-methylimidazol-1'-ylidene)methylene] ruthenium(II) dihexafluorophosphate.*

$Ru(C_9H_{14}N_4)(CH_3CN)_4(PF_6)_2$: ^{19}F-NMR(C_2D_3N, 400MHz): δ -72.70 (d, 12F, ^1J= 709.99 Hz).

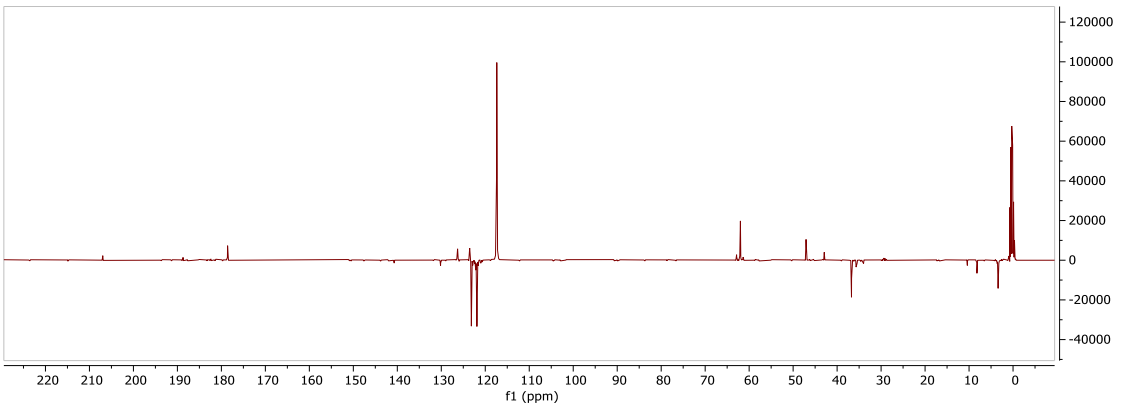

Spectrum 18 - ^{13}C DEPTQ NMR spectrum of *tetrakis(acetonitrile) [1,1-Bis(3'-methylimidazol-1'-ylidene)methylene] ruthenium(II) dihexafluorophosphate.*

$Ru(C_9H_{14}N_4)(CH_3CN)_4(PF_6)_2$: ^{13}C-NMR(C_2D_3N, 400MHz): δ 178.56 (**6**), 126.31 (**2**), 123.22 (**4**), 122.03 (**5**), 117.36 (**2**), 61.94 (**7**), 47.11, 36.5 (**3**), 3.29 (**1**) , 0.70 (**1**)

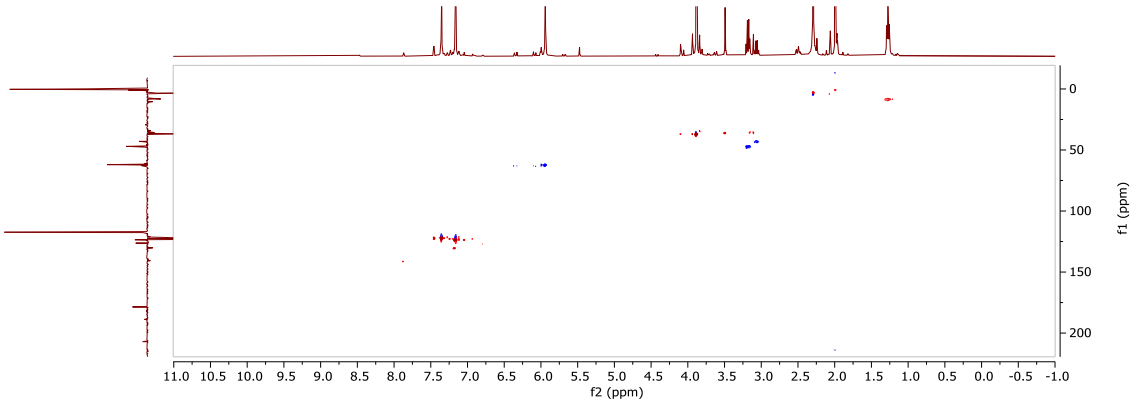

Spectrum 19 - ^{1}H-^{13}C HSQC NMR spectrum of *tetrakis(acetonitrile) [1,1-Bis(3'-methylimidazol-1'-ylidene)methylene] ruthenium(II) dihexafluorophosphate.*

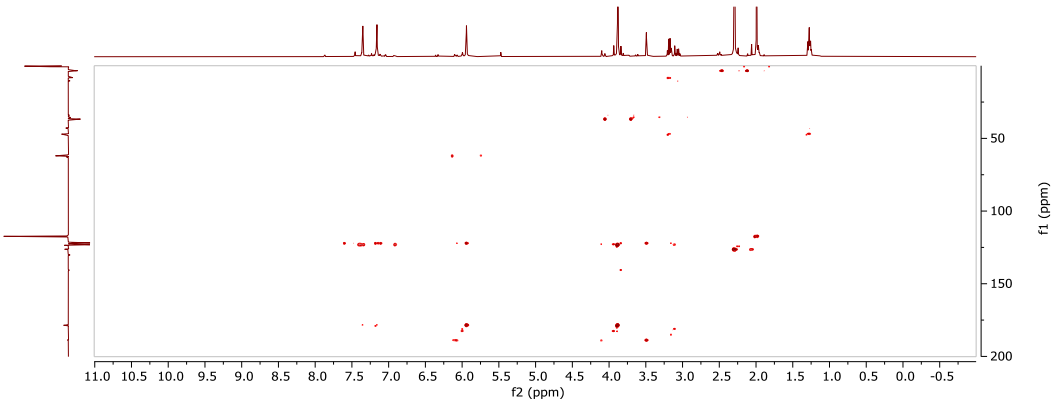

Spectrum 20 - ^{1}H-^{13}C HMBC NMR spectrum of *tetrakis(acetonitrile) [1,1-Bis(3'-methylimidazol-1'-ylidene)methylene] ruthenium(II) dihexafluorophosphate.*

4.7 Synthesis of *trans*-Ru(ACN)$_2$(bipy)(b(MI)M)(PF$_6$)$_2$ (**9a**)

Procedure

A 25mL Schlenk was charged with 84 mg (1 eq) of *(1,5-cyclooctadiene)ruthenium(II) dichloride polymer* and with 130 mg (1 eq) of *1,1'-bis(3-methyl-imidazolium)methylene diiodide*. The tube was set under argon cycling vacuum and argon three times, then 4mL (75eq) of anhydrous and degassed *ACN* were added. The solution was left stirring at reflux for 2 h, then 200 uL (5 eq) of degassed *TEA* was added. The mixture was left reacting for 48 h at reflux, or till the red solution was homogeneous, then the hot solution was cannula filtrated under argon in a second 25 mL Schlenk tube and dried under vacuum. The solution was cooled to room temperature, 46 mg (1 eq) of *2,2'-bipyridine* were added, and was left reacting for 2 h at 50°C. Then 220 mg (4 eq) of *potassium hexafluorophosphate* were added, and the solvent was removed, producing an orange powder. Next, 10 mL of *water* were poured into the flask, producing a dark oil at the bottom. The mixture was left under stirring for 2 h, the trituration yielding a bright orange powder. The mixture was filtered over gooch, the orange powder was washed with *water* (2 x 5 mL) and *diethyl ether* (3 x 5 mL). The collected product was dried overnight (75% yield).

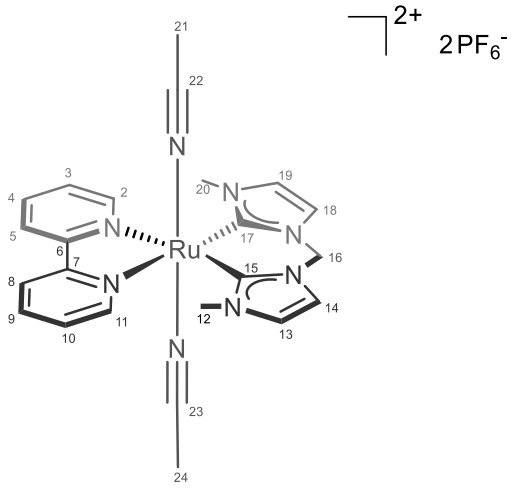

Figure 46 - The structure of *trans-(diacetonitrile) (2,2'-bipyridine) [1,1-Bis(3'-methyl-imidazol-1'-ylidene)methylene] ruthenium(II) dihexafluorophosphate.*

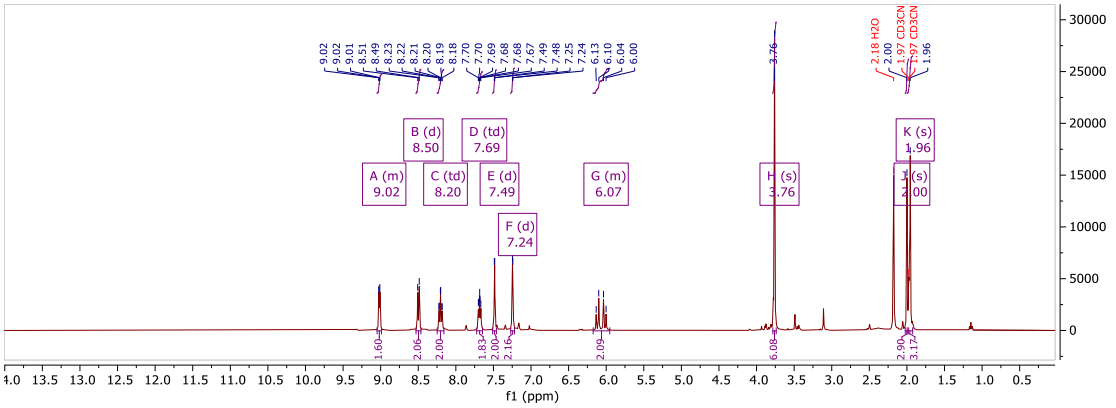

Spectrum 21 - ^{1}H NMR spectrum of *trans-(diacetonitrile) (2,2'-bipyridine) [1,1-Bis(3'-methyl-imidazol-1'-ylidene)methylene] ruthenium(II) dihexafluorophosphate.*

$Ru(C_9H_{14}N_4)(C_{10}H_8N_2)(C_2H_3N)_2(PF_6)_2$: ^{1}H-NMR($CD_3CN$, 400MHz): δ 9.01(d, 2H, $^{3}J_{H3\text{-}H2/H10\text{-}H11}$ = 5.3Hz, **2 + 11**), 8.50 (d, 2H, $^{3}J_{H5\text{-}H4/H8\text{-}H9}$= 8.7 Hz, **5 + 8**), 8.21 (td, 2H, $^{3}J_{H3\text{-}H2/H3\text{-}H4/\ H10\text{-}H11/\ H10\text{-}H9}$ = 7.5Hz, **4 + 9**), 7.68 (td, 2H, $^{3}J_{H4\text{-}H3/H4\text{-}H5/\ H9\text{-}H10/\ H9\text{-}H8}$ = 6.3 Hz, $^{4}J_{H4\text{-}H2/H9\text{-}H11}$ = 1.2 Hz, **3 + 10**), 7.49 (d, 2H, $^{3}J_{H14\text{-}H13/H18\text{-}H19}$ = 2.0 Hz, **14 + 18**), 7.24 (d, 2H, $^{3}J_{H13\text{-}H14/H19\text{-}H18}$ = 2.3 Hz, **13 + 19**), 6.12 (d, 1H, $^{2}J_{H16}$ = 13.8 Hz, **16**), 6.02 (d, 1H, $^{2}J_{H16}$ = 13.8 Hz, **16**), 3.76 (s, 6H, **12 + 20**), 2.00 (s, 6H, **21**).

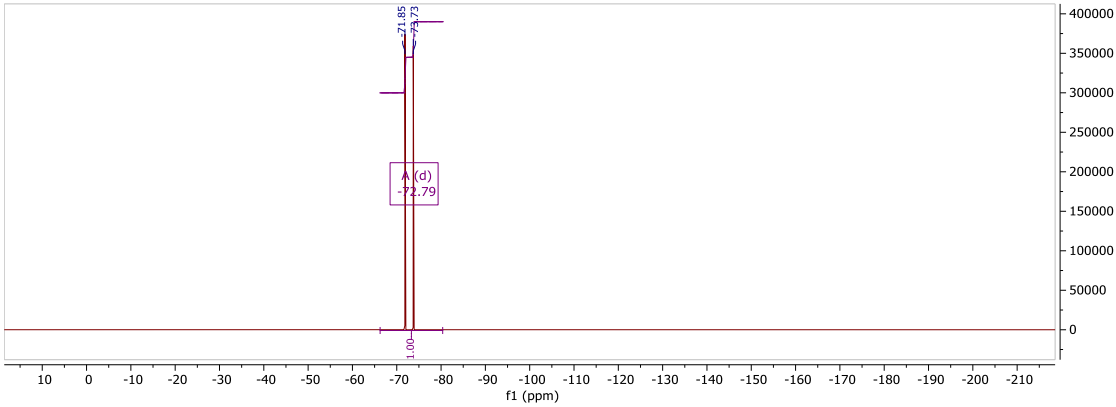

Spectrum 22 - ^{19}F NMR spectrum of *trans-(diacetonitrile) (2,2'-bipyridine) [1,1-Bis(3'-methyl-imidazol-1'-ylidene)methylene] ruthenium(II) dihexafluorophosphate.*

$Ru(C_9H_{14}N_4)(C_{10}H_8N_2)(C_2H_3N)_2(PF_6)_2$: ^{19}F-NMR($CD_3CN$, 400MHz): δ -72.79(d, 6F, ^{1}J= 675.25Hz).

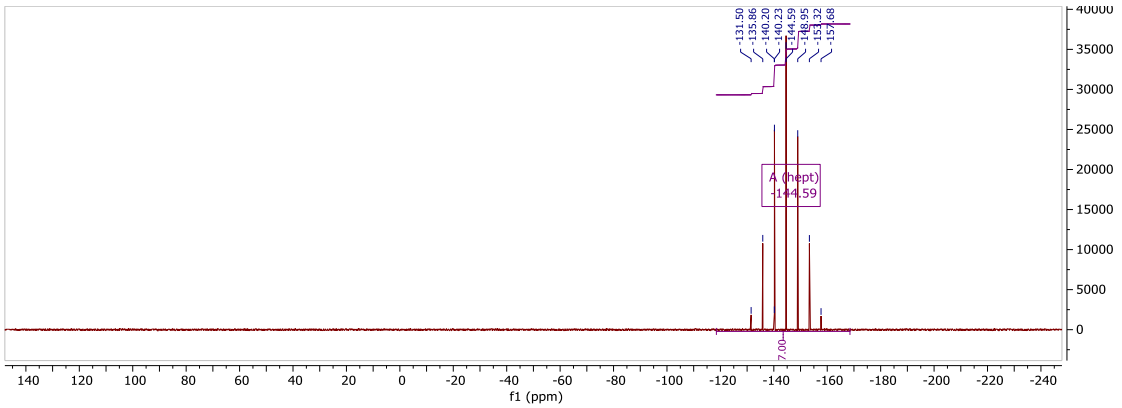

Spectrum 23 - ^{31}P NMR spectrum of *trans-(diacetonitrile) (2,2'-bipyridine) [1,1-Bis(3'-methyl-imidazol-1'-ylidene)methylene] ruthenium(II) dihexafluorophosphate.*

$Ru(C_9H_{14}N_4)(C_{10}H_8N_2)(C_2H_3N)_2(PF_6)_2$: ^{31}P-NMR($CD_3CN$, 400MHz): δ -144.59 (hept, 2P, ^1J= 727.19Hz).

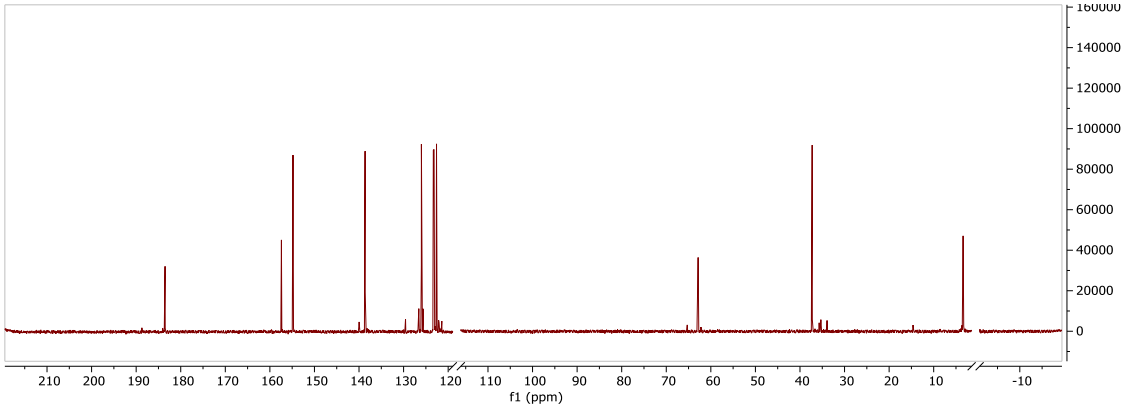

Spectrum 24 - ^{13}C NMR spectrum of *trans-(diacetonitrile) (2,2'-bipyridine) [1,1-Bis(3'-methyl-imidazol-1'-ylidene)methylene] ruthenium(II) dihexafluorophosphate.*

$Ru(C_9H_{14}N_4)(C_{10}H_8N_2)(C_2H_3N)_2(PF_6)_2$: ^{13}C-NMR($CD_3CN$, 400MHz): δ (ppm) 183.51 (**15 + 17**), 157.56 (**6 + 7**), 154.97 (**2 + 11**), 138.86 (**4 + 9**), 126.01 (**22 + 23**), 123.36 (**13 + 19**), 123.18 (**5 + 8**), 122.63 (**14 + 18**), 62.86 (**16**), 37.33 (**12 + 20**), 3.48 (**21 + 24**).

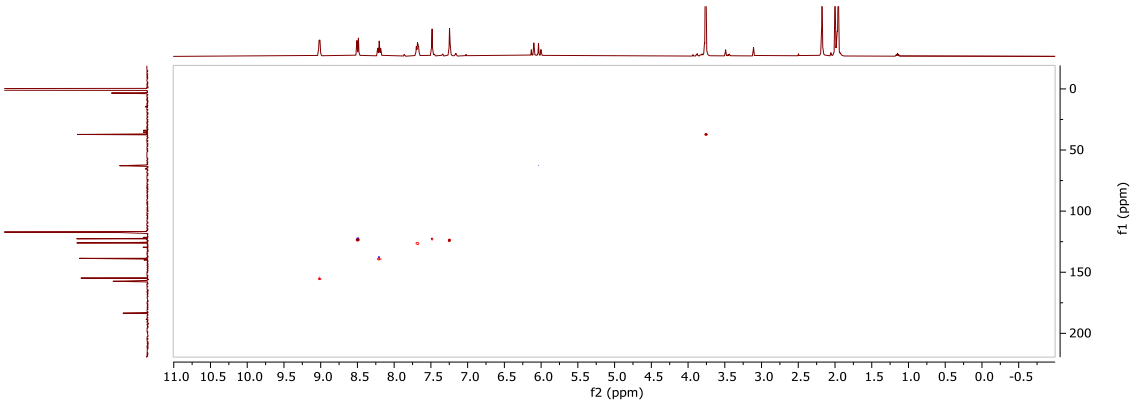

Spectrum 25 - ^{1}H-^{13}C HSQC NMR spectrum of *trans-(diacetonitrile) (2,2'-bipyridine) [1,1-Bis(3'-methyl-imidazol-1'-ylidene)methylene] ruthenium(II) dihexafluorophosphate.*

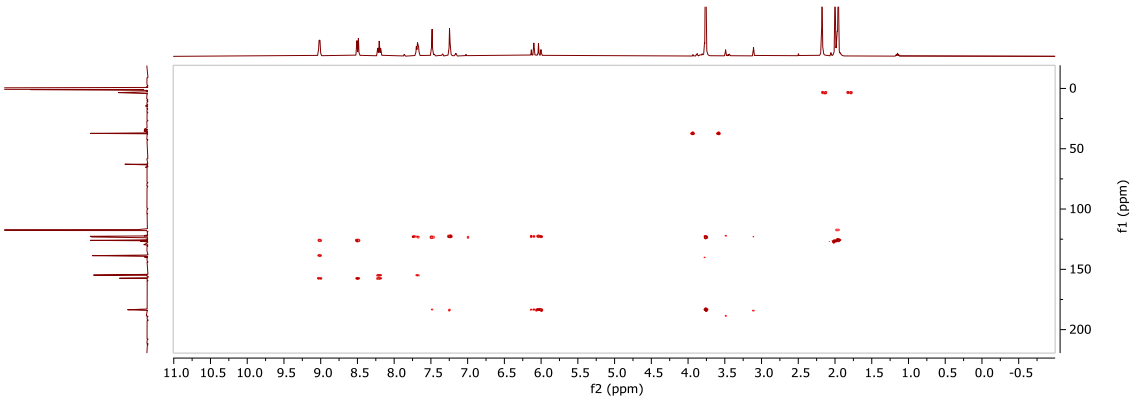

Spectrum 26 - ^{1}H-^{13}C HMBC NMR spectrum of *trans-(diacetonitrile) (2,2'-bipyridine) [1,1-Bis(3'-methyl-imidazol-1'-ylidene)methylene] ruthenium(II) dihexafluorophosphate.*

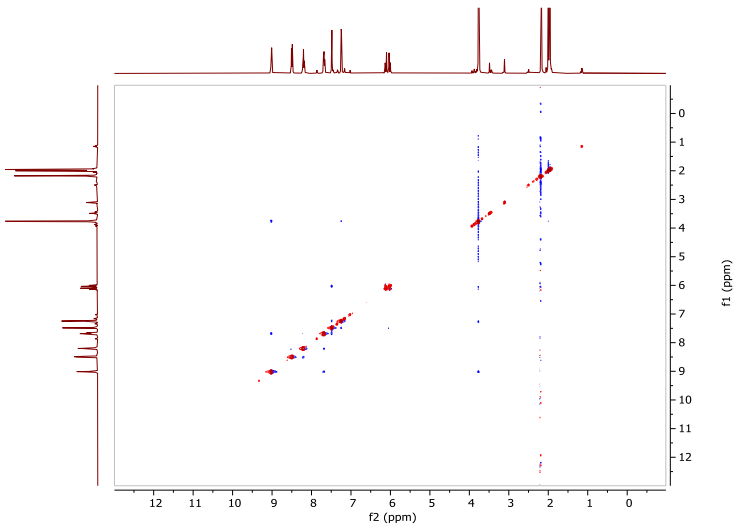

Spectrum 27 - ^{1}H-^{13}C NOESY NMR spectrum of *trans-(diacetonitrile) (2,2'-bipyridine) [1,1-Bis(3'-methyl-imidazol-1'-ylidene)methylene] ruthenium(II) dihexafluorophosphate.*

4.8 Synthesis of *cis*-Ru(ACN)$_2$(bipy)(b(MI)M)(PF$_6$)$_2$ (**10a**)

Procedure

A 15 mL pressure tube was charged with 120 mg (0.30 mmol, 1 eq) of *trans-(diacetonitrile) (2,2'-bipyridine) [1,1-Bis(3'-methyl-imidazol-1'-ylidene)methylene]ruthenium(II) dihexafluorophosphate*, then 10 mL of dry and degassed *ACN* were added under argon counterflow. The pressure tube was sealed and placed in an oil bath at 120°C. After 96 h, the solution was cooled, and the solvent was removed. The residue was dissolved in boiling *methanol* and crystallized overnight. The resulting red crystals were isolated via filtration, washed with *diethyl ether* (3 x 5 mL), and dried under vacuum (80% yield).

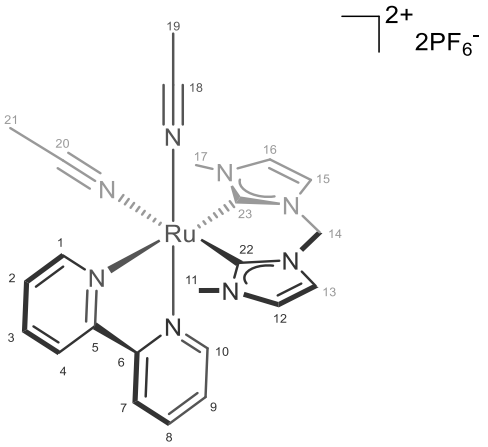

Figure 47 - The structure of *cis-(diacetonitrile) (2,2'-bipyridine) [1,1-Bis(3'-methyl-imidazol-1'-ylidene)methylene] ruthenium(II) dihexafluorophosphate*.

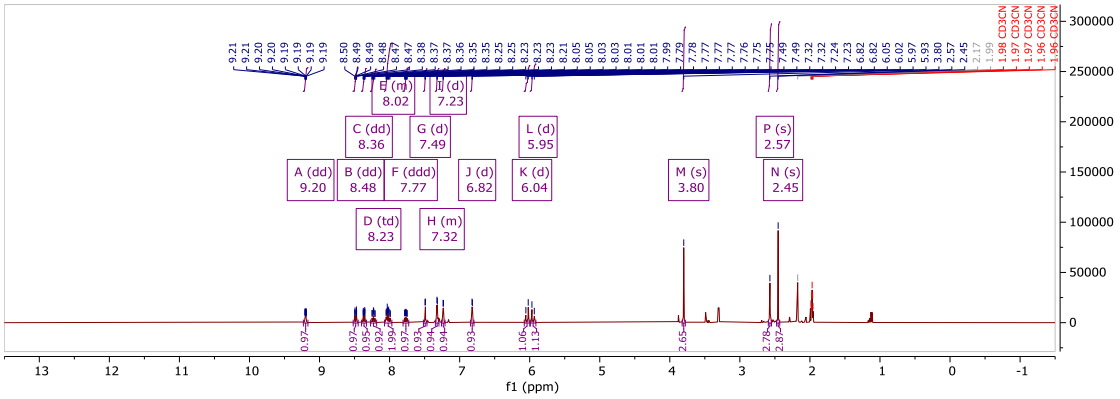

Spectrum 28 - ^{1}H NMR spectrum of *cis-(diacetonitrile) (2,2'-bipyridine) [1,1-Bis(3'-methyl-imidazol-1'-ylidene)methylene] ruthenium(II) dihexafluorophosphate.*

$Ru(C_9H_{14}N_4)(C_{10}H_8N_2)(C_2H_3N)_2(PF_6)_2$: ^{1}H-NMR($C_2H_3N$, 400MHz): δ 9.20(d, 1H, $^{3}J_{H1\text{-}H2}$= 6.4Hz, **1**), 8.48 (d, 1H, $^{3}J_{H4\text{-}H3}$ = 8.0Hz, **4**), 8.37 (d, 1H, $^{3}J_{H10\text{-}H9}$ = 7.8Hz, **10**), 8.23 (td, 1H, $^{3}J_{H2\text{-}H1\ /\ H2\text{-}H3}$ = 7.8Hz, $^{4}J_{H2\text{-}H4}$ =1.5Hz, **2**), 8.02 (m, 2H, **3+7**), 7.77 (ddd, ^{3}J =7.0Hz, ^{3}J =5.7Hz, $^{3}J_{H9\text{-}H7}$ =1.3Hz, **8**), 7.49 (d, 1H, $^{3}J_{H15\text{-}H16}$ =1.7Hz, **15**), 7.32 (m, 2H, **9+16**), 7.23 (d, 1H, $^{3}J_{H13\text{-}H12}$ = 2.1Hz, **13**), 6.82 (d, 1H, $^{3}J_{H12\text{-}H13}$ =2.1Hz, **12**), 6.04 (d, 1H, $^{1}J_{H14}$ = 13.3Hz, **14**), 5.95 (d, 1H, $^{1}J_{H14}$ = 13.3Hz, **14**) 3.80 (s, 3H, **17**) 2.57 (s, 3H, **11**), 2.46 (s, 3H, **19**).

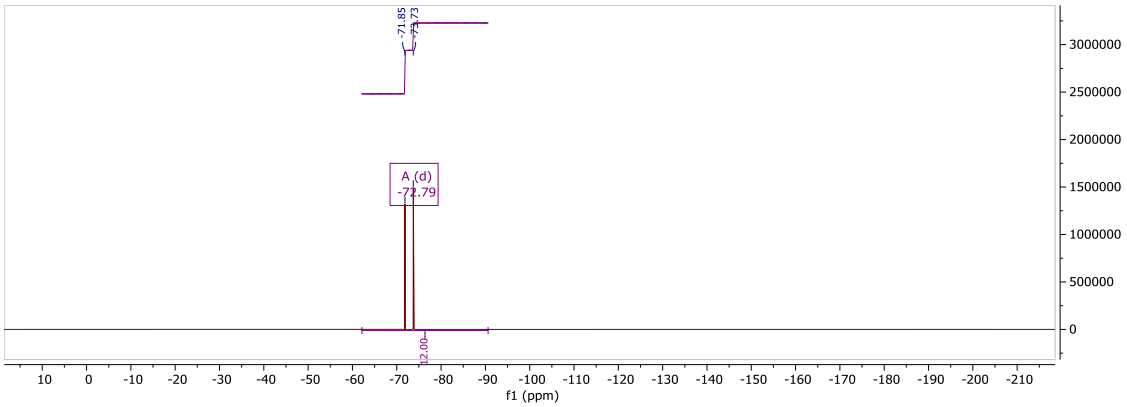

Spectrum 29 - ^{19}F NMR spectrum of *cis-(diacetonitrile) (2,2'-bipyridine) [1,1-Bis(3'-methyl-imidazol-1'-ylidene)methylene] ruthenium(II) dihexafluorophosphate.*

$Ru(C_9H_{14}N_4)(C_{10}H_8N_2)(C_2H_3N)_2(PF_6)_2$: ^{19}F-NMR($C_2H_3N$, 400MHz): δ -72.79 (d, 12F, J= 714.6Hz).

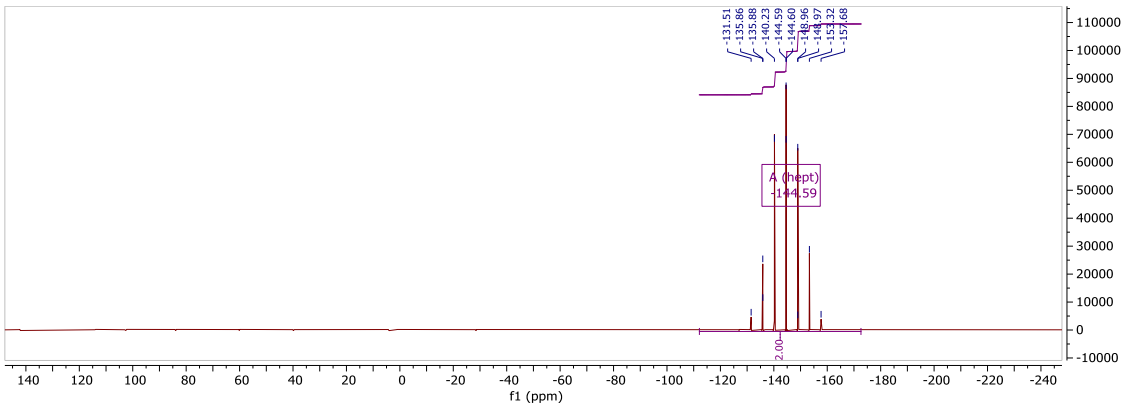

Spectrum 30 - ^{31}P NMR spectrum of *cis-(diacetonitrile) (2,2'-bipyridine) [1,1-Bis(3'-methyl-imidazol-1'-ylidene)methylene] ruthenium(II) dihexafluorophosphate*.

$Ru(C_9H_{14}N_4)(C_{10}H_8N_2)(C_2H_3N)_2(PF_6)_2$: ^{31}P-NMR($C_2H_3N$, 400MHz): δ -144.6 (hept, 2P, J= 698.5.6Hz).

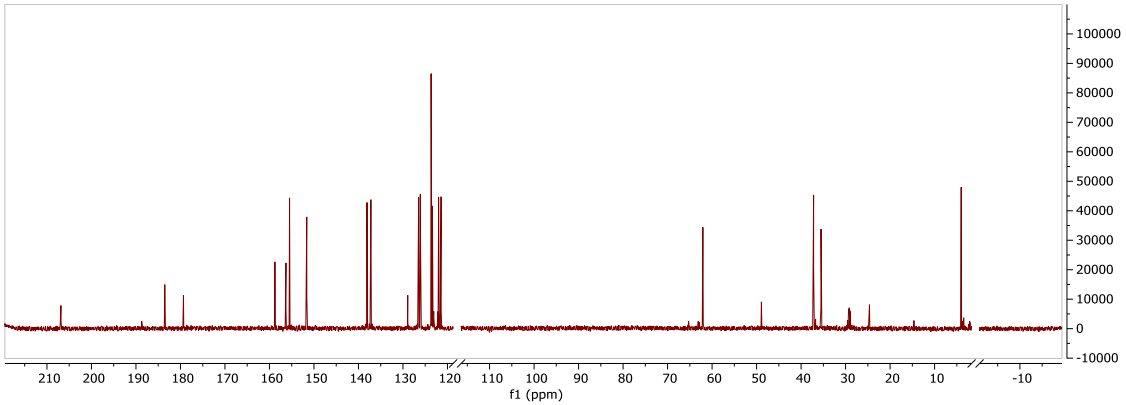

Spectrum 31 - ^{13}C NMR spectrum of *cis-(diacetonitrile) (2,2'-bipyridine) [1,1-Bis(3'-methyl-imidazol-1'-ylidene)methylene] ruthenium(II) dihexafluorophosphate*.

$Ru(C_9H_{14}N_4)(C_{10}H_8N_2)(C_2H_3N)_2(PF_6)_2$: ^{13}C-NMR($C_2H_3N$, 400MHz): δ (ppm) 183.53 (**23**), 179.32 (**22**), 158.78 (**6**), 156.26 (**5**), 151.64 (**1**), 155.50 (**10**), 138.10 (**2**), 137.23 (**3**), 129.55 (**18**), 126.50 (**9**), 126.07 (**8**), 123.71 (**16**), 123.67 (**7**), 123.47 (**4**), 122.04 (**15**), 121.49 (**13**), 123.71 (**12**), 62.09 (**14**), 37.27(**17**), 35.49(**11**), 4.25 (**19**)

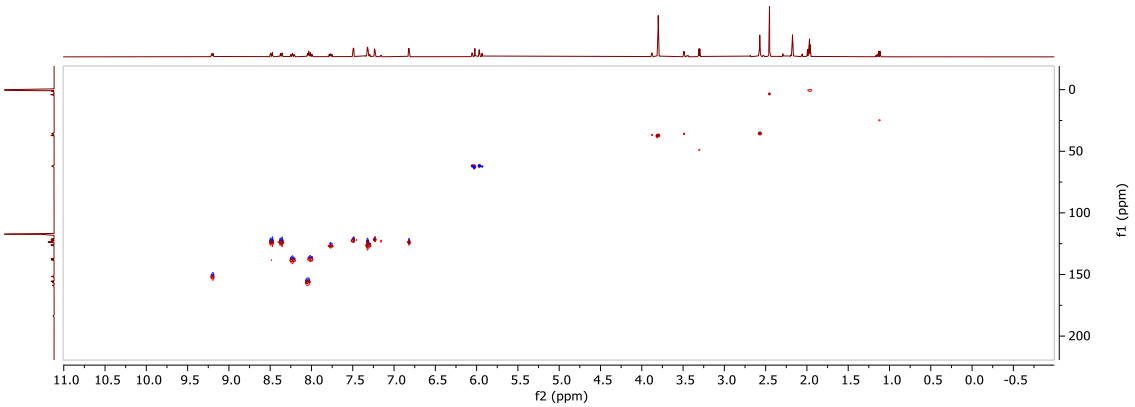

Spectrum 32 - ^{1}H-^{13}C HSQC NMR spectrum of *cis-(diacetonitrile) (2,2'-bipyridine) [1,1-Bis(3'-methyl-imidazol-1'-ylidene)methylene] ruthenium(II) dihexafluorophosphate*.

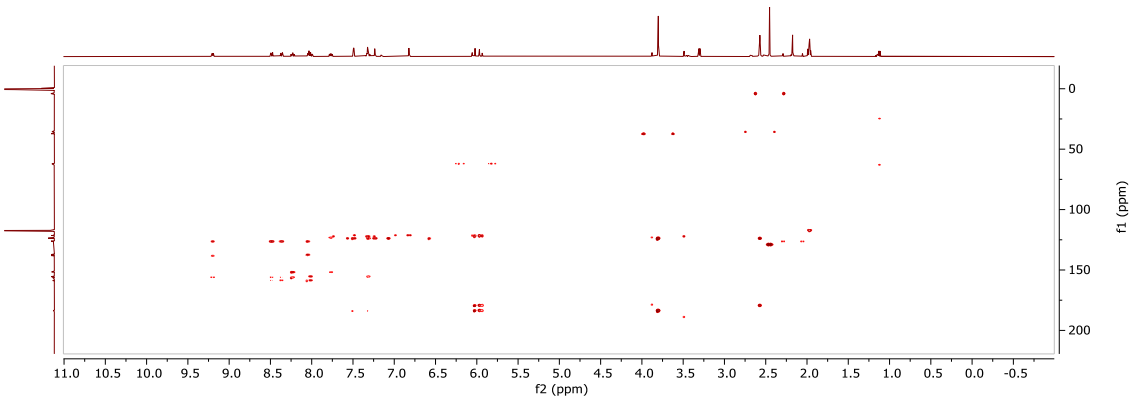

Spectrum 33 - ^{1}H-^{13}C HMBC NMR spectrum of *cis-(diacetonitrile) (2,2'-bipyridine) [1,1-Bis(3'-methyl-imidazol-1'-ylidene)methylene] ruthenium(II) dihexafluorophosphate*.

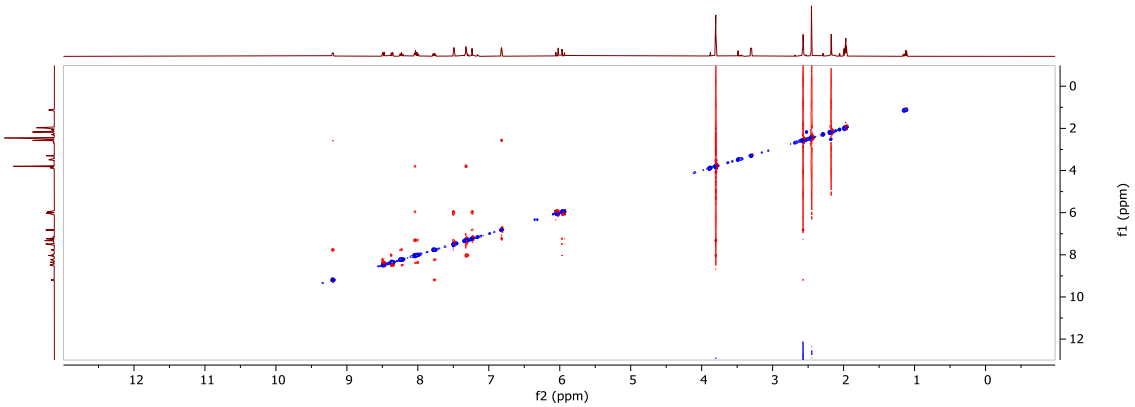

Spectrum 34 - ^{1}H-^{13}C NOESY NMR spectrum of *cis-(diacetonitrile) (2,2'-bipyridine) [1,1-Bis(3'-methyl-imidazol-1'-ylidene)methylene] ruthenium(II) dihexafluorophosphate*.

4.9 Synthesis of *trans*-$Ru(ACN)_2(AMPY)(b(MI)M)(PF_6)_2$ (**11**)

Procedure

A 25 mL Schlenk was charged with 84 mg (0.30 mmol, 1 eq) of *(1,5-cyclooctadiene)(dichloro) ruthenium(II) polymer* and with 130 mg (0.30 mmol, 1 eq) of *1,1-bis(3'-methylimidazolium)methylene diiodide*. The tube was set under argon by cycling vacuum and argon for three times, then 4 mL (75 eq) of *ACN* anhydrous and degassed were added. The solution was left stirring at reflux for 2 h, then 200 uL (1.50 mmol, 5eq) of degassed *TEA* were added. The mixture was left reacting for 48 h at reflux, or till the red solution is homogeneous, then the hot solution was cannula filtrated under argon in a second 25 mL Schlenk tube and dried under vacuum. The orange solid was dissolved in 4 mL of anhydrous and degassed *DCM*, and subsequently, 80 uL (0.30 mmol, 1 eq) of *2-picolylamine* were added. The homogeneous solution was left reacting for 40 minutes at room temperature till a white solid precipitated. *Potassium hexafluorophosphate* (1.2 mmol, 210 mg) was added to the mixture. The solution was reduced in volume and *water* was added (25 mL), the resulting suspension was triturated for 4 h till a fine white powder was obtained. The solid was isolated via filtration over gooch, washed with *water* (2 x 5 mL), *diethyl ether* (3 x 10 mL) and was dried under vacuum (75% yield).

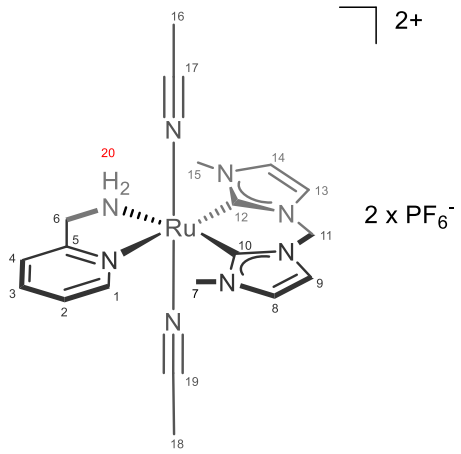

Figure 48 - The structure of *trans-(diacetonitrile)[1,1-bis(3'-methyl-imidazol-2'-yliden)methylene](2-pycolilamine) ruthenium(II) dihexafluorophosphate*.

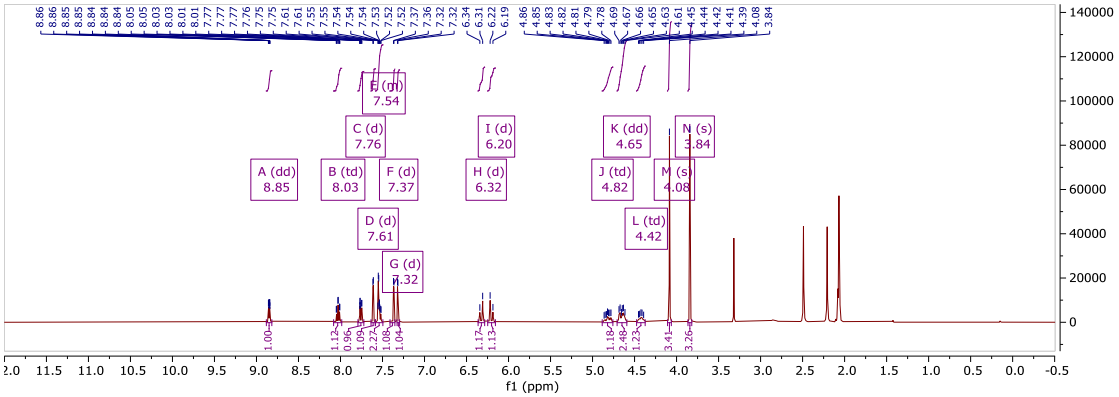

Spectrum 35 - ^{1}H NMR spectrum of *trans-(diacetonitrile)[1,1-bis(3'-methyl-imidazol-2'-yliden)methylene](2-pycolilamine) ruthenium(II) dihexafluorophosphate.*

$Ru(C_9H_{14}N_4)(C_{10}H_8N_2)(C_2H_3N)_2(PF_6)_2$: ^{1}H-NMR($C_3D_6O$, 400MHz): δ 8.86(dd, 1H, $^{3}J_{H1\text{-}H2}$ = 5.6Hz, $^{4}J_{H1\text{-}H3}$ = 1.3 Hz **1**), 8.03 (td, 1H, $^{3}J_{H3\text{-}H4\ /\ H3\text{-}H2}$ =7.68 Hz, $^{4}J_{H3\text{-}H1}$=1.8 Hz, **3**), 7.76 (d, 1H, $^{3}J_{H4\text{-}H3}$ = 8.3 Hz, **4**), 7.61 (d, 1H, $^{3}J_{H13\text{-}H14}$ = 2.2 Hz, **13**), 7.54 (m, 2H, **2 + 9**), 7.37 (d, 1H, $^{3}J_{H14\text{-}H13}$ = 2.3 Hz, **14**), 7.32 (d, 1H, J= 2.3 Hz, **8**), 6.32 (d, 1H, $^{2}J_{H11\text{-}H11}$= 13.3 Hz, **11**), 6.20 (d, 1H, $^{2}J_{H11\text{-}H11}$=13.3 Hz, **11**), 4.82 (td, 1H, $^{2}J_{H6\text{-}H6}$ = 12.00 Hz, $^{3}J_{H6\text{-}H20}$ = 4.91 Hz, **6**), 4.65 (dd, 2H, $^{2}J_{H6\text{-}H6}$ = 15.9 Hz, $^{3}J_{H20\text{-}H6}$ = 5.00 Hz, **20**), 4.42 (td, 1H, $^{2}J_{H6\text{-}H6}$ = 12.00 Hz, $^{3}J_{H6\text{-}H20}$ = 4.91 Hz, **6**), 4.08 (s, 3H, **15**), 3.84 (s, 3H, **7**), 2.49 (s, 6H, **16 +18**) 2.20 (s, 3H, **16 +18**).

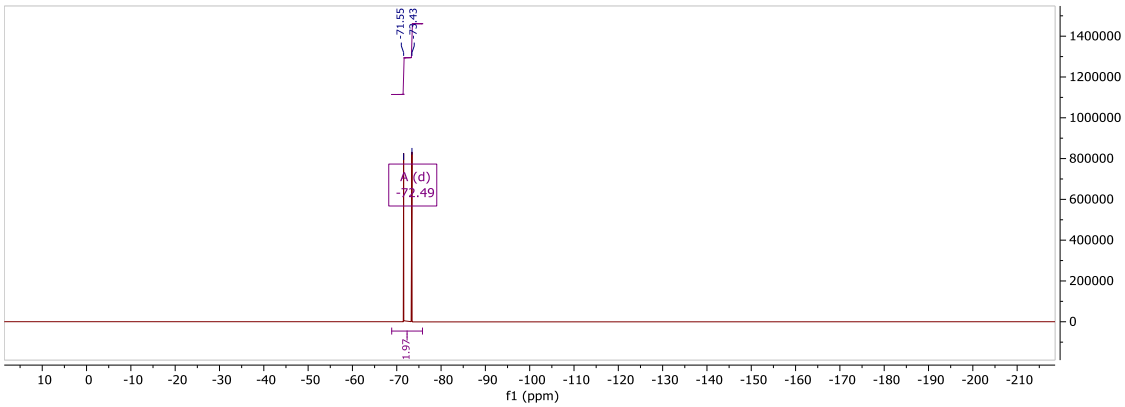

Spectrum 36 - ^{19}F NMR spectrum of *trans-(diacetonitrile)[1,1-bis(3'-methyl-imidazol-2'-yliden)methylene](2-pycolilamine) ruthenium(II) dihexafluorophosphate.*

$Ru(C_9H_{14}N_4)(C_{10}H_8N_2)(C_2H_3N)_2(PF_6)_2$: ^{19}F-NMR($C_3D_6O$, 400MHz): δ -72.49 (d, 12F, ^{1}J= 714.6Hz).

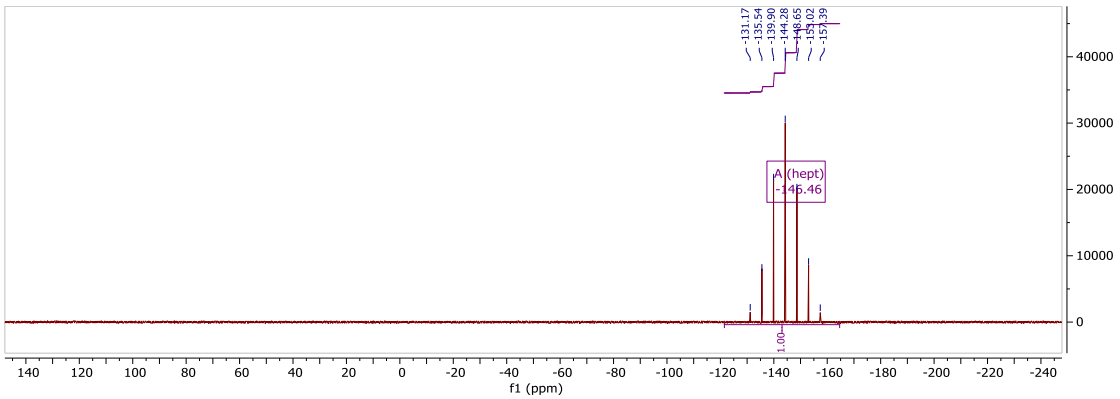

Spectrum 37 - ^{31}P NMR spectrum of *trans-(diacetonitrile)[1,1-bis(3'-methyl-imidazol-2'-yliden)methylene](2-pycolilamine) ruthenium(II) dihexafluorophosphate*.

$Ru(C_9H_{14}N_4)(C_{10}H_8N_2)(C_2H_3N)_2(PF_6)_2$: ^{31}P-NMR($C_3D_6O$, 400MHz): δ -146.46 (hept, 2P, ^{1}J= 698.5.6Hz).

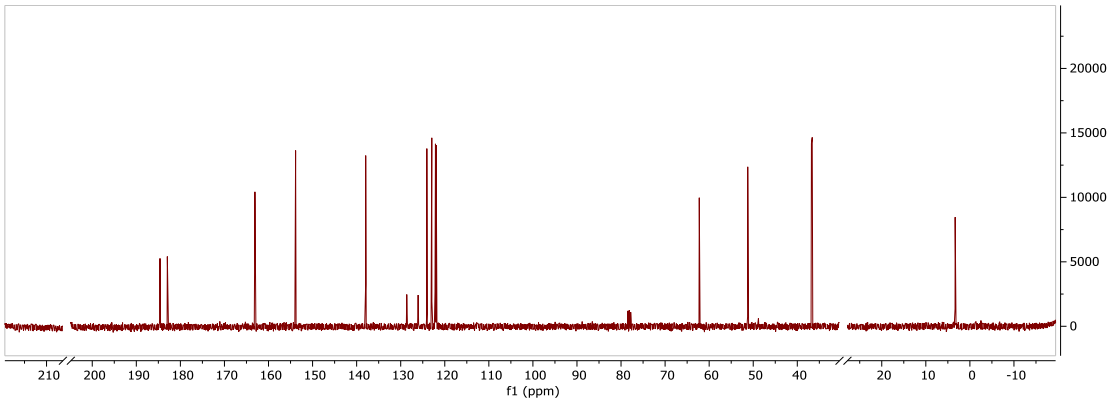

Spectrum 38 - ^{13}C NMR spectrum of *trans-(diacetonitrile)[1,1-bis(3'-methyl-imidazol-2'-yliden)methylene](2-pycolilamine) ruthenium(II) dihexafluorophosphate*.

$Ru(C_9H_{14}N_4)(C_{10}H_8N_2)(C_2H_3N)_2(PF_6)_2$: ^{13}C-NMR($C_3D_6O$, 400MHz): δ (ppm) 184.64 (**12**), 182.94 (**10**), 163.11 (**5**), 153.95 (**1**), 137.94 (**3**), 128.67 (**17**), 126.08 (**19**) 124.07 (**2**), 122.99 (**14**), 122.95 (**8**), 122.21 (**4**), 122.12 (**13**), 121.95 (**9**), 62.18 (**11**), 51.30 (**6**), 36.81 (**15**), 36.63 (**7**), 3.29(**16 + 18**).

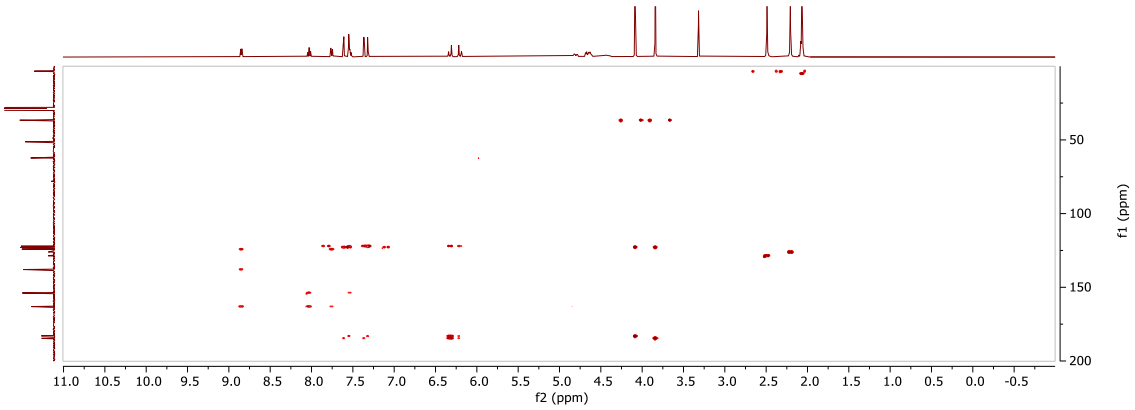

Spectrum 39 - ^{1}H-^{13}C HMBC NMR spectrum of *trans-(diacetonitrile)[1,1-bis(3'-methyl-imidazol-2'-yliden)methylene](2-pycolilamine) ruthenium(II) dihexafluorophosphate*.

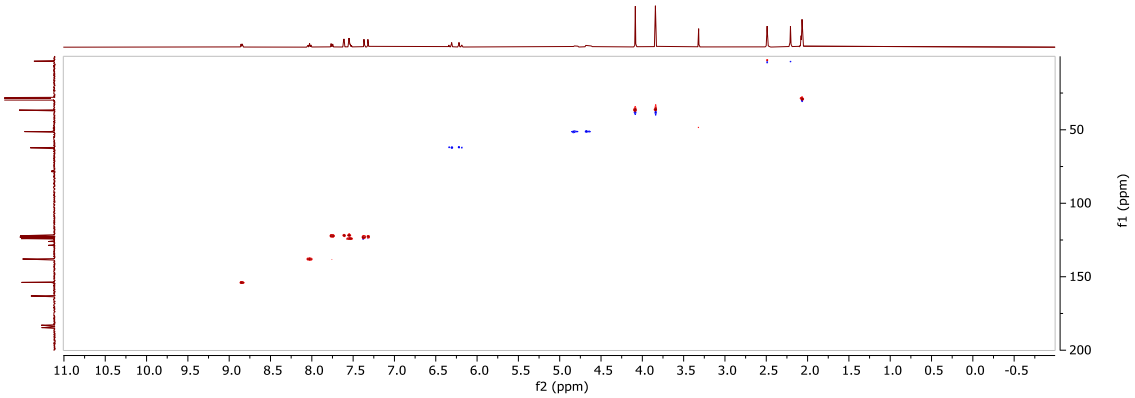

Spectrum 40 - ^{1}H-^{13}C HSQC NMR spectrum of *trans-(diacetonitrile)[1,1-bis(3'-methyl-imidazol-2'-yliden)methylene](2-pycolilamine) ruthenium(II) dihexafluorophosphate*.

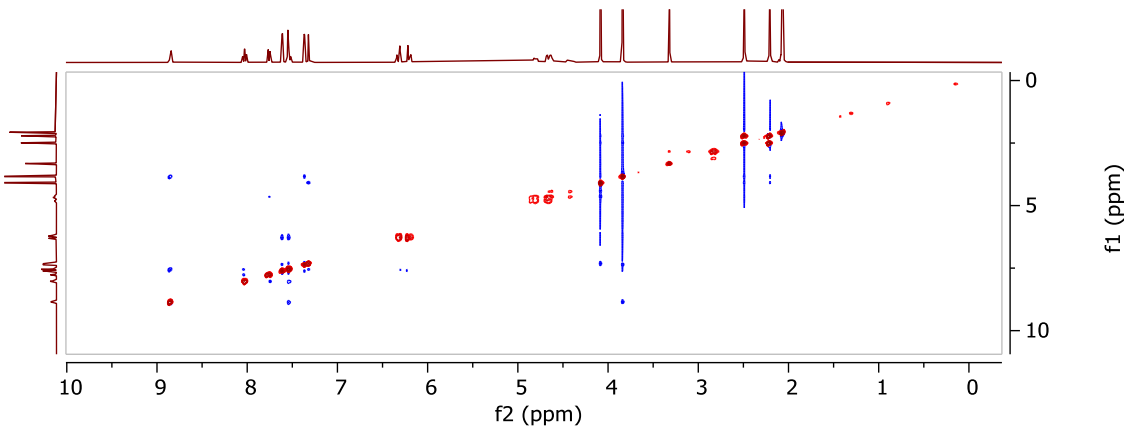

Spectrum 41 - ^{1}H-^{13}C NOESY NMR spectrum of *trans-(diacetonitrile)[1,1-bis(3'-methyl-imidazol-2'-yliden)methylene](2-pycolilamine) ruthenium(II) dihexafluorophosphate*.

4.10 Synthesis of *trans*-$Ru(ACN)_2(b(MI)M)(EN)(PF_6)_2$ (**12**)

Procedure

A 25 mL Schlenk was charged with 84 mg (0.30 mmol, 1 eq) of *(1,5-cyclooctadiene)(dichloro) ruthenium(II) polymer* and with 130 mg (0.30 mmol, 1 eq) of *1,1-bis(3'-methylimidazolium)methylene diiodide*. The tube was set under argon by cycling vacuum and argon for three times, then 4 mL (75 eq) of *ACN* anhydrous and degassed were added. The solution was left stirring at reflux for 2 h, then 200uL (1.50 mmol, 5eq) of degassed *TEA* were added. The mixture was left reacting for 48h at reflux, or till the red solution is homogeneous, then the hot solution was cannula filtrated under argon in a second 25 mL Schlenk tube. Subsequently, 25 uL (0.30 mmol, 1 eq) of *1,2-ethylenediamine* were added. The homogeneous solution was left reacting for 40 minutes at room temperature till a white solid precipitated. *Potassium hexafluorophosphate* (1.2 mmol, 210 mg) was added to the mixture. The solution was reduced in volume and *water* was added (25 mL), the resulting suspension was triturated for 24 h till a fine white powder was obtained. The solid was isolated via filtration over Gooch, washed with *water* (2 x 5 mL), *diethyl ether* (3 x 10 mL), and was dried under vacuum (75% yield).

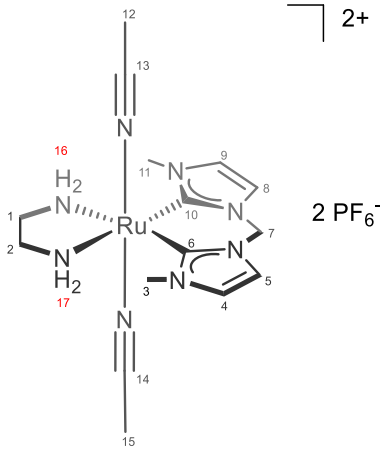

Figure 49 - The structure of *trans-(diacetonitrile)[1,1-bis(3'-methyl-imidazol-2'-yliden)methylene](1,2-ethylenediamine) ruthenium(II) dihexafluorophosphate*.

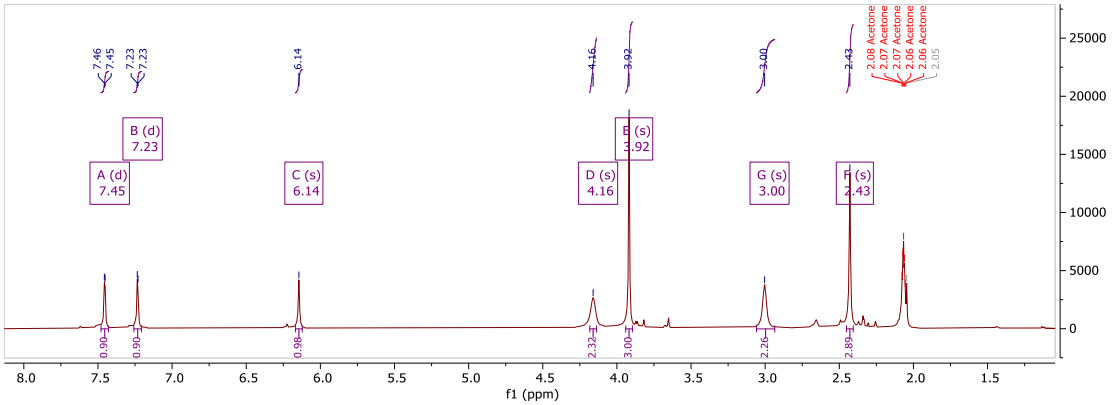

Spectrum 42 - ^{1}H NMR spectrum of *trans-(diacetonitrile)[1,1-bis(3'-methyl-imidazol-2'-yliden)methylene](1,2-ethylenediamine) ruthenium(II) dihexafluorophosphate.*

$Ru(C_9H_{14}N_4)(C_2H_8N_2)(C_2H_3N)_2(PF_6)_2$: ^{1}H-NMR($C_3D_6O$, 400MHz): δ 7.45 (d, 2H, $^{3}J_{H5\text{-}H4\ /\ H8\text{-}H9}$ = 2.16 Hz, **5 + 8**), 7.23 (d, 2H, $^{3}J_{H4\text{-}H5\ /\ H9\text{-}H8}$ =2.16 Hz, **4 + 9**), 6.15 (s, 2H, **7**), 4.16 (s, 4H, **16 + 17**), 3.91 (a, 6H, **3 + 11**), 3.00 (s, 4H, **1 + 2**), 2.43 (s, 6H, **12 + 15**).

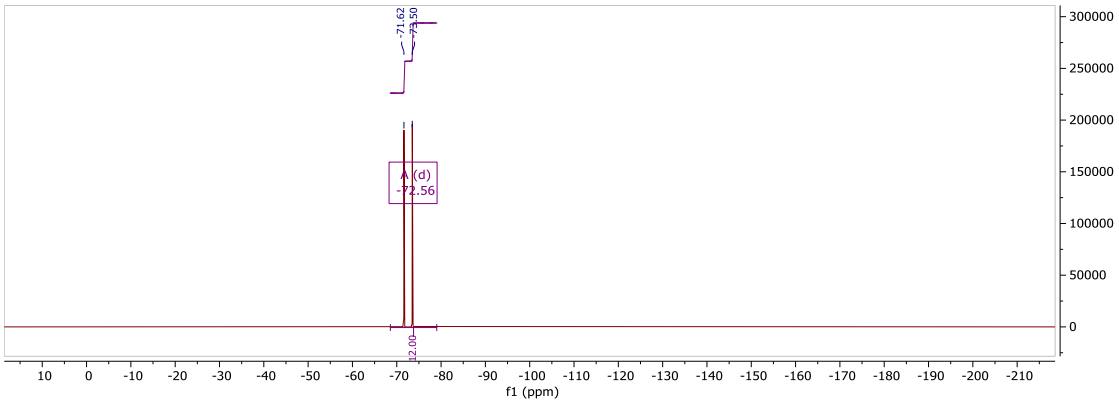

Spectrum 43 - ^{19}F NMR spectrum of *trans-(diacetonitrile)[1,1-bis(3'-methyl-imidazol-2'-yliden)methylene](1,2-ethylenediamine) ruthenium(II) dihexafluorophosphate.*

$Ru(C_9H_{14}N_4)(C_2H_8N_2)(C_2H_3N)_2(PF_6)_2$: ^{19}F-NMR($C_3D_6O$, 400MHz): δ -72.56 (d, 12F, ^{1}J= 647.12 Hz).

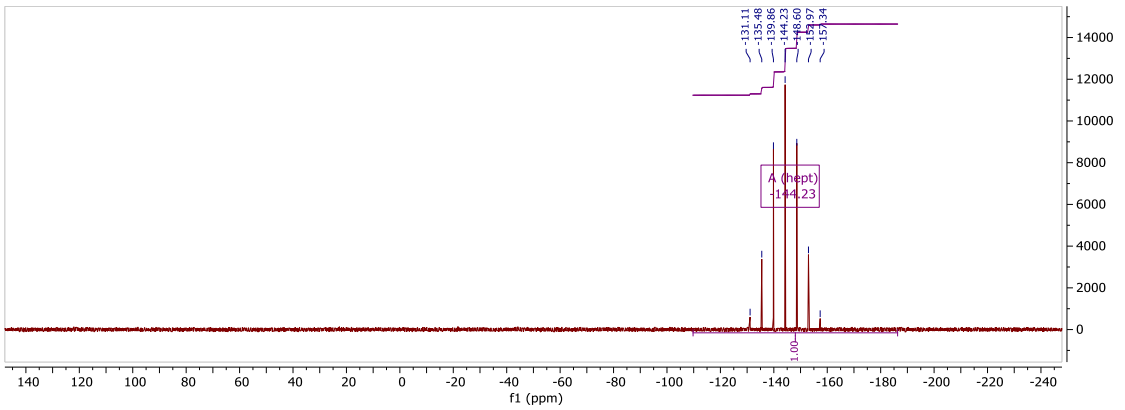

Spectrum 44 – ^{31}P NMR spectrum of *trans-(diacetonitrile)[1,1-bis(3'-methyl-imidazol-2'-yliden)methylene] (1,2-ethylenediamine) ruthenium(II) dihexafluorophosphate*.

$Ru(C_9H_{14}N_4)(C_2H_8N_2)(C_2H_3N)_2(PF_6)_2$: ^{31}P-NMR($C_3D_6O$, 400MHz): δ -144.23 (hept, 2P, ^{1}J= 706.99 Hz).

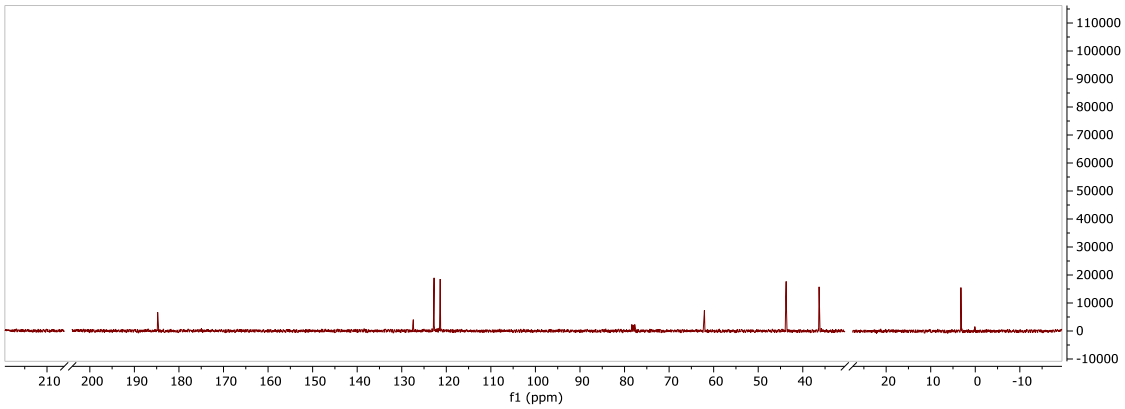

Spectrum 45 - ^{13}C NMR spectrum of *trans-(diacetonitrile)[1,1-bis(3'-methyl-imidazol-2'-yliden)methylene](1,2-ethylenediamine) ruthenium(II) dihexafluorophosphate*.

$Ru(C_9H_{14}N_4)(C_{10}H_8N_2)(C_2H_3N)_2(PF_6)$: ^{13}C-NMR($C_3D_6O$, 400MHz): δ (ppm) 184.90 (**6 + 10**), 127.34 (**13 + 14**), 122.86 (**5 + 8**), 121.43 (**4 + 9**), 62.00 (**7**), 43.68 (**1 + 2**), 36.28 (**3+11**) 3.15 (**12 +15**).

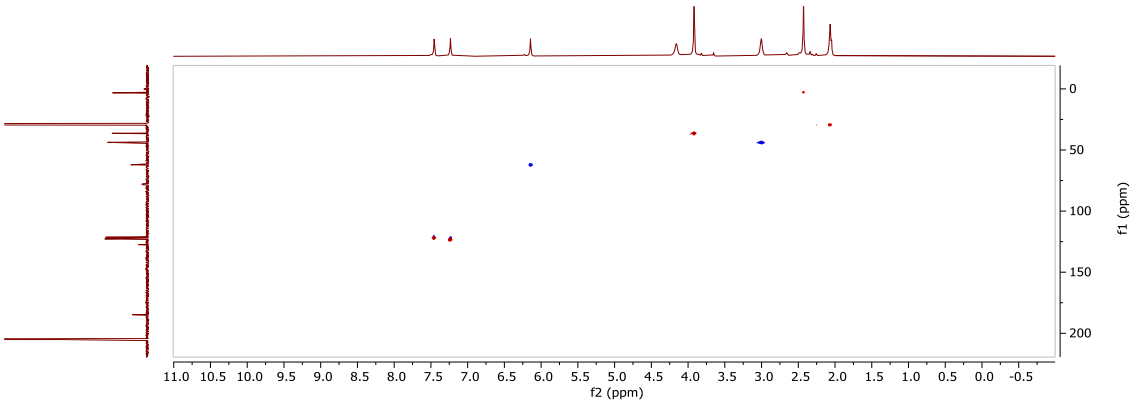

Spectrum 46 - ^{1}H-^{13}C HSQC NMR spectrum of *trans-(diacetonitrile)[1,1-bis(3'-methyl-imidazol-2'-yliden)methylene] (1,2-ethylenediamine) ruthenium(II) dihexafluorophosphate.*

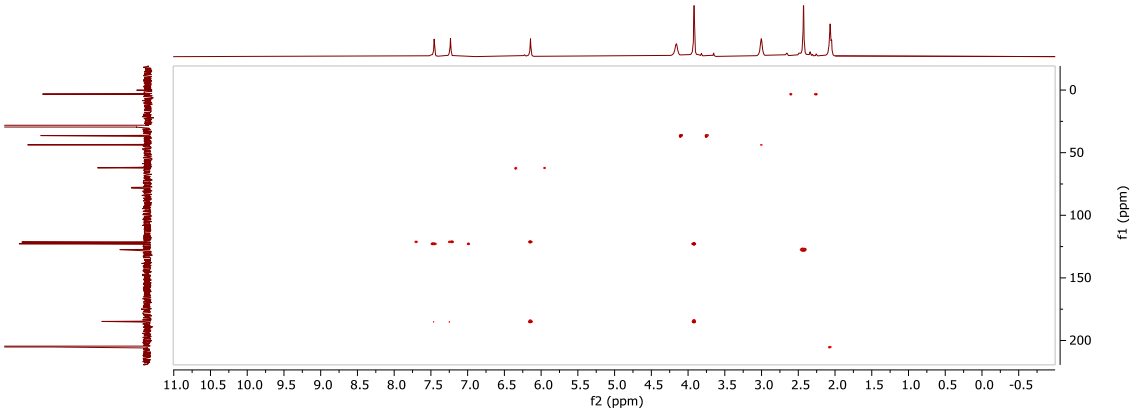

Spectrum 47 - ^{1}H-^{13}C HMBC NMR spectrum of *trans-(diacetonitrile)[1,1-bis(3'-methyl-imidazol-2'-yliden)methylene](1,2-ethylenediamine) ruthenium(II) dihexafluorophosphate.*

4.11 Synthesis of *trans*-Ru(ACN)$_2$(b(MI)M)(dppp)(PF$_6$)$_2$ (**13**)

Procedure

A 25 mL Schlenk was charged with 84 mg (0.30 mmol, 1 eq) of ruthenium(II) *(1,5-cyclooctadiene)(dichloro) ruthenium(II) polymer* and with 130 mg (0.30 mmol,1 eq) of *1,1-bis(3'-methylimidazolium)methylene diiodide*. The tube was set under argon cycling vacuum and argon 3 times, then 4 mL (75 eq) of *ACN* anhydrous and degassed were added. The solution was left stirring at reflux for 2 h, then 200 uL (1.50 mmol, 5 eq) of degassed *TEA* were added. The mixture was left reacting for 48 h at reflux, or till the red solution is homogeneous, then the hot solution was cannula filtrated under argon in a second 25 mL Schlenk tube and dried under vacuum. The orange solid was dissolved in 4 mL of anhydrous and degassed *DCM*, and subsequently, 124 mg (0.30 mmol, 1 eq) of *1,3-bis(diphenylphosphino)propane* were added. The homogeneous solution was left reacting for 3 h at room temperature, then 220 mg (1.2 mmol, 1 eq) of *potassium hexafluorophosphate* were added, and *water* (3mL) was poured into the solution under vigorous stirring. The organic phase was separated and extraction with *DCM* (3 x 3 mL) was carried out on the remaining acquous phase. The organic phase was dried under vacuum and dissolved in *acetone*, the solution was loaded for flash colum chormatography using neutral deactivated alumina as the stationary phase and a 1:1 mixture of *acetone*/*DCM* as eluent. The solvent was removed at the rotary evaporator, obtaining the product as a white solid which was further dried overnight under vacuum. (R_F = 0.72, 40% yield)

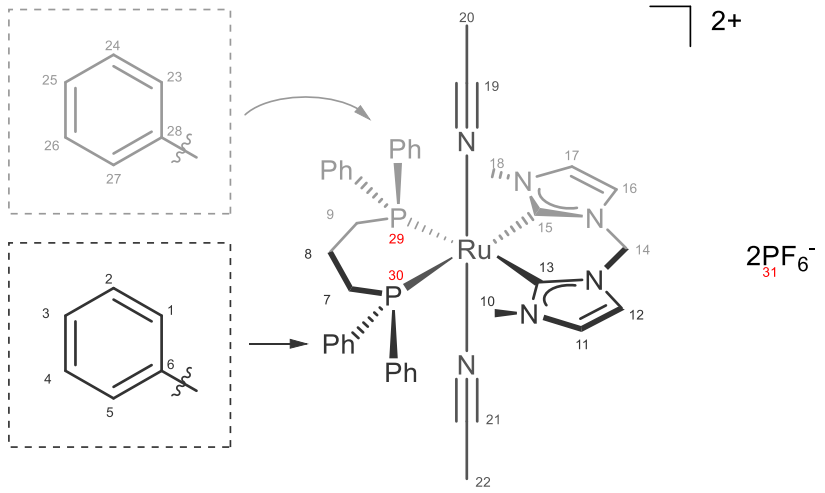

Figure 50 - The structure of *trans-[1,1-Bis(3'-methylimidazol-1'-ylidene)methylene][1,3-bis(diphenylphosphino)propane](diacetonitrile) ruthenium(II) dihexafluorophosphate.*

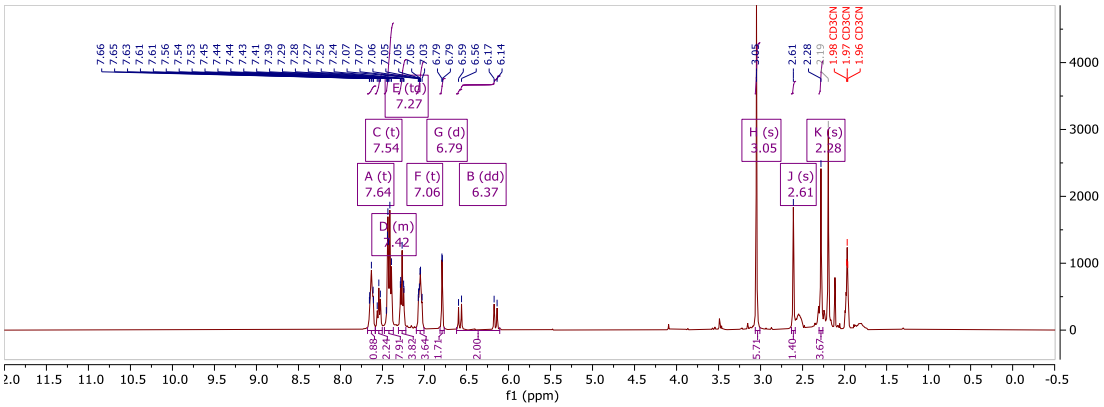

Spectrum 48 - ^{1}H NMR spectrum of *trans-[1,1-Bis(3'-methylimidazol-1'-ylidene)methylene][1,3-bis(diphenylphosphino)propane](diacetonitrile) ruthenium(II) dihexafluorophosphate.*

$Ru(C_9H_{14}N_4)(C_{27}H_{26}P_2)(C_2H_3N)(PF_6)_2$: ^{1}H-NMR($CD_3CN$, 400MHz): δ (ppm) 7.64 (t, 4H, ^{3}J = 7.70 Hz, **1 + 5**), 7.55 (t, 2H, ^{3}J=7.19Hz, **3**), 7.41 (m, 8H, **2 + 4 + 25 + 12 + 16**), 7.26 (t, 4H, J=7.29Hz, **24 + 26**), 7.06 (t, 4H,), 6.79 (d, 2H, $^{3}J_{H11\text{-}H12\ /\ H17\text{-}H16}$= 1.94Hz, **11 + 17**), 6.58 (d, 1H, $^{1}J_{H14}$ = 14.27, **14**), 6.16 (d, 1H, $^{1}J_{H14}$ = 14.27, **14**), 3.05 (s, 6H, **10 + 18**), 2.61 (s, 6H, **20 + 22**), 2.54 (m, 2H, **7 + 9**), 2.19 (m, 5H, **8 + 20 + 22**), 1.97 (m, 2H, **8**).

NOTE: *coupling constant are partially assigned due to phosphorous coupling effect on the NMR spectra.*

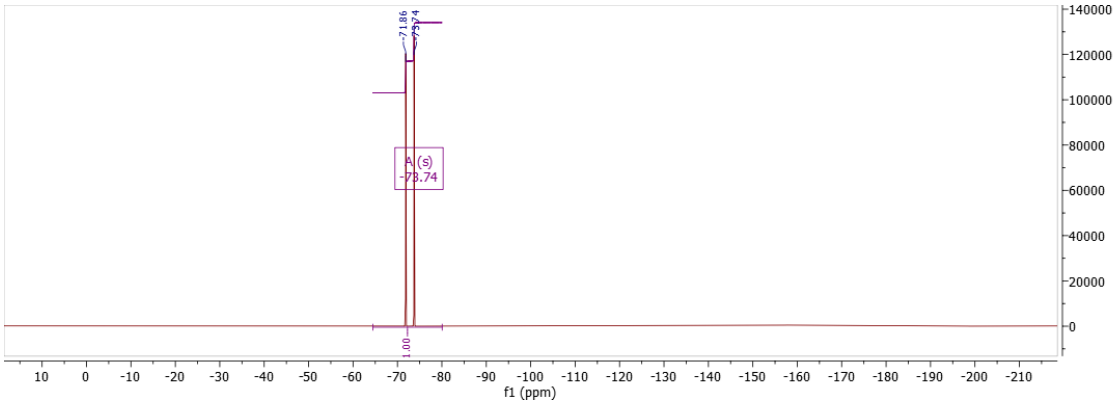

Spectrum 49 - ^{19}F NMR spectrum of *trans-[1,1-Bis(3'-methylimidazol-1'-ylidene)methylene][1,3-bis(diphenylphosphino)propane](diacetonitrile) ruthenium(II) dihexafluorophosphate.*

$Ru(C_9H_{14}N_4)(C_{27}H_{26}P_2)(C_2H_3N)(PF_6)_2$: ^{19}F-NMR($CD_3CN$, 400MHz): δ (ppm) -71.59(d, 12F, ^{1}J= 714.6Hz).

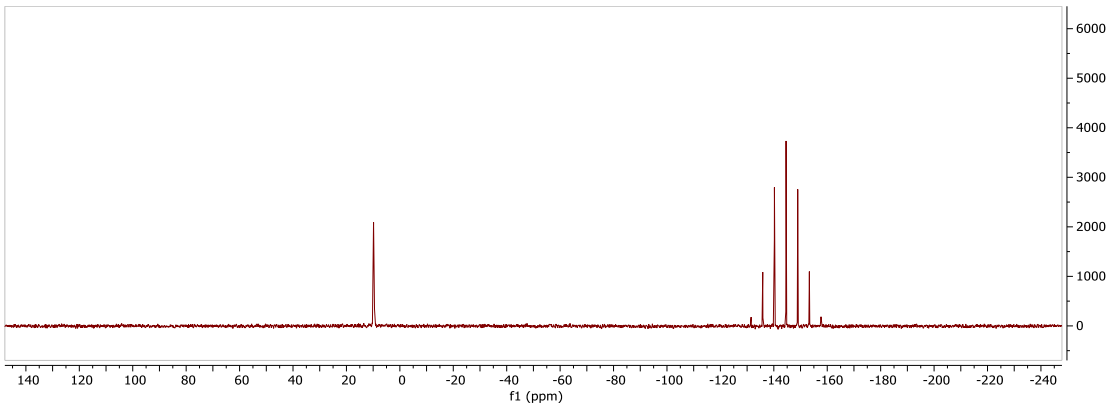

Spectrum 50 – ^{31}P NMR spectrum of *trans-[1,1-Bis(3'-methylimidazol-1'-ylidene)methylene][1,3-bis(diphenylphosphino)propane](diacetonitrile) ruthenium(II) dihexafluorophosphate.*

$Ru(C_9H_{14}N_4)(C_{27}H_{26}P_2)(C_2H_3N)(PF_6)_2$: ^{31}P-NMR(C_2D_3N, 400MHz): δ (ppm) 9.76 (d, 2P, $^3J_{P29\text{-}H9\ /\ P30\text{-}H7}$ = 22.10 Hz, **29 - 30**), -144.9 (hept, 2P, $^1J_{P31\text{-}F}$= 747.39Hz, **31**).

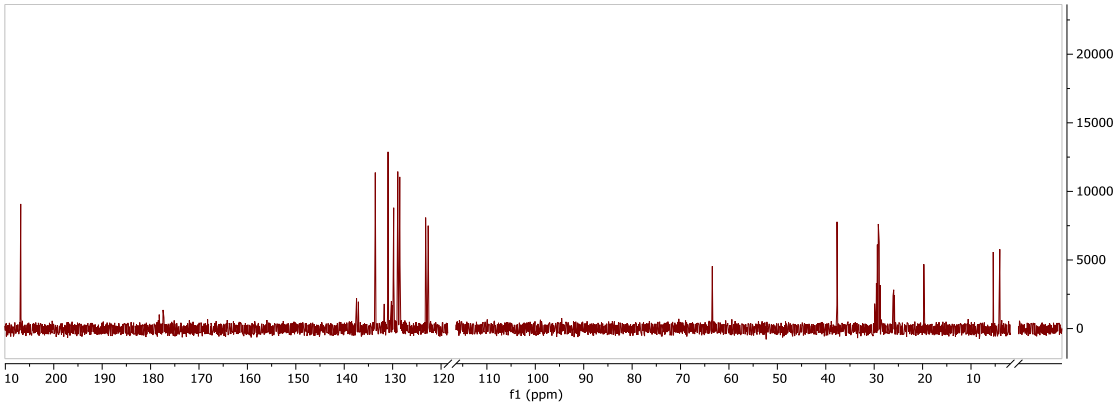

Spectrum 51 - ^{13}C NMR spectrum of *trans-[1,1-Bis(3'-methylimidazol-1'-ylidene)methylene][1,3-bis(diphenylphosphino)propane](diacetonitrile) ruthenium(II) dihexafluorophosphate.*

$Ru(C_9H_{14}N_4)(C_{27}H_{26}P_2)(C_2H_3N)(PF_6)_2$: ^{13}C-NMR($C_2D_3N$, 400MHz): δ (ppm) 177.50 (d, $^3J_{P30\text{-}C15/P29\text{-}C13}$ = 80.02 Hz, **13 + 15**), 137.27 (t, ^1J = 18.90 Hz, **6**), 130.07 (t, ^1J = 17.05 Hz, **28**), 133.67 (t, J = 4.45 Hz, **1 + 5**), 130.94 (t, J = 4.45 Hz, **3**), 131.03 (t, J = 4.45 Hz, **23 + 27**), 129,76 (t, J = 4.45 Hz, **25**), 128.85 (t, J = 4.45 Hz, **2 + 4**), 128.55 (t, J = 4.45 Hz, **24 + 26**), 123.25 (**12 + 16**), 122.64 (**11 + 17**), 63.40 (**14**), 37.66 (**10 + 18**), 25,91 (t, $^1J_{P30\text{-}C7\ /\ P29\text{-}C9}$ = 14.50 Hz, **7 +9**), 19.72 (s, **8**), 5.45 (**20 + 22**).

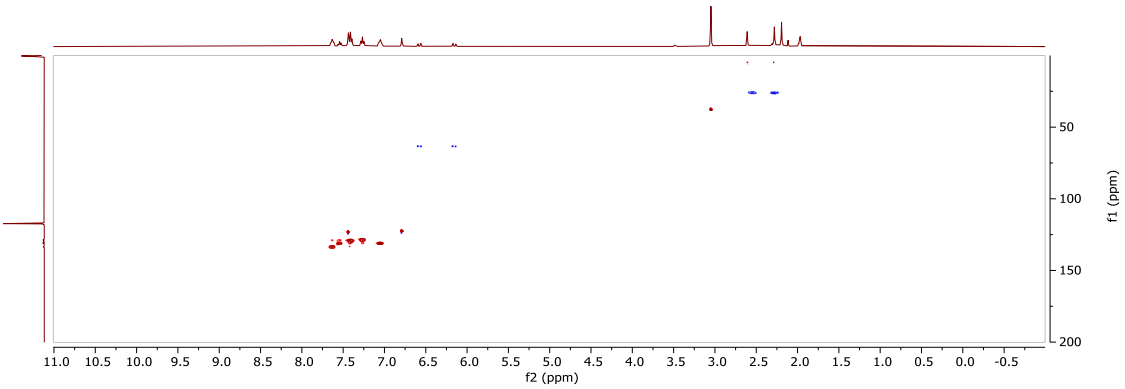

Spectrum 52 - ^{1}H-^{13}C HSQC NMR spectrum of *trans-[1,1-Bis(3'-methylimidazol-1'-ylidene)methylene][1,3-bis(diphenylphosphino)propane](diacetonitrile) ruthenium(II) dihexafluorophosphate.*

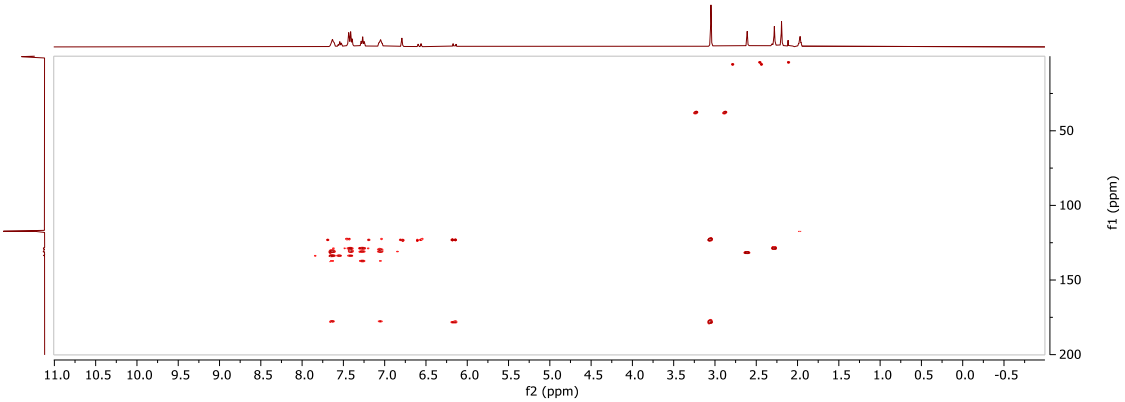

Spectrum 53 - ^{1}H-^{13}C HMBC NMR spectrum of *trans-[1,1-Bis(3'-methylimidazol-1'-ylidene)methylene][1,3-bis(diphenylphosphino)propane](diacetonitrile) ruthenium(II) dihexafluorophosphate.*

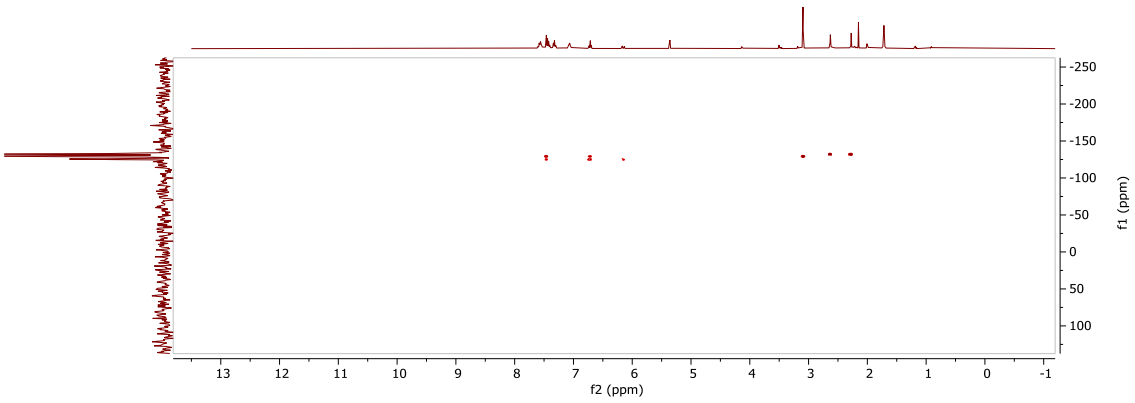

Spectrum 54 - ^{1}H-^{15}N HMBC NMR spectrum of *trans-[1,1-Bis(3'-methylimidazol-1'-ylidene)methylene][1,3-bis(diphenylphosphino)propane](diacetonitrile) ruthenium(II) dihexafluorophosphate.*

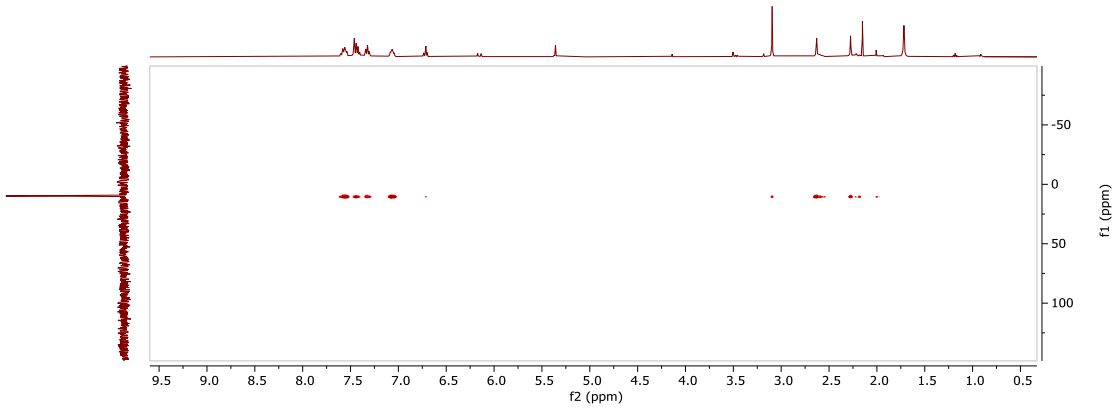

Spectrum 55 - ^{1}H-^{31}P HMBC NMR spectrum of *trans-[1,1-Bis(3'-methylimidazol-1'-ylidene)methylene][1,3-bis(diphenylphosphino)propane](diacetonitrile) ruthenium(II) dihexafluorophosphate*.

4.12 Synthesis of *cis*-Ru(ACN)$_2$(b(MI)M)(dppp)(PF$_6$)$_2$ (**14**)

Procedure

A 15 mL pressure tube was charged with (0.30 mmol, 1 eq) of *trans-[1,1-Bis(3'-methylimidazol-1'-ylidene)methylene][1,3-bis(diphenylphosphino)propane](diacetonitrile) ruthenium(II) dihexafluorophosphate*, then 10 mL of dry and degassed *ACN* were added under argon counterflow. The pressure tube was sealed and placed in an oil bath at 120°C. After 96 h, the solution was cooled, and the solvent was removed. The residue was dissolved in boiling *methanol* and crystallized overnight. The resulting red crystals were isolated via filtration, washed with *diethyl ether* (3 x 5 mL), and dried under vacuum (% yield).

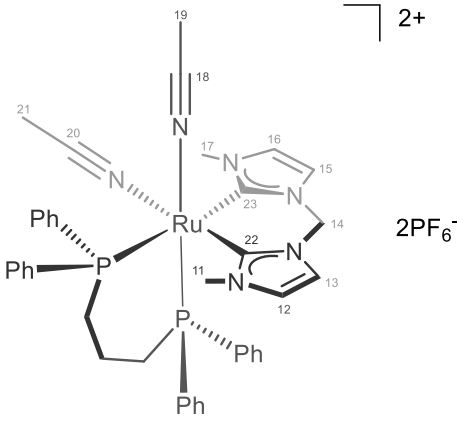

Figure 51 - The structure of *cis-[1,1-Bis(3'-methylimidazol-1'-ylidene)methylene][1,3-bis(diphenylphosphino)propane](diacetonitrile) ruthenium(II) dihexafluorophosphate.*

Characterization

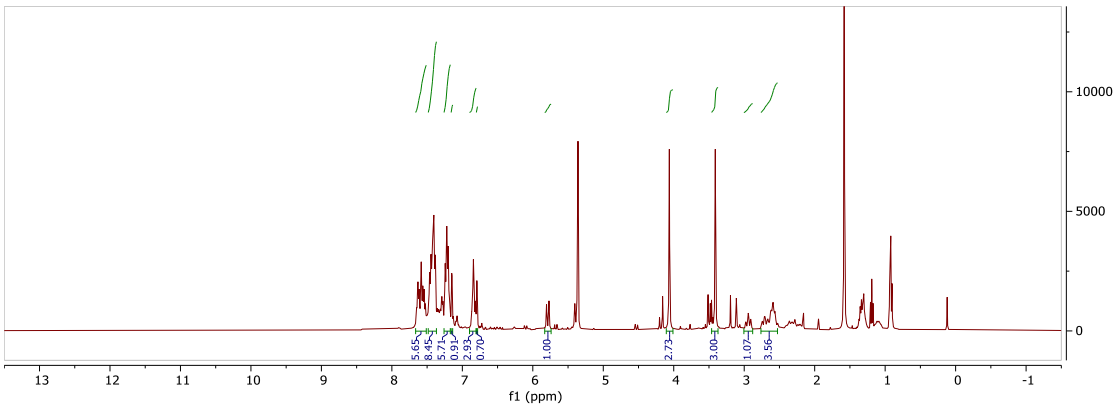

Spectrum 56 - ^{1}H NMR spectrum of *cis-[1,1-Bis(3'-methylimidazol-1'-ylidene)methylene][1,3-bis(diphenylphosphino)propane](diacetonitrile) ruthenium(II) dihexafluorophosphate.*

Ru($C_9H_{14}N_4$)($C_{27}H_{26}P_2$)(C_2D_3N)(PF_6)$_2$: ^{1}H NMR(CD_3CN, 400MHz): δ (ppm) 7.58 (m, 6H), 7.42 (m, 8H), 7.21 (m, 5H), 7.14 (m, 1H), 6.84 (m, 3H), 6.79 (m, 1H), 5.79 (d, 1H, $^1J_{H14}$ = 14.00, **14**),), 5.38 (d, 1H, $^1J_{H14}$ = 14.00, **14**), 4.06 (s, 3H, **11** or **17**), 3.41 (s, 3H, **11** or **17**), 2.94 (t, 1H), 2.64 (m, 4H), 2.32 (m, 1H).

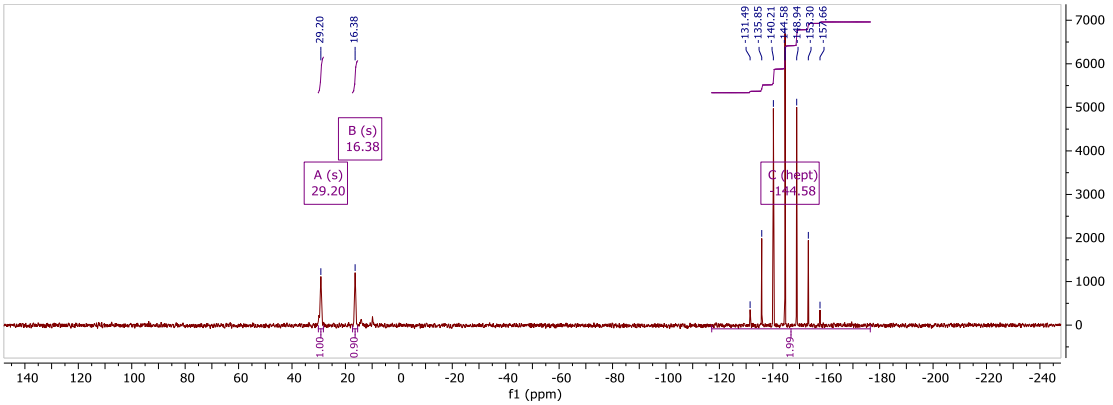

Spectrum 57 – ^{31}P H NMR spectrum of *cis-[1,1-Bis(3'-methylimidazol-1'-ylidene)methylene][1,3-bis(diphenylphosphino)propane](diacetonitrile) ruthenium(II) dihexafluorophosphate*.

$Ru(C_9H_{14}N_4)(C_{27}H_{26}P_2)(C_2H_3N)(PF_6)_2$: ^{31}P-NMR(C_2D_3N, 400MHz): δ (ppm) 29.20 (m, 1P), 16.38 (m, 1P), -144.9 (hept, 2P, $^1J_{P31-F}$= 747.39Hz).

Kinetic – isomerization of *trans*-$Ru(ACN)_2(b(MI)M)(dppp)(PF_6)_2$ (**13**)

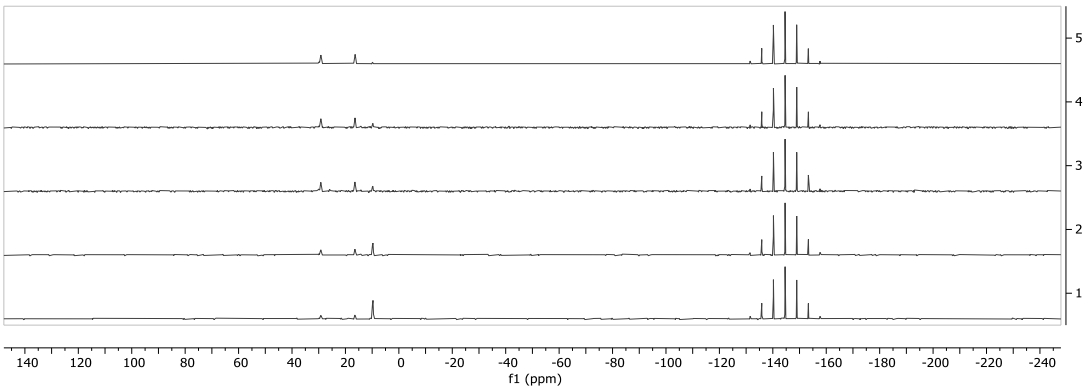

Kinetic 1 – Viewed from the ^{31}P NMR, the evolution of the isomerization process by which the conversion of *trans-[1,1-Bis(3'-methylimidazol-1'-ylidene)methylene][1,3-bis(diphenylphosphino)propane](diacetonitrile) ruthenium(II) dihexafluorophosphate* to *cis-[1,1-Bis(3'-methylimidazol-1'-ylidene)methylene][1,3-bis(diphenylphosphino)propane](diacetonitrile) ruthenium(II) dihexafluorophosphate* was assessed. The reagent consumption is observed by the disappearance of of the related peak falling at 9.76 ppm.

4.13 Synthesis of 2,4,6-trimethylphenyl azide

Procedure

The synthesis of *2,4,6-trimethylphenyl azide* is known, and the same procedure was followed with minor variations.[162] A 50 mL round bottom Schlenk flask was charged under argon counterflow with 5.7 mL (41.0 mmol, 1.0 eq) of *mesityl-aniline* and 90 mL of anhydrous *acetonitrile*. The solution was cooled to -10 °C in a water-table salt ice bath and subsequently 7.3 mL (61.0 mmol, 1.5 eq) of *tert-butyl nitrite* were added dropwise to the solution. After 10 minutes 6.5 mL (49.0 mmol, 1.2 eq) of *azido-trimethyl silane* were added dropwise to the solution, which was left reacting till room temperature was reached in 2 h. The solvent was removed at the rotary evaporator and the dark orange oil was purified via flash filtration through a neutral deactivated alumina plug using *pentane* as eluent. The solvent was removed to obtain the product. Yield 92%.

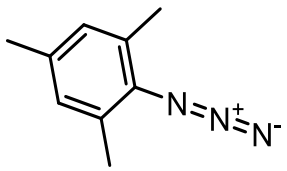

Figure 52 - The structure of *2,4,6-trimethylphenyl azide*.

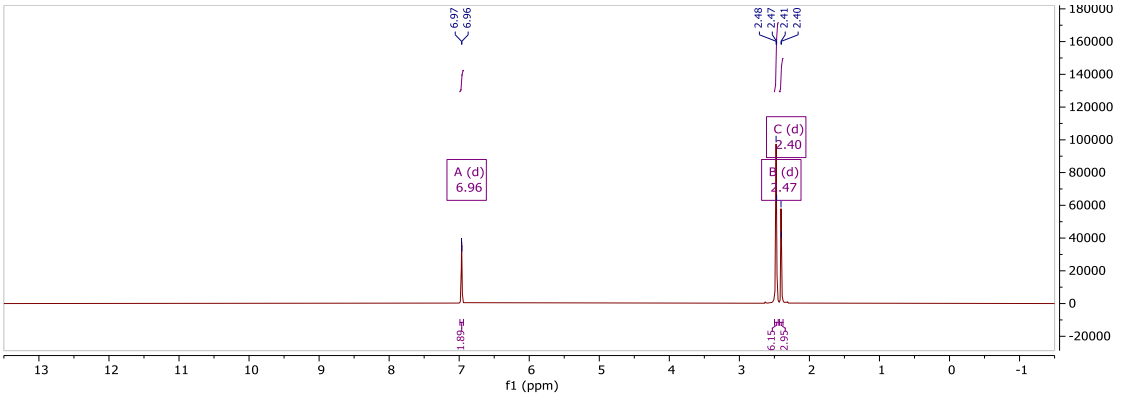

Spectrum 58 - ^{1}H NMR spectrum of *2,4,6-trimethylphenyl azide.*

$C_9H_{11}N_3$: ^{1}H-NMR ($CDCl_3$, 400MHz): δ 6.97 (d, 2H, ^{4}J = 2.1 Hz,), 2.47 (d, ^{4}J = 3.0 Hz, 6H), 2.40 (d, ^{4}J = 2.5 Hz, 3H).

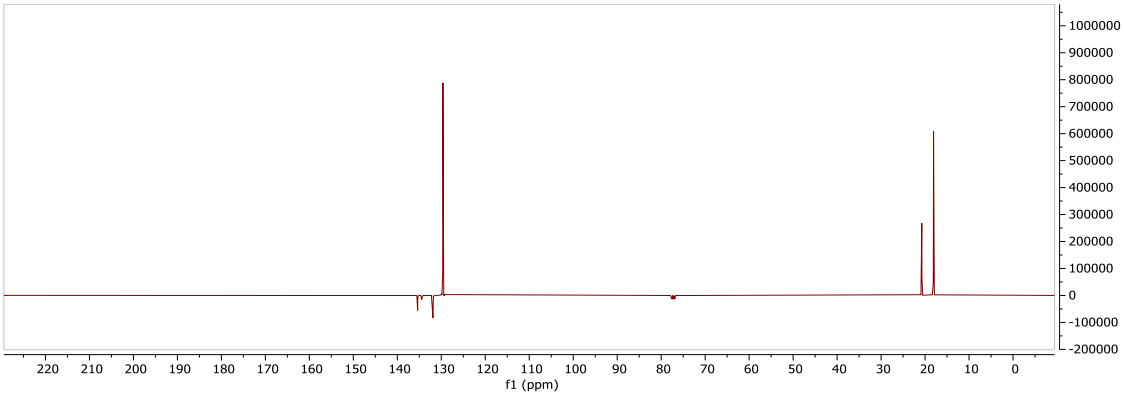

Spectrum 59 - ^{13}C NMR spectrum of *2,4,6-trimethylphenyl azide.*

$C_9H_{11}N_3$: ^{13}C-NMR ($CDCl_3$, 400MHz): δ 135.38, 134.50, 131.90, 129.64, 20.75, 18.08.

4.14 Synthesis of 1-mesityl-1,2,3-triazole

Procedure

The synthesis of *1-aryl-1,2,3-triazoles* is known, and the available literature procedure was followed with minor variations.[163,164]A 500 mL round bottom Schlenk flask was charged with 0.770 g (3.0 mmol, 0.1 eq) of *copper sulfate pentahydrate* and 1.230 g (6.0 mmol, 0.2 eq) of *sodium ascorbate*, and then the air was removed from the reaction vessel cycling vacuum and argon. 100 mL of *water* and *methanol* solution in a 1:1 ratio were added alongside 5.0 g (31.0 mmol, 1 eq) of *mesityl azide*. Subsequently, 8.6 mL (62.0 mmol, 2 eq) of *trimethylsilyl acetylene* were added dropwise to the solution, and the mixture was left reacting under stirring for 7 days at 25°C. The mixture was reduced in volume, and 200 mL of a 15 % water-based *ammonia* solution were added. The mixture was stirred for 10 h, then extraction with solvent was carried out using first 200 mL and then 2 x 50 mL aliquots of *ethyl acetate*. The organic solution was washed with 2 x 50 mL of water, with 50 mL of *brine* afterward, and dried with *sodium sulfate*. After filtration, the solvent was removed, and a pale-yellow solid was isolated. The isolated bulk solid contained the desired product, and the TMS-protected *1-mesityl-4-TMS-1,2,3-triazole* in a 1:3 ratio. The compounds were dissolved in a 1:1 water and methanol solution containing *potassium carbonate* and placed at 70 °C for 3 days. The methanol was removed at the rotary evaporator, and extraction with DCM was conducted. The organic phase was washed with 50 mL of water, 50 mL of *brine* and then dried with *sodium sulfate*. The solvent was removed, and the white powder was washed with 3 x 20 mL aliquots of cold *diethyl ether,* obtaining the final product. Yield 70%.

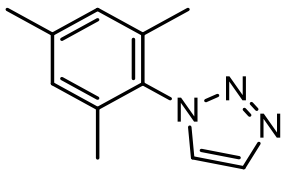

Figure 53 - The structure of *1-mesityl-1,2,3-triazole*.

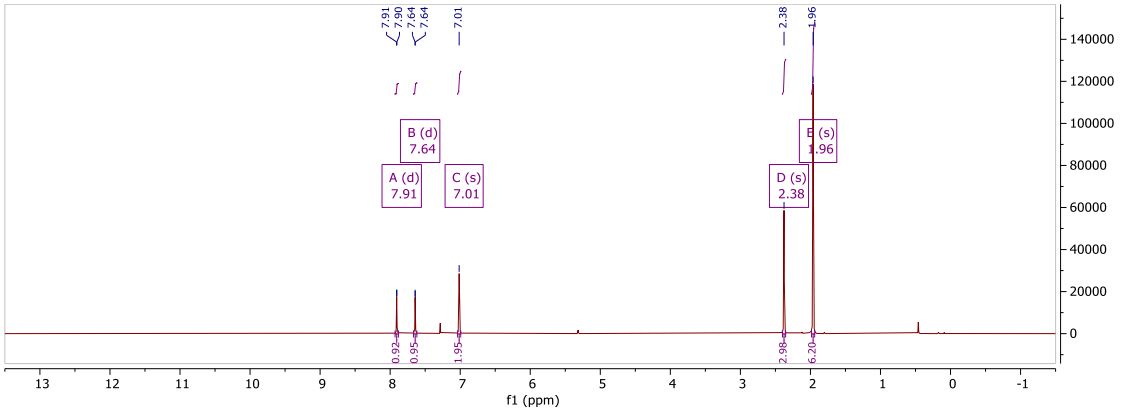

Spectrum 60 - ^{1}H NMR spectrum of *1-mesityl-1,2,3-triazole*.

$C_{11}H_{13}N_3$: ^{1}H-NMR ($CDCl_3$, 400MHz): δ (ppm) 7.91 (s, 1H), 7.64 (s, 1H), 7.02 (s, 2H), 2.38 (s, 3H), 1.96 (s, 6H).

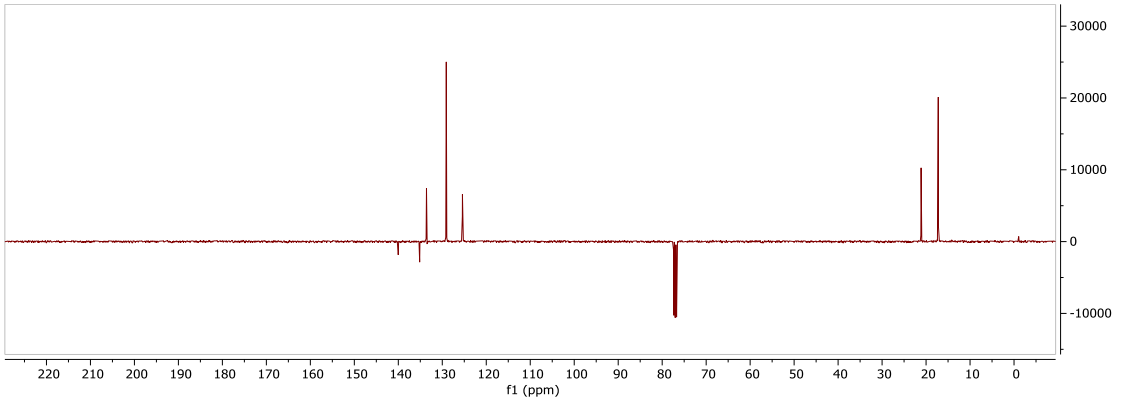

Spectrum 61 - ^{13}C NMR spectrum of *1-mesityl-1,2,3-triazole*.

$C_{11}H_{13}N_3$: ^{13}C-NMR ($CDCl_3$, 400MHz): δ (ppm) 140.03, 135.15, 133.59, 129.10, 125.44, 21.13, 17.24.

4.15 Synthesis of methylene bis(trifluoromethanesulfonate)

Procedure

The synthesis of *methylene bis-trifluoromethanesulfonate* is known, and the same procedure was followed with minor variations.[165]A Schlenk tube was charged with 0.5 g (17.0 mmol, 1.0 eq) of *paraformaldehyde* and the air was removed by cycling vacuum and argon. 3 mL (17.0 mmol, 1.1 eq) of *trifluoromethanesulfonic anhydride* were added dropwise to the bulk solid under stirring, and the mixture was transferred to an oil bath at 60°C. After 24h the excess of *trifluoromethanesulfonic anhydride* was neutralized using anhydrous *methanol* and the black mixture was filtered through a silica plug using dry *DCM* as eluent. The solvent was removed at the rotatory evaporator obtaining a pale-yellow oil. Yield 11%.

Note: The product is volatile and can be detected as residue in the nitrogen trap of the evaporator, to avoid product loss use a water-ice bath, and two liquid nitrogen cold traps.

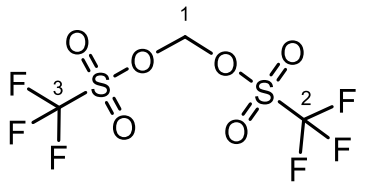

Figure 54 - The structure of *methylene bis(trifluoromethanesulfonate)*.

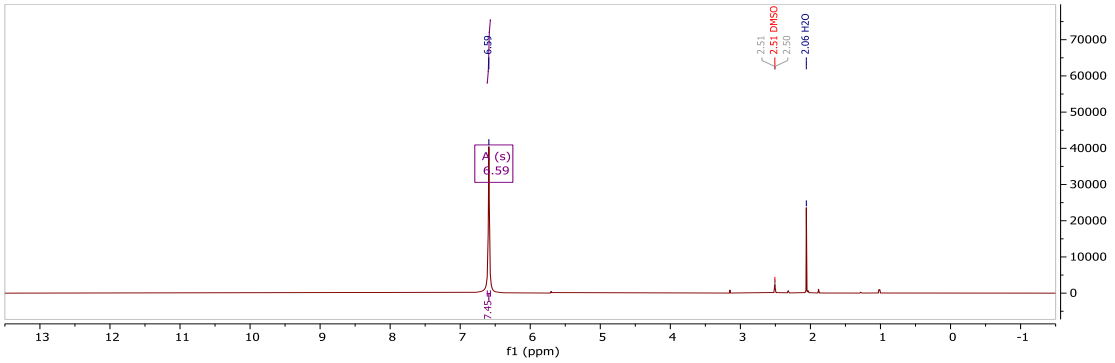

Spectrum 62 - ^{1}H NMR spectrum of *methylene bis(trifluoromethanesulfonate).*

$C_3H_2F_6O_6S_2$: ^{1}H-NMR (DMSO-D6, 400MHz): δ 6.60 (s, 2H)

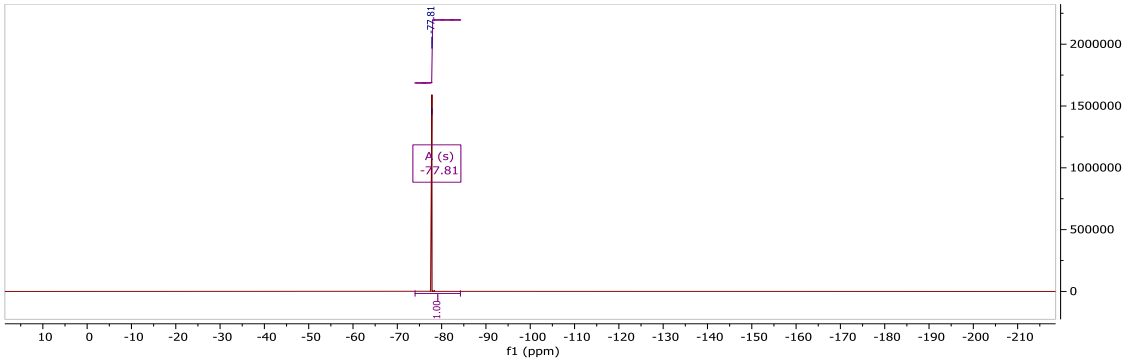

Spectrum 63 - ^{19}F NMR spectrum of *methylene bis(trifluoromethanesulfonate).*

$C_3H_2F_6O_6S_2$: ^{19}F-NMR (DMSO-D6, 400MHz): δ 77.81 (s, 6F)

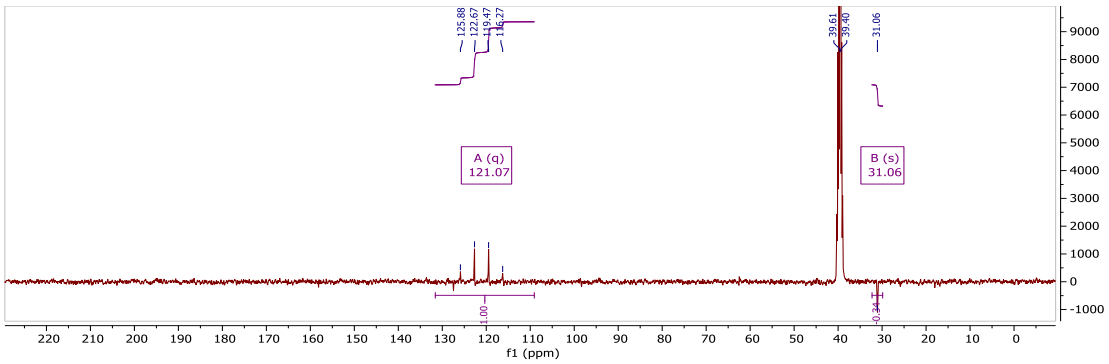

Spectrum 64 - ^{13}C NMR spectrum of *methylene bis(trifluoromethanesulfonate).*

$C_3H_2F_6O_6S_2$: ^{13}C-NMR (DMSO-D6, 400MHz): δ 121.30 (q, 2C, $^{1}J_{C2\text{-}F\ /\ C3\text{-}F}$ = 340 Hz, **2 + 3**), 30.90 (s, 1C, **1**).

4.16 Synthesis of 1,1-bis(1'-mesityl-1',2',3'-triazolium) methylene ditrifluoromethanesulfonate

Procedure

A Schlenk tube was heated while applying vacuum and left cooling till room temperature. 320 mg (1.7 mmol, 2 eq) of *mesityl-1,2,3-triazole* were added and the air was removed cycling vacuum and argon in the flask. The solid was dissolved using 15 mL of anhydrous *ACN*. 267mg (0.9 mmol, 1 eq) of *methylene bis-trifluoromethanesulfonate* diluted in 15 mL of anhydrous *ACN* were later added with a syringe dropwise to the solution under vigorous stirring. The reacting mixture was transferred to an oil bath after 1 h and left reacting for the following 24 h at reflux. The solvent was removed obtaining a pale-yellow solid which was further purified with *pentane* washings (2 x 15mL). The product was dried overnight. Yield 93%.

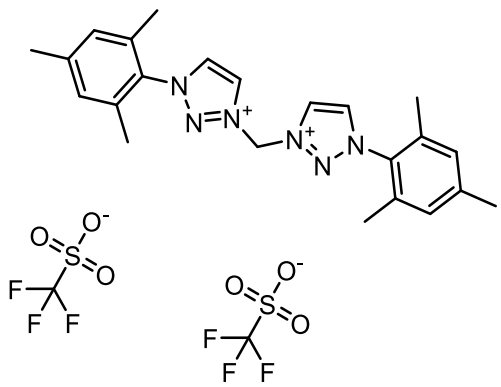

Figure 55 - The structure of *1,1-bis(1'-mesityl-1',2',3'-triazolium) methylene ditrifluoromethanesulfonate.*

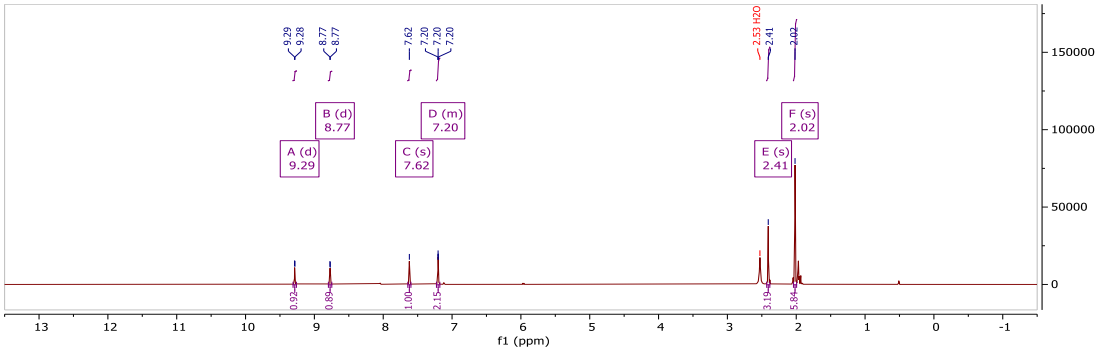

Spectrum 65 - ^{1}H NMR spectrum of *1,1-bis(1'-mesityl-1',2',3'-triazolium) methylene ditrifluoromethanesulfonate.*

$C_{25}H_{28}N_6F_6O_6S_2$: ^{1}H-NMR (CD_3CN, 400MHz): δ (ppm) 9.28 (d, J = 1.64 Hz, 2H), 8.77 (d, J = 1.64 Hz, 2H), 7.62 (s, 2H), 7.2 (s, 2H), 2.41 (s, 6H), 2.02 (s, 12H)

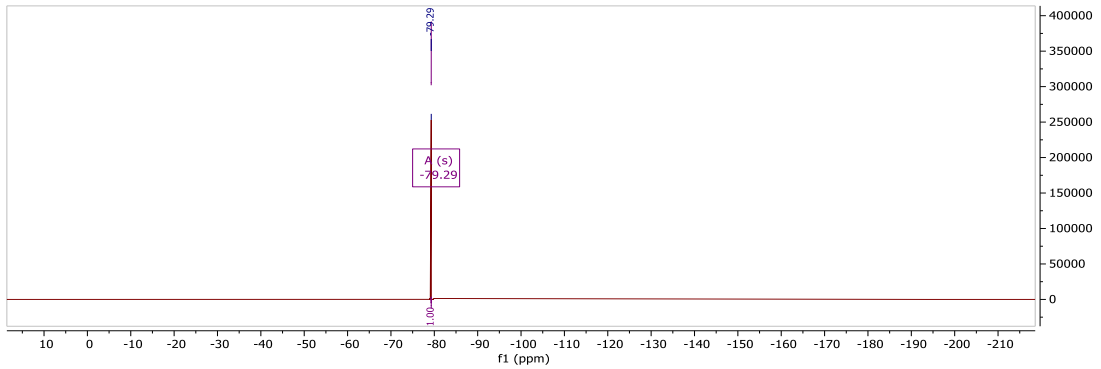

Spectrum 66 - ^{19}F NMR spectrum of *1,1-bis(1'-mesityl-1',2',3'-triazolium) methylene ditrifluoromethanesulfonate.*

$C_{25}H_{28}N_6F_6O_6S_2$: ^{19}F-NMR (CD_3CN, 400MHz): δ (ppm) -79.29 (s, 6F)

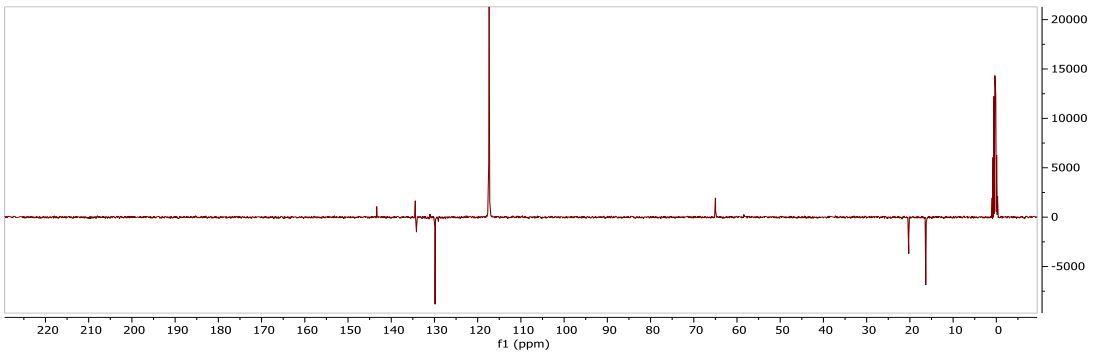

Spectrum 67 - ^{13}C NMR spectrum of *1,1-bis(1'-mesityl-1',2',3'-triazolium) methylene ditrifluoromethanesulfonate.*

$C_{25}H_{28}N_6F_6O_6S_2$: ^{13}C-NMR (CD_3CN, 400MHz): δ (ppm) 143.33, 134.43, 134.33, 134.16, 129.87, 64.97, 20.29, 16.34

4.17 Synthesis of *trans*-Ru(ACN)$_2$(bipy)(bTM)(PF6)$_2$ (**16**)

Procedure

A 50 mL Schlenk tube was charged with 111 mg (0.30 mmol, 1 eq) of *(diacetonitrile)(1,5-cyclooctadiene)(dichloro) ruthenium(II)* and 206 mg (0.30 mmol, 1 eq) of *1,1-bis(3'-mesityl-1',2',3'-triazolium)-methylene ditrifluoromethanesulfonate*. Next, air was purged from the tube by cycling vacuum and argon 3 times, then 200 uL of *TEA* and 10 mL of *ACN* were added under argon counterflow. The tube was sealed, placed in an oil bath, and the solution was brought at reflux under vigorous stirring. After 36 h the solution was removed from the bath and cooled to RT, then 46 mg (0.30 mmol, 1 eq) of *2,2'-bipyridine* were added under argon counterflow. Afterward, the mixture was left reacting at 50°C under stirring. After 24 h, the solution was reduced in volume, and water was added to precipitate the product as an oil. The mixture was triturated for 4 h, producing a fine orange powder which was isolated via filtration over gooch G3. The product was washed with *water* (2 x 15 mL) and *diethyl ether* (3 x 5 mL). Next, the solid was dissolved in *DCM* and loaded into a flash chromatography column charged with neutral deactivated alumina, and the compounds were eluted with a 9:1 mixture of *DCM* and *ACN*, yielding the desired product (RF 0.6) and *trans-(diacetonitrile)bis[1,1-Bis(3'-mesytil-1',2',3'-triazol-5'-ylidene)methylene] ruthenium(II) dihexafluorophosphate* (RF 0.7). *trans-(diacetonitrile) (2,2'-bipyridine) [1,1-Bis(3'-mesytil-1',2',3'-triazol-5'-ylidene)methylene] ruthenium(II) dihexafluorophosphate* was isolated after removing the solvent (50% yield).

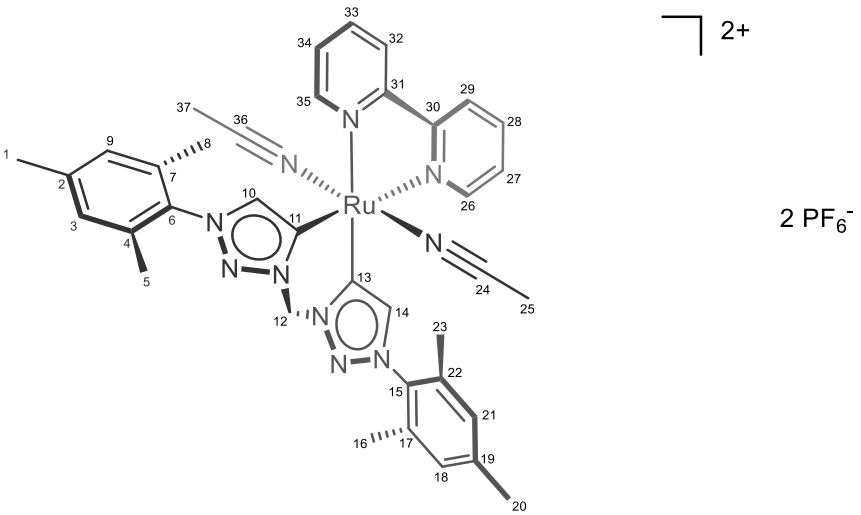

Figure 56 - The structure of *trans-(diacetonitrile) (2,2'-bipyridine) [1,1-Bis(3'-mesytil-1',2',3'-triazol-5'-ylidene)methylene] ruthenium(II) dihexafluorophosphate.*

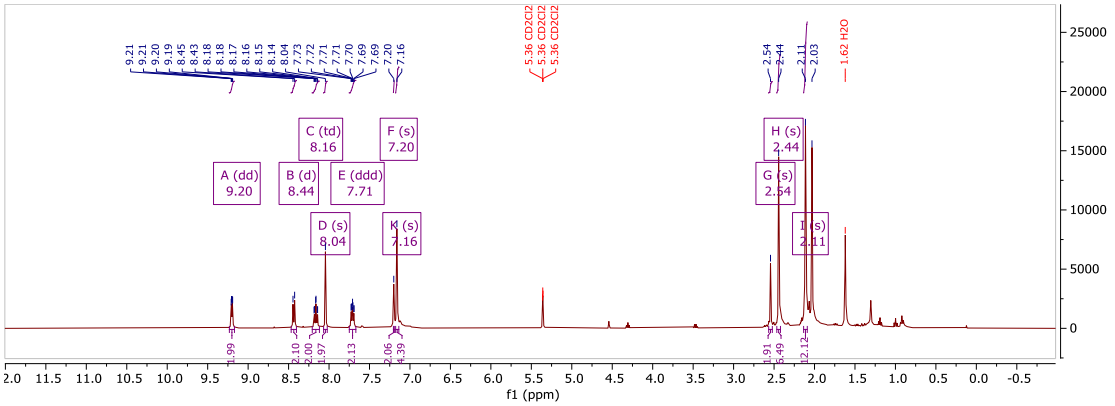

Spectrum 68 - ^{1}H NMR spectrum of *trans-(diacetonitrile) (2,2'-bipyridine) [1,1-Bis(3'-mesytil-1',2',3'-triazol-5'-ylidene)methylene] ruthenium(II) dihexafluorophosphate.*

$Ru(C_{23}H_{26}N_6)(C_{10}H_8N_2)(C_2H_3N)_2(PF_6)_2$: ^{1}H-NMR($CD_2Cl_2$, 400MHz): δ 9.20 (d, 2H, $^{3}J_{H26-H27}$, $_{H35-H34}$ = 5.25 Hz , **26 + 35**), 8.44 (d, 2H, $^{3}J_{H32-H33}$, $_{H29-H28}$ = 8.12 Hz, **29 + 32**), 8.16 (td, 2H, $^{3}J_{H34-H35}$, $_{H34-H33, H27-H26, H27-H28}$ = 8.00 Hz, $^{4}J_{H27-H29}$, $_{H34-32}$ = 1.52 Hz, **27 + 34**), 8.04 (s, 2H, **10 + 14**), 7.71 (dd, 2H, , $^{3}J_{H28-H29}$, $_{H28-H27, H33-H34, H33-H32}$ = 7.66 Hz, $^{4}J_{H28-H26, H33-H35}$ = 1.14 Hz, **28 + 33**), 7.20 (s, 2H, **12**), 7.16 (s, 4H, **3 + 9 + 18 + 21**), 2.54 (s, 3H, **25 + 37**), 2.44 (s, 6H, **1 + 20**), 2.11 (s, 12H, **5 + 8 + 16 + 23**).

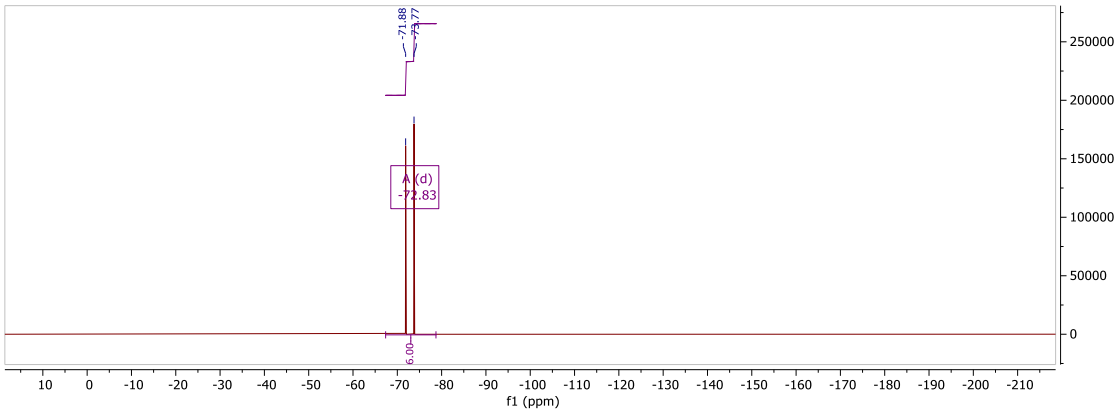

Spectrum 69 - ^{19}F NMR spectrum of *trans-(diacetonitrile) (2,2'-bipyridine) [1,1-Bis(3'-mesytil-1',2',3'-triazol-5'-ylidene)methylene] ruthenium(II) dihexafluorophosphate.*

$Ru(C_{23}H_{26}N_6)(C_{10}H_8N_2)(C_2H_3N)_2(PF_6)_2$: ^{19}F-NMR($CD_2Cl_2$, 400MHz): δ -72.83 (d, 12F, J= 714.6Hz).

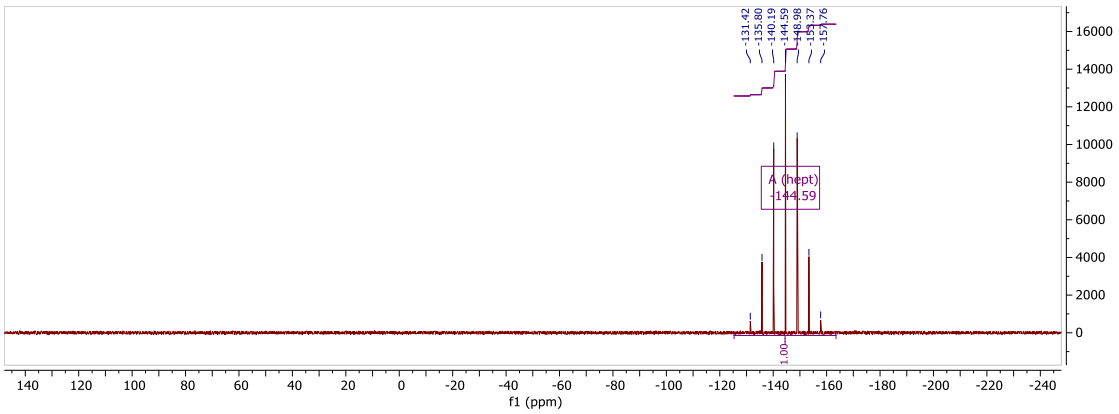

Spectrum 70 - ^{31}P NMR spectrum of *trans-(diacetonitrile) (2,2'-bipyridine) [1,1-Bis(3'-mesytil-1',2',3'-triazol-5'-ylidene)methylene] ruthenium(II) dihexafluorophosphate.*

$Ru(C_{23}H_{26}N_6)(C_{10}H_8N_2)(C_2H_3N)_2(PF_6)_2$: ^{31}P-NMR($CD_2Cl_2$, 400MHz): δ -144.59 (hept, 2P, J= 698.5.6Hz).

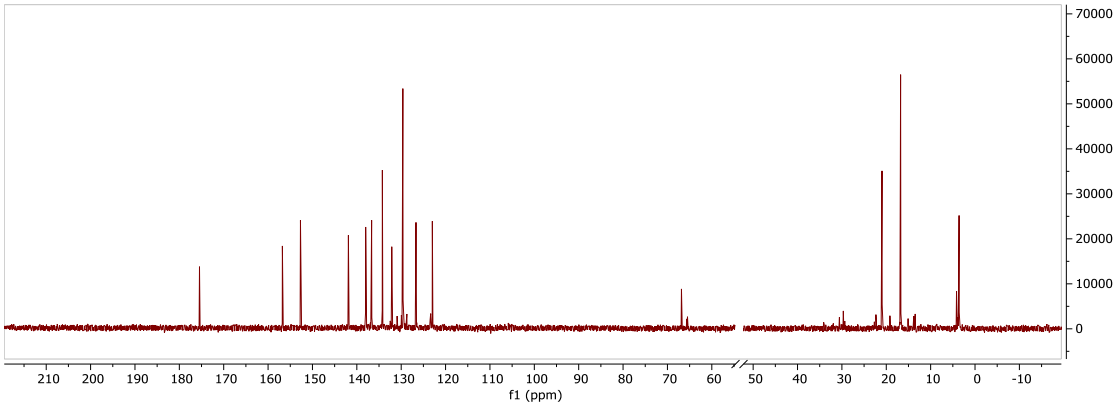

Spectrum 71 - ^{13}C NMR spectrum of *trans-(diacetonitrile) (2,2'-bipyridine) [1,1-Bis(3'-mesytil-1',2',3'-triazol-5'-ylidene)methylene] ruthenium(II) dihexafluorophosphate.*

$Ru(C_{23}H_{26}N_6)(C_{10}H_8N_2)(C_2H_3N)_2(PF_6)_2$: ^{13}C-NMR ($CD_2Cl_2$, 400MHz): δ (ppm) 175.47 (**11 + 13**), 156.78 (**30 + 31**), 152.86 (**26 + 35**), 141.90 (**2 + 19**), 138.09 (**27 + 34**), 136.61 (**10 + 14**), 134.23 (**4 + 7 + 17 + 22**), 132.19 (**6 + 15**), 129.72 (**3 + 9 + 18 + 21**), 126.77 (**28 + 33**), 123.48 (**24 + 36**), 123.08 (**29 + 32**), 66.85 (**12**), 20.90 (**1 + 20**), 16.77 (**5 + 8 + 16 + 23**) , 3.58 (4.19) (**25 + 37**).

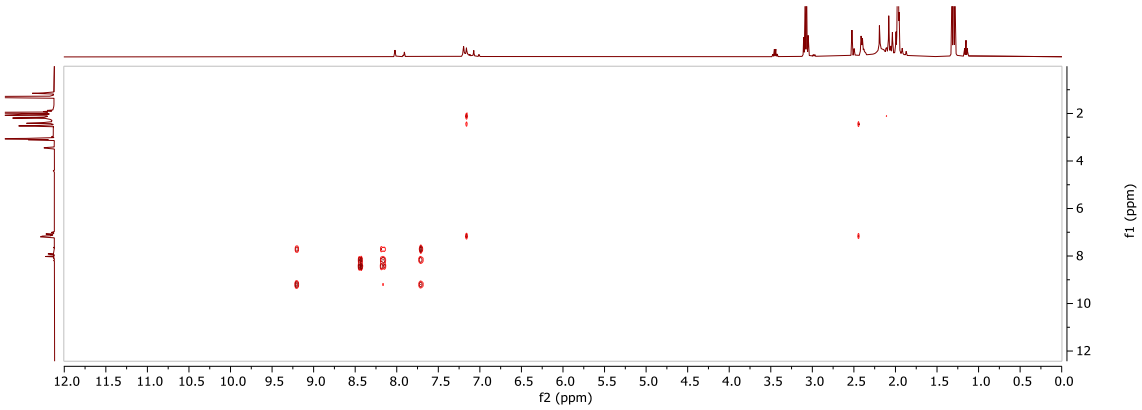

Spectrum 72 - ^{1}H-^{1}H COSY NMR spectrum of *trans-(diacetonitrile) (2,2'-bipyridine) [1,1-Bis(3'-mesytil-1',2',3'-triazol-5'-ylidene)methylene] ruthenium(II) dihexafluorophosphate.*

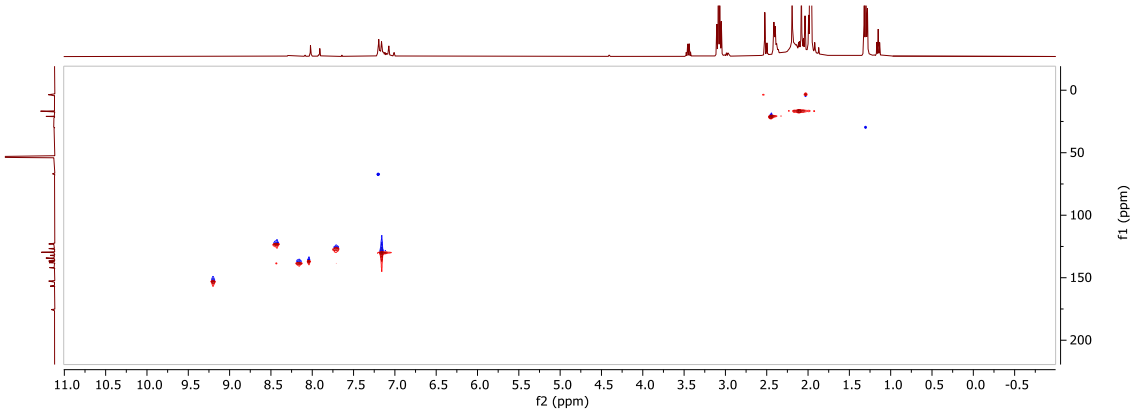

Spectrum 73 - ^{1}H-^{13}C HSQC NMR spectrum of *trans-(diacetonitrile) (2,2'-bipyridine) [1,1-Bis(3'-mesytil-1',2',3'-triazol-5'-ylidene)methylene] ruthenium(II) dihexafluorophosphate.*

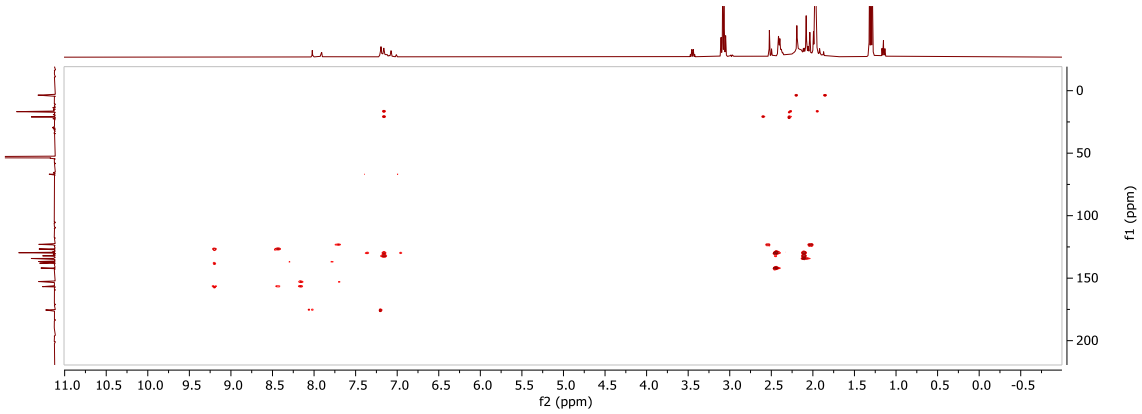

Spectrum 74 - ^{1}H-^{13}C HMBC NMR spectrum of *trans-(diacetonitrile) (2,2'-bipyridine) [1,1-Bis(3'-mesytil-1',2',3'-triazol-5'-ylidene)methylene] ruthenium(II) dihexafluorophosphate.*

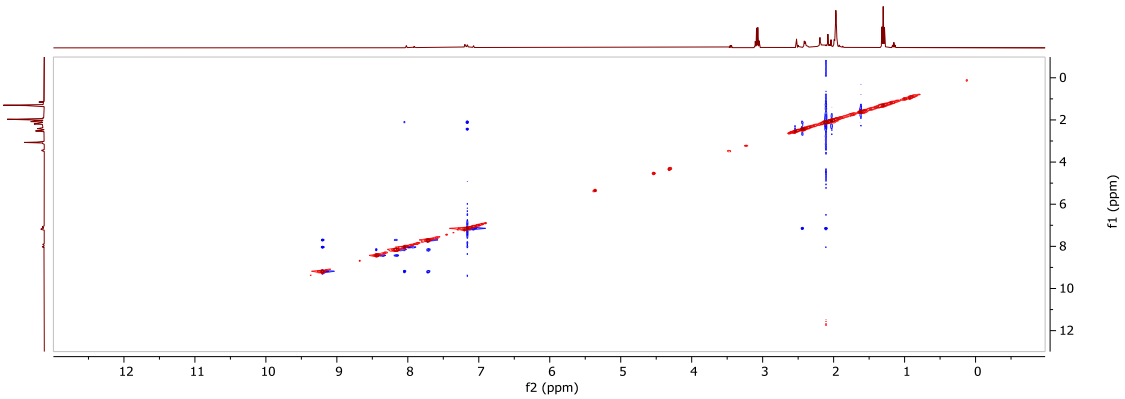

Spectrum 75 - ^{1}H-^{13}C NOESY NMR spectrum of *trans-(diacetonitrile) (2,2'-bipyridine) [1,1-Bis(3'-mesytil-1',2',3'-triazol-5'-ylidene)methylene] ruthenium(II) dihexafluorophosphate.*

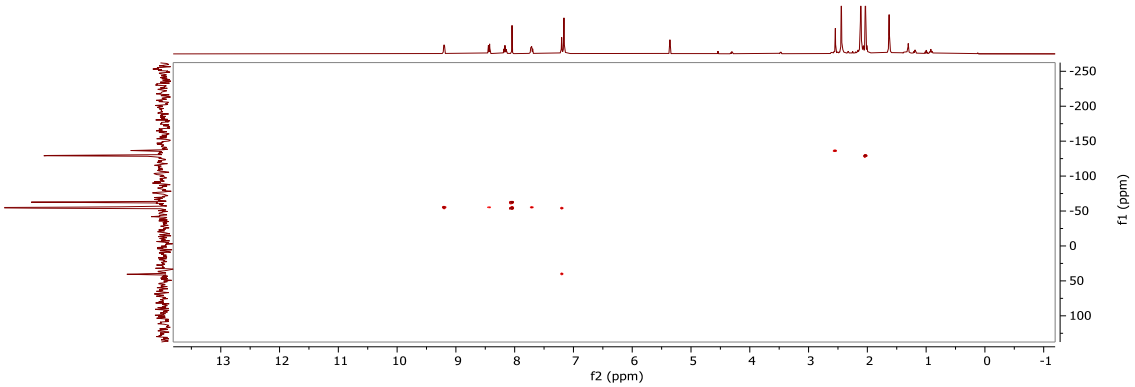

Spectrum 76 - ^{1}H-^{15}N HMBC NMR spectrum of *trans-(diacetonitrile) (2,2'-bipyridine) [1,1-Bis(3'-mesytil-1',2',3'-triazol-5'-ylidene)methylene] ruthenium(II) dihexafluorophosphate.*

4.18 Reaction profile: $[Ru(COD)(Cl_2)]_n$ activation

Procedure

A 5 mm J-young tube was charged with 10.1 mg (0.04 mmol, 1.0 eq) of *1,5-cyclooctadiene)(dichloro) ruthenium(II) polymer,* then air was removed by cycling vacuum and argon (3 times). Subsequently, 500 uL of degassed deuterated *ACN* and 25 uL of degassed *TEA* were added. The tube was sealed and placed in an oil bath at reflux. A ^{1}H NMR spectrum was collected every 4 h to generate the reaction profile.

NMR spectra

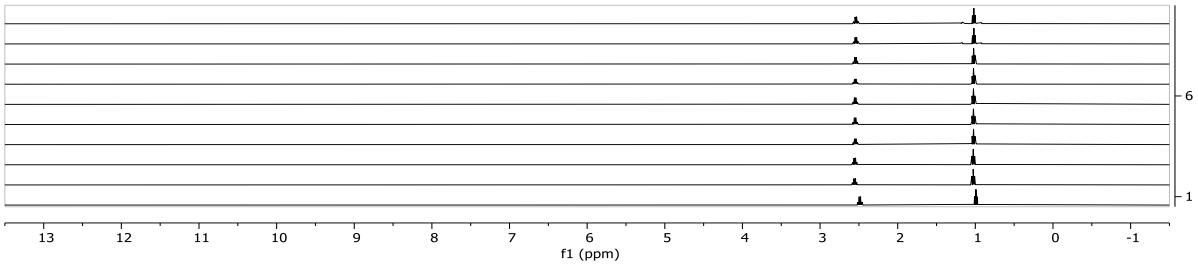

Kinetic 2 - ^{1}H NMR spectra collected from the reacting mixture arranged stacked, acquired at times t=0, 2, 4, 6, 8, 10, 12, 16, 20, 24, 28, 32h, T = 80°C. Reagents: 10.1mg of (1,5-cyclooctadiene)ruthenium(II) dichloride polymer, 25 uL of TEA, and 500 uL of CD_3CN (above).

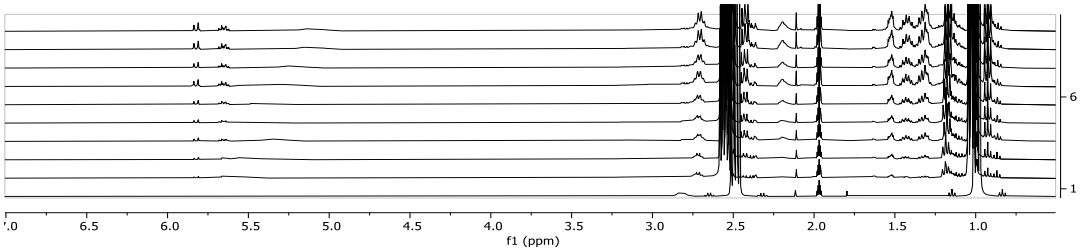

Kinetic 3 - Magnification of the stacked spectra above (Kinetic 2) displaying the spectrum region of interest.

4.19 Reaction profile: $Ru(ACN)_4[b(MI)M]X_2$ formation

Procedure

A 5 mm J-young tube was charged with 10.1 mg (0.04 mmol, 1.0 eq) of *(1,5-cyclooctadiene)(dichloro) ruthenium(II) polymer* and 15.6 mg (0.04 mmol, 1.0 eq) of *1,1-bis(3'-methylimidazolium)methylene diiodide*. The air was removed by cycling vacuum and argon (3 times), then 500 uL of degassed deuterated *ACN* were added, alongside 25 uL of degassed *TEA*. The tube was sealed and placed in an oil bath at reflux. A ^{1}H NMR spectrum was collected every 4 h to generate the reaction profile.

NMR spectra

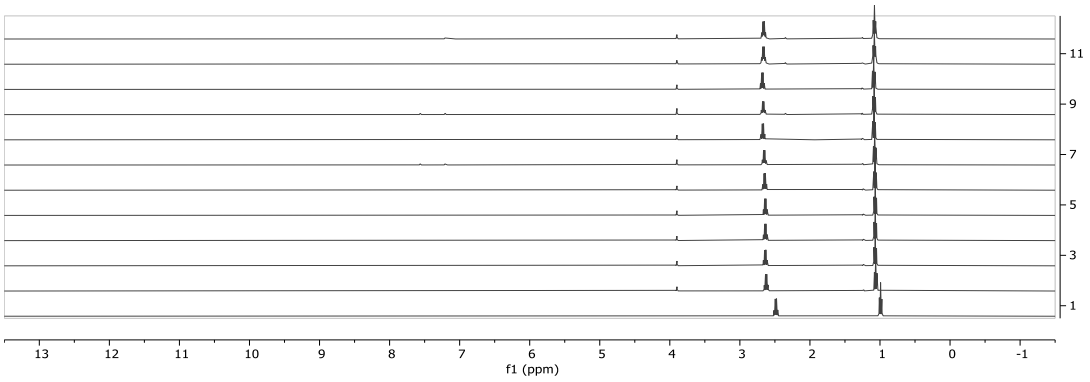

Kinetic 4 - ^{1}H NMR spectra collected from the reacting mixture arranged stacked, acquired at times t=0, 2, 4, 6, 8, 10, 12, 16, 20, 24, 28, 32h, T = 80°C. Reagents: 10.1mg of *(1,5-cyclooctadiene)ruthenium(II) dichloride polymer*, 15.6mg of *1,1-bis(3'-methylimidazolium)methylene diiodide*, 25 uL of *TEA*, and 500 uL of *CD_3CN*.

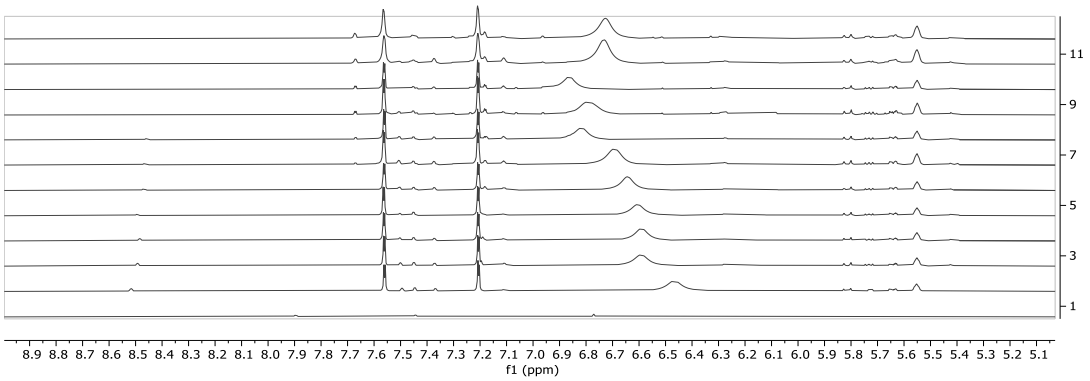

Kinetic 5 - Magnification of the stacked spectra above (Kinetic 4) displaying the spectrum region of interest.

4.20 Reaction profile: bipy coordination to $Ru(ACN)_4[b(MI)M]X_2$

Procedure

A 5 mm J-young tube was charged with 10.1 mg (0.04 mmol, 1.0 eq) of *(1,5-cyclooctadiene)(dichloro) ruthenium(II) polymer* and 15.6 mg (0.04 mmol, 1.0 eq) of *1,1-bis(3'-methylimidazolium)methylene diiodide*. The air was removed by cycling vacuum and argon (3 times), then 500 uL of degassed deuterated *ACN* were added, alongside 25 uL (0.18 mmol, 5 eq) of degassed *TEA*. The tube was sealed and placed in an oil bath at reflux for 36 h. Then 5.6 mg (0.04 mmol, 1.0 eq) of *2,2'-bipyridine* were added under argon counterflow, and the tube was quickly loaded into the NMR device to collect the ^{1}H NMR reaction profile. After 1 h, the temperature was increased to 50 °C to drive the reaction to completion.

NMR spectra

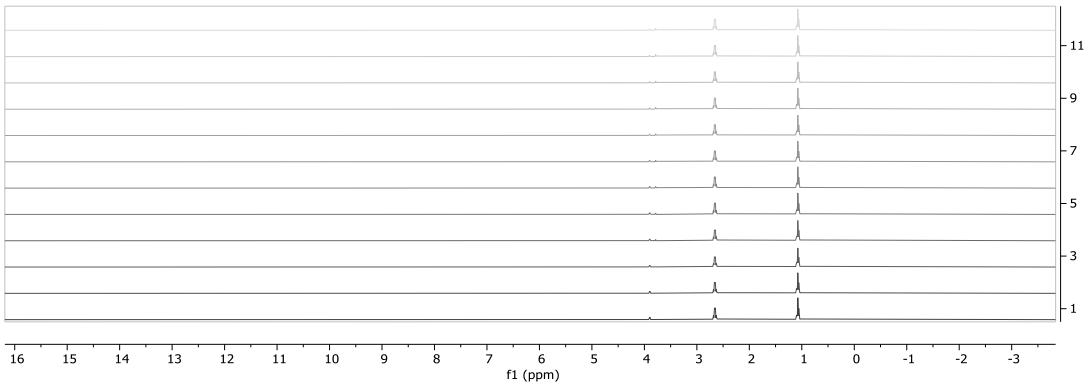

Kinetic 6 - ^{1}H NMR spectra collected from the reacting mixture arranged stacked, acquired every 3 minutes, T = 25°C, after the addition of 5.6 mg of *2,2'-bipyridine* to a solution originally containing: 10.1 mg of *(1,5-cyclooctadiene)ruthenium(II) dichloride polymer*, 15.6 mg of *1,1-bis(3'-methylimidazolium)methylene diiodide*, 25 uL of *TEA*, and 500 uL of CD_3CN (36 h at T = 80 °C).

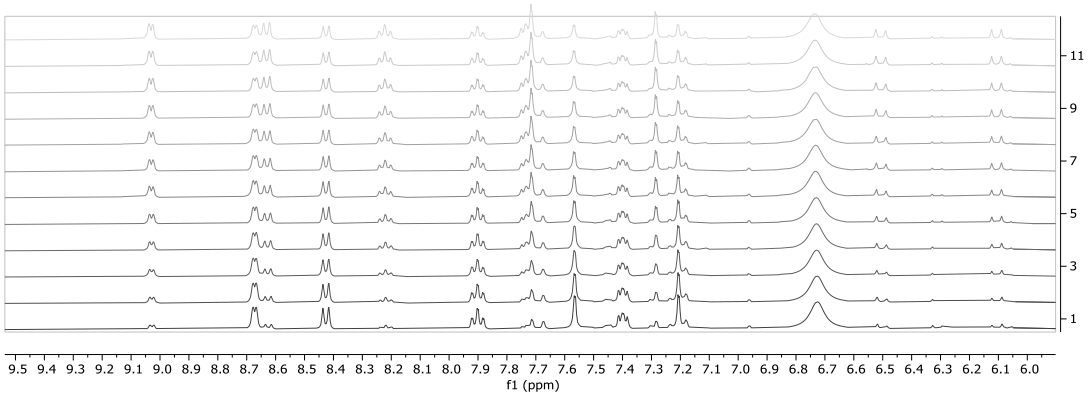

Kinetic 7 - Magnification of the stacked spectra above (Kinetic 6) displaying the spectrum region of interest.

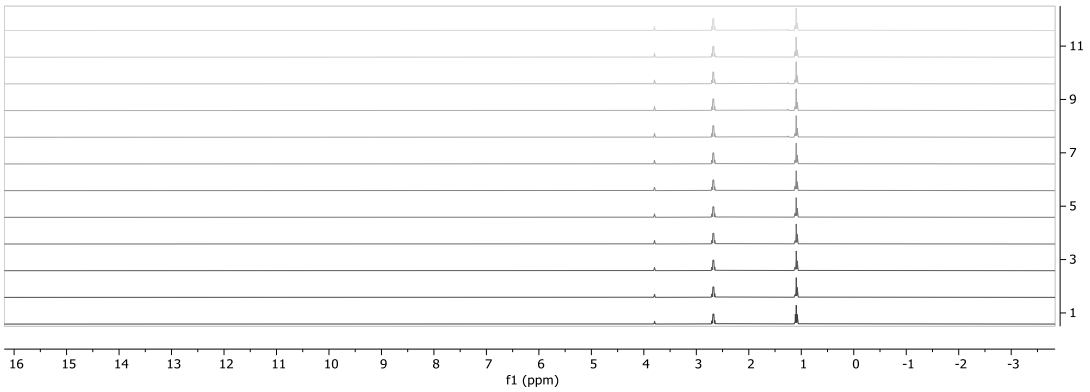

Kinetic 8 - ^{1}H NMR spectra collected from the reacting mixture arranged stacked, acquired every 3 minutes, T = 50°C, after the addition of 5.6 mg of *2,2'-bipyridine* to a solution originally containing: 10.1 mg of *(1,5-cyclooctadiene)ruthenium(II) dichloride polymer*, 15.6 mg of *1,1-bis(3'-methylimidazolium)methylene diiodide*, 25 uL of *TEA*, and 500 uL of *CD_3CN* (36 h at T = 80 °C).

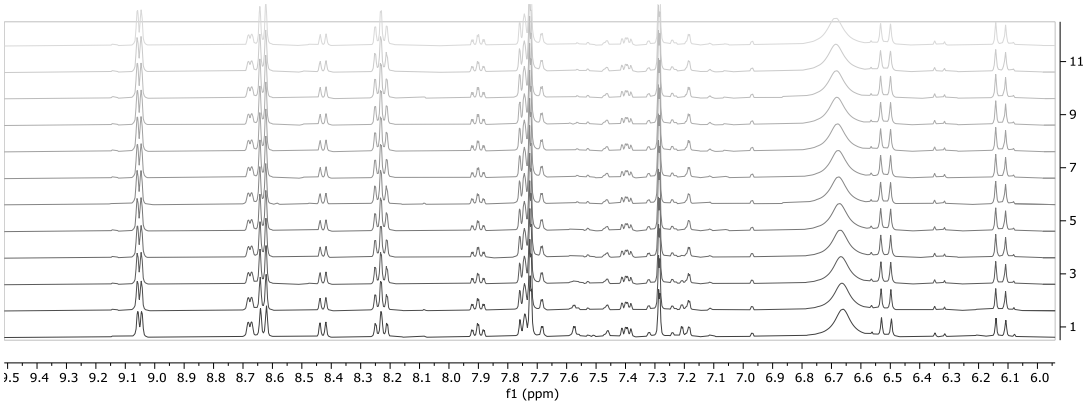

Kinetic 9 - Magnification of the stacked spectra above (Kinetic 8) displaying the spectrum region of interest.

4.21 Material and apparatus for catalytic hydrogen auto-transfer reactions

- 25 mL Schlenk tube equipped with Rotaflo stopcock, 1 cm stirring bar, and 14/23 silicone stoppers.
- *Acetophenone* purification procedure: 1) treated with *sodium permanganate* for 18h at RT, 2) distilled, 3) treated with *potassium carbonate*, 4) distilled under argon, 5) dried over molecular sieves 4 Å overnight, 6) fractionally distilled under argon, 7) FPT.
- *Isopropyl alcohol* purification: 1) Treated with *sodium* overnight, 2) fractionally distilled under argon, 3) FPT.
- *Tert butanol* purification: 1) Treated with *sodium* overnight at 35 °C, 2) fractionally distilled under argon, 3) FPT.

  Note: Do not use silicone stoppers as they slowly react with *isopropoxide* and *isopropanol* vapors, decomposing.

4.22 Transfer hydrogenation catalysis

TH reaction protocol

A 25 mL schlenk tube with a stirring bar was heated using a heat gun and left cooling under a vacuum until it reached room temperature. The tube was placed under argon and 1.0 mL of the 1.0 mM catalyst stock solution were added, and the solvent was removed under vacuum. 10 mL of anhydrous and degassed *isopropyl alcohol* were added under argon counterflow, alongside 117 uL (1.0 mmol, 1.0 eq) of degassed *acetophenone*. The tube was moved to an oil bath placed at 90°C for 5 minutes. Then 200 uL of the 0.1 M isopropoxide stock solution were added to trigger the reaction. The reaction mixture was sampled via a syringe under argon counterflow and each sample was promptly quenched in cold deuterated *chloroform*. Sample to chloroform ratio 1:7.

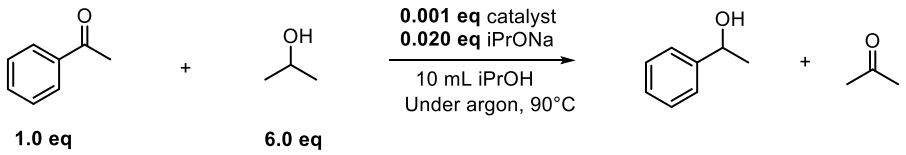

Scheme 23 - Transfer hydrogenation catalysis general reaction scheme.

1.0 mM catalyst stock solution preparation

A round bottom schlenk flask was charged with 0.01 mmol of catalyst (ten times the amount required for a catalytic test). The air was removed from the container by cycling vacuum and argon (3 times). Then 10 mL of anhydrous and degassed *DCM* or *isopropyl alcohol* were added according to the complex solubility.

0.1 M isopropoxide stock solution preparation

Sodium isopropoxide solution 0.1M, from purified *isopropyl alcohol*: 1) a 25 mL Schlenk tube equipped with Rotaflo stopcocks, glass stoppers, and Glindemann O-rings was charged with 10 mL of *isopropyl alcohol*, 2) 23 mg (1.0 mmol, 8E-3 eq) sodium were added under argon counter flow, and the mixture was left reacting overnight.

Note: Do not use silicone stoppers as they slowly react with *isopropoxide* and *isopropyl alcohol* vapors, decomposing.

Catalytic TH: control reaction

The TH reaction protocol reported above was followed in each step, except that the catalyst was not loaded. The reaction profile is herein reported.

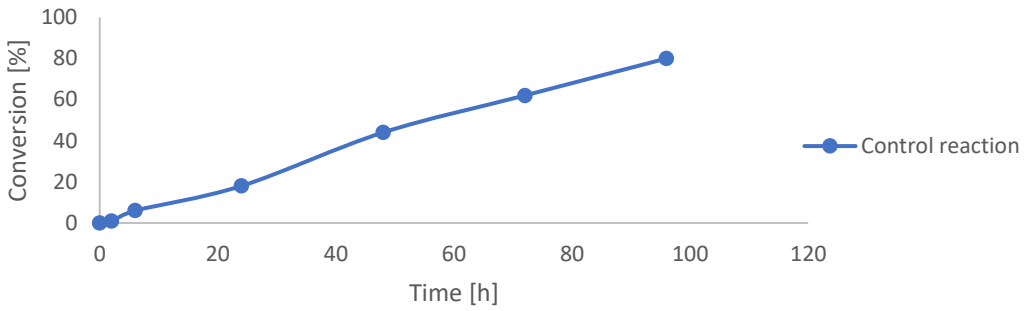

Figure 57 - Reaction profile obtained during the control reaction via analysis of samples collected under argon counterflow.

Catalytic TH: *trans*-complexes

The reaction profiles of the transfer hydrogenation reaction were conducted using the trans-complexes following the described TH reaction protocol. The collected samples were analyzed through ^{1}H NMR spectroscopy, and the conversion was calculated based on the normalized sum of integrals of reactants and products. No side products were detected.

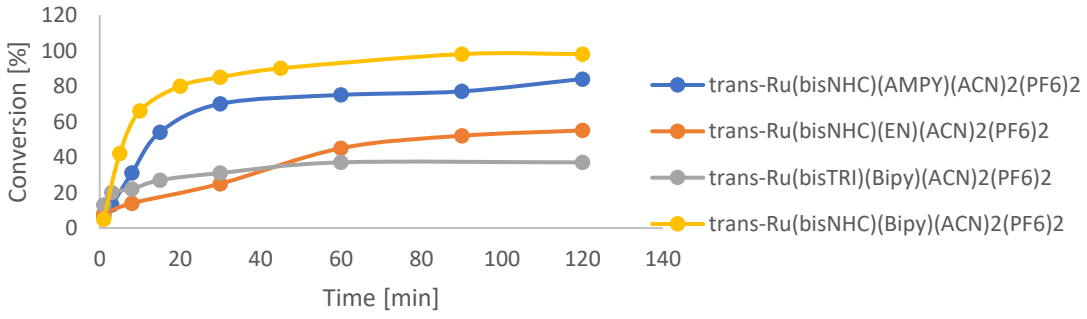

Figure 58 – Reaction profiles obtained via analysis of samples collected under argon counterflow from the reaction mixture. Each profile is the result of the average of two single profiles.

Catalytic TH: quench control reaction

A control reaction was conducted to test the effectiveness of the quenching method with *chloroform*. Two distinct TH hydrogenation reactions were performed employing *trans-(diacetonitrile) (2,2'-bipyridine) [1,1-Bis(3'-methyl-imidazol-1'-ylidene)methylene] ruthenium(II) dihexafluorophosphate* (**9a**) as catalyst. The protocol described at the beginning of this Section was carefully followed in the first catalytic test. Instead, in the second one, each sample collected from the reaction was quenched using *diethyl ether* and filtered over silica before conducting GC-FID analysis to construct the reaction profile. As expected, the combined effect of dilution, temperature, and insolubility does not provide the condition for the reaction to continue in *chloroform*, and the two reaction profiles are equivalent.

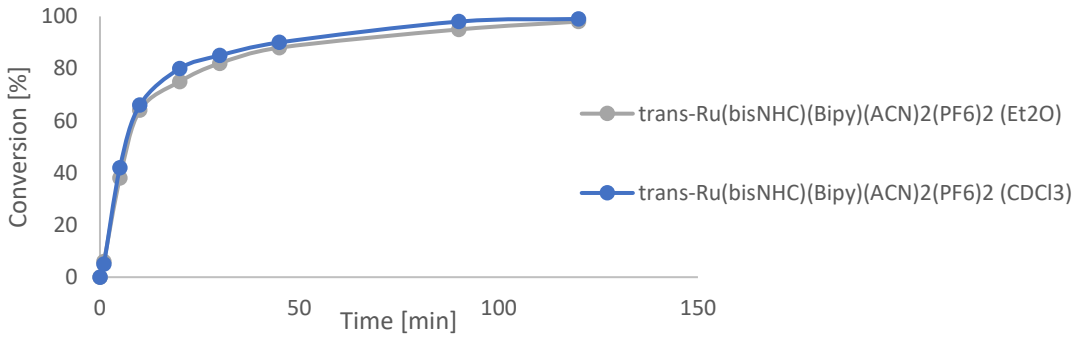

Figure 59 - Reaction profiles obtained via analysis of samples collected under argon counterflow from the reaction mixture.

Catalytic TH: *cis*-complexes

The reaction profiles of the transfer hydrogenation reaction were conducted using the *trans*-complexes following the described TH reaction protocol. The collected samples were analyzed through ^{1}H NMR spectroscopy, and the conversion was calculated based on the normalized sum of integrals of reactants and products. No side products were detected.

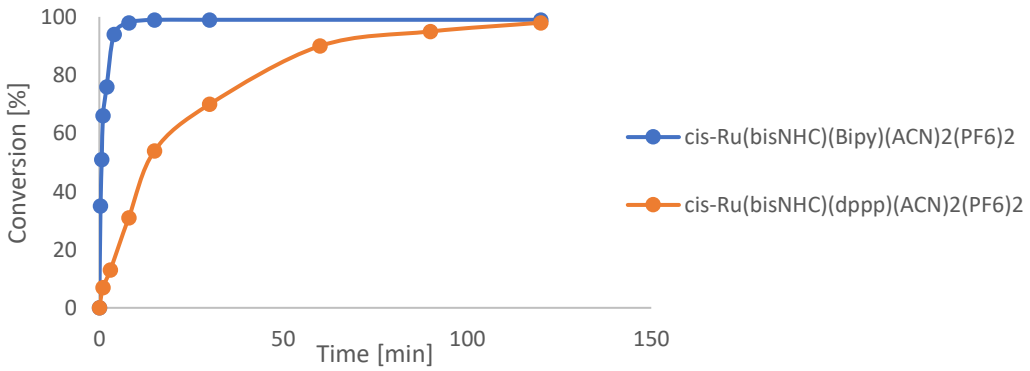

Figure 60 - Reaction profiles obtained via analysis of samples collected under argon counterflow from the reaction mixture. Each profile is the result of the average of two single profiles.

4.23 Direct C-H arylation of 2-phenylpyridine

Typic catalytic procedure:

A 5 mL round bottom Schlenk flask was charged with 5.0 mg (0.01 mmol, 0.1 eq) of *tetrakis(acetonitrile) [1,1-bis(3'-methylimidazol-2'-ylidene)methylene]ruthenium(II) dihexafluorophosphate*, 1.8 mg (0.02 mmol, 0.3 eq) of *potassium acetate* and 18.0 mg (0.13 mmol, 3.0 eq) of *potassium carbonate*. The air was removed by cycling argon and vacuum. Subsequently, 300 uL of *N-methyl-pyrrolidone* were added under argon counterflow, followed by 15.1 uL (0.13 mmol, 2 eq) of *iodobenzene* and 9.6 uL (0.07 mmol, 1 eq) of *2-phenylpyridine*. The flask was sealed and placed in an oil bath for 12 successive hours, and then a sample was collected and diluted with deuterated chloroform to determine yield (98%).

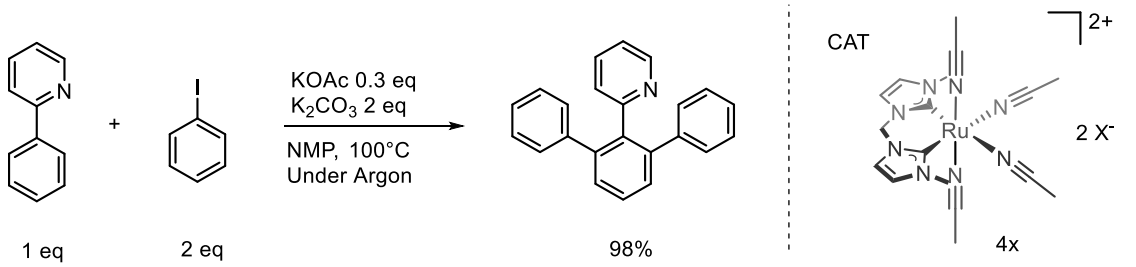

Scheme 24 – General reaction scheme depicting the diarylation of *2-phenylpyridine* using iodobenzene as an arylating agent, *tetrakis(acetonitrile) [1,1-bis(3'-methylimidazol-2'-ylidene)methylene]ruthenium(II) dihexafluorophosphate* as a catalyst and *potassium carbonate* as the internal base for cyclometallation.

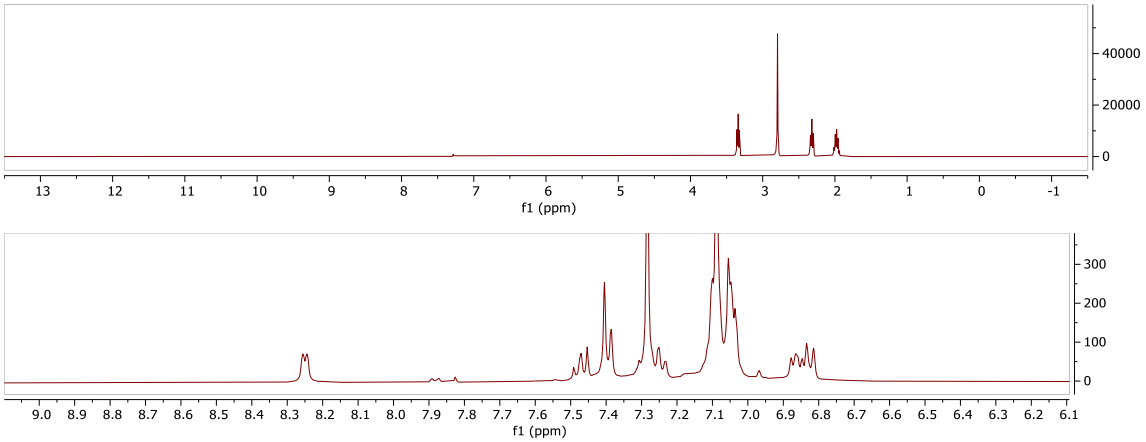

Figure 61 – ^{1}H NMR spectrum of a diluted sample of the crude reaction mixture, where the only visible signals are related to *NMP* (above). A fragment of the latter spectrum, highlighting the aromatic region where the product's signals fall.

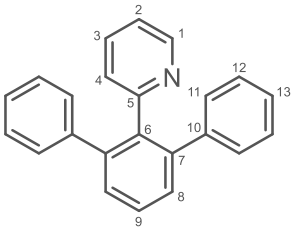

Figure 62 – General structure of *2-[(2',6'-diphenyl)phenyl]pyridine.*

Characterization

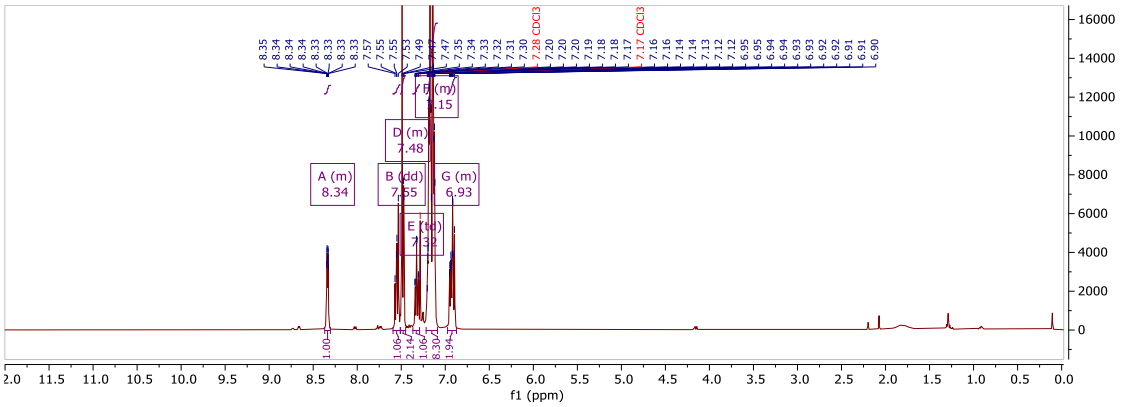

Spectrum 77 - ^{1}H NMR spectrum of *2-[(2',6'-diphenyl)phenyl]pyridine.*

($C_{23}H_{17}N$): ^{1}H NMR (CD_3Cl, 400MHz): δ 8.33 (d, 1H, 4.75 Hz, **1**), 7.55 (m, 1H, **4**), 7.48 (m, 2H), 7.32 (td, 1H, 7.39 Hz, 1.62 Hz, **2**), 7.15 (m, 8H, **11**+**12**+**13**), 6.92 (m, 2H, **8**).

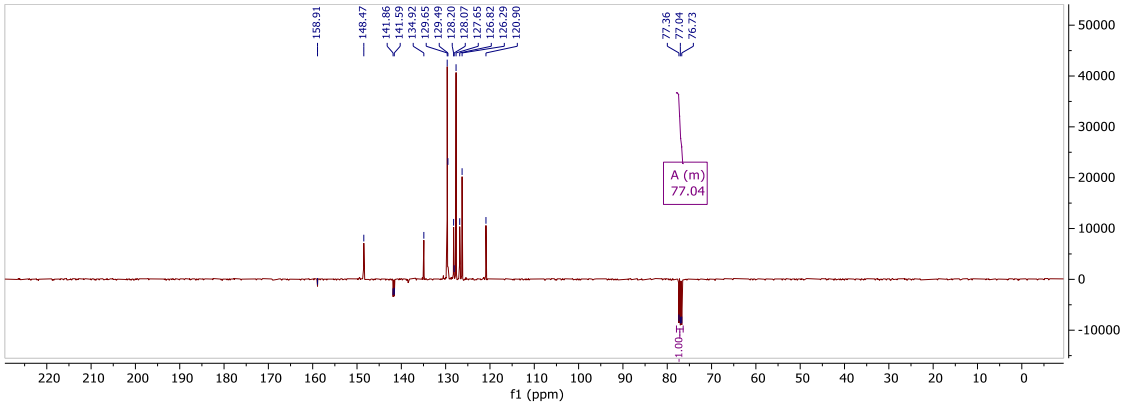

Spectrum 78 - DEPTQ NMR spectrum of *2-[(2',6'-diphenyl)phenyl]pyridine.*

($C_{23}H_{17}N$): ^{13}C DEPTQ NMR (CD_3Cl, 400MHz): δ 158.91, 148.47, 141.86, 141.59, 134.92, 129.65, 129.49, 128.20, 127.65, 126.82, 126.29, 120.90.

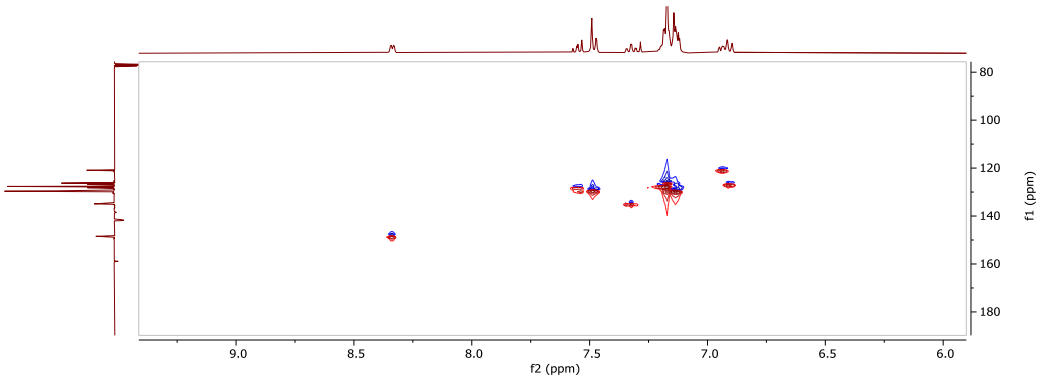

Spectrum 79 - ^{1}H-^{13}C HSQC NMR spectrum of *2-[(2',6'-diphenyl)phenyl]pyridine.*

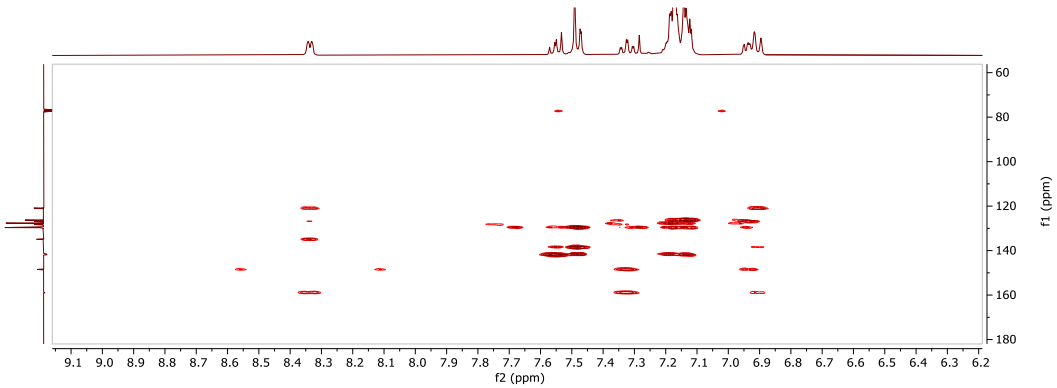

Spectrum 80 - ^{1}H-^{13}C HMBC NMR spectrum of *2-[(2',6'-diphenyl)phenyl]pyridine.*

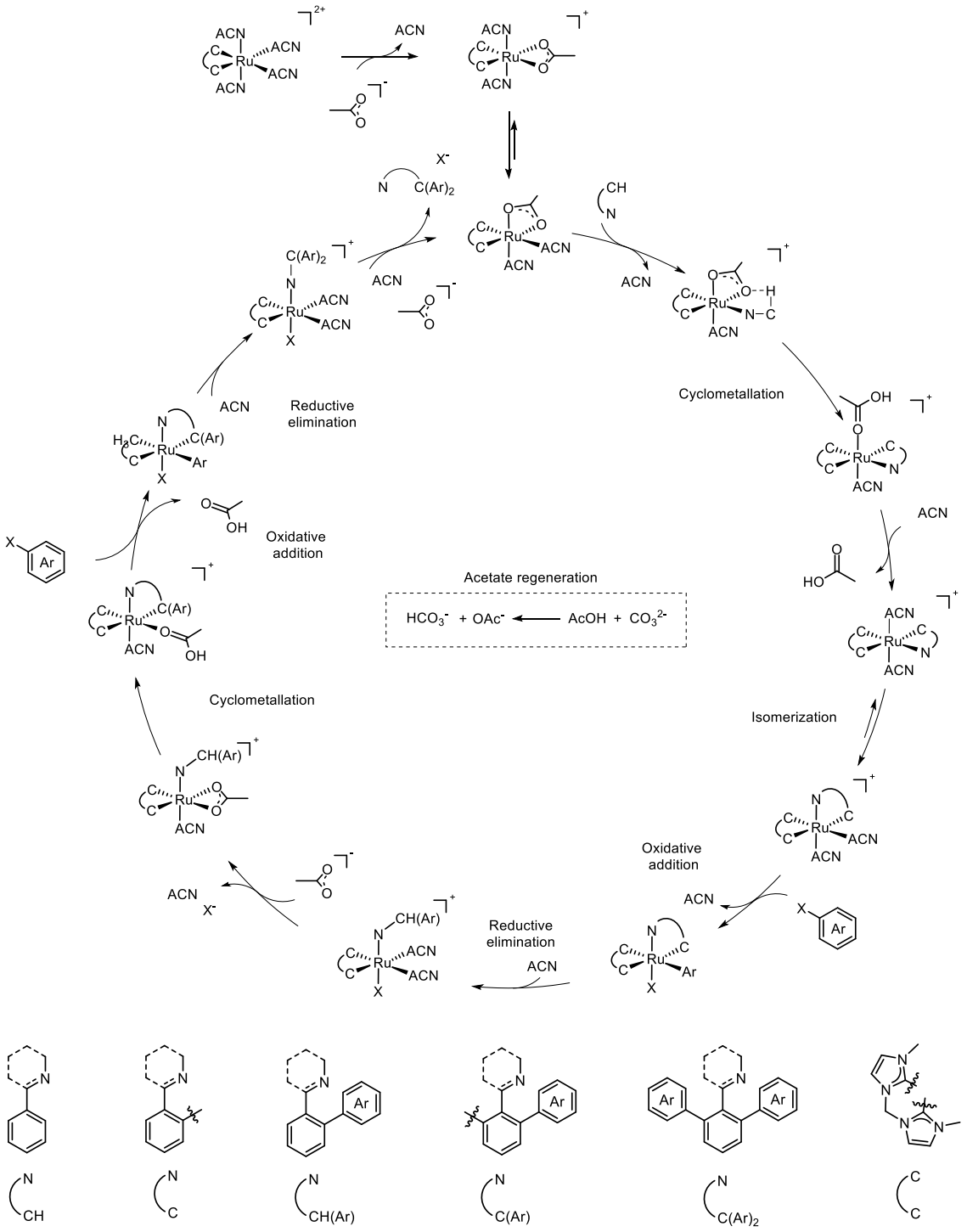

Figure 63 – Proposed reaction mechanism of the ruthenium(II) catalyzed direct C-H *orto*-diarylation for a generic aromatic compound featuring an amino-based directing group.

5 REFERENCES

(1) Hopkinson, M. N.; Richter, C.; Schedler, M.; Glorius, F. An Overview of N-Heterocyclic Carbenes. *Nature* **2014**, *510* (7506), 485–496. https://doi.org/10.1038/nature13384.

(2) Dumas, J. B.; Peligot, E. Memoire Sur l'esprit-de-Bois et Les Divers Composese Etheres Qui En Proviennent. *Ann. Chim. Phys.* **1835**, No. 58, 5–74.

(3) Arduengo, A. J.; Harlow, R. L.; Kline, M. A Stable Crystalline Carbene. *J. Am. Chem. Soc.* **1991**, *113* (1), 361–363. https://doi.org/10.1021/ja00001a054.

(4) Jacobsen, H.; Correa, A.; Poater, A.; Costabile, C.; Cavallo, L. Understanding the M(NHC) (NHC=N-Heterocyclic Carbene) Bond. *Coordination Chemistry Reviews* **2009**, *253* (5–6), 687–703. https://doi.org/10.1016/j.ccr.2008.06.006.

(5) Hoffmann, R. Trimethylene and the Addition of Methylene to Ethylene. *J. Am. Chem. Soc.* **1968**, *90* (6), 1475–1485. https://doi.org/10.1021/ja01008a016.

(6) Arduengo, A. J.; Bock, H.; Chen, H.; Denk, M.; Dixon, D. A.; Green, J. C.; Herrmann, W. A.; Jones, N. L.; Wagner, M.; West, R. Photoelectron Spectroscopy of a Carbene/Silylene/Germylene Series. *J. Am. Chem. Soc.* **1994**, *116* (15), 6641–6649. https://doi.org/10.1021/ja00094a020.

(7) Ullah, F.; Bajor, G.; Veszprémi, T.; Jones, P. G.; Heinicke, J. W. Stabilization of Unsymmetrically Annelated Imidazol-2-Ylidenes with Respect to Their Higher Group 14 Homologues by n-/π-HOMO Inversion. *Angew. Chem. Int. Ed.* **2007**, *46* (15), 2697–2700. https://doi.org/10.1002/anie.200604516.

(8) Bourissou, D.; Guerret, O.; Gabbaï, F. P.; Bertrand, G. Stable Carbenes. *Chem. Rev.* **2000**, *100* (1), 39–92. https://doi.org/10.1021/cr940472u.

(9) Heinemann, C.; Müller, T.; Apeloig, Y.; Schwarz, H. On the Question of Stability, Conjugation, and "Aromaticity" in Imidazol-2-Ylidenes and Their Silicon Analogs. *J. Am. Chem. Soc.* **1996**, *118* (8), 2023–2038. https://doi.org/10.1021/ja9523294.

(10) Arduengo, A. J.; Goerlich, J. R.; Marshall, W. J. A Stable Diaminocarbene. *J. Am. Chem. Soc.* **1995**, *117* (44), 11027–11028. https://doi.org/10.1021/ja00149a034.

(11) Wanzlick, H. W. Aspects of Nucleophilic Carbene Chemistry. *Angew. Chem. Int. Ed. Engl.* **1962**, *1* (2), 75–80. https://doi.org/10.1002/anie.196200751.

(12) Taton, T. A.; Chen, P. A Stable Tetraazafulvalene. *Angew. Chem. Int. Ed. Engl.* **1996**, *35* (9), 1011–1013. https://doi.org/10.1002/anie.199610111.

(13) Hillier, A. C.; Sommer, W. J.; Yong, B. S.; Petersen, J. L.; Cavallo, L.; Nolan, S. P. A Combined Experimental and Theoretical Study Examining the Binding of *N* -Heterocyclic Carbenes (NHC) to the Cp*RuCl (Cp* = η^5 -C_5Me_5) Moiety: Insight into Stereoelectronic Differences between Unsaturated and Saturated NHC Ligands. *Organometallics* **2003**, *22* (21), 4322–4326. https://doi.org/10.1021/om034016k.

(14) Tolman, C. A. Steric Effects of Phosphorus Ligands in Organometallic Chemistry and Homogeneous Catalysis. *Chem. Rev.* **1977**, *77* (3), 313–348. https://doi.org/10.1021/cr60307a002.

(15) Huynh, H. V. Electronic Properties of N-Heterocyclic Carbenes and Their Experimental Determination. *Chem. Rev.* **2018**, *118* (19), 9457–9492. https://doi.org/10.1021/acs.chemrev.8b00067.

(16) Huynh, H. V.; Han, Y.; Jothibasu, R.; Yang, J. A. ^{13}C NMR Spectroscopic Determination of Ligand Donor Strengths Using N-Heterocyclic Carbene Complexes of Palladium(II). *Organometallics* **2009**, *28* (18), 5395–5404. https://doi.org/10.1021/om900667d.

(17) Crabtree, R. H. Abnormal, Mesoionic and Remote N-Heterocyclic Carbene Complexes. *Coordination Chemistry Reviews* **2013**, *257* (3–4), 755–766. https://doi.org/10.1016/j.ccr.2012.09.006.

(18) Chianese, A. R.; Kovacevic, A.; Zeglis, B. M.; Faller, J. W.; Crabtree, R. H. Abnormal C5-Bound N-Heterocyclic Carbenes: Extremely Strong Electron Donor Ligands and Their Iridium(I) and Iridium(III) Complexes. *Organometallics* **2004**, *23* (10), 2461–2468. https://doi.org/10.1021/om049903h.

(19) Hu, X.; Meyer, K. New Tripodal N-Heterocyclic Carbene Chelators for Small Molecule Activation. *Journal of Organometallic Chemistry* **2005**, *690* (24–25), 5474–5484. https://doi.org/10.1016/j.jorganchem.2005.07.119.
(20) Aldeco-Perez, E.; Rosenthal, A. J.; Donnadieu, B.; Parameswaran, P.; Frenking, G.; Bertrand, G. Isolation of a C5-Deprotonated Imidazolium, a Crystalline "Abnormal" N-Heterocyclic Carbene. *Science* **2009**, *326* (5952), 556–559. https://doi.org/10.1126/science.1178206.
(21) Guisado-Barrios, G.; Bouffard, J.; Donnadieu, B.; Bertrand, G. Crystalline 1H-1,2,3-Triazol-5-Ylidenes: New Stable Mesoionic Carbenes (MICs). *Angewandte Chemie International Edition* **2010**, *49* (28), 4759–4762. https://doi.org/10.1002/anie.201001864.
(22) Bouffard, J.; Keitz, B. K.; Tonner, R.; Guisado-Barrios, G.; Frenking, G.; Grubbs, R. H.; Bertrand, G. Synthesis of Highly Stable 1,3-Diaryl-1 *H* -1,2,3-Triazol-5-Ylidenes and Their Applications in Ruthenium-Catalyzed Olefin Metathesis. *Organometallics* **2011**, *30* (9), 2617–2627. https://doi.org/10.1021/om200272m.
(23) Crabtree, R. H. NHC Ligands versus Cyclopentadienyls and Phosphines as Spectator Ligands in Organometallic Catalysis. *Journal of Organometallic Chemistry* **2005**, *690* (24–25), 5451–5457. https://doi.org/10.1016/j.jorganchem.2005.07.099.
(24) Gusev, D. G. Donor Properties of a Series of Two-Electron Ligands. *Organometallics* **2009**, *28* (3), 763–770. https://doi.org/10.1021/om800933x.
(25) Hahn, F. E.; Jahnke, M. C. Heterocyclic Carbenes: Synthesis and Coordination Chemistry. *Angew. Chem. Int. Ed.* **2008**, *47* (17), 3122–3172. https://doi.org/10.1002/anie.200703883.
(26) Normand, A. T.; Cavell, K. J. Donor-Functionalised N-Heterocyclic Carbene Complexes of Group 9 and 10 Metals in Catalysis: Trends and Directions. *Eur J Inorg Chem* **2008**, *2008* (18), 2781–2800. https://doi.org/10.1002/ejic.200800323.
(27) Marion, N.; Nolan, S. P. N-Heterocyclic Carbenes in Gold Catalysis. *Chem. Soc. Rev.* **2008**, *37* (9), 1776. https://doi.org/10.1039/b711132k.
(28) Valente, C.; Çalimsiz, S.; Hoi, K. H.; Mallik, D.; Sayah, M.; Organ, M. G. The Development of Bulky Palladium NHC Complexes for the Most-Challenging Cross-Coupling Reactions. *Angew. Chem. Int. Ed.* **2012**, *51* (14), 3314–3332. https://doi.org/10.1002/anie.201106131.
(29) Kantchev, E. A. B.; O'Brien, C. J.; Organ, M. G. Palladium Complexes of N-Heterocyclic Carbenes as Catalysts for Cross-Coupling Reactions—A Synthetic Chemist's Perspective. *Angew. Chem. Int. Ed.* **2007**, *46* (16), 2768–2813. https://doi.org/10.1002/anie.200601663.
(30) Würtz, S.; Glorius, F. Surveying Sterically Demanding N-Heterocyclic Carbene Ligands with Restricted Flexibility for Palladium-Catalyzed Cross-Coupling Reactions. *Acc. Chem. Res.* **2008**, *41* (11), 1523–1533. https://doi.org/10.1021/ar8000876.
(31) Fortman, G. C.; Nolan, S. P. N-Heterocyclic Carbene (NHC) Ligands and Palladium in Homogeneous Cross-Coupling Catalysis: A Perfect Union. *Chem. Soc. Rev.* **2011**, *40* (10), 5151. https://doi.org/10.1039/c1cs15088j.
(32) Prakasham, A. P.; Ghosh, P. Nickel N-Heterocyclic Carbene Complexes and Their Utility in Homogeneous Catalysis. *Inorganica Chimica Acta* **2015**, *431*, 61–100. https://doi.org/10.1016/j.ica.2014.11.005.
(33) Lazreg, F.; Nahra, F.; Cazin, C. S. J. Copper–NHC Complexes in Catalysis. *Coordination Chemistry Reviews* **2015**, *293–294*, 48–79. https://doi.org/10.1016/j.ccr.2014.12.019.
(34) Samojłowicz, C.; Bieniek, M.; Grela, K. Ruthenium-Based Olefin Metathesis Catalysts Bearing *N* -Heterocyclic Carbene Ligands. *Chem. Rev.* **2009**, *109* (8), 3708–3742. https://doi.org/10.1021/cr800524f.
(35) Vougioukalakis, G. C.; Grubbs, R. H. Ruthenium-Based Heterocyclic Carbene-Coordinated Olefin Metathesis Catalysts. *Chem. Rev.* **2010**, *110* (3), 1746–1787. https://doi.org/10.1021/cr9002424.
(36) Mata, J. A.; Poyatos, M.; Peris, E. Structural and Catalytic Properties of Chelating Bis- and Tris-N-Heterocyclic Carbenes. *Coordination Chemistry Reviews* **2007**, *251* (5–6), 841–859. https://doi.org/10.1016/j.ccr.2006.06.008.
(37) Gardiner, M. G.; Ho, C. C. Recent Advances in Bidentate Bis(N-Heterocyclic Carbene) Transition Metal Complexes and Their Applications in Metal-Mediated Reactions. *Coordination Chemistry Reviews* **2018**, *375*, 373–388. https://doi.org/10.1016/j.ccr.2018.02.003.
(38) Gridnev, A. A.; Mihaltseva, I. M. Synthesis of 1-Alkylimidazoles. *Synthetic Communications* **1994**, *24* (11), 1547–1555. https://doi.org/10.1080/00397919408010155.

(39) Herrmann, W. A.; Elison, M.; Fischer, J.; Köcher, C.; Artus, G. R. J. Metal Complexes of N-Heterocyclic Carbenes—A New Structural Principle for Catalysts in Homogeneous Catalysis. *Angew. Chem. Int. Ed. Engl.* **1995**, *34* (21), 2371–2374. https://doi.org/10.1002/anie.199523711.
(40) Herrmann, W. A.; Schwarz, J.; Gardiner, M. G. High-Yield Syntheses of Sterically Demanding Bis(N-Heterocyclic Carbene) Complexes of Palladium ·. *Organometallics* **1999**, *18* (20), 4082–4089. https://doi.org/10.1021/om990326k.
(41) Chemistry A European J - 2009 - Heckenroth - On the Electronic Impact of Abnormal C4-Bonding in N-Heterocyclic Carbene-1.Pdf.
(42) Taige, M. A.; Zeller, A.; Ahrens, S.; Goutal, S.; Herdtweck, E.; Strassner, T. New Pd–NHC-Complexes for the Mizoroki–Heck Reaction. *Journal of Organometallic Chemistry* **2007**, *692* (7), 1519–1529. https://doi.org/10.1016/j.jorganchem.2006.11.050.
(43) Herrmann, W. A.; Schwarz, J.; Gardiner, M. G.; Spiegler, M. Homoleptic Chelating N-Heterocyclic Carbene Complexes of Palladium and Nickel. *Journal of Organometallic Chemistry* **1999**, *575* (1), 80–86. https://doi.org/10.1016/S0022-328X(98)00980-2.
(44) Eur J Inorg Chem - 2009 - Vinh Huynh - Formation of Homoleptic Tetracarbene versus cis-Chelating Dicarbene Complexes of.Pdf.
(45) Eur J Inorg Chem - 2016 - Luo - Nickel Complexes of Pyridine-Functionalized N-Heterocyclic Carbenes Syntheses Structures .Pdf.
(46) Angew Chem Int Ed - 2009 - Liu - Direct Synthesis of Iron Cobalt Nickel and Copper Complexes of N-Heterocyclic Carbenes-1.Pdf.
(47) Lin, I. J. B.; Vasam, C. S. Preparation and Application of N-Heterocyclic Carbene Complexes of Ag(I). *Coordination Chemistry Reviews* **2007**, *251* (5–6), 642–670. https://doi.org/10.1016/j.ccr.2006.09.004.
(48) Cao, C.; Zhuang, Y.; Zhao, J.; Peng, Y.; Li, X.; Shi, Z.; Pang, G.; Shi, Y. Binuclear Palladium Complexes Bridged by Dicarbene with Different Lengths and Their Application in Mizoroki–Heck Reaction. *Inorganica Chimica Acta* **2010**, *363* (14), 3914–3918. https://doi.org/10.1016/j.ica.2010.07.054.
(49) Subramanium, S. S.; Slaughter, L. M. Direct Observation of a Carbonylation Reaction Relevant to CO/Alkene Copolymerization in a Methylpalladium Carbonyl Complex Containing a Bis(N-Heterocyclic Carbene) Ligand. *Dalton Trans.* **2009**, No. 35, 6930. https://doi.org/10.1039/b908689g.
(50) Poyatos, M.; Sanaú, M.; Peris, E. New Rh(I) and Rh(III) Bisimidazol-2-Ylidene Complexes: Synthesis, Reactivity, and Molecular Structures. *Inorg. Chem.* **2003**, *42* (8), 2572–2576. https://doi.org/10.1021/ic026212+.
(51) Kühnel, E.; Shishkov, I. V.; Rominger, F.; Oeser, T.; Hofmann, P. Synthesis and Structures of Copper(I) Complexes with Phosphino-Functionalized N-Heterocyclic Carbenes (NHCP) and Bis-N-Heterocyclic Carbenes (Bis-NHC). *Organometallics* **2012**, *31* (22), 8000–8011. https://doi.org/10.1021/om300701u.
(52) Nirmala, M.; Saranya, G.; Viswanathamurthi, P.; Bertani, R.; Sgarbossa, P.; Malecki, J. G. Organonickel Complexes Encumbering Bis-Imidazolylidene Carbene Ligands: Synthesis, X-Ray Structure and Catalytic Insights on Buchwald-Hartwig Amination Reactions. *Journal of Organometallic Chemistry* **2017**, *831*, 1–10. https://doi.org/10.1016/j.jorganchem.2016.12.029.
(53) A. Herrmann, W.; Reisinger, C.-P.; Spiegler, M. Chelating N-Heterocyclic Carbene Ligands in Palladium-Catalyzed Heck-Type Reactions. *Journal of Organometallic Chemistry* **1998**, *557* (1), 93–96. https://doi.org/10.1016/S0022-328X(97)00736-5.
(54) Hohloch, S.; Suntrup, L.; Sarkar, B. Arene–Ruthenium(II) and −Iridium(III) Complexes with "Click"-Based Pyridyl-Triazoles, Bis-Triazoles, and Chelating Abnormal Carbenes: Applications in Catalytic Transfer Hydrogenation of Nitrobenzene. *Organometallics* **2013**, *32* (24), 7376–7385. https://doi.org/10.1021/om4009185.
(55) Harlang, T. C. B.; Liu, Y.; Gordivska, O.; Fredin, L. A.; Ponseca, C. S.; Huang, P.; Chábera, P.; Kjaer, K. S.; Mateos, H.; Uhlig, J.; Lomoth, R.; Wallenberg, R.; Styring, S.; Persson, P.; Sundström, V.; Wärnmark, K. Iron Sensitizer Converts Light to Electrons with 92% Yield. *Nature Chem* **2015**, *7* (11), 883–889. https://doi.org/10.1038/nchem.2365.
(56) Weskamp, T.; Böhm, V. P. W.; Herrmann, W. A. N-Heterocyclic Carbenes: State of the Art in Transition-Metal-Complex Synthesis. *Journal of Organometallic Chemistry* **2000**, *600* (1–2), 12–22. https://doi.org/10.1016/S0022-328X(00)00035-8.
(57) Jamali, S.; Milić, D.; Kia, R.; Mazloomi, Z.; Abdolahi, H. Organoplatinum(Ii) Complexes Containing Chelating or Bridging Bis(N-Heterocyclic Carbene) Ligands: Formation of a

Platinum(Ii) Carbonate Complex by Aerial CO2 Fixation. *Dalton Trans.* **2011**, *40* (37), 9362. https://doi.org/10.1039/c1dt10736d.
(58) Angew Chem Int Ed - 2010 - Boyd - Reduction of a Chelating Bis NHC Palladium II Complex to -bis NHC 2Pd2H A.Pdf.
(59) Wanniarachchi, Y. A.; Khan, M. A.; Slaughter, L. M. An Unusually Static, Sterically Hindered Silver Bis(N-Heterocyclic Carbene) Complex and Its Use in Transmetalation. *Organometallics* **2004**, *23* (25), 5881–5884. https://doi.org/10.1021/om0493098.
(60) Baron, M.; Tubaro, C.; Basato, M.; Biffis, A.; Natile, M. M.; Graiff, C. Dinuclear N-Heterocyclic Dicarbene Gold Complexes in I–III and III–III Oxidation States: Synthesis and Structural Analysis. *Organometallics* **2011**, *30* (17), 4607–4615. https://doi.org/10.1021/om2004145.
(61) Zamora, M. T.; Ferguson, M. J.; McDonald, R.; Cowie, M. Unsymmetrical Dicarbenes Based on *N* -Heterocyclic/Mesoionic Carbene Frameworks: A Stepwise Metalation Strategy for the Generation of a Dicarbene-Bridged Mixed-Metal Pd/Rh Complex. *Organometallics* **2012**, *31* (15), 5463–5477. https://doi.org/10.1021/om3004543.
(62) Tkatchouk, E.; Mankad, N. P.; Benitez, D.; Goddard, W. A.; Toste, F. D. Two Metals Are Better Than One in the Gold Catalyzed Oxidative Heteroarylation of Alkenes. *J. Am. Chem. Soc.* **2011**, *133* (36), 14293–14300. https://doi.org/10.1021/ja2012627.
(63) Zamora, M. T.; Ferguson, M. J.; McDonald, R.; Cowie, M. Carbene-Anchored/Pendent-Imidazolium Species as Precursors to Di-N-Heterocyclic Carbene-Bridged Mixed-Metal Complexes. *Dalton Trans.* **2009**, No. 35, 7269. https://doi.org/10.1039/b906884h.
(64) Garrison, J. C.; Youngs, W. J. Ag(I) N-Heterocyclic Carbene Complexes: Synthesis, Structure, and Application. *Chem. Rev.* **2005**, *105* (11), 3978–4008. https://doi.org/10.1021/cr050004s.
(65) Rieb, J.; Dominelli, B.; Mayer, D.; Jandl, C.; Drechsel, J.; Heydenreuter, W.; Sieber, S. A.; Kühn, F. E. Influence of Wing-Tip Substituents and Reaction Conditions on the Structure, Properties and Cytotoxicity of Ag(I)– and Au(I)–Bis(NHC) Complexes. *Dalton Trans.* **2017**, *46* (8), 2722–2735. https://doi.org/10.1039/C6DT04559F.
(66) Poyatos, M.; Mata, J. A.; Peris, E. Complexes with Poly(N-Heterocyclic Carbene) Ligands: Structural Features and Catalytic Applications. *Chem. Rev.* **2009**, *109* (8), 3677–3707. https://doi.org/10.1021/cr800501s.
(67) Ahrens, S.; Zeller, A.; Taige, M.; Strassner, T. Extension of the Alkane Bridge in BisNHC−Palladium−Chloride Complexes. Synthesis, Structure, and Catalytic Activity. *Organometallics* **2006**, *25* (22), 5409–5415. https://doi.org/10.1021/om060577a.
(68) Perrin, L.; Clot, E.; Eisenstein, O.; Loch, J.; Crabtree, R. H. Computed Ligand Electronic Parameters from Quantum Chemistry and Their Relation to Tolman Parameters, Lever Parameters, and Hammett Constants. *Inorg. Chem.* **2001**, *40* (23), 5806–5811. https://doi.org/10.1021/ic0105258.
(69) Poyatos, M.; McNamara, W.; Incarvito, C.; Clot, E.; Peris, E.; Crabtree, R. H. A Weak Donor, Planar Chelating Bitriazole N-Heterocyclic Carbene Ligand for Ruthenium(II), Palladium(II), and Rhodium. *Organometallics* **2008**, *27* (9), 2128–2136. https://doi.org/10.1021/om800021c.
(70) Teng, Q.; Huynh, H. V. Determining the Electron-Donating Properties of Bidentate Ligands by ^{13}C NMR Spectroscopy. *Inorg. Chem.* **2014**, *53* (20), 10964–10973. https://doi.org/10.1021/ic501325j.
(71) Baker, M. V.; Brown, D. H.; Simpson, P. V.; Skelton, B. W.; White, A. H.; Williams, C. C. Palladium, Rhodium and Platinum Complexes of Ortho-Xylyl-Linked Bis-N-Heterocyclic Carbenes: Synthesis, Structure and Catalytic Activity. *Journal of Organometallic Chemistry* **2006**, *691* (26), 5845–5855. https://doi.org/10.1016/j.jorganchem.2006.09.037.
(72) Berding, J.; Lutz, M.; Spek, A. L.; Bouwman, E. Synthesis of Novel Chelating Benzimidazole-Based Carbenes and Their Nickel(II) Complexes: Activity in the Kumada Coupling Reaction. *Organometallics* **2009**, *28* (6), 1845–1854. https://doi.org/10.1021/om8010596.
(73) Biffis, A.; Gazzola, L.; Tubaro, C.; Basato, M. Alkyne Hydroarylation in Ionic Liquids Catalyzed by Palladium(II) Complexes. *ChemSusChem* **2010**, *3* (7), 834–839. https://doi.org/10.1002/cssc.201000039.
(74) Biffis, A.; Gazzola, L.; Gobbo, P.; Buscemi, G.; Tubaro, C.; Basato, M. Alkyne Hydroarylations with Chelating Dicarbene Palladium(II) Complex Catalysts: Improved and Unexpected Reactivity Patterns Disclosed Upon Additive Screening. *Eur J Org Chem* **2009**, *2009* (19), 3189–3198. https://doi.org/10.1002/ejoc.200900321.

(75) Biffis, A.; Tubaro, C.; Buscemi, G.; Basato, M. Highly Efficient Alkyne Hydroarylation with Chelating Dicarbene Palladium(II) and Platinum(II) Complexes. *Adv Synth Catal* **2008**, *350* (1), 189–196. https://doi.org/10.1002/adsc.200700271.
(76) Kreisel, K. A.; Yap, G. P. A.; Theopold, K. H. A Chelating N-Heterocyclic Carbene Ligand in Organochromium Chemistry. *Organometallics* **2006**, *25* (19), 4670–4679. https://doi.org/10.1021/om060514s.
(77) Vivancos, Á.; Albrecht, M. Influence of the Linker Length and Coordination Mode of (Di)Triazolylidene Ligands on the Structure and Catalytic Transfer Hydrogenation Activity of Iridium(III) Centers. *Organometallics* **2017**, *36* (8), 1580–1590. https://doi.org/10.1021/acs.organomet.7b00140.
(78) Horn, S.; Gandolfi, C.; Albrecht, M. Transfer Hydrogenation of Ketones and Activated Olefins Using Chelating NHC Ruthenium Complexes. *Eur J Inorg Chem* **2011**, *2011* (18), 2863–2868. https://doi.org/10.1002/ejic.201100143.
(79) Farrell, K.; Melle, P.; Gossage, R. A.; Müller-Bunz, H.; Albrecht, M. Transfer Hydrogenation with Abnormal Dicarbene Rhodium(III) Complexes Containing Ancillary and Modular Poly-Pyridine Ligands. *Dalton Trans.* **2016**, *45* (11), 4570–4579. https://doi.org/10.1039/C5DT04656D.
(80) Farrell et al. - 2016 - Transfer Hydrogenation with Abnormal Dicarbene Rho.Pdf.
(81) Gandolfi, C.; Heckenroth, M.; Neels, A.; Laurenczy, G.; Albrecht, M. Chelating NHC Ruthenium(II) Complexes as Robust Homogeneous Hydrogenation Catalysts. *Organometallics* **2009**, *28* (17), 5112–5121. https://doi.org/10.1021/om900356w.
(82) Angew Chem Int Ed - 2007 - Heckenroth - Neutral Ligands with Exceptional Donor Ability for Palladium-Catalyzed Alkene.Pdf.
(83) Chemistry A European J - 2014 - Liu - A Heteroleptic Ferrous Complex with Mesoionic Bis 1 2 3-triazol-5-ylidene Ligands .Pdf.
(84) Ogba, O. M.; Warner, N. C.; O'Leary, D. J.; Grubbs, R. H. Recent Advances in Ruthenium-Based Olefin Metathesis. *Chem. Soc. Rev.* **2018**, *47* (12), 4510–4544. https://doi.org/10.1039/C8CS00027A.
(85) Fürstner, A.; Ackermann, L.; Beck, K.; Hori, H.; Koch, D.; Langemann, K.; Liebl, M.; Six, C.; Leitner, W. Olefin Metathesis in Supercritical Carbon Dioxide. *J. Am. Chem. Soc.* **2001**, *123* (37), 9000–9006. https://doi.org/10.1021/ja010952k.
(86) Huang, J.; Stevens, E. D.; Nolan, S. P.; Petersen, J. L. Olefin Metathesis-Active Ruthenium Complexes Bearing a Nucleophilic Carbene Ligand. *J. Am. Chem. Soc.* **1999**, *121* (12), 2674–2678. https://doi.org/10.1021/ja9831352.
(87) Scholl, M.; Trnka, T. M.; Morgan, J. P.; Grubbs, R. H. Increased Ring Closing Metathesis Activity of Ruthenium-Based Oiefin Metathesis Catalysts Coordinated with Imidazolin-2-Ylidene Ligands.
(88) Clapham, S. E.; Hadzovic, A.; Morris, R. H. Mechanisms of the H2-Hydrogenation and Transfer Hydrogenation of Polar Bonds Catalyzed by Ruthenium Hydride Complexes. *Coordination Chemistry Reviews* **2004**, *248* (21–24), 2201–2237. https://doi.org/10.1016/j.ccr.2004.04.007.
(89) Fache, F.; Schulz, E.; Tommasino, M. L.; Lemaire, M. Nitrogen-Containing Ligands for Asymmetric Homogeneous and Heterogeneous Catalysis. *Chem. Rev.* **2000**, *100* (6), 2159–2232. https://doi.org/10.1021/cr9902897.
(90) Blaser, H.; Malan, C.; Pugin, B.; Spindler, F.; Steiner, H.; Studer, M. Selective Hydrogenation for Fine Chemicals: Recent Trends and New Developments. *Adv Synth Catal* **2003**, *345* (1–2), 103–151. https://doi.org/10.1002/adsc.200390000.
(91) Noyori, R. Asymmetric Catalysis: Science and Opportunities (Nobel Lecture) Copyright© The Nobel Foundation 2002. We Thank the Nobel Foundation, Stockholm, for Permission to Print This Lecture. *Angew. Chem. Int. Ed.* **2002**, *41* (12), 2008. https://doi.org/10.1002/1521-3773(20020617)41:12<2008::AID-ANIE2008>3.0.CO;2-4.
(92) Noyori, R.; Takaya, H. BINAP: An Efficient Chiral Element for Asymmetric Catalysis. *Acc. Chem. Res.* **1990**, *23* (10), 345–350. https://doi.org/10.1021/ar00178a005.
(93) Cuevas, J. V.; Garcia-Herbosa, G. Base-Catalyzed Dehydrogenation of Palladium(II) Amino to i.Mm. o Complexes.
(94) Arliguie, T.; Chaudret, B.; Morris, R. H.; Sella, A. Monomeric and Dimeric Ruthenium(II) .Eta.2-Dihydrogen Complexes with Tricyclohexylphosphine Co-Ligands. *Inorg. Chem.* **1988**, *27* (4), 598–599. https://doi.org/10.1021/ic00277a006.

(95) Esteruelas, M. A.; Oro, L. A. Dihydrogen Complexes as Homogeneous Reduction Catalysts. *Chem. Rev.* **1998**, *98* (2), 577–588. https://doi.org/10.1021/cr970322u.
(96) Joó, F. Aqueous Biphasic Hydrogenations. *Acc. Chem. Res.* **2002**, *35* (9), 738–745. https://doi.org/10.1021/ar0100733.
(97) Wang, D.; Astruc, D. The Golden Age of Transfer Hydrogenation. *Chem. Rev.* **2015**, *115* (13), 6621–6686. https://doi.org/10.1021/acs.chemrev.5b00203.
(98) Corma, A.; Navas, J.; Sabater, M. J. Advances in One-Pot Synthesis through Borrowing Hydrogen Catalysis. *Chem. Rev.* **2018**, *118* (4), 1410–1459. https://doi.org/10.1021/acs.chemrev.7b00340.
(99) Irrgang, T.; Kempe, R. 3d-Metal Catalyzed N- and C-Alkylation Reactions via Borrowing Hydrogen or Hydrogen Autotransfer. *Chem. Rev.* **2019**, *119* (4), 2524–2549. https://doi.org/10.1021/acs.chemrev.8b00306.
(100) Reed-Berendt, B. G.; Polidano, K.; Morrill, L. C. Recent Advances in Homogeneous Borrowing Hydrogen Catalysis Using Earth-Abundant First Row Transition Metals. *Org. Biomol. Chem.* **2019**, *17* (7), 1595–1607. https://doi.org/10.1039/C8OB01895B.
(101) Shimizu, K. Heterogeneous Catalysis for the Direct Synthesis of Chemicals by Borrowing Hydrogen Methodology. *Catal. Sci. Technol.* **2015**, *5* (3), 1412–1427. https://doi.org/10.1039/C4CY01170H.
(102) Seretis, A.; Diamantopoulou, P.; Thanou, I.; Tzevelekidis, P.; Fakas, C.; Lilas, P.; Papadogianakis, G. Recent Advances in Ruthenium-Catalyzed Hydrogenation Reactions of Renewable Biomass-Derived Levulinic Acid in Aqueous Media. *Front. Chem.* **2020**, *8*, 221. https://doi.org/10.3389/fchem.2020.00221.
(103) European Environment Agency. *Energy and Environment Report 2008*; Publications Office: LU, 2008.
(104) Armaroli, N.; Balzani, V. The Future of Energy Supply: Challenges and Opportunities. *Angew Chem Int Ed* **2007**, *46* (1–2), 52–66. https://doi.org/10.1002/anie.200602373.
(105) Blankenship, R. E. *Molecular Mechanisms of Photosynthesis*; Blackwell Science: Oxford ; Malden, MA, 2002.
(106) Eisenberg, R.; Nocera, D. G. Preface: Overview of the Forum on Solar and Renewable Energy. *Inorg. Chem.* **2005**, *44* (20), 6799–6801. https://doi.org/10.1021/ic058006i.
(107) Grätzel, M. Photoelectrochemical Cells. **2001**, *414*.
(108) Gonçalves, L. M.; De Zea Bermudez, V.; Ribeiro, H. A.; Mendes, A. M. Dye-Sensitized Solar Cells: A Safe Bet for the Future. *Energy Environ. Sci.* **2008**, *1* (6), 655. https://doi.org/10.1039/b807236a.
(109) Polo, A. S.; Itokazu, M. K.; Murakami Iha, N. Y. Metal Complex Sensitizers in Dye-Sensitized Solar Cells. *Coordination Chemistry Reviews* **2004**, *248* (13–14), 1343–1361. https://doi.org/10.1016/j.ccr.2004.04.013.
(110) Argazzi, R.; Murakami Iha, N. Y.; Zabri, H.; Odobel, F.; Bignozzi, C. A. Design of Molecular Dyes for Application in Photoelectrochemical and Electrochromic Devices Based on Nanocrystalline Metal Oxide Semiconductors. *Coordination Chemistry Reviews* **2004**, *248* (13–14), 1299–1316. https://doi.org/10.1016/j.ccr.2004.03.026.
(111) Hagfeldt, A.; Graetzel, M. Light-Induced Redox Reactions in Nanocrystalline Systems. *Chem. Rev.* **1995**, *95* (1), 49–68. https://doi.org/10.1021/cr00033a003.
(112) Wasielewski, M. R. Photoinduced Electron Transfer in Supramolecular Systems for Artificial Photosynthesis. *Chem. Rev.* **1992**, *92* (3), 435–461. https://doi.org/10.1021/cr00011a005.
(113) Gao, F.; Wang, Y.; Zhang, J.; Shi, D.; Wang, M.; Humphry-Baker, R.; Wang, P.; Zakeeruddin, S. M.; Grätzel, M. A New Heteroleptic Ruthenium Sensitizer Enhances the Absorptivity of Mesoporous Titania Film for a High Efficiency Dye-Sensitized Solar Cell. *Chem. Commun.* **2008**, No. 23, 2635. https://doi.org/10.1039/b802909a.
(114) Yu, Q.; Liu, S.; Zhang, M.; Cai, N.; Wang, Y.; Wang, P. An Extremely High Molar Extinction Coefficient Ruthenium Sensitizer in Dye-Sensitized Solar Cells: The Effects of π-Conjugation Extension. *J. Phys. Chem. C* **2009**, *113* (32), 14559–14566. https://doi.org/10.1021/jp904096g.
(115) Gao, F.; Wang, Y.; Shi, D.; Zhang, J.; Wang, M.; Jing, X.; Humphry-Baker, R.; Wang, P.; Zakeeruddin, S. M.; Grätzel, M. Enhance the Optical Absorptivity of Nanocrystalline TiO_2 Film with High Molar Extinction Coefficient Ruthenium Sensitizers for High Performance Dye-Sensitized Solar Cells. *J. Am. Chem. Soc.* **2008**, *130* (32), 10720–10728. https://doi.org/10.1021/ja801942j.

(116) Vougioukalakis, G. C.; Philippopoulos, A. I.; Stergiopoulos, T.; Falaras, P. Contributions to the Development of Ruthenium-Based Sensitizers for Dye-Sensitized Solar Cells. *Coordination Chemistry Reviews* **2011**, *255* (21–22), 2602–2621. https://doi.org/10.1016/j.ccr.2010.11.006.
(117) Wang, P.; Zakeeruddin, S. M.; Moser, J. E.; Nazeeruddin, M. K.; Sekiguchi, T.; Grätzel, M. A Stable Quasi-Solid-State Dye-Sensitized Solar Cell with an Amphiphilic Ruthenium Sensitizer and Polymer Gel Electrolyte. *Nature Mater* **2003**, *2* (6), 402–407. https://doi.org/10.1038/nmat904.
(118) Matheu, R.; Ertem, M. Z.; Gimbert-Suriñach, C.; Sala, X.; Llobet, A. Seven Coordinated Molecular Ruthenium–Water Oxidation Catalysts: A Coordination Chemistry Journey: Focus Review. *Chem. Rev.* **2019**, *119* (6), 3453–3471. https://doi.org/10.1021/acs.chemrev.8b00537.
(119) Hey, D. A.; Reich, R. M.; Baratta, W.; Kühn, F. E. Current Advances on Ruthenium(II) N-Heterocyclic Carbenes in Hydrogenation Reactions. *Coordination Chemistry Reviews* **2018**, *374*, 114–132. https://doi.org/10.1016/j.ccr.2018.06.005.
(120) Poyatos, M.; Mas-Marzá, E.; Sanaú, M.; Peris, E. Synthesis and Reactivity of New Chelate-N-Heterocyclic Biscarbene Complexes of Ruthenium. *Inorg. Chem.* **2004**, *43* (5), 1793–1798. https://doi.org/10.1021/ic035307o.
(121) Saha, S.; Ghatak, T.; Saha, B.; Doucet, H.; Bera, J. K. Steric Control at the Wingtip of a Bis-N-Heterocyclic Carbene Ligand: Coordination Behavior and Catalytic Responses of Its Ruthenium Compounds. *Organometallics* **2012**, *31* (15), 5500–5505. https://doi.org/10.1021/om300469n.
(122) Cheng, Y.; Lu, X.-Y.; Xu, H.-J.; Li, Y.-Z.; Chen, X.-T.; Xue, Z.-L. Bis-N-Heterocyclic Carbene Ruthenium(II) Carbonyl Complexes: Synthesis, Structural Characterization and Catalytic Activities in Transfer Hydrogenation of Ketones. *Inorganica Chimica Acta* **2010**, *363* (2), 430–437. https://doi.org/10.1016/j.ica.2009.11.015.
(123) Gill, T. P.; Mann, K. R. Photochemical Properties of the Cyclopentadienyl(.Eta.6-Benzene)Ruthenium(II) Cation. The Synthesis and Reactions of a Synthetically Useful Intermediate: The Cyclopentadienyltris(Acetonitrile)Ruthenium(II) Cation. *Organometallics* **1982**, *1* (3), 485–488. https://doi.org/10.1021/om00063a014.
(124) Zuccaccia, D.; Bellachioma, G.; Cardaci, G.; Zuccaccia, C.; Macchioni, A. Aggregation Tendency and Reactivity toward AgX of Cationic Half-Sandwich Ruthenium(Ii) Complexes Bearing Neutral N,O-Ligands. *Dalton Trans.* **2006**, No. 16, 1963. https://doi.org/10.1039/b514269e.
(125) Terasawa, J.; Kondo, H.; Matsumoto, T.; Kirchner, K.; Motoyama, Y.; Nagashima, H. "Unsymmetrical" Diruthenium Amidinates in Which the μ_2-Amidinate Bridge Is Perpendicular to the Ru−Ru Axis: Synthesis and Reactions of Derivatives of [(η^5-C_5Me_5)Ru(μ-Amidinate)Ru(η^5-C_5H_5)]$^+$. *Organometallics* **2005**, *24* (11), 2713–2721. https://doi.org/10.1021/om050091e.
(126) Fernandez, S.; Pfeffer, M.; Ritleng, V.; Sirlin, C. An Effective Route to Cycloruthenated N-Ligands under Mild Conditions. *Organometallics* **1999**, *18* (12), 2390–2394. https://doi.org/10.1021/om9901067.
(127) Alvarez, P.; Gimeno, J.; Lastra, E.; García-Granda, S.; Van Der Maelen, J. F.; Bassetti, M. Synthesis and Reactivity of Indenyl Ruthenium(II) Complexes Containing the Labile Ligand 1,5-Cyclooctadiene (COD): Catalytic Activity of [Ru(η^5-C_9H_7)Cl(COD)]. *Organometallics* **2001**, *20* (17), 3762–3771. https://doi.org/10.1021/om010205w.
(128) Widegren, J. A.; Weiner, H.; Miller, S. M.; Finke, R. G. Improved Synthesis and Crystal Structure of Tetrakis(Acetonitrile)(H4-1,5-Cyclooctadiene)Ruthenium(II) Bis[Tetrafluoroborate(1 −)]. *Journal of Organometallic Chemistry* **2000**.
(129) S0022-328x_2800_2981336-4.Pdf.
(130) Albers, M. O.; Ashworth, T. V.; Oosthuizen, H. E.; Singleton, E.; Merola, J. S.; Kacmarcik, R. T. (η^4-1, 5-Cyclooctadiene)Ruthenium(II) Complexes. In *Inorganic Syntheses*; Kaesz, H. D., Ed.; John Wiley & Sons, Inc.: Hoboken, NJ, USA, 2007; pp 68–77. https://doi.org/10.1002/9780470132579.ch14.
(131) Rach, S. F.; Kühn, F. E. Nitrile Ligated Transition Metal Complexes with Weakly Coordinating Counteranions and Their Catalytic Applications. *Chem. Rev.* **2009**, *109* (5), 2061–2080. https://doi.org/10.1021/cr800270h.
(132) Poyatos, M.; Mas-Marzá, E.; Sanaú, M.; Peris, E. Synthesis and Reactivity of New Chelate-N-Heterocyclic Biscarbene Complexes of Ruthenium. *Inorg. Chem.* **2004**, *43* (5), 1793–1798. https://doi.org/10.1021/ic035307o.

(133) Huynh, H. V.; Han, Y.; Jothibasu, R.; Yang, J. A. ^{13}C NMR Spectroscopic Determination of Ligand Donor Strengths Using N-Heterocyclic Carbene Complexes of Palladium(II). *Organometallics* **2009**, *28* (18), 5395–5404. https://doi.org/10.1021/om900667d.
(134) Rapaport, I.; Helm, L.; Merbach, A. E.; Bernhard, P.; Ludi, A. High-Pressure NMR Kinetics. Part 34. Variable-Temperature and Variable-Pressure NMR Kinetic Study of Solvent Exchange on Hexaaquaruthenium(3+) and -(2+) and Hexakis(Acetonitrile)Ruthenium(2+). *Inorg. Chem.* **1988**, *27* (5), 873–879. https://doi.org/10.1021/ic00278a025.
(135) Meerwein, H.; Schmidt, R. Ein neues Verfahren zur Reduktion von Aldehyden und Ketonen. *Justus Liebigs Ann. Chem.* **1925**, *444* (1), 221–238. https://doi.org/10.1002/jlac.19254440112.
(136) Ponndorf, W. Der reversible Austausch der Oxydationsstufen zwischen Aldehyden oder Ketonen einerseits und primären oder sekundären Alkoholen anderseits. *Z. Angew. Chem.* **1926**, *39* (5), 138–143. https://doi.org/10.1002/ange.19260390504.
(137) Sasson, Y.; Blum, J. Dichlorotris(Triphenylphosphine)Ruthenium-Catalyzed Hydrogen Transfer from Alcohols to Saturated and a,b-Unsaturated Ketones. *Journal of Organometallic Chemistry* **1975**, *40* (13), 1887–1896. https://doi.org/10.1021/jo00901a004.
(138) Chowdhury, R. L.; Backvall, J.-E. Efficient Ruthenium-Catalysed Transfer Hydrogenation of Ketones by Propan-2-Ol. *Journal of the Chemical Society, Chemical Communications* **1991**, No. 16, 1063–1064. https://doi.org/10.1039/C39910001063.
(139) Gunanathan, C.; Milstein, D. Bond Activation and Catalysis by Ruthenium Pincer Complexes. *Chem. Rev.* **2014**, *114* (24), 12024–12087. https://doi.org/10.1021/cr5002782.
(140) Figliolia, R.; Cavigli, P.; Comuzzi, C.; Del Zotto, A.; Lovison, D.; Strazzolini, P.; Susmel, S.; Zuccaccia, D.; Ballico, M.; Baratta, W. CNN Pincer Ruthenium Complexes for Efficient Transfer Hydrogenation of Biomass-Derived Carbonyl Compounds. *Dalton Trans.* **2020**, *49* (2), 453–465. https://doi.org/10.1039/C9DT04292J.
(141) Baldino, S.; Facchetti, S.; Zanotti-Gerosa, A.; Nedden, H. G.; Baratta, W. Transfer Hydrogenation and Hydrogenation of Commercial-Grade Aldehydes to Primary Alcohols Catalyzed by 2-(Aminomethyl)Pyridine and Pincer Benzo[*h*]Quinoline Ruthenium Complexes. *ChemCatChem* **2016**, *8* (13), 2279–2288. https://doi.org/10.1002/cctc.201600420.
(142) Jin, W.; Wang, L.; Yu, Z. A Highly Active Ruthenium(II) Pyrazolyl–Pyridyl–Pyrazole Complex Catalyst for Transfer Hydrogenation of Ketones. *Organometallics* **2012**, *31* (15), 5664–5667. https://doi.org/10.1021/om300602w.
(143) Pardatscher, L.; Hofmann, B. J.; Fischer, P. J.; Hölzl, S. M.; Reich, R. M.; Kühn, F. E.; Baratta, W. Highly Efficient Abnormal NHC Ruthenium Catalyst for Oppenauer-Type Oxidation and Transfer Hydrogenation Reactions. *ACS Catal.* **2019**, *9* (12), 11302–11306. https://doi.org/10.1021/acscatal.9b03677.
(144) Böth, A. D.; Sauer, M. J.; Baratta, W.; Kühn, F. E. Abnormal NHC Ruthenium Catalysts: Mechanistic Investigations of Their Preparation and Steric Influence on Catalytic Performance. *Catal. Sci. Technol.* **2022**, *12* (18), 5597–5603. https://doi.org/10.1039/D2CY01036D.
(145) Housecroft, C. E.; Sharpe, A. G. Inorganic Chemistry.
(146) Docherty, J. H.; Lister, T. M.; Mcarthur, G.; Findlay, M. T.; Domingo-Legarda, P.; Kenyon, J.; Choudhary, S.; Larrosa, I. Transition-Metal-Catalyzed C–H Bond Activation for the Formation of C–C Bonds in Complex Molecules. *Chem. Rev.* **2023**, *123* (12), 7692–7760. https://doi.org/10.1021/acs.chemrev.2c00888.
(147) Nareddy, P.; Jordan, F.; Szostak, M. Recent Developments in Ruthenium-Catalyzed C–H Arylation: Array of Mechanistic Manifolds. *ACS Catal.* **2017**, *7* (9), 5721–5745. https://doi.org/10.1021/acscatal.7b01645.
(148) Simonetti, M.; Cannas, D. M.; Just-Baringo, X.; Vitorica-Yrezabal, I. J.; Larrosa, I. Cyclometallated Ruthenium Catalyst Enables Late-Stage Directed Arylation of Pharmaceuticals. *Nature Chem* **2018**, *10* (7), 724–731. https://doi.org/10.1038/s41557-018-0062-3.
(149) Simonetti, M.; Perry, G. J. P.; Cambeiro, X. C.; Juliá-Hernández, F.; Arokianathar, J. N.; Larrosa, I. Ru-Catalyzed C–H Arylation of Fluoroarenes with Aryl Halides. *J. Am. Chem. Soc.* **2016**, *138* (10), 3596–3606. https://doi.org/10.1021/jacs.6b01615.
(150) Johnston, A. J. S.; Ling, K. B.; Sale, D.; Lebrasseur, N.; Larrosa, I. Direct *Ortho* -Arylation of Pyridinecarboxylic Acids: Overcoming the Deactivating Effect of Sp ^{2} -Nitrogen. *Org. Lett.* **2016**, *18* (23), 6094–6097. https://doi.org/10.1021/acs.orglett.6b03085.
(151) Oi, S.; Aizawa, E.; Ogino, Y.; Inoue, Y. Ortho-Selective Direct Cross-Coupling Reaction of 2-Aryloxazolines and 2-Arylimidazolines with Aryl and Alkenyl Halides Catalyzed by Ruthenium Complexes. *J. Org. Chem.* **2005**, *70* (8), 3113–3119. https://doi.org/10.1021/jo050031i.

(152) Ackermann, L.; Born, R.; Álvarez-Bercedo, P. Ruthenium(IV) Alkylidenes as Precatalysts for Direct Arylations of Alkenes with Aryl Chlorides and an Application to Sequential Catalysis. *Angew Chem Int Ed* **2007**, *46* (33), 6364–6367. https://doi.org/10.1002/anie.200701727.
(153) Arockiam, P. B.; Fischmeister, C.; Bruneau, C.; Dixneuf, P. H. C□H Bond Functionalization in Water Catalyzed by Carboxylato Ruthenium(II) Systems. *Angewandte Chemie* **2010**, *122* (37), 6779–6782. https://doi.org/10.1002/ange.201002870.
(154) Ferrer Flegeau, E.; Bruneau, C.; Dixneuf, P. H.; Jutand, A. Autocatalysis for C–H Bond Activation by Ruthenium(II) Complexes in Catalytic Arylation of Functional Arenes. *J. Am. Chem. Soc.* **2011**, *133* (26), 10161–10170. https://doi.org/10.1021/ja201462n.
(155) Požgan, F.; Dixneuf, P. H. Ruthenium(II) Acetate Catalyst for Direct Functionalisation of Sp^2-C□H Bonds with Aryl Chlorides and Access to Tris- Heterocyclic Molecules. *Adv Synth Catal* **2009**, *351* (11–12), 1737–1743. https://doi.org/10.1002/adsc.200900350.
(156) Ackermann, L.; Lygin, A. V.; Hofmann, N. Ruthenium-Catalyzed Oxidative Annulation by Cleavage of C□H/N□H Bonds. *Angewandte Chemie* **2011**, *123* (28), 6503–6506. https://doi.org/10.1002/ange.201101943.
(157) Findlay, M. T.; Hogg, A. S.; Douglas, J. J.; Larrosa, I. Improving the Sustainability of the Ruthenium-Catalysed *N*-Directed C–H Arylation of Arenes with Aryl Halides. *Green Chem.* **2023**, *25* (6), 2394–2400. https://doi.org/10.1039/D2GC03860A.
(158) Kolb, H. C.; Finn, M. G.; Sharpless, K. B. Click Chemistry: Diverse Chemical Function from a Few Good Reactions. *Angew. Chem. Int. Ed.* **2001**, *40* (11), 2004–2021. https://doi.org/10.1002/1521-3773(20010601)40:11<2004::AID-ANIE2004>3.0.CO;2-5.
(159) Chen, L.; Malollari, K. G.; Uliana, A.; Hartwig, J. F. Ruthenium-Catalyzed, Chemoselective and Regioselective Oxidation of Polyisobutene. *J. Am. Chem. Soc.* **2021**, *143* (12), 4531–4535. https://doi.org/10.1021/jacs.1c00125.
(160) Borys, A. M. An Illustrated Guide to Schlenk Line Techniques. *Organometallics* **2023**, *42* (3), 182–196. https://doi.org/10.1021/acs.organomet.2c00535.
(161) Yang, C.-H.; Beltran, J.; Lemaur, V.; Cornil, J.; Hartmann, D.; Sarfert, W.; Fröhlich, R.; Bizzarri, C.; De Cola, L. Iridium Metal Complexes Containing N-Heterocyclic Carbene Ligands for Blue-Light-Emitting Electrochemical Cells. *Inorg. Chem.* **2010**, *49* (21), 9891–9901. https://doi.org/10.1021/ic1009253.
(162) Barral, K.; Moorhouse, A. D.; Moses, J. E. Efficient Conversion of Aromatic Amines into Azides: A One-Pot Synthesis of Triazole Linkages. *Org. Lett.* **2007**, *9* (9), 1809–1811. https://doi.org/10.1021/ol070527h.
(163) Eisenberger, P.; Bestvater, B. P.; Keske, E. C.; Crudden, C. M. Hydrogenations at Room Temperature and Atmospheric Pressure with Mesoionic Carbene-Stabilized Borenium Catalysts. *Angew. Chem. Int. Ed.* **2015**, *54* (8), 2467–2471. https://doi.org/10.1002/anie.201409250.
(164) Fletcher, J. T.; Walz, S. E.; Keeney, M. E. Monosubstituted 1,2,3-Triazoles from Two-Step One-Pot Deprotection/Click Additions of Trimethylsilylacetylene. *Tetrahedron Letters* **2008**, *49* (49), 7030–7032. https://doi.org/10.1016/j.tetlet.2008.09.136.
(165) Anneser, M. R.; Haslinger, S.; Pöthig, A.; Cokoja, M.; Basset, J.-M.; Kühn, F. E. Synthesis and Characterization of an Iron Complex Bearing a Cyclic Tetra-N-Heterocyclic Carbene Ligand: An Artifical Heme Analogue? *Inorg. Chem.* **2015**, *54* (8), 3797–3804. https://doi.org/10.1021/ic503043h.

6 LIST OF PUBLISHED AND DRAFTED ARTICLES

Insights on the Anion Effect in N-heterocyclic Carbene Based Dinuclear Gold(I) Catalysts

Authors:

Filippo Campagnolo, Matteo Bevilacqua, Marco Baron, Cristina Tubaro, Andrea Biffis, Daniele Zuccaccia

Abstract:

Dinuclear bisNHC (bis(N-heterocyclic carbene)) gold(I) complexes **3a** and **4a** of general formula [Au_2Br_2(bisNHC)] were tested as catalysts in the cycloisomerization of N-(prop-2-yn-yl)benzamide and in the hydromethoxylation of 3-hexyne in the presence of silver(I) activators bearing different counteranions. The catalytic performance in the same reactions of mononuclear NHC complexes (**1a**, **2a**) was studied as well. The results highlighted the fundamental role of both NHC ligand and counterion in the catalytic cycles and activation process: dinuclear catalysts exhibit higher initial activity even under milder conditions but suffer in terms of stability with respect to mono NHCs. Furthermore, a new dinuclear bisNHC gold(I) complex **2c** of general formula [$Au_2(OTs)_2$(bisNHC)] (OTs = p-toluenesulfonate) was successfully synthesized and characterized by means of NMR and ESI-MS analyses.

DOI:

https://doi.org/10.1002/cplu.202300421

Experimental and Theoretical Investigation of Ion Pairing in Gold(III) Catalysts

Authors:

Jacopo Segato, Eleonora Aneggi, Walter Baratta, Filippo Campagnolo, Leonardo Belpassi, Paola Belanzoni, and Daniele Zuccaccia

Abstract:

The ion pairing structure of the possible species present in solution during the gold(III)- catalyzed hydration of alkynes: [(ppy)Au(NHC)Y]X_2 and [(ppy)Au(NHC)X]X [ppy = 2-phenylpyridine, NHC = NHCiPr = 1,3-bis(2,6-di-isopropylphenyl)-imidazol-2-ylidene; NHC = NHCmes = 1,3-bis(2,4,6-trimethylphenyl)-imidazol-2-ylidene X = Cl^-, BF_4^-, OTf^-; Y = H_2O and 3-hexyne] are determined. The nuclear overhauser effect nuclear magnetic resonance (NMR) experimental measurements integrated with a theoretical description of the system (full optimization of different ion pairs and calculation of the Coulomb potential surface) indicate that the preferential position of the counterion is tunable through the choice of the ancillary ligands (NHCiPr, NHCmes, ppy, and Y) in [(ppy)Au(NHC)(3-hexyne)]X_2 activated complexes that undergo nucleophilic attack. The counterion can approach near NHC, pyridine ring of ppy, and gold atom. From these positions, the anion can act as a template, holding water in the right position for the outer-sphere attack, as observed in gold(I) catalysts.

DOI:

https://doi.org/10.1021/acs.organomet.3c00293

Solvent-free selective oxidation of benzyl alcohol using Ru loaded ceria-zirconia catalysts

Authors:

Eleonora Aneggi, Filippo Campagnolo, Jacopo Segato, Daniele Zuccaccia, Walter Baratta, Jordi Llorca, Alessandro Trovarelli

Abstract:

Selective oxidation of alcohols to aldehydes or ketones is a fundamental process in organic chemistry and the development of green and sustainable transformations are strongly required. Herein, we focused on the development of Ru-based catalysts deposited over ceria-zirconia supports (CZRu) for the solvent free oxidation of benzyl alcohol using air as oxidant, which is a cheap and safe process and meets to the atom economy and environment requirements. XPS characterization of the material reveals that the formation of RuO_2 on the surface is necessary to achieve higher catalytic activity. The activity is strongly related to the reducibility of the material and to the close interaction between ceria-zirconia and RuO_2, with the likely formation of Ru-O-Ce arrangements. The greater mobility of oxygen due to the formation of bridging oxygens in Ru-O-Ce and to the formation of superoxide species (O_2^-) over Ce^{3+} sites, significantly boosts the selective oxidation of alcohols. CZRu is a promising material with a remarkable 61% alcohol conversion at 90 °C without solvents; it also exhibits high activity (55% conversion) and complete selectivity (100%) for the selective oxidation of 1-phenylethanol to acetophenone. Overall, the formulation is among the most active reported so far under solvent free conditions and molecular oxygen. In addition, the reaction over CZRu exhibits an environmental factor (E-factor) lower than 1 (0.95) confirming the sustainability of the proposed process.

DOI:

https://doi.org/10.1016/j.mcat.2023.113049

Sustainable Solvent-Free Selective Oxidation of Benzyl Alcohol Using Ru(0) Supported on Alumina

Authors:

Eleonora Aneggi, Filippo Campagnolo, Daniele Zuccaccia, Walter Baratta, Jordi Llorca and Alessandro Trovarelli

Abstract:

The selective oxidation of primary alcohols into their corresponding carbonyl compounds is challenging because of the easy over-oxidization to acids and esters. The traditional reaction requires large amounts of solvent and oxidant, causing serious environmental issues. Recently, several efforts have been made to transform the reaction into a more sustainable process. Here, we investigated the solvent-free oxidation of benzyl alcohol using air as a green oxidant in the presence of ruthenium supported on alumina and zirconia, thereby meeting atom economy and environmental requirements. The materials were extensively characterized and, in addition to their activity, selectivity, and reusability, the environmental sustainability of the process was assessed according to green chemistry metrics. XRD, TEM, and XPS analyses suggest that the formation of metallic Ru on the support plays a key role in the catalytic activity. Ru supported on alumina, after a reduction treatment, achieves good activity (62% conversion) and a complete selectivity in a very sustainable process (without a solvent and with air as oxidant), as indicated by the very low E-factor value. The formulation is very stable and maintains high activity after recycling.

DOI:

https://doi.org/10.3390/inorganics11050177

Postprandial kinetics of digestive function in rainbow trout (*Oncorhynchus mykiss*): genes expression, enzymatic activity and blood biochemistry as a practical tool for nutritional studies

Authors:

Giulia Pascon, Enrico Daniso, Gloriana Cardinaletti, Maria Messina, Filippo Campagnolo, Daniele Zuccaccia and Francesca Tulli

Abstract:

Postprandial kinetics of genes expression of gastric (chitinase, pepsinogen) and intestinal (alkaline phosphatase, maltase) digestive enzymes and nutrient transporters (peptide transporter 1, sodium-glucose transporter 1), Brush Border Membrane (BBM) enzymes activity (alkaline phosphatase, leucine aminopeptidase, maltase, saccharase) and blood biochemistry (triglycerides, cholesterol, protein, albumin, glucose, amino acids) through NMR spectroscopy, were investigated in rainbow trout (*Oncorhynchus mykiss*) fed a commercial aquafeed. For this purpose, fish were starved 72 h and digestive tract and blood were sampled before the meal and at 1.5, 3, 6, 9, 12, and 24 h after feeding (T0, T1.5, T3, T6, T9, T12 and T24). The postprandial kinetic showed that the expression of the genes involved in digestion and nutrient transport, the activity of BBM enzymes, and the presence of metabolites in blood were stimulated in different ways by the presence of feed in the digestive tract. The expression of most genes peaked 3 h after meal except gastric pepsinogen and maltase in distal intestine that peaked at T9 and T12, respectively. The activity of BBM enzymes were stimulated differently based on the intestine tract. The plasma proteins level increased from T1.5 until T9, while the other blood parameters unvariated during the postprandial period. This study supplied useful information about the physiological effects a single meal as a potential tool for planning nutritional studies involving the digestive functions.

DOI:

https://doi.org/10.1016/j.cbpa.2023.111559

On the mechanism of ruthenium(II)-aNHC homogeneous catalyzed hydrogen auto-transfer reactions

Authors:

Filippo Campagnolo, Walter Baratta, Fritz E. Kühn, Daniele Zuccaccia

Abstract:

Ruthenium(II) complexes bearing aNHC-phosphine ligands showed remarkable activity in hydrogen auto-transfer reactions. The hydrogenation of ketones using sacrificial alcohols and the inverse Oppenauer oxidation reaction are assumed to follow the same reaction mechanisms, even if they are often conducted with different experimental protocols. The development of a unique reaction protocol shared between reductive and oxidative pathways highlighted the role of the base in both activation equilibria and in the decomposition of the catalysts. A structure/reactivity correlation study proved that a linear free energy relationship subsists for all substrates used, implicating a strong dependency on the substrate steric hindrance, consistent with an inner sphere mechanism. Furthermore, the slope steepness inversion in the two reactions suggests a difference in the reaction mechanism.

DOI:

Draft

Assessing the ion-pairing effect in Gold(I) catalyzed alkyne hydroalkoxylation, a DOSY NMR approach

Authors:

Filippo Campagnolo, Eleonora Aneggi, Daniele Zuccaccia

Abstract:

In recent years, homogeneous gold(I) catalysis caught attention as a growing field in the development of organic chemistry reactions promoted by L-Au-X compounds (L = an ancillary ligand, and X^- = a counterion), which mainly involve nucleophilic additions to carbon–carbon unsaturated bonds. The alkyne hydroalkoxylation reaction is among the most studied gold(I)-catalyzed reactions, as it provides an excellent framework to develop a robust complex by tuning the ligand (L) and studying the counterion (X-) effect. Indeed, the counterion, usually regarded as a spectator ion, here instead plays a pivotal role in the reaction mechanism. Optimizing the choice of the counterion becomes hence crucial because of its involvement in the reaction's key steps: 1) the pre-equilibrium, where the coordination of the alkynes takes place moving the counterion from the inner sphere to the outer sphere ion pair configuration, 2) the nucleophilic attack, where the just formed gold-alkyne complex undergoes nucleophilic attack by a nucleophile (Nu-H), and 3) the protodeauration, where the gold-carbon bond is cleaved by a proton in the newly formed organogold intermediate, giving the desired product and regenerating the catalyst. In the hydroalkoxylation reaction, where the rate-determining step (RDS) is the nucleophilic attack, the p-toluenesulfonate anion (OTs^-) provides the best compromise for achieving an efficient catalyst, thanks to its intermediate coordinating ability, basicity, and hydrogen bond acceptor property. These properties are assumed to affect the actual ion-pairing ratio during catalysis between the cation (L-Au-R^+) and the counterion (X^-), but the ion-pairing ratio constitutes an elusive and complex quantity to asses experimentally, particularly under catalytic conditions. Taking advantage of diffusion-ordered spectroscopy (DOSY) NMR, we observed the average hydrodynamic volumes of different L-Au-X catalysts under catalytic conditions, which from the ion-pairing ratio of each species was obtained. The experimental results highlighted how the ion-pairing ratio is a fundamental parameter to consider, but also that the basic properties of the anion matter, as the trifluoromethanesulfonate (OTf-) and OTs^- anions displayed the same average ratio despite different catalytic performances.

DOI:

Draft

ACKNOWLEDGMENTS

Finding words compelling enough to express my gratitude to the extraordinary people who supported me during my PhD is no easy task. To all those who stood by me, your support has been like a compass when I felt lost. Thank you all for being an integral part of this journey. To begin with, I would like to express my deep appreciation for my mentor, Professor Daniele Zuccaccia, whose guidance has been essential throughout these years. His wisdom has been both enlightening and enriching, inspiring me to strive for more. I extend my heartfelt gratitude to my dear friend, Gabriele Pirodda, for the invaluable support he provided throughout the years. I owe much of my current standing to his unwavering help. Next, I would like to sincerely thank the entire Kühn group at TUM, whose warm welcome made my six-month journey a life-changing experience. To Dr. Alexander Böth, Micheal Sauer, Nicole Dietl, Carla Hoefer, and Johannes Mayr, thanks for the time we shared. Among them, Alexander left an indelible mark, thanks to his resolute composure under stress that will always be a source of inspiration. I would also mention Alberto Piccoli and Dr. Denise Lovison, who I also met at TUM, and with whom I shared the experience of being a researcher abroad. I extend my sincere appreciation to the organometal chemistry group at Udine, particularly Dr. Maurizio Ballico and Marta Busato. Maurizio, your unparalleled expertise in organometallic chemistry is unmatched, and to Marta, I wish you the very best in all your future challenges. My gratitude also goes to Dario Alessi, with whom I shared the trenches over these three years. Our collaborative efforts have been the backbone of this journey, and I am thankful for the time we shared. Finally, I would like to thank my amazing parents and family, to whom I owe the most. Their love, encouragement, and belief in my abilities have been my driving force. This accomplishment is as much yours as it is mine. I am profoundly grateful for the love and support you have shown me.